2023 YOUNG LEADER IN DISPLAY AND PG WORKSHOP

第十届兩岸三地研究生顯示技術研討會

21-22 AUGUST 2023

The Hong Kong University of Science and Technology

YOUNG LEADER IN DISPLAY AND PG WORKSHOP

第十屆兩岸三地研究生顯示技術研討會

21-22 AUGUST 2023

The Hong Kong University of Science and Technology

Table of Contents

Foreword ii

2023 PGWS Committees iii

Program v

Campus WIFI Access ix

Instruction for Oral and Poster Presentation x

Campus Map xi

Index of Abstract xiii

Foreword

Welcome to the Tenth Cross-Strait Postgraduate Workshop on Displays and Young Leaders in Displays. This year marks the Tenth Year Anniversary of PGWS. This Workshop was started ten years ago by Professor NS Xu of SYSU, Professor David Shieh of NCTU and myself. The first one was held in HKUST, and has been rotating between various locations across the Taiwan Strait. It was organized entirely by PG students with help from the staff.

The idea of the Workshop is to have young researchers sharing their results and experiences. Over the years, this goal has been achieved remarkably and many students from different Universities started collaborating after the Workshop. Quite a few projects have resulted in joint publications. Many of the students maintain contacts with each other after their graduation, especially for those who remain in the display research and manufacturing industry. It is very satisfying for us to see the younger generation taking over the baton.

Since five years ago, we have included students from other Universities. We are glad to see that this year, more Universities are involved and we have a record breaking attendance of over 200 people. Overall, 13 Universities are represented, including, SYSU, NYCU, SusTech, SCUT, SZU, PKU(SZ), FZU, IMECAS, SEU, JNU, HBU, SHU and HKUST. Since last year, we have started a Young Leaders in Displays Symposium. Each University is requested to recommend one speaker to the Symposium.

Since this is the Tenth Anniversary, the students have arranged an interesting social program for their celebration. It includes a friendly soccer tournament, and a boat trip around Hong Kong harbor. We are sure that everyone will enjoy these events. As always, the academic exchange will surely be enlightening and rewarding. We are sure that many research collaborations and ideas will be stimulated by this Workshop, resulting in joint publications and research proposals and research grants. Collaborative research is becoming important and much funding opportunities have been created in the newly recognized Greater Bay Area. This PGWS will surely grow into a platform for research collaborations. We wish all the participants best of luck in their future endeavors.

Honorary Chairs

NS Xu, David Shieh and H Kwok

2023 PGWS Committees

Conference Honorary Chair

Prof Hoi Sing Kwok
Executive Director of SKL
Department of ECE, HKUST

Prof Han-Ping D. Shieh
Emeritus Professor
National Yang Ming Chiao Tung University

Prof Ningsheng Xu
President
Fudan University

Conference Chair

Prof Man Wong
Director, SKL of ADT
Department of ECE, HKUST

Organizing Committee

Prof Zhiyong Fan
Professor
Department of ECE, HKUST

Prof Abhishek Srivastava
Associate Professor
Department of ECE, HKUST

Prof Ken Tseng
Research Assistant Professor
Department of ECE, HKUST

Prof Zhihe Xia
Research Assistant Professor
Department of ECE, HKUST

Conference Secretary

Dr Fion Yeung
Senior Manager, SKL of ADT
Department of ECE, HKUST

Ms Yiying Wang
Officer, SKL of ADT
Department of ECE, HKUST

Ms Denise Tong
Assistant Officer, SKL of ADT
Department of ECE, HKUST

Overseas Organizing Committee

Prof Boru Yang
Professor
Sun Yat-Sen University

Prof Enguo Chen
Professor
Fuzhou Univseristy

Prof Vincent Chen
Professor
South China University of Technology

Prof Zhaojun Liu
Associate Professor
Southern University of Science and Technology

Prof Di Geng
Assistant Professor
University of Chinese Academy of Sciences

Prof Guijun Li
Assistant Professor
Shenzhen University

Prof Lei Lu
Assistant Professor
Peking University

Prof Zong Qin
Associate Professor
Sun Yat-Sen University

Prof Wanlong Zhang
Assistant Professor
Shenzhen University

Student Committee

Mr Runxiao Shi
Chair
Department of ECE, HKUST

Ms Tengteng Lei
Vice-Chair
Department of ECE, HKUST

Program

All the times are local Hong Kong Time (HKT).

Day 1: 21 August, 2023 (Mon)

Session	Time (HK Time)	Activity	Speaker	Poster Session
	08:15-08:45	Registration		
	08:45-08:55	Opening of Young Leaders in Displays Session Photo Taking	Prof. Man WONG (HKUST) Prof. Andrew POON (HKUST)	
Session 1 (Young Leaders in Displays) Session chair: Shi Runxiao (HKUST)	08:55-09:15	An Integrated Analog Front-End System on Flexible Substrate for the Acquisition of Bio-Potential Signals	Shi Runxiao	
	09:15-09:35	The fluorescent electrophoretic display based on $CsPbBr_3$@TiO_2 particles	Liu Guangyou	
	09:35-09:55	Heterogeneous Integration of Atomically-Thin Indium Tungsten Oxide Transistors for Low-Power 3D Monolithic Complementary Inverter	Lin MengChun	
	09:55-10:15	Color Conversion with Hollow Cylindrical Blue Micro-LEDs	Huang Wenjun	
	10:15-10:35	Investigation of flexible ITZO Phototransistors for Deep Ultraviolet Light Detection and Response Properties	Lin Delang	
	10:35-10:55	Tea Break		
Session 2 (Young Leaders in Displasy) Session chair: Lin Delang (SCUT)	10:55-11:10	Post-Annealing Enhanced Electrical Performance of Self-Aligned Top-Gate Amorphous In-Ga-Zn-O TFTs with Ultrathin AlO_x Gate Insulator	Li Jiye	
	11:10-11:30	Stable quantum dots glasses for laser projection display	Du Aochen	
	11:30-11:50	Liquid Crystal Polymer Phase Plates Fabricated by Direct Laser Writing	Zou Xin	
	11:50-12:10	Ultra-scaled Dual-gate IGZO TFT with Record-low Contact Pitch of sub-80nm, Ultra-high I_{ON} of 68.4 μA/μm and Low *SS*	Wu Zijing	
	12:10-12:30	Investigation of Color Deviation in MicroMini-LED Display	Lin Weihan	

	12:30-14:00	Lunch (Location: China Garden)	
	14:00-14:10	Opening of Postgraduate Workshop Photo Taking	Prof. H. S. KWOK
Session 3 (Active-matrix device and sensor integration) Session chair: Li JiYe (PKU)	14:10-14:30	An Active-Matrix Piezoelectric Tactile Sensor Array with In-Pixel Amplifier and Non-Uniformity Compensation	Lei Tengteng
	14:30-14:50	Fluorination-Mitigated High-Current Degradation of Amorphous InGaZnO Thin-Film Transistors	Wang Yanxin
	14:50-15:10	Infrared Sensitive Thin-Film Phototransistor Made on Glass Substrate for Active Matrix Sensing Application	Tsai HsuEn
	15:10-15:30	A Kinetic Model for Intrinsic Donor-Defects in Metal-Oxide Semiconductors	Wang Yuqi
	15:30-15:50	Multisensory and Multifunctional Electronic Skin based on Core-shell CsPbBrPDMS Perovskite Microspheres	Cai Junhu
	15:50-16:10	Tea Break	
Session 4 (Liquid crystal technology and E-paper) Session chair: Zou Xin (SZU)	16:10-16:30	The Transparent E-paper Based on Microcup Electrophoretic Display	Liu Jie
	16:30-16:50	Advanced Thin-Film Polarizers and Their Applications	Cheng Yuechu
	16:50-17:10	Switchable Optical Differential Operation of Two-dimensional Intensity and Phase Based on Liquid Crystal Polarization Gratings	Peng Weiwei
	17:10-17:30	Plasma-enhanced transferring process for one-step patterning of stretchable transparent silver nanowire electrodes and its applications on touching detection	Gu Yifan
	17:30-18:50	Welcome Reception & Poster Author Interview (Location: Outside LTK)	
	19:00-22:00	Football Match (Location: FYT Sports Center)	

Day 2: 22 August, 2023 (Tue)

Session	Time (HK Time)	Activity	Speaker
	08:30-09:00	Registration	
	09:00-09:10	Light Journal	
Session 5 (Quantum-dot and perovskite in display) Session chair: Du Aochen (FZU)	09:10-09:30	Stable Spectral and High Color Purity Blue Perovskite Duantum Dots and Devices	Lan Xi
	09:30-09:50	High-performance inverted quantum rods light-emitting diode	Liao Zebing
	09:50-10:10	Click Chemistry-Assisted Fabrication of Quantum Dot-Embedded Optical Fiber Tips for Sensing Applications	Li Shang
	10:10-10:30	The Strategies to Improve the Morphology of the Inkjet Printing Perovskite Microarrays	Zhu Mingchao
	10:30-10:50	Tea Break	
Session 6 (HUD and 3D display) Liu Guangyou (SYSU)	10:50-11:10	Illumination and Shadow Rendering in Polygon-Based Computer-Generated Holography	Dong Jiaqi
	11:10-11:30	Using time and spatial multiplexing to reduce speckle for augmented reality head-up display	Chen YenJung
	11:30-11:50	Computational vision-correcting near-eye light field displays by manipulating vector sampling rays	Qiu Yuqing
	11:50-12:10	Viewing Angle Improvement of the Floating Display System Based on Dihedral Corner Reflector Array	Tsai ChengHsun
	12:10-12:30	A multi-focal-plane head-up display using polarization multiplexing	Yi Liu
	12:30-14:00	Lunch (Location: China Garden and Uni-Bistro)	
Session 7 (Micro-LED display) Session chair: Huang Wenjun (SUSTech)	14:00-14:20	Advancements in high quality InGaNGaN multiple quantum wells Micro-LEDs on free-standing GaN substrate: from material to display	Liu Yibo
	14:20-14:40	High-Yield Transfer of Flip-Chip Structure Micro-LED by Flexible Film	Li Jiayi
	14:40-15:00	Enhancing the Front LEE of Micro-LEDs via Sidewall Transparent Oxide	Xia Tianwen
	15:00-15:20	The full-color micro-LED display with quantum dots inkjet printing	Lin Yonghong

	15:20-15:40	Design and Application of Micro-LED Pico-Projection Based on Image Fiber	Jin Huajian
	15:40-16:00	Monolithically Integrated Micro-LED and AlGaNGaN High Electron Mobility Transistor for Display	Liu Yaying
	16:00-16:20	Closing + Young Leader Award Photo Taking	SYSU, NYCU, HKUST
	16:20-16:40	Tea Break	
	16:40-17:30	Lab Tour	SKL, CDR, NFF
	17:30	Coach boarding from CYT to Hotel Banquet	
Conference banquet	17:30-21:30	Location: Crowne Plaza Hong Kong Kowloon East Closing & Best Oral & Best Poster Award Ceremony	To Be Confirmed

Day 3: 23 August, 2023 (Wed)

A boat trip will be arranged for participants to enjoy the beautiful scenery of Hong Kong coastlines. We will board at Tsim Sha Tsui public pier, where a boat will take us to Po Toi Island for seafood lunch. Guests can also enjoy swimming in the sea after lunch. In the evening, we will then return to Tsim Sha Tsui Pier for sightseeing of the Victoria Harbor and going ashore.

10:00 Gathering at HKUST

10:45 (Close to Tsim Sha Tsui MTR Exit L6)

11:00 Boarding at Tsim Sha Tsui Pier

12:30 Lunch at Po Tai Island

15:00 Swimming and Sightseeing

17:30 Arriving Tsim Sha Tsui Pier

Campus WIFI Access

Please scan the QR code for instructions on campus WIFI access.

Instruction for Oral and Poster Presentation

General Information for Oral presentation speaker

Location: Lecture Theatre LT-J		
Date: 21,22 August, 2023 (Mon and Tue)		
Total Length	**Presentation Time**	**Q/A (at end of each presentation)**
20 minutes	**15 minutes**	**5 minutes**

Please prepare your PowerPoint in a USB. Kindly test and load your presentation slides during morning registration or office break session. Our student helper will be in service to assist.

General Information for Poster presentation speaker

Location: Outside Lecture Theatre LT-J		
Date: 21 August, 2023 (Mon)		
Size of the poster: 950 mm x 1360 mm		
Mounting Time	**Presentation Time**	**Removal Time**
08:00 ~ 08:45	**17:30-18:50**	**Same Day before 23:00**

Presenting authors are required to set up their materials at designed mounting time and at least one of the authors is required to be attendance during the poster.

Please post the posters according to the poster numbers.

Campus Map


CAMPUS MAP 大學地圖
LEE SHAU KEE CAMPUS 李兆基校園
Main venue: Lecture Theatre LT-J
2023 PGWS
North (Main) Entrance 北門入口
South Entrance 南門入口
Information 詢問處
Lecture Theatre 演講廳
Gown Service Counter 畢業袍服務處
Souvenirs Shop (Self pick-up point) 精品店(自取點)
Catering 餐廳及飯堂
Collection of Diploma 領取證書
Lifts 電梯
Congregation Venue 典禮會場
Photo Backdrop 攝影角
Flower Pop-up Booth 花束臨時銷售點
Shuttle Bus Station 穿梭巴士車站
Car Park (Open on Saturdays only) 停車場(只於星期六開放)

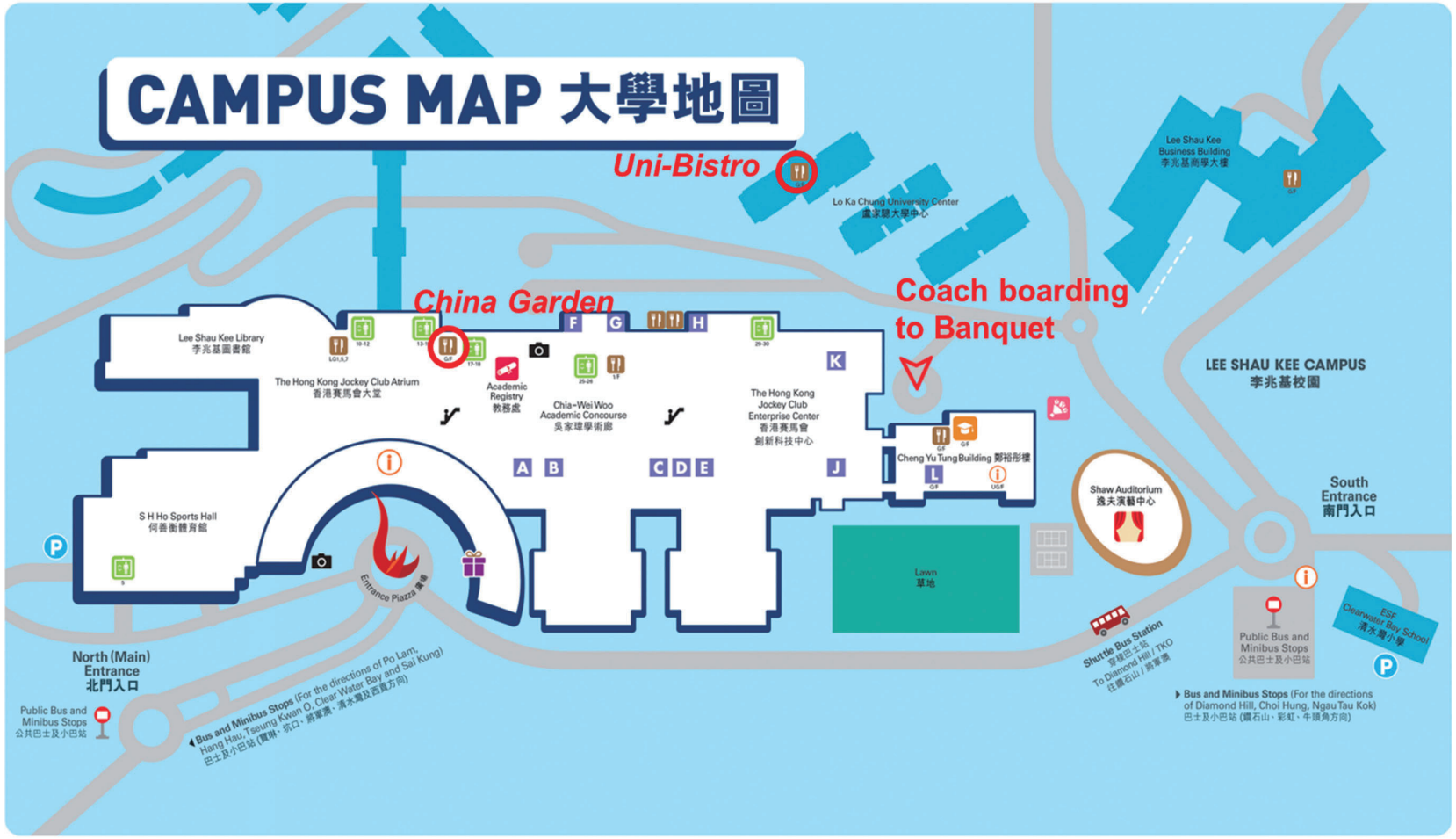
CAMPUS MAP 大學地圖
Uni-Bistro
China Garden
Coach boarding to Banquet
Lee Shau Kee Business Building 李兆基商學大樓
Lo Ka Chung University Center 盧家聰大學中心
LEE SHAU KEE CAMPUS 李兆基校園
Lee Shau Kee Library 李兆基圖書館
The Hong Kong Jockey Club Atrium 香港賽馬會大堂
Academic Registry 教務處
Chia-Wei Woo Academic Concourse 吳家瑋學術廊
The Hong Kong Jockey Club Enterprise Center 香港賽馬會創新科技中心
Cheng Yu Tung Building 鄭裕彤樓
S H Ho Sports Hall 何善衡體育館
Entrance Piazza 廣場
Lawn 草地
Shaw Auditorium 逸夫演藝中心
South Entrance 南門入口
North (Main) Entrance 北門入口
Public Bus and Minibus Stops 公共巴士及小巴站
Bus and Minibus Stops (For the directions of Po Lam, Hang Hau, Tseung Kwan O, Clear Water Bay and Sai Kung) 巴士及小巴站 (寶琳、坑口、將軍澳、清水灣及西貢方向)
Shuttle Bus Station 穿梭巴士站 To Diamond Hill / TKO 往鑽石山 / 將軍澳
Public Bus and Minibus Stops 公共巴士及小巴站
Bus and Minibus Stops (For the directions of Diamond Hill, Choi Hung, Ngau Tau Kok) 巴士及小巴站 (鑽石山、彩虹、牛頭角方向)
ESF Clearwater Bay School 清水灣小學
Information 詢問處
Lecture Theatre 演講廳
Catering 餐廳及飯堂
Lifts 電梯
Photo Backdrop 攝影角
Shuttle Bus Station 穿梭巴士車站
Gown Service Counter 畢業袍服務處
Souvenirs Shop (Self pick-up point) 精品店(自取點)
Collection of Diploma 領取證書
Congregation Venue 典禮會場
Flower Pop-up Booth 花束臨時銷售點
Car Park (Open on Saturdays only) 停車場(只於星期六開放)

Index of Abstract

Oral Presentations

Young Leaders in Displays		
Name	**Title of Abstract**	**Page No.**
Shi Runxiao	An Integrated Analog Front-End System on Flexible Substrate for the Acquisition of Bio-Potential Signals	YL 002
Liu Guangyou	The fluorescent electrophoretic display based on $CsPbBr_3$@TiO_2 particles	YL 003
Lin MengChun	Heterogeneous Integration of Atomically-Thin Indium Tungsten Oxide Transistors for Low-Power 3D Monolithic Complementary Inverter	YL 004
Huang Wenjun	Color Conversion with Hollow Cylindrical Blue Micro-LEDs	YL 005
Lin Delang	Investigation of flexible ITZO Phototransistors for Deep Ultraviolet Light Detection and Response Properties	YL 006
Li Jiye	Post-Annealing Enhanced Electrical Performance of Self-Aligned Top-Gate Amorphous In-Ga-Zn-O TFTs with Ultrathin AlO_x Gate Insulator	YL 007
Du Aochen	Stable quantum dots glasses for laser projection display	YL 008
Zou Xin	Liquid Crystal Polymer Phase Plates Fabricated by Direct Laser Writing	YL 009
Wu Zijing	Ultra-scaled Dual-gate IGZO TFT with Record-low Contact Pitch of sub-80nm, Ultra-high ION of 68.4 μA/μm and Low SS	YL 010
Lin Weihan	Investigation of Color Deviation in MicroMini-LED Display	YL 011
Oral		
Lei Tengteng	An Active-Matrix Piezoelectric Tactile Sensor Array with In-Pixel Amplifier and Non-Uniformity Compensation	OR 002
Wang Yanxin	Fluorination-Mitigated High-Current Degradation of Amorphous InGaZnO Thin-Film Transistors	OR 003
Tsai HsuEn	Infrared Sensitive Thin-Film Phototransistor Made on Glass Substrate for Active Matrix Sensing Application	OR 004
Wang Yuqi	A Kinetic Model for Intrinsic Donor-Defects in Metal-Oxide Semiconductors	OR 005
Junhu Cai	Multisensory and Multifunctional Electronic Skin based on Core-shell $CsPbBr_3$/PDMS Perovskite Microspheres	OR 006
Liu Jie	The Transparent E-paper Based on Microcup Electrophoretic Display	OR 007
Cheng Yuechu	Advanced Thin-Film Polarizers and Their Applications	OR 008
Peng Weiwei	Switchable Optical Differential Operation of Two-dimensional Intensity and Phase Based on Liquid Crystal Polarization Gratings	OR 009
Gu Yifan	Plasma-enhanced transferring process for one-step patterning of stretchable transparent silver nanowire electrodes and its applications on touching detection	OR 010
Lan Xi	Stable Spectral and High Color Purity Blue Perovskite Duantum Dots and Devices	OR 011
Liao Zebing	High-performance inverted quantum rods light-emitting diode	OR 012
Jia Siqi	Ligand Modification of ZnO Nanocrystals for High Performance Quantum Dot Light Emitting Diodes	OR 013
Zhu Mingchao	The Strategies to Improve the Morphology of the Inkjet Printing Perovskite Microarrays	OR 015
Dong Jiaqi	Illumination and Shadow Rendering in Polygon-Based Computer-Generated Holography	OR 016
Chen YenJung	Using time and spatial multiplexing to reduce speckle for augmented reality head-up display	OR 017
Qiu Yuqing	Computational vision-correcting near-eye light field displays by manipulating vector sampling rays	OR 018
Tsai ChengHsun	Viewing Angle Improvement of the Floating Display System Based on Dihedral Corner Reflector Array	OR 019
Yi Liu	A multi-focal-plane head-up display using polarization multiplexing	OR 020

Liu Yibo	Advancements in high quality InGaNGaN multiple quantum wells Micro-LEDs on free-standing GaN substrate: from material to display	OR 021
Li Jiayi	High-Yield Transfer of Flip-Chip Structure Micro-LED by Flexible Film	OR 022
Xia Tianwen	Enhancing the Front LEE of Micro-LEDs via Sidewall Transparent Oxide	OR 023
Lin Yonghong	The full-color micro-LED display with quantum dots inkjet printing	OR 024
Jin Huajian	Design and Application of Micro-LED Pico-Projection Based on Image Fiber	OR 025
Liu Yaying	Monolithically Integrated Micro-LED and AlGaNGaN High Electron Mobility Transistor for Display	OR 026

Poster Presentations

Poster No.	Name	Title of Abstract	Page No.
01	Huang BoWei	High Performance Ultra-Nanosheet Indium Zinc Oxide Transistor for BEOL Compatible Applications	PO 002
02	Zhu Jianming	Enhanced Stability of Elevated-Metal Metal-Oxide a-IGZO TFTs through Controlled Defect Generation and Elimination	PO 003
03	Zhang Yuhan	Improvement for Electrical Performance of Self-Aligned Top-Gate Amorphous InGaZnO Thin-Film Transistors with Pre-Annealed SiOx Buffer	PO 004
04	Ma Zhikang	High-Mobility Dual-Gate a-IGZO/a-IZO/a-IGZO Thin-Film Transistors	PO 005
05	Xie Xinying	Conductive Indium-Tin-Zinc Oxide Formed by Oxygen Plasma Treatment	PO 006
06	Jiang Wei	The effects of the temperature of fluorination treatment on the reliability of an indium-gallium-zinc oxide thin-film transistor	PO 007
07	Xu Lin	Temperature-Controlled Dip-Coating Carbon Nanotube Thin-Film Transistor	PO 008
08	Liu Shilin	Enhanced Performance of Self-Powered PTAA/MAPbCl3 Single Crystal Film Heterojunction Ultraviolet Photodetector Based on Homologous bromides passivation	PO 009
09	Yang Mei	Wearable Piezoelectric Sensor Based on PVDF/ZnO Composite Membrane and ITZO TFT	PO 010
10	Huang Tengyan	High Photo Response of High-Indium InZnO Thin-Film Transistors	PO 011
11	Wang Tianqi	Bio-Inspired Ultrasensitive Optical-Electrical Strain Sensor for Human Motion Detection	PO 012
12	Liu Zong	An “Intelligent” Gas Sensor Array based on IGZO Thin Film Transistors	PO 013
13	Huang BorJiun	A High-Reliability, Capacitorless, 1-to-4 Sharing Architecture Gate Driver with a-Si H TFTs for TFT-LCD Application	PO 014
14	Wu WeiLin	Power and Color Shift Analysis of Driving MicroLED Display with Gamma 2.2 Correction in Low Grayscale	PO 015
15	Wu Xinzao	Progress Review of Driving Method and Color Evaluation for Color Electrophoretic Display	PO 016
16	Fan Qitian	Passive Matrix Driving Method of Alternating Current Electroluminescence with Multiple Grey Levels	PO 017
17	Deng Zhaoyu	A VCO-Based ADC Circuit Using N-Type Oxide TFTs	PO 018
18	Zhang Wenhao	Design of High-Precision Horizontal Synchronization Circuit in Micro-LED Display Driver	PO 019
19	Liu Zhaoyong	A Review on Micro-LED Display Integrating Metasurface Structures in Controlling Emission Angles	PO 020
20	Li Zichun	Recent Progress of Quantum Dot Photoresist-Based Full-Color Micro-LED	PO 023
21	Fengfeng	Unraveling the Enhancements in Radiant Flux Density by Scaling-down AlGaN Ultraviolet-C MicroLEDs	PO 025
22	Li Chunxiao	Change in Field of Micro-LED Brought by GaN Substrate	PO 026
23	Zhengui Fan	Micro-LED structure using metasurface for collimation	PO 028

24	Zhanghu Mengyuan	Enhancing Device Performance of Micro-LEDs through the Ideality Factor	PO 029
25	Zhang Jingyang	Optimization of a normally-off in-situ Integration HEMT-LED enabled by P-GaN Selective Epitaxy Growth	PO 030
26	Zeng Jingnan	The Effect of ITO Thickness on Metal Grating Linear Polarized Micro LED	PO 031
27	Yin Yanzhen	Light-field Three-dimensional Displays Based on a Mini-LED Displays	PO 032
28	Wang Juan	Enhancing the Light Extraction Efficiency of AlGaN-based DUV Micro-LED by Optimizing the Chip Sidewall Inclined Angle	PO 033
29	Sheng Yujia	Perovskite crystals for Full-color Micro-display	PO 034
30	Yang Hang	Size-Independent Current Density-Voltage Characteristic of Micro-LEDs	PO 035
31	Liu Xinyi	GaN Micro-LED Array Based Underwater Wireless Optical Communication Using Flip-Chip Technology	PO 038
32	Yao Ziming	Micro LED pixel-level collimator for direct-type pico-projectors	PO 039
33	Liang Tao	Research progress on Micro-LED light extraction and beam shaping	PO 040
34	Zheng Xingke	Double perovskite for full color E-paper display	PO 041
35	Deng Liwen	Coaxial spherical cavity Micro-LED for near-eye display based on curved surface metal bonding engineering	PO 042
36	Yao Lisheng	A single layer all-optical diffraction neural network based on liquid crystal	PO 043
37	Liu Liu	A Realization of Dynamic Continuous Adjustable Phase Based on Liquid Crystal-Integrate All-dielectric Metasurface	PO 044
38	Shi Haidong	High Order Laguerre Gaussian Generation System based on liquid crystal	PO 045
39	Ma Xiaoxin	The complete LCD design process based on Empyrean Technology platform	PO 046
40	Liu Cong	High Efficiency Full-phase Continuous Modulator Based on Liquid Crystal Metasurface	PO 047
41	Yu Xinyi	Passive Vibration Sensor Using Deformed Helix Ferroelectric Liquid Crystal Electro-Optical Modulator	PO 048
42	Yi-Yang Gao	Advanced Color Conversion LCD with Photoluminescent Color Filter and In-Cell Polarizer	PO 050
43	Zhao Zhiqing	Integrated Display and Communication High-capacity MIMO Visible Light Communication Enabled by LCDs with mini-LED Backlight	PO 051
44	Peng Lisha	Progress Review in Materials and Structures toward Stretchable Light-Emitting Diodes	PO 053
45	Zhou Tao	Improving the Response Time of Electrophoretic Display by Waveform with invisible Shaking	PO 054
46	Shi Jintao	Key printing processes and applications of roll-to-roll in flexible display	PO 056
47	Zhu Simu	A Stretchable Electrophoretic Display Device for Textile Display Application	PO 057
48	Zeng Debo	Sealing Considerations for Electrophoretic Displays of Ink-on-Array	PO 058
49	Yang Jinglan	Increasing Particle Response Speed with Mixed Surfactants in Electrophoretic Display	PO 059
50	Xiong Feng	Surface Modification of Black Electrophoretic Particles via Thiol-Ene Click Reactions	PO 060
51	Liu Yunhe	A Transparent Electrophoretic Display Prototype Based on In-Plane Lateral Driving	PO 061
52	Li Zhuohang	Cation modified composite film to optimize the bi-stability of transparent electrophoretic display	PO 062
53	Zhang Zhiqing	High efficiency pure blue perovskite light-emitting diode based on interface engineering	PO 063
54	Fengning Yang	Innovative Interfacial Engineering of Hole Transport Material for High-Performance Perovskite Photovoltaics	PO 064
55	Song Jianxin	Pixelated Polarized Luminescent Color Filters Based on Down-converting Nanorods	PO 065
56	Xiang Guohong	Transparent Quantum Dot Light-Emitting Diodes with a Current Focusing Structure	PO 066
57	Chen Xiaogang	Synthesis and Optical Properties of Fluorine Doped Double-cationic Perovskite Quantum Dots Molecular Sieve Composites	PO 067

58	Chen HanSyuan	Correction Algorithm of AR-HUD Holographic Image Based on Distortion Model	PO 068
59	Qimeng Wang	Research on Light Field 3D Display Based on Field Sequential Color Image Source	PO 069
60	Jiang Haonan	An AR Retina Projection Optical System with Switchable Multi-viewpoints Based on Dammann Grating	PO 070
61	Debjyoti BHADRA	Photopatterned nanoparticle films for advanced photonic and optoelectronic applications	PO 071
62	Cheung Shunkong	Exploring the Intermediate State in CoFeB Pillar Devices Integrated with Thin Film Transistors	PO 072
63	Chen Yi	Laser-induced Film Release, Bending and Movement under Electrostatic Field	PO 073
64	Zhou Hanqin	Electronic Properties of (NixGa1-x)2O3 Alloys by First Principles Investigation	PO 074
65	Wu Xuezhao	Optimization of information computational capacity for an alternating-driven magnetic tunnel junction	PO 075
66	Timothy Chan	Laser-enhanced nanoimprinting of optical metasurfaces with fluorescent materials	PO 076
67	Zhuo Dingyu	Uniformity Improvement in a Floating Aerial Display Using Off-axis Freeform-mirror	PO 077
68	Cheng YuChia	Simulation of a 2D array of 1×12 wavelength selective switches with LCoS	PO 078
69	Long Quanzhou	All Optical Diffraction Neural Network Digital Recognition Based on Photoalignment Technology	PO 079
70	Cheng Yunfan	A New Fast Elemental Image Array Rendering Method for Computer generated Integral Imaging Light Field Display	PO 080
71	Lin Zijian	Waveguide Coupler Based on Polarization Volume Gratings for Large Full-color Field of View	PO 081
72	Huo Yipeng	A new One-Drop-Filling (ODF) machine	PO 082
73	Zhang Daquan	Large-scale planar and spherical light-emitting diodes based on arrays of perovskite quantum wires	PO 083
74	Tang Wenying	Micro-heater Integrated Nanotube Array Gas Sensor for Parts-Per-Trillion Level Gas Detection and Single Sensor-based Gas Discrimination	PO 084
75	Long Zhenghao	A perovskite nanowire array based bionic eye integrated with color imaging and signal preprocessing functions	PO 085
76	Shu Lei	Highly Efficient Blue Light-Emitting Diodes Based on Perovskite Film with Vertically Graded Bandgap and Organic Grain Boundary Passivation Shells	PO 086
77	Zhu Yiyi	Designing Efficient and Aesthetically Pleasing Semitransparent Perovskite Solar Cells for Building-Integrated Photovoltaics: A Biomimetic Approach	PO 087
78	Kumar Mallem	Record External Quantum Efficiency of Blue Quantum Rod Light Emitting Diodes achieved with Positive Aging Effect	PO 088
79	Wang Hongteng	Invisibly Patterning Silver Nanowire Electrode through the Plateau-Rayleigh Instability	PO 089

Abstract from Young Leaders in Display

An Integrated Analog Front-End System on Flexible Substrate for the Acquisition of Bio-Potential Signals

Runxiao Shi[1], Zhihe Xia[1] and Man Wong[1,2]

[1]State Key Laboratory on Advanced Displays and Optoelectronics and Technologies, Department of Electronic and Computer Engineering, The Hong Kong University of Science and Technology, Hong Kong, China

[2]The Hong Kong University of Science and Technology Shenzhen Research Institute, Shenzhen 518057, China

Presently described is the application of a versatile, low-temperature thin-film transistor (TFT) technology to the implementation on a flexible substrate [1] of an analog front-end (AFE) system for the acquisition of bio-potential signals (Fig. 1). The technology is based on semiconducting amorphous indium-gallium-zinc oxide (IGZO). IGZO is used as a semiconductor in TFTs and as a conductor in capacitors (Fig. 2).

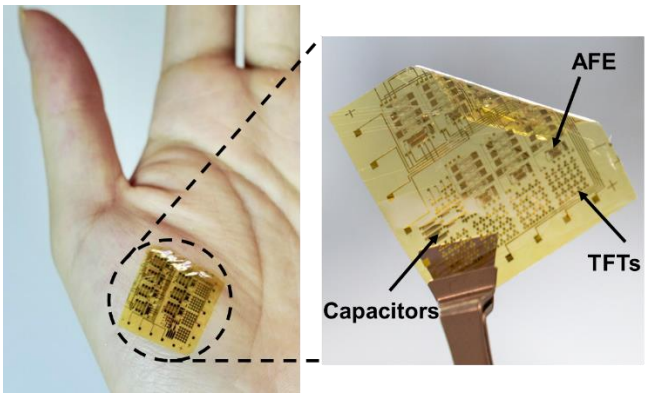

Fig. 1. Photography of the AFE for the acquisition of bio-potential signals on flexible substrate.

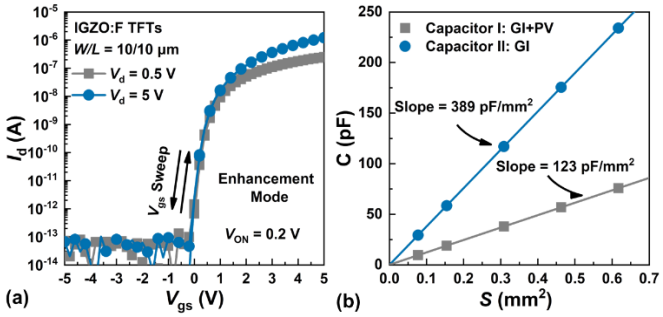

Fig. 2. (a) The transfer characteristics of the IGZO TFTs. (b) The dependence of the capacitance on the area.

The AFE system consists of three monolithically integrated constituent components: a bias-filter circuit with a bio-compatible low cut-off frequency of ~1 Hz, a 4-stage differential amplifier offering a large gain-bandwidth product of ~955 kHz and an additional notch filter exhibiting over 30 dB suppression of the power-line noise (Fig. 3). Respectively built using conductive IGZO electrode with thermally induced donor-agents and enhancement-mode fluorinated IGZO TFTs with exceptionally low leakage current, both capacitors and resistors with significantly reduced footprints have been realized. Defined as the ratio of the gain-bandwidth product of an AFE system to its area, a record-setting figure-of-merit of ~86 kHz/mm^2 has been achieved. This is about an order of magnitude larger than the < 10 kHz/mm^2 of the nearest benchmark. Requiring no supplementary off-substrate signal-conditioning components and occupying an area ~11 mm^2, the stand-alone AFE system has been successfully applied to measure electromyography (EMG) and electrocardiography (ECG) as shown in Fig. 4.

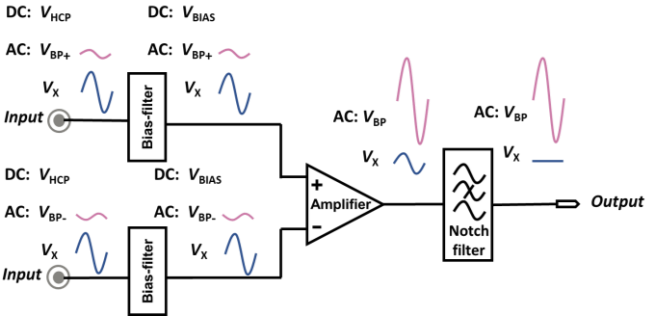

Fig. 3. The evolution of the signal components through the constituent components of the AFE system.

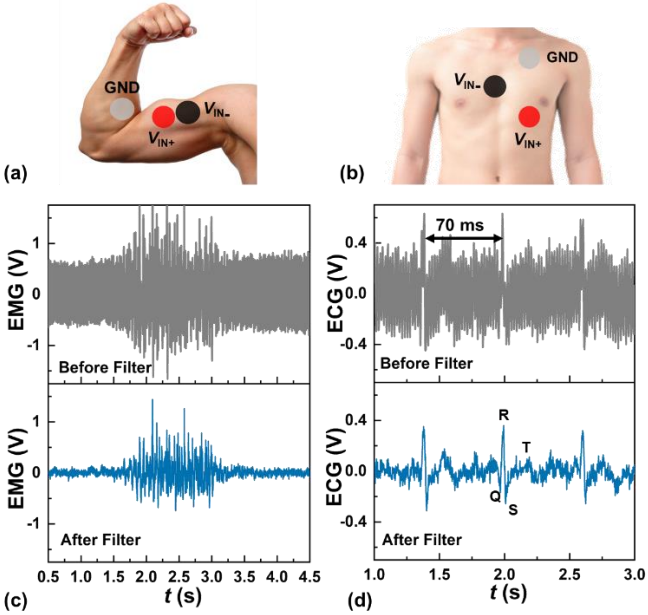

Fig. 4. In-vitro measurement of the EMG and ECG using the fabricated AFE system. Placement of the three electrodes during the acquisition of (a) EMG and (b) ECG. (c) EMG signals acquired when the biceps are exercised. (d) ECG signals acquired from the chest.

References

[1] Shi, Runxiao, et al. "An Integrated Analog Front-End System on Flexible Substrate for the Acquisition of Bio-Potential Signals." Advanced Science (2023): 2207683.

The fluorescent electrophoretic display based on $CsPbBr_3$@TiO_2 particles

Guangyou Liu[1], Xinzao Wu[1], Feng Xiong[1], Zhuohang Li[1], Xidu Wang[2], Zong Qin[1], Bo-Ru Yang[1,]*

[1] State Key Laboratory of Optoelectronic Materials and Technologies, Guangdong Province Key Laboratory of Display Material and Technology, School of Electronics and Information Technology, Sun Yat-Sen University, Guangzhou 510275, People's Republic of China.

[2] *School of Electronics and Information Engineering, South China University of Technology, Guangzhou, 510640, China.*

*Email: paulyang68@me.com

Abstract

With the development of Inter of Things (IoT), the current display demands low-power consumption, flexibility, sunlight visibility, and wearability. Compared with the liquid crystal and organic light emitting diode, the electrophoretic display (EPD) has obvious advantages, such as high ambient contrast ratio (ACR), bistability, low power consumption, and flexibility [1]. Therefore, EPD is suitable for outdoor, long-term, flexible, and stretchable electronic displays. At present, EPD is widely applied in electronic books, electronic shelf labels, bus signs, smart blackboards, smart windows etc. [1-3]. However, current EPD usually only be used under sunlight and white light illumination, with certain light source dependence. To increase the application scenarios of EPD, the fluorescent electrophoretic particles can be introduced, which can be applied in the anti-counterfeiting and multicolor display.

The preparation process of TiO_2@$CsPbBr_3$ is shown in Figure 2, in which white TiO_2 particles are ball-milled with silane coupling agent (KH570) in toluene to graft the hydroxyl groups on TiO_2 particles' surface (TiO_2-MPS). Then, the perovskite nanocrystals ($CsPbBr_3$) are grown on TiO_2 ($CsPbBr_3$@TiO_2-MPS) by pouring the perovskite precursor solution into the toluene of TiO_2-MPS solution. In addition, fluorescent electrophoretic particles coated with polymers were obtained by polymerized $CsPbBr_3$@TiO_2 ($CsPbBr_3$@TiO_2-MPS-PLMA) particles with polymer monomers (LMA). To balance the ratio of the $CsPbBr_3$ loading content on the TiO_2 particles, the $CsPbBr_3$@TiO_2 can exhibit the ideal white state of TiO_2 and the high luminescence efficiency of $CsPbBr_3$.

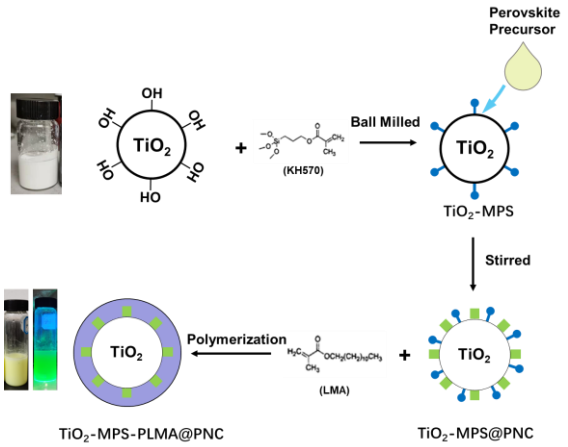

Figure 2 Preparation of fluorescent electrophoretic particles $CsPbBr_3$@TiO_2-PLMA.

To investigate the driving effect of fluorescent particles, we have prepared the EPD device. Two ITO electrodes adhere with OCA, which is filled with electrophoretic ink consisting of negatively charged white fluorescent particles and positively charged black particles. When the ink is filled, the device shows a grey state. When +15V is given to the upper electrode, the black and white particles are separated. The negatively charged white particles are driven to the upper electrode, and the device shows a white state. When the device is in a white state, the EPD can show a green state under the UV light. On the other hand, when the upper electrode is given -15 V, the positively charged black particles are driven to the upper electrode, which makes the EPD exhibit a black state. Through positive and negative voltage regulation and UV light, the EPD based on fluorescent electrophoretic particles can achieve a black-white-green tristate display, shown in Figure 3.

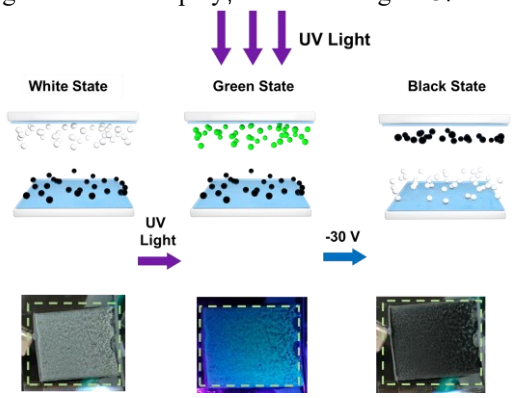

Figure 3 The illustration and photographs of fluorescent EPD switching between white, green, and black state under UV light and sunlight at 30 V.

References

[1] Yang B-R. "E-Paper Displays". John Wiley & Sons Ltd, Chichester, ISBN: 978-1-119-74558-7, 2022.

[2] G. Liu, J. Liu, Q. Fan, Y. Liu, Z. Zeng, Z. Li, X. Wu, M. Yang, B-R. Yang, "High transmittance, fast response, and high contrast ratio smart window with lateral driving electrophoretic display", Chemical Engineering Journal (2023), doi: https://doi.org/10.1016/j.cej.2023.144133.

[3] M. Yang, G. Liu, Z. Zeng, S. Zhang, J. Liu, Z. Qin, Z. Chen, B-R. Yang, "Dual-Mode Switching E-Paper by Negative Electrorheological Fluid with Reversible Silica Networks", Advanced Materials Technologies, (2022) 2200371.

Heterogeneous Integration of Atomically-Thin Indium Tungsten Oxide Transistors for Low-Power 3D Monolithic Complementary Inverter

Meng-Chun Lin, Zhen-Hao Li, Tsung-Che Chiang, Po-Tsun Liu
Dept. of Photonics, College of Electrical and Computer Engineering, National Yang Ming Chiao Tung University, Hsinchu 30010, Taiwan

The rapid advancement of technology in the semiconductor industry has led to the development of monolithic 3D Integrated Circuit(M3D-IC) as a promising solution to overcome area constrains and to surpass the limitation of Moore's law. This work explores the utilization of thin-film transistors(TFTs) to enable M3D technology, particularly focusing on fabrication of vertically-stacked logic circuits to enhance device density. By integrating heterogeneous materials in the complementary inverter, the study aims to achieve high voltage gain and large noise margin, crucial for ensuring reliable signal transmission.

To address the challenges associated with mismatch issues in electrical properties in traditional logic circuits, this study proposes the integrated circuit using p-channel polycrystalline silicon(poly-Si) and n-channel amorphous oxide semiconductor(AOS) materials. This combination offers larger flexibility in achieving comparable electrical properties and enables lower power dissipation through complementary configuration. Moreover, the introduction of amorphous indium tungsten oxide(a-IWO) enhanced carrier mobility and improves the thermal stability, migrating short channel effects and degradation issue.

To further optimize the gate control ability and subthreshold swing, the ultra nano-sheet(UNS) architecture is also explored. This helps operating in fully depleting mode and inhibiting short channel effect. By scaling down the channel of the a-IWO TFTs to about 3 to 4 atomic layers, the carrier transported like 2D materials and without sacrificing carrier mobility. The a-IWO TFTs showed the impressive electrical characteristics, including high mobility of 24cm^2 V^{-1} s^{-1}, near-ideal subthreshold swing of 63mV dec^{-1}, low leakage current below 10^{-13}A, negligible hysteresis of 0mV, a high on/off current ratio exceeding 10^9, low contact resistance of 0.44kΩ-μm, and remarkable stability after encapsulating a passivation layer.

The electrical properties of the n-channel a-IWO TFTs matched well with those of the p-channel poly-Si TFT, rendering the proposed complementary metal-oxide-semiconductor technology superior for various application. The designed inverter was able to achieve a high voltage gain of 152V V^{-1} at a low supply voltage of 1.5V. Furthermore, the margin noise was 80% of the supply voltage and could operate within a symmetrical window. Notably, the inverter achieves pico-watt static power consumption, attributed to the wide energy bandgap of the a-IWO channel and the atomically-thin channel designed.

Overall, this vertically-stacked complementary field-effect transistor(CFET) structure offers high energy-efficiency, enabling an increase in circuit density on chip to align with the advancements of next generation semiconductor technology.

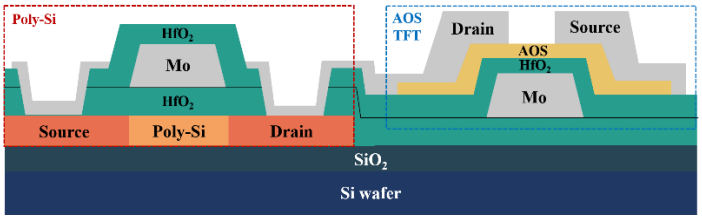

Fig. 1. Structure schematic of the complementary metal-oxide-semiconductor(CMOS) with p-channel poly-Si TFT and n-channel a-IWO TFT.

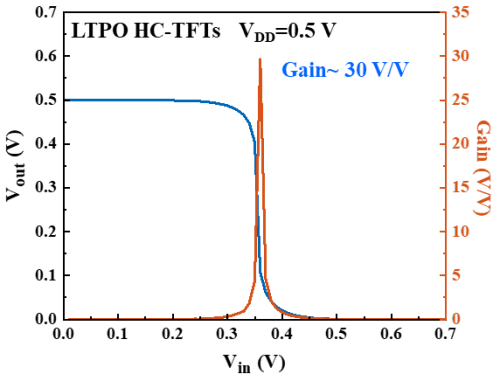

Fig. 2. Voltage gain of the inverter.

References

[1] Li, Z.-H., Chiang, T.-C., Kuo, P.-Y., Tu, C.-H., Kuo, Y., Liu, P.-T., *Heterogeneous Integration of Atomically-Thin Indium Tungsten Oxide Transistors for Low-Power 3D Monolithic Complementary Inverter. Adv. Sci. 2023, 10, 2205481.* https://doi.org/10.1002/advs.202205481.

Color Conversion with Hollow Cylindrical Blue Micro-LEDs

Wenjun Huang*, Zhaojun Liu**

*** Department of Electrical and Electronic Engineering, Southern University of Science and Technology, Shenzhen, China**

****liuzj@sustech.edu.cn**

This paper proposes a novel approach to achieve color conversion in micro light-emitting diodes (Micro-LEDs) using a hollow cylindrical design, which allows the printing of quantum dots (QDs) in a hollow place. We investigated the color conversion capabilities of 60, 70, 80, and 90 um hollows, and demonstrated a 3x3 array. This approach reduces the thickness of the quantum dots on the LED surface and eliminates the need for a thick black matrix, thereby reducing the problem of light crosstalk [1]. This hollow cylindrical design has potential applications in displays and lighting technologies.

The Micro-LED devices were fabricated as follows. The Micro-LED mesa structures were defined using SiO2 as a hard mask and etched using Cl_2/BCl_3 inductively coupled plasma (ICP) down to the n-GaN layer, resulting in an etching thickness of 1.0μm. A transparent current spreading layer and ohmic contact layer of 110nm indium-tin oxide (ITO) was deposited using magnetron sputtering with a step power growth of 30 W and 50 W, respectively. The sample underwent rapid thermal annealing after the ITO lift-off process. A 50 nm Al_2O_3 passivation layer was then deposited using thermal atomic layer deposition (ALD) at 300℃, and the contact hole was patterned using Cl_2/BCl_3 ICP to expose the ITO layer. Negative and positive electrodes of 20/150/50/120nm Ti/Al/Ti/Au were deposited using electron-beam evaporation. Finally, a 20/150nm Ti/Al reflective mirror was deposited on the sidewall of the mesa to prepare the lighting-up hollow cylindrical Micro-LED devices.

The second step involved printing the QDs onto the hollow cylindrical Micro-LED devices. Four different sizes of hollow cylindrical structures and two sizes of Micro-LEDs were used in the study: D1 (R1=50μm, r1=45μm), D2 (R2=50μm, r2=40μm), D3 (R3=40μm, r3=35μm), and D4 (R4=40μm, r4=35μm). The QDs were printed into the middle of the hollow using a printer with a specific volume of red and green QDs. Subsequently, the novel structure was subjected to a characterization analysis.

Figure 1 shows the IV curves for four samples, which indicate that their performance is almost the same, except for D2 and D4, which exhibit lower leakage current compared to D1 and D3, respectively. The wavelength detection and resulting image are shown in Figure 2. In addition, the study also prepared a 3x3 array design to demonstrate the application of this novel structure for color conversion.

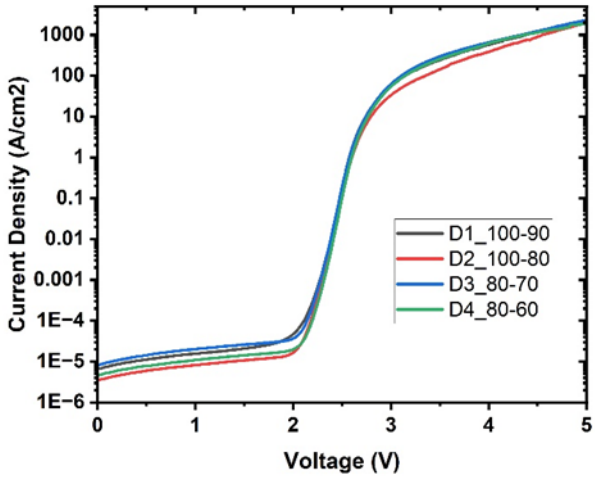

Fig. 1. Current-Voltage characteristic of different sizes of hollow cylinder Micro-LED

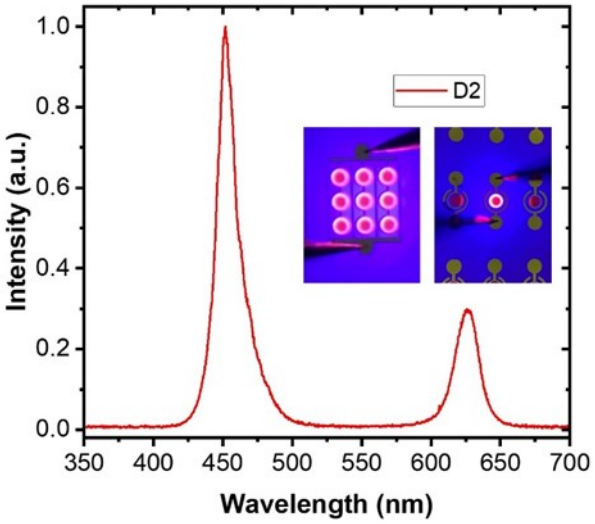

Fig. 2. Spectrum of color conversion of hollow cylinder Micro-LED D2 with red QDs

References

[1] Hyun BR, J Phys Chem Lett, 12(29), 6946 (2021)

[2] Yibo Liu, Journal of Physics D-Applied Physics, 55(31), 315107 (2022)

Investigation of flexible ITZO Phototransistors for Deep Ultraviolet Light Detection and Response Properties

Delang Lin*, Rongsheng Chen*, **

***School of Microelectronics, South China University of Technology, Guangzhou, China.**

****State Key Laboratory of Advanced Displays and Optoelectronics Technologies, Department of Electronic and Computer Engineering, The Hong Kong University of Science and Technology, Hong Kong, China**

The three-terminal metal oxide-based deep ultraviolet (DUV) phototransistors are electronic devices designed to detect and respond to light in the deep ultraviolet region of the electromagnetic spectrum. They are widely used in various applications, benefiting industries such as aerospace, healthcare, and environmental monitoring.

Herein, we propose a flexible InSnZnO DUV phototransistor with the multifunctional laminated organic (MLO) passivation layer (PVL), which can effectively suppress the response of ZnO-based DUV phototransistors to UVA radiation, achieving a high rejection ratio and field-effect mobility (μ_{fe}).

The transfer curves of flexible ITZO DUV phototransistors, measured in the dark and under 365 nm/254 nm light illumination, were illustrated in Fig. 1(a). The ITZO DUV phototransistor exhibited competitive electrical properties in the dark. Moreover, the device showed a small negative drift in its transfer curves and a slight increase in the off-state current under 365 nm NUV light illumination due to the isolation of NUV light by the MLO layer. However, under 254 nm DUV light illumination, there was a considerable increase in I_{ds}, demonstrating the strong response properties to DUV light. The output characteristics of ITZO phototransistors showed an excellent ohmic contact between channel and S/D electrode, as shown in Fig. 1(b).

To mitigate the influence of the PPC effect and improve the optical response rate of the device, the preparation process and structure of the ITZO active layer have been optimized. As depicted in Fig. 2(a), the ITZO DUV phototransistor, prepared at an argon-to-oxygen ratio of 10:6 and a substrate deposition temperature of 300 °C, exhibited a faster response and shorter recovery time.

The optical response characteristic curves of the devices with varying channel lengths are shown in Fig. 2(d). The ITZO DUV phototransistors with a channel width-to-length ratio of 300μm:100μm demonstrated increased photoresponse currents and faster response rates. The dynamic photoresponse measurements of the ITZO DUV phototransistor was illustrated in Fig. 2(c). For these phototransistors, R_{254nm} tended to decrease with increasing P_{in} from 10 μW/cm^2 to 50 μW/cm^2, owing to the sublinear relationship between P_{in} and I_{photo} ($I_{photo} \propto P_{in}\alpha$, $\alpha < 1$). In order to effectively suppress the PPC effect, a positive gate voltage pulse was applied to the ITZO DUV phototransistor during the recovery process, and the I_{ds} immediately returned to their original level.

Due to the absorption effect of MLO films on NUV, the photocurrent of the DUV phototransistor to NUV was suppressed to a low level, as depicted in Fig. 2(d). Therefore, the ITZO DUV phototransistor achieved a rejection ratio comparable to that of Ga_2O_3-based phototransistors.

Overall, the ZnO-based DUV phototransistors have been demonstrated, and the optoelectronic performance has been enhanced by optimizing their preparation process and structure.

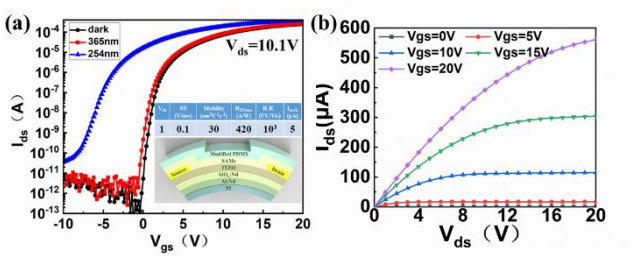

Fig. 1. (a)Transfer curves in the dark and under illumination and (b) the output curves in the dark of the ITZO phototransistor.

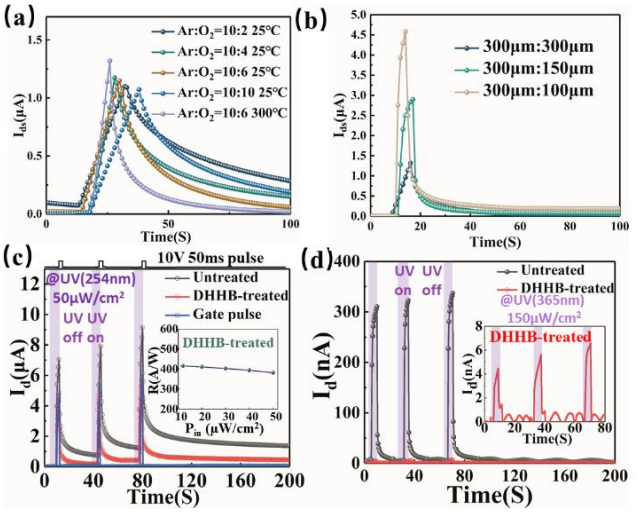

Fig. 2. 254nm optical response characteristic curves of ITZO DUV phototransistor prepared under (a) different deposition conditions and (b) different aspect ratios, time-dependent photoresponse curves under UV (c) 254 nm and (d) 365 nm.

References

[1] D. Lin, C. Zhou, D. Luo, B. Liu and R. Chen, "Flexible InSnZnO Thin Film Phototransistors for Deep Ultraviolet Detection," IEEE Electron Device Letters, vol. 44, no. 7, pp. 1120-1123, July 2023, doi: 10.1109/LED.2023.3273212.

Post-Annealing Enhanced Electrical Performance of Self-Aligned Top-Gate Amorphous In-Ga-Zn-O TFTs with Ultrathin AlO_x Gate Insulator

Jiye Li*, Yuqing Zhang**, Yuhan Zhang*, Xinwei Wang, Lei Lu*, and Shengdong Zhang****

***School of Electrical and Computer Engineering, Peking University, Shenzhen 518055, China**

****Department of Electronic and Computer Engineering, The Hong Kong University of Science and Technology, Hong Kong 999077, China**

*****School of Advanced Materials, Peking University, Shenzhen 518055, China**

Amorphous InGaZnO (a-IGZO) thin-film transistors (TFTs) are promising for next-generation displays and low-power circuits [1]. To enable advanced applications, reducing the thickness of the gate insulator (GI) with high-k materials is crucial [2]. However, inherent defects and the deposition process can degrade the GI/a-IGZO interface, impacting the performance of self-aligned top-gate (SATG) a-IGZO TFTs [3]. Therefore, post-deposition treatments are necessary to establish low-defect interfaces and realize high-performance ultrathin-GI SATG TFTs.

Fig. 1(a)-(c) show the schematic cross-section and major fabrication steps of the SATG a-IGZO TFT with 4 nm AlO_x GI (Fig. 1(d)). Fig. 2(a) shows the poor performance of the TFTs with 4-nm AlO_x GI, characterized by a high off-current (I_{off}) and negative threshold voltage (V_{th}). By comparison, post-annealing in N_2 or O_2 at 300 °C (Fig. 2(b) and (c)) both effectively reduced I_{off} and improved electrical parameters (Table 1). Notably, O_2 annealing demonstrated the best performance, with decent field effect mobility (μ_{FE}) of 11.1 cm^2/Vs, positive V_{th} of 0.23 V, and near-ideal subthreshold swing (SS) of 61.6 mV/decade, indicating reduced interface trap density.

C-V measurements (Fig. 3(a)) revealed stretched-out behavior in non-annealed TFTs, indicating the presence of shallow-level defects including hydrogen (H) and oxygen vacancies (Fig. 3(b)). Annealing successfully suppressed these defects, as confirmed by the absence of stretched-out behavior. Specifically, N_2 annealing eliminated H-related defects through diffusion, while O_2 annealing suppressed both H and O-related defects through diffusion and repair mechanisms, as depicted in Fig. 4. Therefore, these results further confirm the crucial role of post-annealing in enhancing the electrical performance of SATG AOS TFTs.

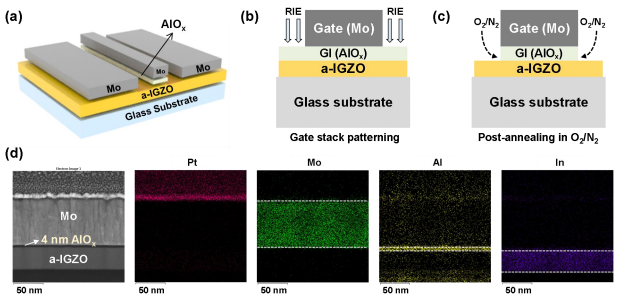

Fig. 1. (a) The schematic cross-sectional views of the fabricated TFTs. (b)(c) The illustrates of gate stacking patterning and post-annealing. (d) TEM image and energy-dispersive spectroscopy (EDS) images of the fabricated TFTs.

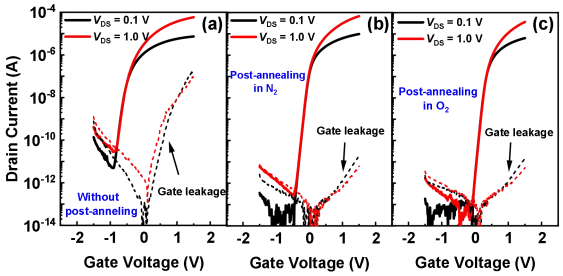

Fig. 2. Transfer curves of fabricated SATG a-IGZO TFTs (a) without post-annealing, (b) with post-annealing in N_2, and (c) with post-annealing in O_2.

Table 1. Electrical parameters of the SATG a-IGZO TFTs with different post-annealing conditions.

TFT sample	V_{th} (V)	μ_{FE} ($cm^2V^{-1}s^{-1}$)	SS (mV/dec)	I_g (A)
Without post-annealing	-0.63	8.7	77.5	$<10^{-6}$
Post-annealing in N_2	-0.13	13.1	67.3	$<10^{-11}$
Post-annealing in O_2	0.23	11.1	61.6	$<10^{-11}$

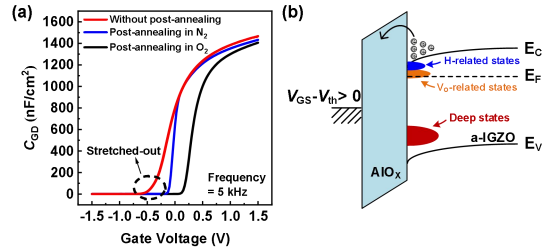

Fig. 3. (a) *C-V* curves of the TFTs with different post-annealing conditions. (b) Energy band diagrams at the AlO_x/a-IGZO interface.

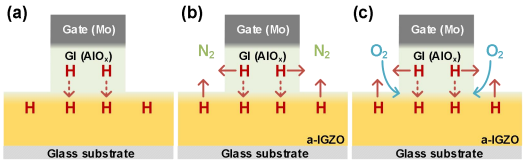

Fig. 4. Schematic migration process of hydrogen in the AlO_x and a-IGZO layers of the SATG TFTs (a) without post-annealing, (b) with post-annealing in N_2, and (c) with post-annealing in O_2.

References

[1] J. Troughton *et al.*, *J. Mater. Chem. C,* vol. 7, pp. 12388 -12414, (2019).

[2] M. Si *et al.*, *Nat. Electron.,* vol. 5, pp. 164-170, (2022).

[3] Y. H. Chang *et al.*, *Appl. Phys. Lett.,* vol. 108, p. 03350 2, (2016).

Stable quantum dots glasses for laser projection display

Aochen Du[1,2], Xingke Zheng[2], Yun Ye[1,2,*], Enguo Chen[1,2], Sheng Xu[1,2], Tailiang Guo[1,2]

[1]College of Physics and Information Engineering, Fuzhou University, Fuzhou 350108, China

[2]Fujian Science & Technology Innovation Laboratory for Optoelectronic Information of China, Fuzhou 350108, China

***Corresponding author, E-mail: yeyun07@fzu.edu.cn**

Laser diodes (LDs), as compared to light emitting diodes (LEDs), have gained significant prominence in various critical domains including automotive headlights, outdoor lighting, laser projection, and laser cinemas. LDs offer distinct advantages such as high brightness, extended irradiation distance, and compact size, while effectively overcoming the issue of "efficiency droop" at higher power densities.[1]

Due to their intriguing photoelectronic properties, such as tunable bandgap, high color purity, long diffusion length, high absorption coefficient, and high carrier mobility, there has been a dedicated effort to fabricate efficient perovskite quantum dots for applications in the display field.[2] However, perovskite quantum dots tend to degrade and fail under external environmental stimuli such as light, heat, and humid air, which hinders their practical applications.[3] By growing perovskite quantum dots in situ within a glasses substrate and leveraging the dense network structure of inorganic glass for seamless encapsulation, the quantum dots can be effectively isolated from the external environment.[4] This approach efficiently addresses the stability issues of quantum dots and broadens their application prospects in fields such as solid-state lighting, backlight displays, and laser projection. Fig. 1 (a) illustrates the mix electroluminescence (EL) spectra of blue LDs, green emitting perovskite quantum dots glasses, and red emitting ceramic phosphors, showcasing emissions in blue, green, and red colors. Figure 1 (a) showcases the EL spectra of blue LDs and green-emitting perovskite quantum dot glasses. As the laser power increases, the luminescence of the glass initially intensifies and then diminishes, which is attributed to thermal quenching.

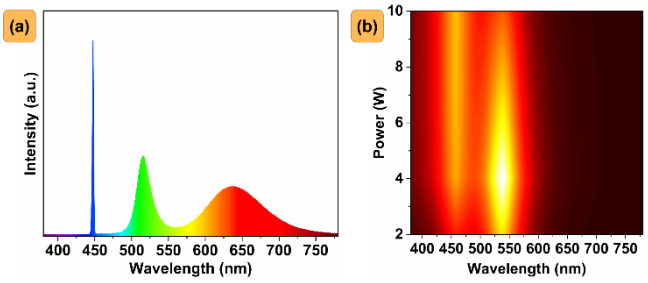

Fig. 1. EL spectra. (a) green emitting perovskite quantum dots glasses and red emitting ceramic phosphors, (b) green emitting perovskite quantum dots glasses

To investigate the damage state of perovskite quantum dot glass under high-power laser irradiation, a finite element method was employed to simulate the process, as illustrated in Fig. 2.

The governing equation for each boundary of the geometric model is Eq. (1).

$$\begin{cases} \begin{cases} K\dfrac{\partial T}{\partial z}\Big|_{z=d} = Q(x,y,z,t)+h\left[T'-T(r,0,t)\right]+\varepsilon\sigma\left[T^4-T^4(r,0,t)\right] \\ K\dfrac{\partial T}{\partial z}\Big|_{z=0} = h\left[T'-T(r,0,t)\right]+\varepsilon\sigma\left[T^4-T^4(r,0,t)\right] \end{cases} \\ \begin{cases} K\dfrac{\partial T}{\partial x}\Big|_{x=0}=0, K\dfrac{\partial T}{\partial x}\Big|_{x=l}=0 \\ K\dfrac{\partial T}{\partial y}\Big|_{y=0}=0, K\dfrac{\partial T}{\partial y}\Big|_{y=l}=0 \end{cases} \end{cases} \tag{1}$$

h is the convective heat transfer coefficient of the material, ε is the surface emissivity of the material, σ is Stefan-Boltzmann constant.

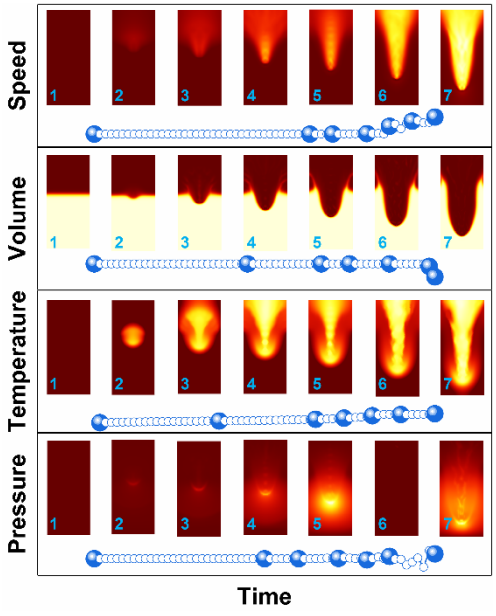

Fig. 2. The process of damage caused by high-power lasers

References

[1] A. C. Du, Q. Y. Du, X. Liu, et al. *J. Inorg. Mater.*, 36, 883 (2021).

[2] A. C. Du, D. B. Shen, W. X. Zhao, et al. *Nanoscale*, 15, 8675 (2023).

[3] A. C. Du, W. X. Zhao, Y. Peng, et al. *Nanomaterials*, 13, 17 (2023).

[4] A. C. Du, W. X. Zhao, Y. Ye, et al. *J. Soc. Inf. Display*, 31, 466 (2023).

Liquid Crystal Polymer Phase Plates Fabricated by Direct Laser Writing

Xin ZOU*, Cong LIU*, Wanlong ZHANG*, Ting LEI*, Xiaocong YUAN*
***Nanophotonics Research Center, Institute of Microscale Optoelectronics,**
Shenzhen University, Shenzhen, 518060, China

Optical vortex is a type of structured beam that carry orbital-angular momentum (OAM) with different topological charge numbers [1]. Optical vortex beams are widely used in optical communication field, including improving the capacity of communication system, and transmitting messages as a carrier. In this paper, we fabricate liquid crystal polymer phase plates to generate vortex beams by femtosecond 3D direct laser writing. Instead of using traditional photoresist, we compound liquid crystal monomers to create different structures [2].

The two-photon direct laser writing technique is of high resolution of 100 nm, which implements high accuracy of our structures. We have produced phase plates that generate vortex beams with different topological charge numbers. Fig.1(a) shows the spiral phase plate (SPP) we design with diameter of 25μm and a total height difference *h* of 1.33um. The fabricated SPP is presented under polarization optical microscope as shown in Fig. 1(b).

The interference system for the vortex beam characterization is illustrated in Fig. 2. The fabricated SPP is insert between two objective lenses for laser beam coupling. By interfering with the reference beam, the interference pattern is observed by the CCD, as shown in Fig. 3(a). The vortex beam profiles with a ring-shaped pattern, the sharp centric dark spot can be seen in visible region [3]. With the interference beam coupled, the presence of the vortex is indicated by the fringe "dislocation defects" at the center of the vortex as shown in Fig.3(b).

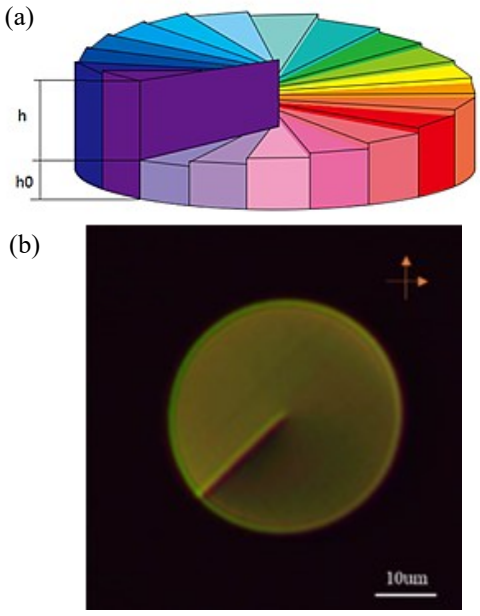

Fig. 1 (a)The schematic image of a SPP with a topological charge (l =1); (b) The fabricated SPP under polarization optical microscope

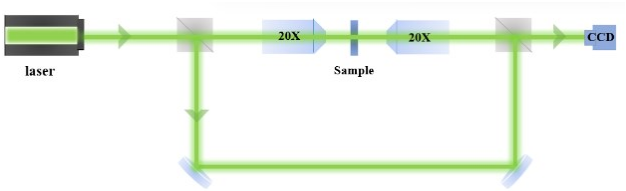

Fig. 2 Experimental setup for vortex beam interference imaging.

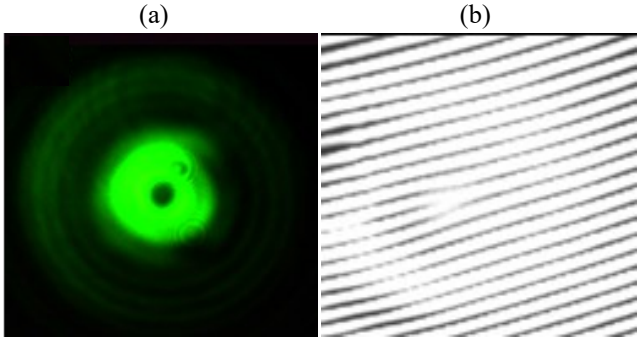

Fig. 3 (a) Images of SPP under polarization optical microscope; (b) A sharp doughnut shape with a uniform ring was found at visible light. (c) Interference pattern between a plane wave and a vortex beam from the SPP with topological charge 1.

In summary, the direct laser writing by Nanoscribe presents the new way to fabricate liquid crystal polymer structures with the unique birefringent properties other than the normal photoresists, indicating the new possibilities in photonics application.

Acknowledgement

The financial support from the National Natural Science Foundation of China (NSFC) 62005180 is gratefully acknowledged.

References

[1] Heming Wei, Abhishek K. Amrithanath, Sridhar Krishnaswamy. *IEEE Photonics. Technol. Lett.*, 31(8), (2019).

[2] del Pozo, Marc, Colm Delaney, Marina Pilz da Cunha, Michael G. Debije, Larisa Florea, and Albert Schenning. *Small Structures*, 2100158, (2022).

[3] Zhou Junchao, Lin Pao Tai. *Optics and Laser Technology*, 156, (2022).

Ultra-scaled Dual-gate IGZO TFT with Record-low Contact Pitch of sub-80 nm, Ultra-high ION of 68.4 μA/μm and Low SS

Zijing Wu*1,2, Ziheng Bai**1, Kaifei Chen1,2, Jiebin Niu1, Wendong Lu1,2, Menggan Liu1,2, Fuxi Liao1,2, Jiawei Wang1, Peiwen Zhang1, Congyan Lu1, Lingfei Wang1, Nianduan Lu1, Di Geng1, Guanhua Yang1, Ling Li***1 and Ming Liu1***

[1]State Key Lab of Fabrication Technologies for Integrated Circuits, Institute of Microelectronics, Chinese Academy of Sciences (IMECAS), Beijing, China.

[2]University of Chinese Academy of Sciences, Beijing, China.

For the first time, scaling down the contact pitch of IGZO TFT to sub-80nm without penalty of electrical characteristics is demonstrated in this work. For ultra-scaled TFT, its footprint is characterized by the contact pitch (CP), an important industry metric, which equals to the sum of channel length (L_{CH}) and contact length (L_C) of the device in **Fig. 1a**. L_{CH} scaling naturally leads to higher channel conductance and improves device performance; however, L_C scaling increases contact resistance (R_C), which degrades device properties. While the scalability of L_{CH} in IGZO FET has been well investigated, L_C and its related scaling challenges remain elusive. **Fig. 1b** is the TEM cross-sectional of the DG device structure (Mo/HfO_2/IGZO/Al_2O_3/HfO_2/Ni). The bottom and top insulators are 5nm HfO_2 and 2/8nm Al_2O_3/ HfO_2, and the IGZO is 5nm. The S/D and the TG electrode metal layer (20/15nm Ni/Au) was fabricated by e-beam evaporation.

By using ultra-high vacuum evaporation of Ni contact, as low as contact resistance of R_C=340Ω·μm and contact resistivity of $\rho_C=1.72\times10^{-7}\Omega\cdot cm^2$ are achieved, respectively. At first, we fabricated and characterized "long-channel" DG IGZO TFTs, with L_{CH} in several hundred nm scale, except for a slight shift to positive direction at sub-threshold region, there is no significant I_{DS} degradation as L_C is scaled down from 300nm to 20nm. $R_{TOT}=2R_C+R_{SH}$, where R_{SH} is sheet resistance of IGZO channel. Because the R_{SH} portion is high in "long-channel", even though the L_C is close to or is lower than L_T, the R_C still is not the primary factor. When L_{CH} is several hundred nm, the I_{DS} degradation is insensitive to L_C reduction. Thus, the L_{CH} should be further scaled to investigate L_C shrinking influence in "short channel" devices. Then, we selected L_{CH}=40nm and L_C values of 300nm, 40nm, 30nm, and 20nm to deeply investigate the effect of L_C scaling on "short-channel" devices. **Fig. 2** gives the overlaid I_{DS}-V_G curves at V_{DS}=1V with L_C of (a) 300nm, (b) 40nm, (c) 30nm, and (d) 20nm, respectively. I_{DS} drops abruptly once L_C shrinks below 30nm, proving that the device property is sensitive to L_C shrinkage at short-channel.

By this design, record-low contact pitch of 80nm (L_C=40nm & L_{CH}=40nm) with ultra-high I_{ON} of 68.4μA/μm (@V_{TH}+1V & V_{DS}=1V) and low SS of 83.4mV/dec **(Fig. 3)** is exhibited among all the oxide semiconductor TFTs reported so far, showing great potential to increase packing density on a chip and be widely used in a variety of applications such as 2T0C DRAM.

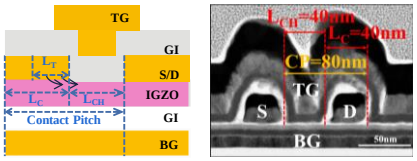

Fig. 1. Device schematic of dual-gate IGZO TFTs and its cross-sectional TEM.

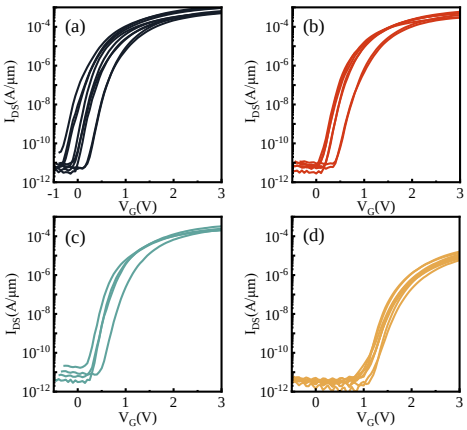

Fig. 2. I_{DS}-V_G characteristics of multiple DG-IGZO TFTs at L_{CH}=40nm with L_C scaling: L_C is scaled from (a) 300nm, (b) 40nm, (c) 30nm to (d) 20nm.

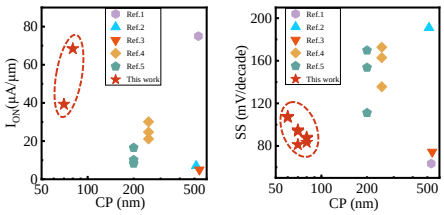

Fig. 3. Benchmark plot of I_{ON} vs. CP, a high I_{ON} of 68.4μA/μm with CP=80nm is achieved and Benchmark plot of SS vs. CP, showing CP=80nm has SS=81.2 mV/dec and CP=70nm has SS=83.4 mV/dec.

References

[1] K. Chen et al., 2022, *VLSI*, pp.298-299.

[2] C. Wang et al., 2022, *VLSI*, pp.294-295.

[3] S. Samanta et al., 2020, *VLSI*, pp.1-2.

[4] S. Subhechha et al., 2022, *VLSI*, pp.292-293.

[5] A. Belmonte et al., 2023, *VLSI*, T17-5.

Investigation of Color Deviation in Micro/Mini-LED Displays

LIN Wei-han[1],,LIU Zhao-jun[2],YANG Mei-hui[1]

1.KONKA group co., Ltd.,Shenzhen 518057,China.

2..Dept. of Electronic and Electrical Engineering, Southern University of Science and Technology, Shenzhen 518055,China

MLED active display technology uses red, green, and blue MLED flip chip devices, which are fixed by die bonder on printed circuit boards (PCB) or glass driver substrates (COB or COG). Compared to LED displays packaged with conventional brackets, COB products are prone to optical crosstalk between pixels due to the lack of reflective cups with LED packaging brackets, which can cause color deviation when viewing MLED display screens from a large angle.

This article will use a MLED chip with a size of 75um to produce a red, green, and blue full color MLED light panel through mass transfer and surface sealing process. The surface sealing material is organic silicon modified epoxy resin mixed with carbon powder, with a sealing thickness of 250um. The sample was subjected to brightness and color coordinate optical testing using CS2000. Rotate the screen according to the angle to test the color coordinate value and brightness value of the sample under different Angle condition. Based on subjective observations, determine the color deviation phenomenon and numerical value of the display screen. Test the optical data of the MLED RGB die and compare it with the changes in screen angle color coordinates and color deviation phenomenon.The sample is shown in Figure 1.

Fig. 1. MLED screen

Facing the screen, the line of sight is at 0 ° to the normal of the screen, which is the standard white field.By rotating the screen angle observation, the MLED direct display screen will experience an angular color deviation phenomenon as the angle of outgoing light increases, from facing the white field to light red and then to light cyan.Through test and calculation, it is found that the inflection point of color coordinate appears at the position of 50 ° ~ 60 °. The color coordinate changes are shown in Fig.2.

As shown in Fig.2, the x coordinate value of the color from 0 ° to 55 ° increases by+0.0121, the y coordinate value increases by+0.0031, and the x value changes by -0.0283 within the range of 55 ° to 85 °. The y value increases by 0.0073, indicating that after 55 °, the white field color gradually turns cyan. The x coordinate of color is related to the energy intensity of red light, and the change in x coordinate is more significant than that in y coordinate, that is, the energy of red light changes significantly at different angles.

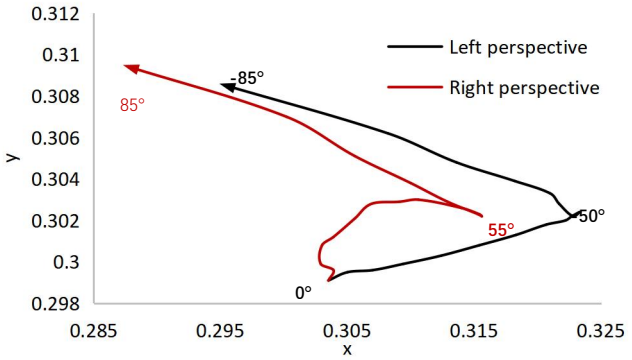

Fig.2.Color coordinate changes from different perspectives

Normalize the brightness data measured from different angles of the screen sample and chip sample to produce a light distribution map. The brightness distribution diagram of the sample test is shown in Fig.3. The distribution of light patterns between the two has undergone significant changes. The light distribution trend of the screen is similar to that of the die chip, both of which are asymmetric from left to right, but the specific shape is different, especially for red light. The folding degree of the die chip is stronger than that of the screen light.

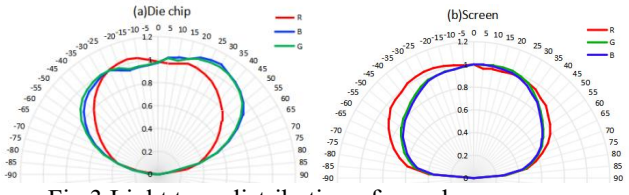

Fig.3.Light type distribution of sample

Through the light type analysis, the color deviation on the surface of MLED screen is related to the light type mismatch and left-right asymmetry of of RGB die chip. The three colors of the screen have a significant deviation from the original three colors of the die chip, which is related to the dispersion of light at different wavelengths after passing through the medium.

The degree of divergence of screen light after sealing is higher than that of die light, with the highest degree of

divergence of red light R, which means that the light escape angle after sealing is greater than that of die state. This may be related to the change in refractive index before and after sealing. The light emitting medium of MLED chip is sapphire, and the epoxy resin used for MLED board is organic silicon modified epoxy resin. The light emitted by the chip reaction layer escapes from the sapphire substrate, causing refraction and total reflection at the interface between the sapphire substrate and the epoxy resin. The refracted light enters the epoxy resin layer. When the light further reaches the interface between epoxy resin and air, it undergoes refraction and total reflection again. The medium through which the optical path passes is shown in Fig.4.

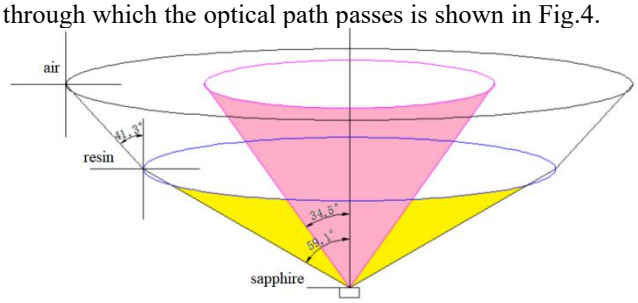

Fig.4.MLED chip and light board escape angle

The degree of R-shaped folding of MLED die chips is stronger than that of GB, but the degree of R-shaped divergence of the sealed light board is higher than that of GB's angular divergence. This may be related to the inconsistent refraction and reflection angles of different wavelengths of light in the same medium, known as dispersion phenomenon.

According to A.L. Cauchy's dispersion empirical formula(1), the refractive index and interface escape angle data of light in the medium for chips with wavelengths of 630nm, 530nm, and 470nm are calculated as Table 1.

$$n(\lambda) = A + \frac{B}{\lambda^2} \quad \text{--------(1)}$$

Table 1. Refractive index and surface escape angle

Color	Sapphire Substrate Refractive Index	Modified Epoxy Resin Refractive Index	Escape angle between substrate and resin interface	Escape angle of resin air interface
R	1.766	1.506	58.5°	41.6°
G	1.772	1.517	58.9°	41.3°
B	1.777	1.526	59.2°	40.9°

The escape angle data calculated in the above table shows that the escape angle of RGB at the interface between the sapphire substrate and resin is about 59°, which includes most of the high-energy emitted light from the die chip. The degree of convergence of red light R is stronger than that of GB. At the interface between resin and air, the escape angle of red light is greater than that of blue-green light. Therefore, the red light changes from the converging light type of the die chip to the divergent light type after the surface of the light board is sealed, and the degree of divergence is stronger than that of blue and green light.

Due to the dispersion of RGB color in the medium, the escape angle of red light is greater than that of blue and green light, and the divergence of red light is stronger than that of blue and green light after passing through the medium. The difference in the intensity attenuation of red, green and blue light causes the angular color deviation of the outgoing light.

References

[1] Chao Tian,Shu- xu Guo,Jing- qiu Liang,et al.Effects of unit size on current density and illuminance of micro-LED- array[J].Opto-electronics Letters,2017,13(2):84.

[2] Zhaojun Liu,Chun-Ho Lin,Byung-Ryool Hyun,et al. Micro-light-emitting diodes with quantum dots in display technology. Light: science & applications, (2020.05) 9:83 P1-P23.

[3] MOHAMED SUFYAN ISLIM,RICARDO X.FERREIRA,XIANGYU HE,et al.Towards 10 Gb/s orthogonal frequency division multiplexing-based visible light communication using a GaN violet micro-LED[J].Photonics Research,2017,5(2):A35-A43.

[4] [Japan] Moriaki wakaki, keieikudo, Takehisa Shibuya. Handbook of optical materials [M]. Translated by Hai-xian ZHOU, Yun-fang CHENG, Beijing: Chemical Industry Press, 2010:328-329.

[5] Xi-mou CHEN. Optics[M], Beijing: Peking University Press, 2011:196-200.

[6] Mian-feng CHEN. Study on the Preparation and Performance of Polysiloxane-modified Epoxy Resin for LED Encapsulation[D]. South China University of Technology,2017.15-16.

[7] Lei WANG, Xiang LUO, Fo-qing CHANG, et al. Effect of refractive index matching on optical performance of green LED microdisplay[J]. Chinese Journal of Liquid Crystals and Displays, 2020, 35(9):900-907.

Abstract from Oral Presentations

An Active-Matrix Piezoelectric Tactile Sensor Array with In-Pixel Amplifier and Non-Uniformity Compensation

Tengteng Lei, Yushen Hu, Man Wong
***Department of Electronic and Computer Engineering, Hong Kong, China**

While offering improved sensitivity, an active-matrix piezoelectric tactile sensor array with monolithically integrated in-pixel amplifiers built using thin-film transistors (TFTs) could suffer degraded response uniformity induced by the inevitable variation of TFT parameters. Presently described is the implementation of a compensation scheme for such variation, leading to a significant improvement in response uniformity. This is demonstrated by the enhanced performance of a compensated 16×16 sensor array.

Sensors converting tactile stimuli to electrical signals are attracting increased attention. For their application in the field of robotics and health monitoring [1], etc., large area, high sensitivity and good uniformity are features to promote. Active-matrix addressing is popularly deployed to regulate the operation of a large-area array of sensing or other functional elements. The most widely known example of this is the flat-panel display, with the active matrix implemented using thin-film transistors (TFTs).

Recently, tactile sensors consisting of polyvinylidene fluoride (PVDF) piezoelectric sensing film and signal-conditioning circuits based on TFTs for improved sensitivity have been reported [2]-[3]. Deployed in each pixel were a dual-gate (DG) TFT for signal coupling and an amplifier for signal magnification. However, degraded response uniformity induced by the inevitable variation of TFT parameters has been observed. Presently described is a scheme for remedying such degradation, leading to improved response uniformity.

The pixel circuit, a timing diagram of the compensation scheme, and photographs of an array and a pixel are displayed in Fig. 1. Shown in Fig. 2 are the current (I)-voltage (V) characteristics of top-gate (TG) and DG TFTs and the variation of their extracted threshold voltage (V_{TH}). The corresponding mean ($\overline{V_{TH}}$) and standard deviation ($\sigma(V_{TH})$) values are summarized.

Addressing of the array is divided into two stages (Fig. 1b): a compensating STAGE 1 and a sensing STAGE 2. During STAGE 1, M3 is off and TFTs M4 and M5 are on. Consequently, the sensing input of M1 is grounded through M5. Since its drain and gate terminals are shorted through M4, M1 is forced to operate in the saturation regime. During STAGE 2, M3 is on to allow offloading of the output; M4 is turned off, thus storing on capacitor C_S of the bias voltage V_B established during STAGE 1 that allows the amplifier consisting of TFTs M1 and M2 to operate in the saturation regime and results in a uniform voltage gain largely determined by the aspect ratio of M1 and M2; M5 is off to isolate the input terminal from the ground.

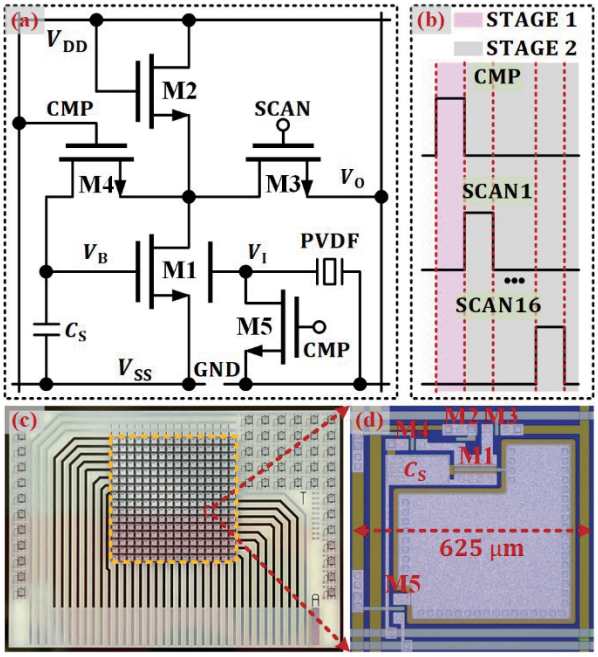

Fig. 1. Circuit and (b) timing diagrams of the proposed tactile pixel; Photographs of (c) a tactile sensor array and (d) a pixel.

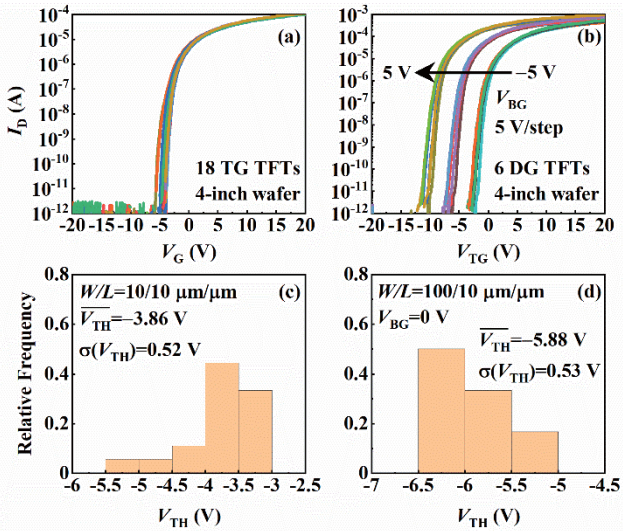

Fig. 2. *I-V* characteristics of (a) TG and (b) DG TFTs; extracted V_{TH} and standard deviation $\sigma(V_{TH})$ of (c) TG and (d) DG TFTs.

References

[1] L. Nela, *et al.*, *Nano Lett.*, 18(3): 2054-2059, 2018.
[2] A. Rasheed, *et al.*, *Sensors*, 19(14): 3241, 2019.
[3] G. Di, *et al.*, *IEEE Sensors J.*, 17(3), 2017.

Fluorination-Mitigated High-Current Degradation of Amorphous InGaZnO Thin-Film Transistors

Yanxin Wang*, Jiye Li*, Fayang Liu*, Yunping Wang*, Shengdong Zhang*, Lei Lu*

***School of Electronic and Computer Engineering, Peking University Shenzhen Graduate School, Shenzhen, Guangdong, China**

To drive more advanced displays, amorphous oxide semiconductor (AOS) thin-film transistors (TFTs) have encountered severe degradation behaviors, and even hard breakdown under high current stresses (HCSs). The underlying mechanism is the self-heating (SH) effect, which is often ascribed to the poor thermal conductivity of AOSs and the thermally induced internal and external defects.[1,2]

The HCS degradations were observed in the output curve of the amorphous InGaZnO (a-IGZO) TFT, as shown in Fig. 1(a). The drain current (I_d) exhibits the linear and then gradual saturation dependences on drain voltage (V_{ds}) in *Stage-I*, while the high saturation current instantly triggers a dramatic I_d uprising in *Stage-II*. The inflection point of output resistance curve precisely define the triggering voltage (V_{tr}) of HCS degradation in *Stage-II*, which is plausibly caused by the SH effect-activated induction of shallow-donor defects from the deep-state defects.[3]

Based on the disclosed mechanism, the a-IGZO was treated with CF_4 plasma to suppress the native defects.[4] As extracted from Fig. 1, the V_{tr} is significantly increased from 23.4 V to 27.9 V by the plasma fluorination. This verifies the suppressing effect of fluorine on the initial total density of deep-state V_O (N_{Vo}), as illustrated in Fig. 2.

To compare the fluorination effect on the defect state transition speed, the time evolution of I_d is characterized under constant V_{ds} and gate voltage (V_{gs}). As shown in Fig. 3, the I_d gradually encounters the linear increasing, fast rising and abrupt collapse. In the linear increasing stage, the linear slopes are 2.36 μA/s and 1.70 μA/s respectively for a-IGZO and a-IGZO:F TFTs, suggesting that the fluorination noticeably reduces the SH-induced donor generation rate (R_{gen}) by 28%, which is much higher than the reduction ratio of N_{Vo} using fluorination treatment. Therefore, the noticeably slower R_{gen} in a-IGZO:F TFTs may not be fully explained by the fluorination-suppressed N_{Vo}. The SH-induced transition rate of N_{Vo} (R_{tran}) of the SH a-IGZO channel is plausibly also reduced by the fluorination treatment. As illustrated in Fig. 2, the fluorine-mitigated R_{tran} and N_{Vo} together contribute to the significant retardation of HCS degradation. The proposed scheme noticeably enhances the high-current applications of oxide TFTs.

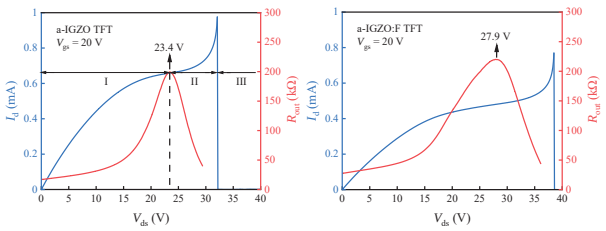

Fig. 1. Output characteristic and output resistance curves of the (a) a-IGZO TFT (b) a-IGZO:F TFT at Vgs = 20 V.

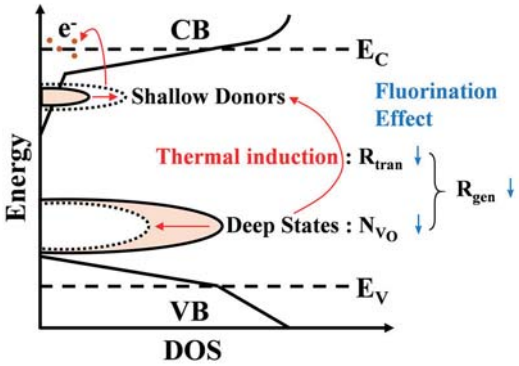

Fig. 2. The mechanism of SH-induced defect transformation, illustrated in the density of states (DOS) in a-IGZO.

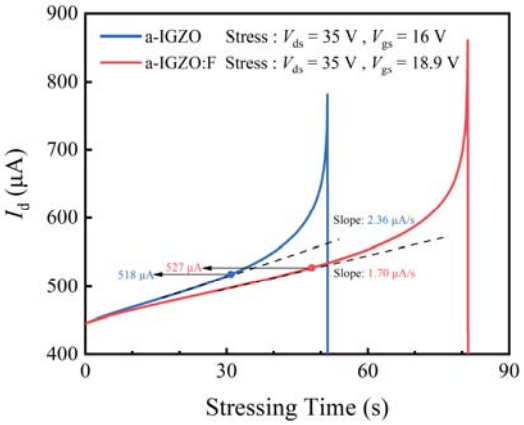

Fig. 3. The evolution of Id of a-IGZO and a-IGZO:F TFTs under SH stresses of the same initial power.

References

[1] Mativenga M and Hong S. *Appl Phys Lett*, 102(2), 023503(2013)

[2] Yang H and Huang TY. *IEEE Trans Electron Devices*, 68(12), 6197(2021)

[3] Zhou YH and Liu FY. *Solid-State Electron*, 195, 108393(2022)

[4] Lu L and Xia ZH. *IEEE Electron Device Lett*, 39(2), 196(2017)

Infrared Sensitive Thin-Film Phototransistor Made on Glass Substrate for Active Matrix Sensing Application

Yi-Cheng Yuan*, Ya-Hsiang Tai*, Hsu-En Tsai*, Her-Yih Shieh** and Hsueh-Shih Chen**

***Department of Photonics and Institute of Electro-Optical Engineering, College of Electrical and Computer Engineering, National Yang Ming Chiao Tung University, Hsinchu, Taiwan, 30010, R.O.C.**

**** Department of Materials Science and Engineering, National Tsing Hua Tung University, Hsinchu, Taiwan, 300, R.O.C.**

The application of image sensors has become increasingly popular for integration with display panels, such as for ambient light, proximity, and fingerprint sensors. However, using visible light for the sensor can negatively impact display performance, and using Ultraviolet (UV) sensing can pose potential health hazards. To avoid these potential risks, an infrared (IR) sensor is the best choice.

We focused on IR signals with a wavelength of 940 nm in this study, and we calculated the corresponding photon energy using the Planck constant and the speed of light. The result of this calculation was approximately 1.32 eV.

$$E_{photon}\& = h\nu = h\frac{C}{\lambda} \times \frac{1}{e}(eV) \approx 1.32eV$$

PbS QDs have a bandgap energy of 1.2 eV. Therefore, when IR radiation is absorbed by the PbS QDs, they generate electron-hole pairs, which can then be collected to produce an electrical signal, making it a desirable material for IR sensing applications.

In our previous work, we reported that the conventional TFT with a gap region between gate and drain, known as the Gap-Type TFT, can be used as a photo sensor. Through TCAD simulation, we discovered that LIBL effect can be observed either in the gap region or near the interface of metal/semiconductor in our recent research. Therefore, we prepare TFTs with and without gap in this study and expect to see the high photocurrent for both structures.

To preliminarily verify the infrared sensitivity of our device, we coated the PbS layer without patterning, and the structure of the gap-type TFT IR sensor is shown in Fig. 4(a).

Fig. 5(a) presents the photocurrent responses of the proposed TFT sensors with a gap in their structure when subjected to IR radiation with a wavelength of 940nm. The experimental results demonstrate that both sensor structures exhibit excellent sensitivity to IR radiation, as evidenced by the noticeable photocurrent response.

Fig. 6 shows the relation between the photocurrent density and the incident IR intensity of our proposed device and the PbS photodiode. As can be seen in the plot, the light sensitivity normalized by the area of our PbS TFT sensor is 1~2 orders larger than the PbS photodiode.

In conclusion, we proposed a device provides a high photocurrent at much smaller area and lower cost compared to other photodiode devices, making it more cost-effective and accessible to a larger user base. Moreover, the proposed device has the potential for various applications in the field of IR sensing.

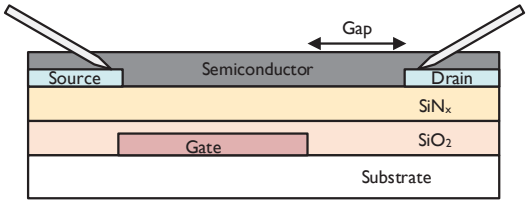

Fig. 4(a). Structures of the gap-type IR TFT sensor

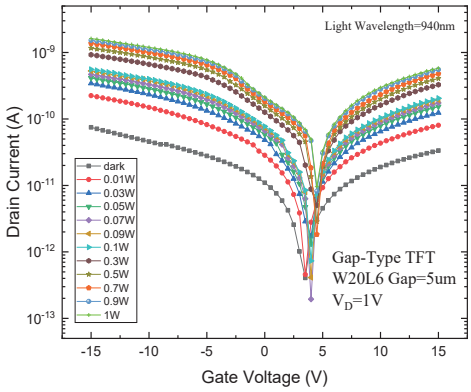

Fig. 5(a). Photocurrent responses of the gap-type TFT

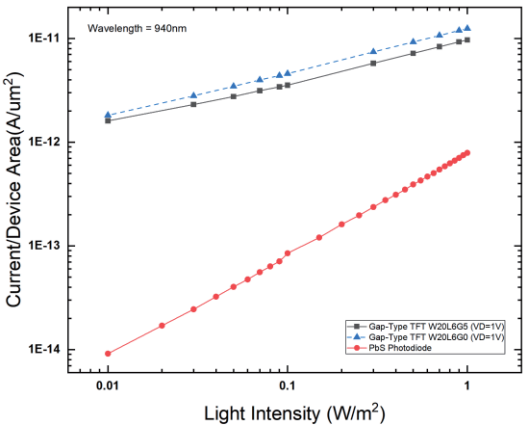

Fig. 6. Comparison of photocurrent density

A Kinetic Model for Intrinsic Donor-Defects in Metal-Oxide Semiconductors

Yuqi Wang[1*], Zhihe Xia[1] and Man Wong[1,2**]

[1]State Key Laboratory of Advanced Displays and Optoelectronics Technologies, Department of Electronic and Computer Engineering, The Hong Kong University of Science and Technology, Hong Kong, China
[2]The Hong Kong University of Science and Technology Shenzhen Research Institute, Shenzhen, China
Email: ywangkm@ust.hk, eemwong@ust.hk

A kinetic model[1] has been proposed, involving oxidant diffusion and an oxidation-reduction reaction for the thermally induced intrinsic donor-defects in common metal-oxide (MO) semiconductors (such as IGZO and ITZO). This leads to a 3-parameter equation governing the time dependence of the concentration of such defects (N_D), which is characterized by measuring the shift in the turn-on voltage (V_{ON}) of a thin-film transistor (TFT) subjected to heat-treatments in different atmospheres for different durations. The model parameters have been extracted, resulting in the determination of relevant activation energies from their temperature dependencies. Such model is applicable to MO semiconductors of different compositions and has been used to study the effect of fluorination on IGZO.[2] Guided by this model, precisely control of the saturation V_{ON} of TFTs has been achieved through an extended oxidation process.[3] These results further illustrate the utility of the model as a tool for developing and optimizing MO TFT technologies.

Shown in Fig. 1 is the schematic of the system under study. A reversible oxidation-reduction reaction (Eq. 1) takes place in the MO film, with respective rate constants k_O and k_R. The oxidant diffuses with a diffusivity K_O through a medium covering the MO. D_O and D_OO denote the reduced/active and oxidized/inactive donor-defects, respectively. It is finally obtained that the time-dependence of the concentration change in N_D can be expressed by a 3-parameter equation after relating ΔN_D to ΔV_{ON}:

$$\underbrace{D_OO}_{N_T-N_D} \rightleftharpoons \underbrace{D_O}_{N_D} + \underbrace{O}_{N_O}. \tag{1}$$

$$\Delta V_{ON} = V_{ON} - V_{ON}|_{t=0} \approx -\frac{q}{C_{ox}}(N_D - N_D|_{t=0}), \tag{2}$$

$$\Delta V_{ON} \approx A(1 - e^{-Bt+C\Delta V_{ON}}), \tag{3}$$

where A, B and C are phenomenological model parameters.

Depending on specific experimental conditions, reasonable approximations can be made to simplify the model equation. When a device is annealed in an inert atmosphere, one has:

$$\Delta V_{ON} \approx -K_R t, \tag{4}$$

where K_R is related to the reduction rate constant k_R. It is found that when a device is annealed at a sufficiently low T, defect generation becomes negligible. When a device is annealed in an oxidizing atmosphere with no defect generation, one obtains a set of modified parameters A_O, B_O and C_O and yields:

$$\Delta V_{ON} \approx A_O(1 - e^{-B_O t+C_O\Delta V_{ON}}). \tag{5}$$

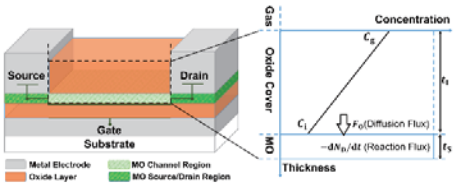

Fig. 1. Cross-section of a bottom-gate TFT (Left) and a schematic (Right) showing the diffusion of oxidants in the oxide cover layer and the oxidation-reduction reaction in the channel portion of the semiconducting MO layer.

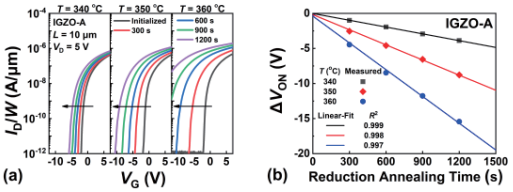

Fig. 2. a) Time evolution of transfer curves of an IGZO TFT initialized and subsequently annealed in N_2 and b) comparison of the measured ΔV_{ON} *vs.* t and the optimal fit curves.

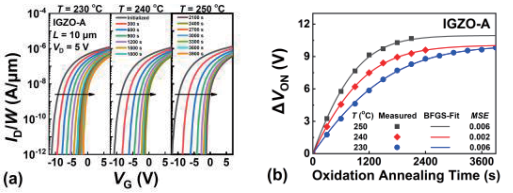

Fig. 3. a) Time evolution of transfer curves of an IGZO TFT initialized and subsequently annealed in O_2 and b) comparison of the measured ΔV_{ON} *vs.* t and the optimal fit curves.

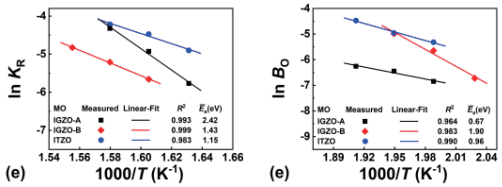

Fig. 4. Arrhenius plot of a) extracted K_R and b) B_O for TFTs based on three different MO thin films.

REFERENCES

[1] Y. Wang, W. Jiang, X. Xie, Z. Xia, and M. Wong, "A Kinetic Model for the Generation and Annihilation of Thermally Induced Carrier Donors in a Semiconducting Metal-Oxide Thin Film," *Small*, vol. 2203346, p. 2203346, Aug. 2022, DOI:10.1002/smll.202203346.

[2] Y. Wang, W. Jiang, Z. Xia, and M. Wong, "Application of a Kinetic Model to the Characterization of Donor-Defects in a Fluorinated Metal-Oxide Semiconductor," *Int. Conf. Disp. Technol.*, vol. 54, pp. 5–7, 2023.

[3] Y. Wang, Z. Xia, and M. Wong, "Dependence of the Transfer Characteristics of Metal-Oxide Thin-Film Transistors on the Temperature of an Extended Oxidizing Heat-Treatment," *IEEE Electron Device Lett.*, vol. 44, no. 3, pp. 452–455, Mar. 2023, DOI:10.1109/LED.2023.3240566.

Multisensory and Multifunctional Electronic Skin based on Core-shell $CsPbBr_3$/PDMS Perovskite Microspheres

Junhu Cai[1], Zexi Lin[1], Wenxiao Zhao[1], Wenyan Zhang[1], Xiaogang Chen[1], Enguo Chen[1,2,], Yun Ye[1,2], Sheng Xu[1,2], Jie Sun[1,2], Qun Yan[1,2], and Tailiang Guo[1,2]*

[1]National & Local United Engineer Laboratory of Flat Panel Display Technology, College of Physics and Information Engineering, Fuzhou University, Fuzhou, China

[2]Fujian Science & Technology Innovation Laboratory for Optoelectronic Information of China, Fuzhou, China

[*]Corresponding author: ceg@fzu.edu.cn

Integrated electronic skin (e-skin) provide information on physiological and environmental parameters. To imitate better or even surmount the perceptive capabilities of human skin, multifunctional and multisensory e-skin is an important trend in the future. Perovskite materials hold great potentials for highly performance and multi-functional photoelectric field. However, poor stability and lack of exploitation of multi-sensing and multifunctional properties limit their application in integrated devices. In this work, we first obtained $CsPbBr_3$/PDMS perovskite microspheres with improved performance and stability through two-step optimization of ligand modification and in-situ coating. The acidic environment provided by benzene sulfonic acid ligands and ring-opening polymerization of silicon monomer are the key conditions for the PDMS shell formation, and are also the decisive factors for the two-step optimization of $CsPbBr_3$. Then, interestingly, by adjusting PDMS shell polymerization environment, gradient photoelectrical properties of $CsPbBr_3$/PDMS microspheres obtained. E-skins based on the performance-differentiated $CsPbBr_3$/PDMS microspheres have capacity sensing the temperature, relative humidity simultaneously, as well as with the function of human-machine collaboration, anti-counterfeiting and so on. It demonstrates the potential application prospects in the integrated device field.

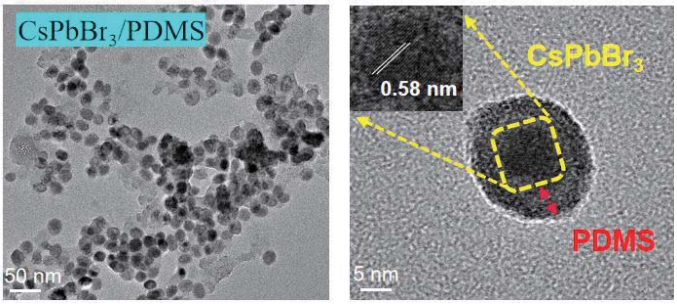

Fig. 1. TEM and HRTEM images of $CsPbBr_3$/PDMS perovskite microspheres.

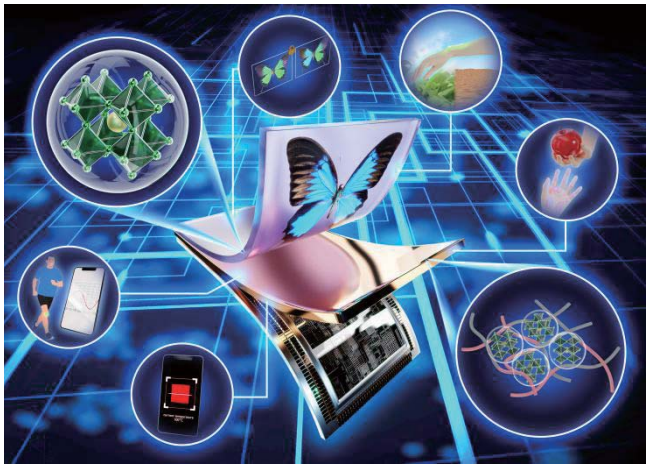

Fig. 2. Multisensory and multifunctional electronic skin based on core-shell $CsPbBr_3$/PDMS perovskite microspheres.

The Transparent E-paper Based on Microcup Electrophoretic Display

*Jie Liu, Guangyou Liu, Yunhe Liu, Xinzao Wu, Hao Shu, Zong Qin, Bo-ru Yang**

State Key Laboratory of Optoelectronic Materials and Technologies, Guangdong Province Key Laboratory of Display Material and Technology, School of Electronics and Information Technology, Sun Yat-Sen University, Guangzhou 510275, People's Republic of China.

***Email:** paulyang68@me.com

Abstract

Electronic paper (E-paper) has advantages such as high contrast [1], bistability, low power consumption [2], eyes protection, large viewing angle, and higher readability [3]. With the advent of the era of Internet of things (IoT), the emergence of various application scenarios has highlighted the importance of E-paper [4]. As a new generation of display technology, E-paper is expected to replace traditional paper and become a new generation of display media [5]. Traditional E-papers achieve display by driving charged particles to the top side of microcapsules or microcups through electric field, as shown in Figure 1(a). However, the transparent E-paper can be achieved by designing transverse electrodes to drive particles to both sides of the microcapsule or micro cup, where the incident light can be transmitted through the devices to ensure the transparent state of E-paper, as shown in Figure 1(b).

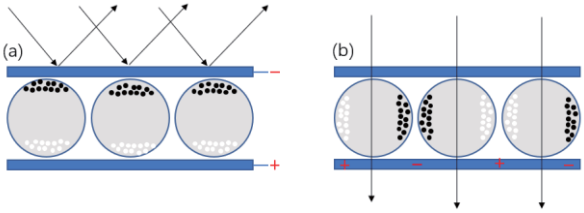

Figure 1 (a) The schematic diagram of traditional E-paper display. (b) The schematic diagram of transparent E-paper display

Herein, we fabricated microcups of various shapes and sizes by mature photolithography technology. Furthermore, transparent E-papers based on In-Plane Switching (IPS-EPD) with microcups was prepared, which can be switched between transparent state and white state. The microcups were prepared by a lithography process, mainly including plasma pretreatment, spin coating photoresist, pre-baking, exposure, post-baking, and development. Process parameters such as pretreatment time, spin coating speed, exposure time, baking temperature, development time, etc., will affect the quality of the microcups After constant adjustment of process parameters, microcups with different shapes, good appearance and high surface flatness were made, as shown in Figure 2(a). Distortion, defects and other problems occurred when the process parameters were inaccurate. Our microcups have a width of 180μm and a microcup wall width of 20μm. Utilizing overlay technology, they are effectively aligned with the underlying IPS electrodes, resulting in improved transmittance.

Finally, we assembled the complete device and placed it on the OLED screen to test the effect as shown in Figure 2(b)-(d). The transmissivity of this transparent E-paper can reach 60%, and the response speed is fast, it only takes 2-3 seconds. The transparent IPS-EPD can be applied in smart windows, smart watch covers, and other display fields.

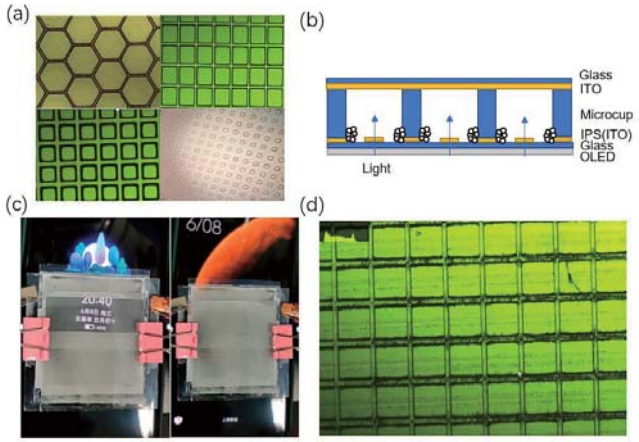

Figure 2 (a) A schematic of the perfection and defects of various microcups. (b) The schematic diagram of device structure. (c) Display effect on mobile phone screen. (d) Microscopic image of particles arranged.

References

[1] Hertel D. Optical measurement standards for reflective e-Paper to predict colors displayed in ambient illumination environments[J]. Color Research and Application, 2018, 43(6): 907-921.

[2] Heikenfeld J, Drzaic P, Jong-souk Yeo, et al. Review Paper: A critical review of the present and future prospects for electronic paper[J]. Journal of the Society for Information Display, 2012, 19(2):129-156.

[3] Ota I, Ohnishi J, Yoshiyama M. Electrophoretic image display (EPID) panel[J]. Proceedings of the IEEE, 1973, 61(7):832-836.

[4] Yang B-R. "E-Paper Displays". John Wiley & Sons Ltd, Chichester, ISBN: 978-1-119-74558-7, 2022.

[5] Comiskey, B., Albert, J., Yoshizawa, H. et al. An electrophoretic ink for all-printed reflective electronic displays. Nature 394, 253–255 (1998).

Advanced Thin-Film Polarizers and Their Applications

Yue-Chu Cheng*, Yi-Yang Gao*, Man-Chun Tseng*, Yeuk-Lung Ho*, Olena Vashchenko*, Valerii Vashchenko*, Shu-Tuen Tang*, Sze-Yan Yeung*, and Hoi-Sing Kwok*

***State Key Laboratory of Advanced Displays and Optoelectronics Technologies,**
Department of Electronic and Computer Engineering,
The Hong Kong University of Science and Technology

Abstract

This paper investigates the efficient fabrication strategies for high-performance ultra-thin polarizers utilizing photo-aligned azo-dyes. The fabricated polarizers demonstrates exceptional dichroism (DR>100), and superior polarization efficiency (PE>99%) with ultra-thin film thickness (200nm). Furthermore, we exhibit the wide-ranging applications of these ultra-thin polarizers in liquid crystal displays and flexible display technologies.

Technical Summary

Polarizers are essential in contemporary display technologies, particularly Liquid Crystal Displays (LCDs). Polarizers are functional in controlling the polarization state and transmission of light, which can be classified into two types: absorptive polarizers and reflective polarizers[1]. With the advancement of technology, there is a growing demand for high-performance displays. A coatable polarizer fabricated through solution processing was proposed for higher-performance and ultra-thin display technologies. The coatable polarizer can be produced inside the display panel as an in-cell polarizer. Ultra-thin azo-dye polarizers are an innovative type of polarizer[2]. In this work, we utilize dichroic azo-dye material, which can absorb light based on the polarization state. Such azo-dye polarizers have several advantages, including ultra-thin film thickness and high dichroic ratio. This type of polarizer can be produced using solution-processing techniques, enabling lower-cost manufacturing processes.

Azo-dyes are a class of organic compounds with a characteristic chemical structure with a double nitrogen bond between two carbon atoms[2]. The molecular structure of dichroic azo-dye AD1 is shown in Figure 1. These dyes often have a rod-like molecular structure, which contributes to their dichroic properties.

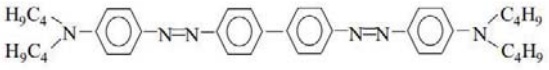

Fig. 1 Molecular structure of dichroic azo-dye AD1

Photoalignment of azo-dyes is a technique used to achieve precise and controllable alignment of the azo-dye molecules in thin film polarizers. In our approach, the photoalignment method achieves the alignment of dichroic AD1 film. Under polarized light exposure, the azo dyes minimize absorption by rotating themselves perpendicular to the irradiated light's polarization[3]. Thus, the AD1 molecules are aligned in a specific direction to achieve anisotropic absorption. This technique allows for precise control of the alignment direction and degree of alignment, which can lead to improved polarizer performance.

The photographs of the fabricated coatable AD1 polarizer are shown in Figure 2. The AD1 polarizer is placed on top of the backlight and covered with a commercial polarizer.

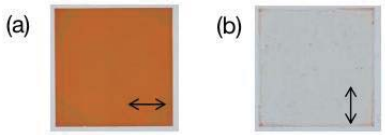

Fig. 2 Photographs of fabricated AD1 polarizer on top of the backlight covered with a commercial polarizer.

The photographs of the in-cell polarizer demo are presented in Figure 3. With a patterned ITO surface, the TN liquid crystal cell can display the "HKUST" and "SKL" logo when a voltage is applied.

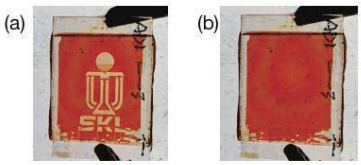

Fig. 3 The photographs of TN mode LCD with AD1 in-cell polarizer.

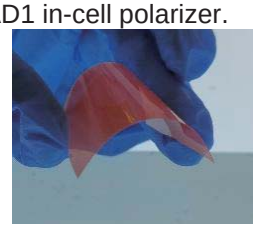

Fig. 4 Thin-film polarizer on flexible substrate

Furthermore, we successfully developed thin-film polarizers on flexible substrates, as exhibited in figure 4. The proposed approach holds promise for flexible display applications, offering low cost, durability, and chemical and thermal stability benefits.

References

[1] Zwick MM. J. Appl. Polym. Sci. 1965;9:2393.

[2] S. Pan, J. Y. Ho, V. G. Chigrinov, H. S. Kwok, ACS Appl Mater Interfaces 2018, 10, 9032.

[3] Chigrinov V, Pikin S, Verevochnikov A, et al. Diffusion model of photoaligning in azo-dye layers[J]. Physical Review E, 2004, 69(6): 061713.

Switchable Optical Differential Operation of Two-dimensional Intensity and Phase Based on Liquid Crystal Polarization Gratings

Weiwei Peng*, Wanlong Zhang*, Xiaocong Yuan*

***Nano-photonics Research Centre, Shenzhen Key Laboratory of Micro-scale Optical Information Technology, Institute of Micro/Nano Optoelectronics, Shenzhen University, 518060, China**

Optical analog computing is a method of using optical devices and materials to perform mathematical operations. According to the design method, optical analog computing devices can be divided into two categories: 4F system method and Green's function method. Optical analog computing devices can achieve different computing functions, such as differentiators, integrators, equation solvers, and spatial frequency filters. Optical analog computing has the advantages of high speed, low power consumption, parallel processing, etc., and can be applied to artificial intelligence, image processing, quantum information and other fields[1] .

Liquid crystal polarization gratings can be easily fabricated by photoalignment technology, which can make the incident ray polarized into left-rotated and right-rotated light emitted at a certain angle. Combining the anisotropy and geometric phase theory of liquid crystals, the liquid crystal polarization gratings and 4f system are constructed to realize differential operations in all-optical analog computing[2].

Utilizing the polarization-sensitive property of liquid crystals, this paper combines line polarizers and twisted nematic liquid crystal voltage modulation technique in the experimental system, and adopts the 4f system method to realize the detection of light intensity and phase of two-dimensional images at different angles, opening up a new way for optical image processing. This method can be applied in the field of bio-photonics involving phase detection. The applicability of liquid crystals to the full spectrum makes it possible to achieve real-time and fast optical discretization of the full light. In addition, liquid crystal gratings are low-cost, easy to mass-produce, and have a simple system structure, making them have broad application prospects.

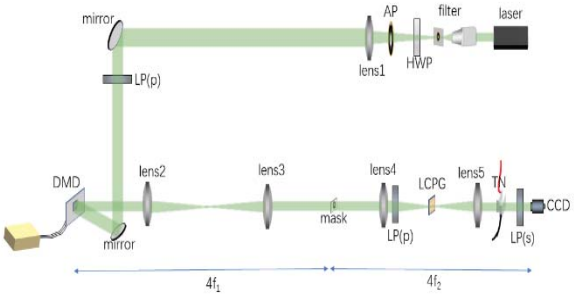

Fig. 1. Optical system diagram.

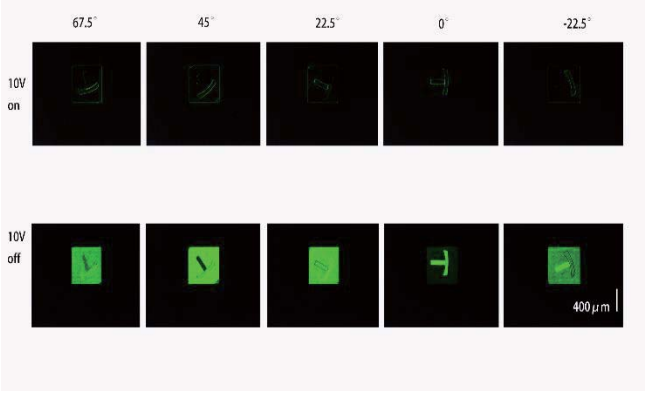

Fig. 2. The experiment was processed for differential operation on a hammer. The first row shows the 10V voltage differential measurements of the twisted nematic liquid crystal at different rotation angles. The second row is the original image processing results seen when the voltage of the twisted nematic liquid crystal is turned off.

References

[1] Dmien Woods. *J.amc.*,215(4),1417-1430(2009).

[2] Shanshan He,Ruisi Wang. *Nanophotonics.*, 11(6), 1083-1108 (2022).

Plasma-enhanced transferring process for one-step patterning of stretchable transparent silver nanowire electrodes and its applications on touching detection

Yifan Gu[1], Zhiguang Qiu[1], Gaofan Zhang[1], Ziyi Wu[1], Simu Zhu[1], Zong Qin[1], Bo-Ru Yang[1,]*

[1] State Key Laboratory of Optoelectronic Materials and Technologies, Guangdong Province Key Laboratory of Display Material and Technology, School of Electronics and Information Technology, Sun Yat-Sen University, Guangzhou, China (*paulyang68@me.com)

Stretchable electronics have been booming in recent years since it breaks through the restraint of rigid form and provides the electronic device with more flexible performance. Specifically, stretchable transparent electrodes (STE) with designed patterns have attracted great attention for its potential in future stretchable electronics applications [1, 2]. In this work, a plasma-enhanced transferring (PE-transferring) process for one-step patterning of silver nanowires (AgNW) STEs was proposed, which achieved excellent performance for the as-prepared STE with arbitrary patterns. As the application, a stretchable touch sensor array was demonstrated in this work as a possible application in the future.

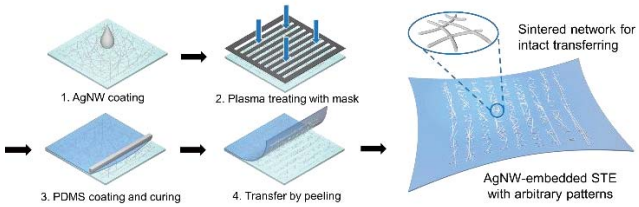

Fig. 1. Patterned STE prepared by the PE-transferring process.

The PE-transferring process was illustrated in **Fig. 1**. Owing to the plasma treatment, the HPMC additives mixed in the AgNW inks were removed in the exposing area. Furthermore, the plasma-treated AgNW network was sintered [3], which led to the intact transferring of AgNW patterns. Thus, the one-step process for preparing STEs with arbitrary patterns was achieved, as only the AgNWs in the exposing area could be transferred to the PDMS layer since the removal of the HPMC additives.

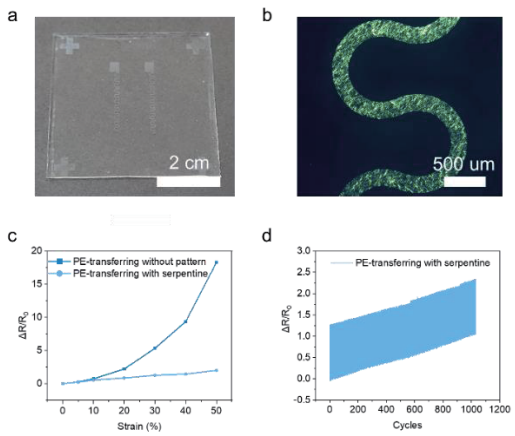

Fig. 2. (a) Photograph of serpentine patterned STE and (b) its enlarged OM image. (c) Resistance variation of different types of STEs under 0-50% strain. (d) Resistance variation of serpentine patterned STE under 30% strain for 1000 cycles.

The photographs of the patterned STE and its enlarged OM image have been shown in **Fig. 2a-b**. Specific serpentine shape [4] has been employed to improve the stretching performance of the STEs ($\Delta R/R_0$ = 1.989 in 50% strain), which was shown in **Fig. 2c-d**. Furthermore, the as-prepared serpentine STEs were utilized to demonstrate a stretchable touch sensor array as a potential application in the future. As shown in **Fig. 3**, the sensing array could accurately recognize the touching point even under 30% strain, which promised its potential in future applications in stretchable electronics.

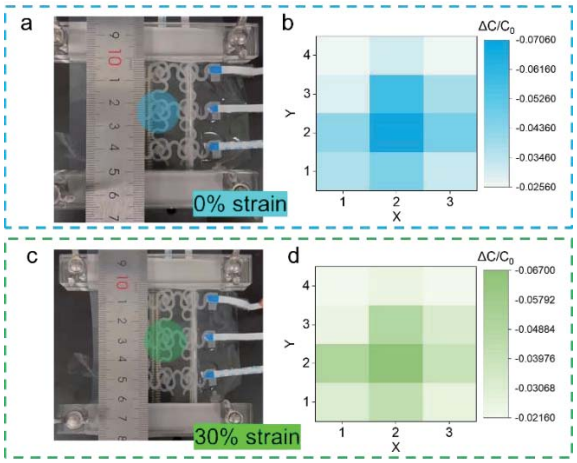

Fig. 3. Photographs of stretchable touch sensor array (a) in normal state and (c) under 30% strain. Heatmap for the touch response of mutual capacitance for all t he pixels when touching pixel (2,2) (b) in normal state and (d) under 30% strain.

References

[1] C. Park, et al. *Appl. Phys. Rev*. 9, 021312, (2022).

[2] N. Matsuhisa, et al. Chem. Soc. Rev. 48, 2946-2966, (2019).

[3] J. Liu, et al. *ACS Appl. Nano Mater*. 4, 1664-1671, 2021.

[4] Z. Wu, et al. *IEEE Sens. J.*, (2023), DOI: 10.1109/JSEN.2023.3296248 (Accepted).

• Stable Spectral and High Color Purity Blue Perovskite Duantum Dots and Devices

Xi Lan, Fanghao Ye, Mengyao Tian, Mingchao Zhu, Jianjing Yi, Mengling Fan, Zhenwei Lin, Guijun Li

Key Laboratory of Optoelectronic Devices and Systems of Ministry of Education and Guangdong Province, Shenzhen University, Shenzhen, China.

Perovskite quantum dots (PQDs) have attracted enormous attention due to their tunable visible spectrum, narrow half-width, wide color gamut (≈140%), and high photoluminescence quantum yields (PLQY). Significant breakthroughs have been achieved in the synthesis of green and red PQDs and the performance of perovskite light-emitting diodes (PeLEDs) based on them. While the low performance of blue PQDs has hindered the development of blue PeLEDs for commercial display applications. From a component engineering perspective, the hybrid halide (Br and Cl) perovskites can adequately perform band-gap cropping and cover the entire blue light range. However, the mixed halide PQDs are prone to lattice mismatch and phase separation, which disrupting the PeLEDs performance. The low formation energy of Cl vacancies in perovskites tends to form Cl vacancies within the band gap, leading to deeper defect energy levels and significantly nonradiative recombination. In addition, when PQDs are applied to LED devices, PQDs with high ligand density need to go through several purification, annealing and other processes, which will reduce the luminous performance and life of quantum dots. In this paper, the basic green PQDs is synthesized by LARP method, and the high color purity blue PQDs with spectral stability are obtained successfully by introducing thiocyanate with 5% chloride ion through post-treatment. Through surface ligand engineering, short-chain ligand and inorganic ligand passivation defects are introduced to optimize the device. Finally, the obtained PQDs have stable photoluminescence and electroluminescence spectra, 467 nm, FMHM 16 nm, the PQDs are aligned, the size is about 8 nm, and the device efficiency EQE is 0.5%. This strategy provides a new idea for the synthesis of blue luminescent PQDs, and provides a research basis for the further realization of efficient and stable PQDs and subsequent devices.

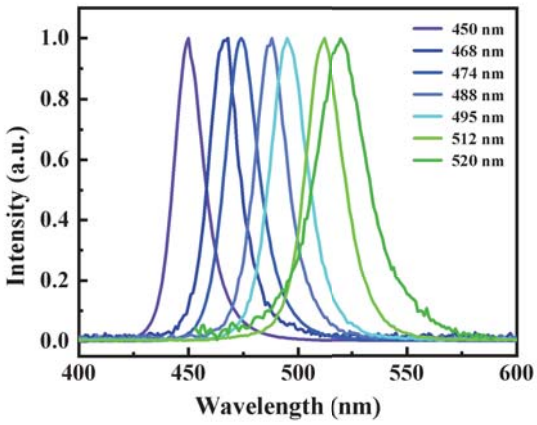

Fig. 1. Photoluminescent spectra

• **Table 1.** PL properties of the samples.

•

Sample	PL Peak (nm)	FWHM (nm)
1	520	27
2	512	20
3	495	19
4	488	17
5	474	18
6	468	16
7	450	15

References

[1] Chenghao Bi, Zhiwei Yao, Xuejiao Sun, Xuecheng Wei, Junxi Wang, and Jianjun Tian* Adv. Mater. 2021, 33, 2006722.

[2] Hanwen Zhu, Guoqing Tong*, Junchun Li, Enze Xu, Xuyong Tao, Yuanyuan Sheng, Jianxin Tang* and Yang Jiang* Adv.Mater.2022, 34, 2205092.

High-performance inverted quantum rods light-emitting diode

Zebing Liao, Kumar Mallem*, Maksym F. Prodanov*, Abhishek K. Srivastava**

***State Key Laboratory on Advanced Displays and Optoelectronics Technologies, Department of Electronics and Computer Engineering, The Hong Kong University of Science and Technology**

As extensive efforts were invested in quantum dot LED, the highest EQE of green and red QLED has achieved close to the theoretical limits of 25 %. Blue QLED also has been improved to 20%. The further improvement was limited by the intrinsic properties-outcoupling efficiency. The emitting light was trapped inside of the QLED device due to different light transmit modes, such as surface plasmons, waveguide mode, and substrate mode. Although many researchers had tried to enhance the outcoupling efficiency by adopting an additional scattering layer or fabricating a well-designed top-emitting QLED device, the final results show a limited improvement. Quantum rods, due to its rods shape, behave with anisotropic emission, which can double the outcoupling efficiency. However, as the result of little research input and inherent flaws, the performance of QRLED still falling behind. The highest EQE and peak luminance of QRLED only achieve 15.7% and 10,4000 cd m^{-2}. There still is enough space to improve it compared to the theoretical limits (40 %).

Here, we developed a high-performance inverted QRLED device. Replacing solution-processed HTL (like PVK, TFB, or Poly-TPD) with small molecule HTL, such as CBP or TCTA, the EQE of the device improved from 4~5 % to 21 %, which is the highest value ever reported and comparable with QDLED. The peak luminance also achieved 110,000 cd m^{-2}.

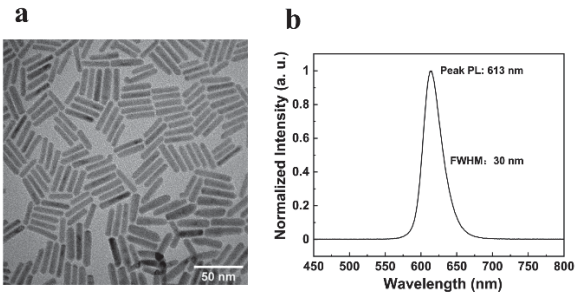

Figure 1 a) The TEM image of CdSe/ZnS QRs, the length of QRs around 20 nm. **b)** The PL spectrum of QRs.

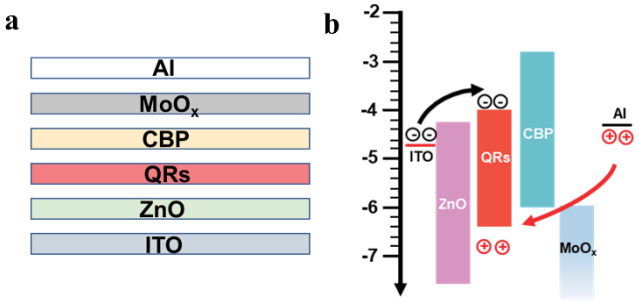

Figure 2 a) The QRLED device structure and **b)** energy level diagram.

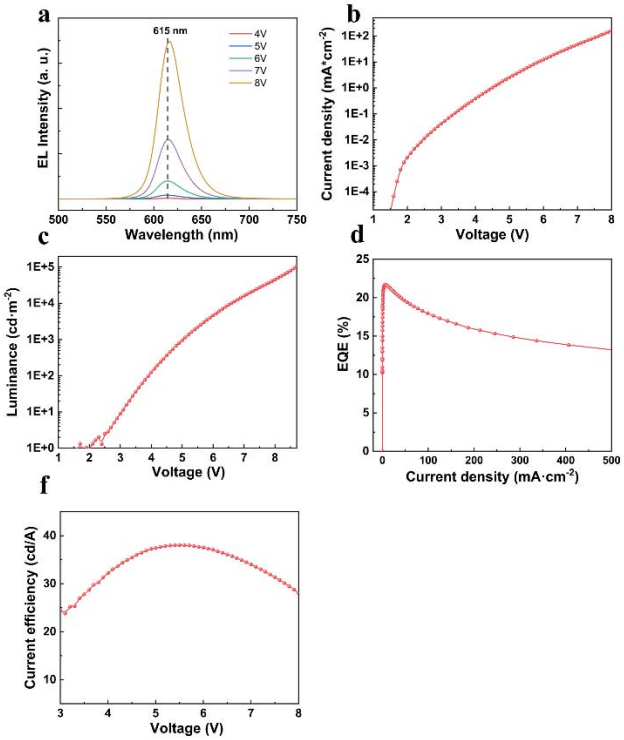

Figure 3 a) The EL spectrum of QRLED at different voltage from 4 V to 8 V. b) The current density verse voltage. c) The luminance verse Voltage. d) The EQE verse current density. f) The current efficiency verse voltage.

References

[1] 1. Mallem, Kumar, et al. "Solution-Processed Red, Green, and Blue Quantum Rod Light-Emitting Diodes." *ACS Applied Materials & Interfaces* 14.16 (2022): 18723-18735.

Ligand Modification of ZnO Nanocrystals for High Performance Quantum Dot Light Emitting Diodes

*Siqi Jia[1,2], Menglei Hu[1,3], Mi Gu[1], Jingrui Ma[1], Depeng Li[1], Guohong Xiang[1], Pai Liu[1], Kai Wang[1], Peyman Servati[3], Wei Kun Ge[1], and Xiao Wei Sun[1]**

[1] Institute of Nanoscience and Applications, and Department of Electrical and Electronic Engineering, Southern University of Science and Technology, Shenzhen 518055, China
[2] Institute of Advanced Displays, Henan Academy of Sciences, Zhengzhou 450046, China
[3] Department of Electrical and Computer Engineering, University of British Columbia, Vancouver, BC V6T 1Z4, Canada

Colloidal quantum dots (QDs) have garnered significant interest due to their narrow emission line width, size-dependent optical properties, and high photoluminescence quantum yield (PLQY).[1–3] Their colloidal nature makes them particularly attractive for realizing low-cost and solution-processable quantum dot light-emitting diodes (QLEDs), which are considered a leading contender for next-generation display applications.[3,4] QLEDs can be thought of as a p-i-n diode, with the QD emission layer as the intrinsic layer, where electron and hole radiative recombination primarily happens. However, the interfacial layers sandwiching the QDs layer are equally important as they provide the charge carrier transportation from the electrodes and injection into the QDs layer.[5,6] In recent years, metal oxide (e.g., ZnO) nanocrystals have been introduced as electron transport layers (ETL) in the QLEDs structure, effectively unleashing the potential of QLEDs.[7] The function of the ZnO nanocrystals and the interplay between ZnO and QD have been studied by researchers, showing that they cannot be neglected in the development of QLEDs.[8,9]

As the electron transport layer in quantum dot light-emitting diodes (QLEDs), ZnO suffers from excessive electrons which lead to luminescence quenching of the quantum dots, and charge-imbalance in QLEDs. Therefore, the interplay between ZnO and quantum dots requires an in depth understanding. In this study, we employed DFT and COSMOSL simulations to investigate the effect of sulfur atoms on ZnO. Based on the simulations, we adopted thiol ligands (specifically 2-Hydroxy-1-ethanethiol) to modify the ZnO nanocrystals. This modification alleviated the excess electrons without causing any additional issues in the charge injection in QLEDs. This modification strategy proved effective in improving the performance of red-emitting QLEDs, achieving an external quantum efficiency of over 23% and a remarkably long lifetime T95 of >12000 h at 1000 cd/m2. Importantly, we investigated the relationship between ZnO layers with different electronic properties and their effect on the adjacent quantum dots through single quantum dot measurement. Our findings show that the ZnO surface defects and electronic properties can significantly impact the device performance, highlighting the importance of optimizing the ZnO-QD interface, and showcasing a promising ligand strategy for the development of highly efficient QLEDs.

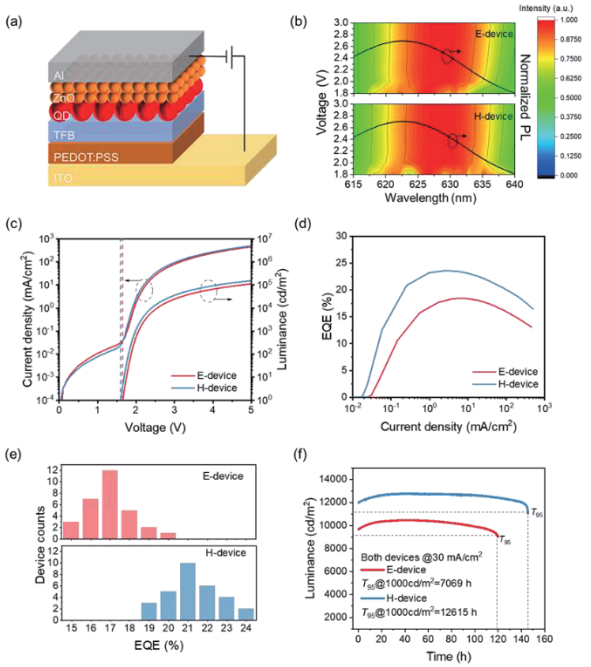

Figure 1. QLED based on different ZnO characterizations. a) Schematic device structure. b) Electroluminescent spectra of E-device and H-device. c) Current-voltage-luminance characteristics. d) External quantum efficiency of E-device and H-device. e) Statistic chart of maximum external quantum efficiency of devices. f) Lifetime of different device.

References

[1]. Liu, M.; Yazdani, N.; Yarema, M.; Jansen, M.; Wood, V.; Sargent, E. H. Colloidal Quantum Dot Electronics. *Nat Electron* 2021, 4 (8), 548–558.

[2]. García de Arquer, F. P.; Talapin, D. v.; Klimov, V. I.; Arakawa, Y.; Bayer, M.; Sargent, E. H. Semiconductor Quantum Dots: Technological Progress and Future Challenges. *Science* (1979) 2021, 373 (6555).

[3]. Jia, S.; Tang, H.; Ma, J.; Ding, S.; Qu, X.; Xu, B.; Wu, Z.; Li, G.; Liu, P.; Wang, K.; Sun, X. W. High Performance Inkjet-Printed Quantum-Dot Light-Emitting Diodes with High

Operational Stability. *Adv Opt Mater* 2021, 2101069, 2101069.

[4]. Triana, M. A.; Hsiang, E. L.; Zhang, C.; Dong, Y.; Wu, S. T. Luminescent Nanomaterials for Energy-Efficient Display and Healthcare. *ACS Energy Lett* 2022, 7 (3), 1001–1020.

[5]. Kagan, C. R.; Lifshitz, E.; Sargent, E. H.; Talapin, D. v. Building Devices from Colloidal Quantum Dots. *Science* (1979) 2016, 353 (6302).

[6]. Yang, Z.; Gao, M.; Wu, W.; Yang, X.; Sun, X. W.; Zhang, J.; Wang, H. C.; Liu, R. S.; Han, C. Y.; Yang, H.; Li, W. Recent Advances in Quantum Dot-Based Light-Emitting Devices: Challenges and Possible Solutions. *Materials Today.* Elsevier B.V. April 1, 2019, pp 69–93.

[7]. Qian, L.; Zheng, Y.; Xue, J.; Holloway, P. H. Stable and Efficient Quantum-Dot Light-Emitting Diodes Based on Solution-Processed Multilayer Structures. *Nat Photonics* 2011, 5 (9), 543–548.

[8]. Yoon, S. Y.; Lee, Y. J.; Yang, H.; Jo, D. Y.; Kim, H. M.; Kim, Y.; Park, S. M.; Park, S.; Yang, H. Performance Enhancement of InP Quantum Dot Light-Emitting Diodes via a Surface-Functionalized ZnMgO Electron Transport Layer. *ACS Energy Lett* 2022, 7 (7), 2247–2255.

[9]. Noh, K.; Kim, M.; Lee, S. H.; Yun, H. S.; Lim, T. H.; Choi, Y.; Kim, K. J.; Jiang, Y.; Beom, K.; Kim, M.; Kim, Y. G.; Lee, P.; Oh, N.; Kim, B. H.; Shin, C.; Lee, H. H.; Yoon, T. S.; Shim, M.; Lim, J.; Kim, K. B.; Cho, S. Y. Effect of Ethanolamine Passivation of ZnO Nanoparticles in Quantum Dot Light Emitting Diode Structure. *Current Applied Physics* 2019, 19 (9), 998–1005.

The Strategies to Improve the Morphology of the Inkjet Printing Perovskite Microarrays

Mingchao Zhu, Xi Lan, Mengyao Tian, Guijun Li
Key Laboratory of Optoelectronic Devices and Systems of Ministry of Education and Guangdong Province, Shenzhen University, Shenzhen, China.

Metal halide perovskites (MHPs) have excellent optical emission properties and can be used in a variety of optoelectronic devices. Multifunctional and low-cost inkjet printing（IJP） is a powerful technology to achieve high-density pixelated perovskite microarrays. However, during the inkjet printing process, the coffee ring or other poor morphology often lead to uneven thickness and seriously reduce the quality of perovskite microarrays. In this work, we study the effect of different ratio of the dual solvents (dodecane and methylbenzene) as well as the number of different printing droplets on the improvement of the morphology, and successfully prepare perovskite microarrays with uniform thickness and good morphology. This work provides a certain reference for preparing perovskite color conversion layers.

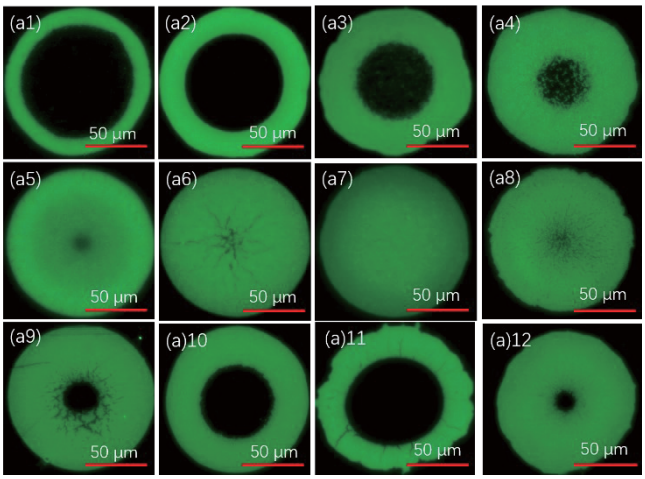

Fig. 1. The 2D PL microscope photographs of microarrays that were printed with different ratio of dual solvents (dodecane : methylbenzene) with (a1) 10:0,(a2) 9:1, (a3) 8:2,(a4) 7:3,(a5) 6:4,(a6) 5:5, (a7) 4:6,(a8) 3:7, (a9) 2:8,(a10) 1:9,(a11) 0:10 and (a12) 4:6 which the solvent without PEO.

References

[1] Giovanni Vescio., et al., High Quality Inkjet Printed Emissive Nanocrystalline Perovskite $CsPbBr_3$ Layers for Color Conversion Layer and LEDs Applications. Adv. Mater. Technol. 2022, 7, 2101525

Illumination and Shadow Rendering in Polygon-Based Computer-Generated Holography

Jiaqi Dong, Bo-Ru Yang, Zong Qin*

***School of Electronics and Information Technology, Sun Yat-sen University, Guangzhou, China**

Holography is one of the most promising 3-dimensional (3D) display techniques since it is the only method to record and reconstruct an arbitrary wavefront without information loss [1]. Instead of traditional optical holography, computer-generated holography (CGH) enables the rendering of arbitrary virtual scenes, making holographic techniques more practical. However, the limited space-bandwidth production of modern spatial light modulators (SLMs) and the low rendering speed astrict the applications of CGH. Compared to the hardware limitation, enhancing the CGH rendering speed is more practical using modern computing hardware with optimized algorithms. Learning-based algorithms can achieve real-time rendering with detailed visual information [2]. However, these algorithms are primarily trained for specific domains, and it is challenging to render ultra-high-definition holograms using neural networks.

We proposed a semi-analytical polygon-based method to achieve both high rendering speed and texture mapping [3]. To synthesize texture information, we first draw the reference triangle in an array; then we can obtain G_r by a fast Fourier transform (FFT). Finally, we determine the rendered triangle's spectrum by sampling G_r according to the affine relation. Figure 1 illustrates the whole process. Since sampling is naturally included in the drawing stage, texture information can be easily synthesized.

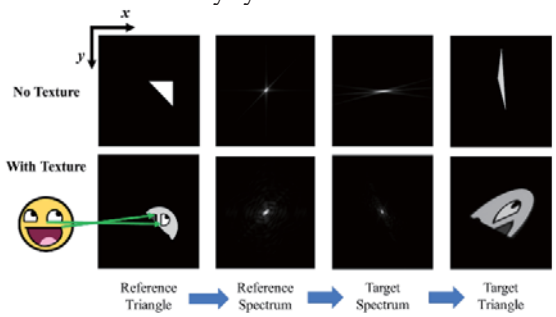

Fig. 1. The semi-analytical rendering process.

As for occlusion handling, we proposed a Z-buffer-based method [4]. We first calculate the depth distribution of the scene and store it in a buffer named "Z-buffer." Next, we copy the "Z-buffer" to another buffer named "Z-tmp" and cover the depth value of the rendered triangle's corresponding position. In the drawing stage, we sample the depth values of the fragment in "Z-buffer" and "Z-tmp" and compare the values to judge if the fragment should be discarded. After this modification, we achieved complex occlusion handling, e.g., three triangles in the same depth occluding each other (see "Overlap" in Fig. 2).

Shadow is the scene's occluded part in the view of the light source, named "light space." By transforming the model into the light space, we can obtain the visible area of the light source. Next, in the drawing stage, we can determine if the fragment is in the invisible area of the light space. Therefore, shadow casting can be achieved with additional occlusion handling. Figure 2 illustrates the rendered results.

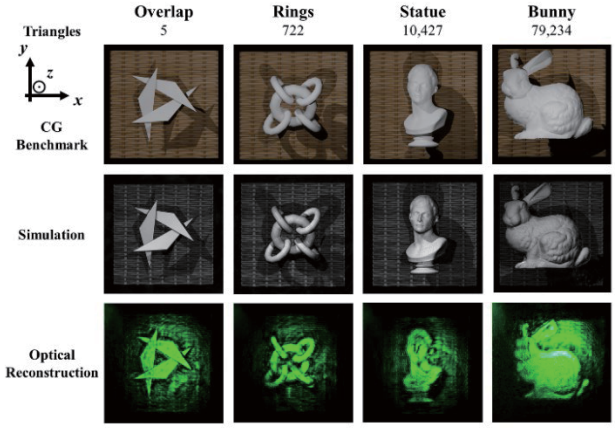

Fig. 2 The simulation and optical reconstruction results with occlusion handling and shadow casting.

As for the rendering speed, we proposed quadrilateral-based semi-analytical rendering to reduce the FFTs and sampling process. Whatsmore, our rendering pipeline can be parallelly optimized because the triangles' depth order does not affect the occlusion handling process. Graphics Processing Units (GPUs) can also accelerate the rendering process. Our rendering pipeline's maximal rendering speed exceeds 5000 triangles per second with the above optimizations.

In this abstract, we introduced our semi-analytical polygon-based method, which can achieve higher efficiency in texture mapping, occlusion handling and shadow casting. In the future, we will further optimize our algorithm's rendering speed and robustness and achieve more visual effects, making the rendered CGH more visually realistic.

References

[1] C. Chang, K. Bang, G. Wetzstein, B. Lee, and L. Gao, *Optica*, 7(11), 1563-1578 (2020).

[2] Y. F. Peng, S. Choi, N. Padmanaban, and G. Wetzstein, *ACM Trans. Graph.*, 39(6), Article 185 (2020).

[3] J. Dong, J. Hu, B.-R. Yang, and Z. Qin, in *Frontiers in Optics + Laser Science 2022 (FIO, LS)*(Optica Publishing Group, Rochester, New York, 2022), p. JW4B.50.

[4] J. Dong, B.-R. Yang, and Z. Qin, *Opt. Express*, 31(9), (2023).

Using time and spatial multiplexing to reduce speckle for augmented reality head-up display

Yen – Jung Chen [1], ***Hung – I Chang***[1], ***You – Si Lin***[1], ***Hoang – Yan Lin***[1]

Graduate Institute of Photonics and Optoelectronics, National Taiwan University, No. 1, Sec. 4, Roosevelt Road, Taipei, 10617, Taiwan

In the research of the Dual-focal-plane Multi-color Head Up Display with Holographic Imaging [1] based on LCoS (Liquid Crystal on Silicon) and holographic projection, the speckle issue caused by using lasers as the light source severely affects the image quality. When the speckle contrast is too large, the image resolution and the edge sharpness of the images may become low , resulting in the driver's inability to quickly understand the road conditions or dashboard information, thus affecting the overall driving experience and even driving safety. This causes problems of driving experience for the driver.

This paper proposes an effective method to reduce the speckle problem by space division multiplexing with color mixing in the experiment. The proposed method, using a time multiplexing [2], adopts a "half-space half-time" configuration to reduce the speckle problem more effectively than the conventional temporal method. We introduce the holographic projection system and the experimental setup, followed by an explanation of the speckle phenomenon and its principles.

In this experiment, an RGB laser device and a single-panel LCoS are used to present holographic images onto the diffuser. The laser device, as shown in Figure. 1, coupled with a chopper, projects red, green, and blue lights separately with two different time sequences. The optical components are used to combine the three different colored light paths before projecting onto the LCoS. Due to the persistence of vision, although the holographic image seen can achieve the combination of RGB into white light, the speckle reduction effect is already achieved by dividing the RGB lasers into two sets with time sequences projection.

Considering the human eye's temporal persistence time of approximately 1/24 second, within this time frame, approximately 4 holographic images can be played: two RG holographic images and two blue holographic images, as shown in Figure. 2. With this design, we can have one additional holographic image within a single temporal persistence time, thereby further reducing the image received by the human eye for the second time.

In this paper, it is known that space multiplexing is utilized to divide a hologram into two regions: one for green phase and the other for red phase, as shown in Fig. 3. By overlapping the holograms of the two colors through an optical path, the speckle can be effectively reduced. We aim to further mitigate the speckle issue by incorporating time multiplexing into the system.

As shown in Fig. 4. presents the preliminary experimental results of temporal multiplexing. When measuring the speckle, we ensured that the measurements were taken in densely populated regions of the hologram to minimize any variations. The speckle contrast for the left image, representing the hologram of green light, is 28.20%.The middle image, representing the hologram of red light, has a speckle contrast of 14.36%. Finally, the right image shows the hologram formed by overlapping the green and red holograms using spatial multiplexing, resulting in a speckle contrast of 11.28% for the resulting yellow light hologram.

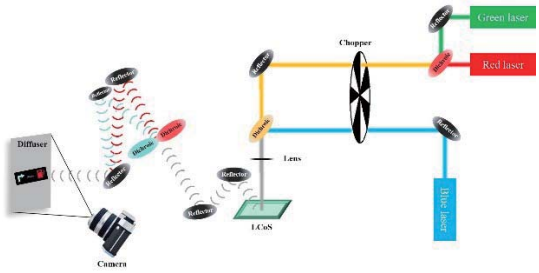

Fig. 1. Experimental Architecture

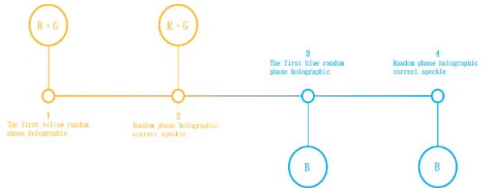

Fig. 2. Persistence of vision within time sequences

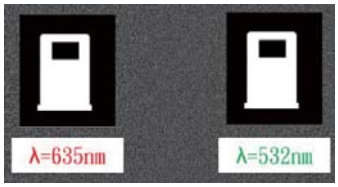

Fig. 3. A hologram is devided into two regions

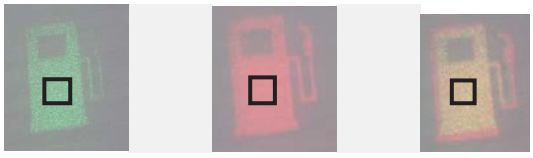

Fig. 4. Comparison of three-color speckle

References

[1] Yu-Ming Hu, " Dual-focal-plane multi-color Head Up Display with Holographic Imaging." Master thesis from National Taiwan University (2022)

[2] Takaki, Yasuhiro, and Masahito Yokouchi. "Speckle-free and grayscale hologram reconstruction using time-multiplexing technique." Optics express 19.8 (2011): 7567-7579.Takaki, Yasuhiro, and Masahito Yokouchi. "Speckle-free and grayscale hologram reconstruction using time-multiplexing technique." Optics express 19.8 (2011): 7567-7579.

Computational vision-correcting near-eye light field displays by manipulating vector sampling rays

Yuqing Qiu*, Bo-Ru Yang*, and Zong Qin*

***School of Electronics and Information Technology, Sun Yat-Sen University, Guangzhou, 510006 China.**

Considering the large population with impaired vision, a vision correction solution that can adapt to refractive errors such as myopia, hyperopia, astigmatism, and high-order aberrations (HOAs) is required for wearable VR/AR devices, as vision-correcting near-eye displays (NEDs).

Wearing a user's own spectacle is unsuitable because a very long eye relief is required, increasing the system volume. Adding additional optics is a common solution many studies considered, e.g., electrically-controlled focus-tunable lens [1] that changes the focal power as needed. Yet, this solution requires a complicated device and cannot deal with astigmatism and HOAs by only changing the focal length. Alternatively, Wu et al. [2] designed an AR NED with added freeform optics that can address most refractive errors, especially astigmatism. However, in addition to the increase in system complexity, different freeform optics must be fabricated for different prescriptions, significantly increasing costs. Computer-generated holography (CGH) was further considered for computational vision correction [3]. However, the CGH itself is way far from practical use. Huang et al. [4] realized vision correction in light field displays by applying heterogeneous prefiltering algorithms in elemental images. The plural elemental images provide a higher degree of freeform in image compensation. Nevertheless, the method eliminates the light field display's ability of 3D display.

This study proposes a new vision-correcting NED to overcome the above issues. Besides myopia and hyperopia, we utilize integral imaging light field displays (InIm-LFDs) to address astigmatism and HOAs. Different prescriptions can be adapted with no hardware modification. Moreover, the InIm-LFD's ability of true-3D display is wholly retained.

First, for myopia or hyperopia, the InIm-LFD directly presents optically nearer or farther images through its ability of computational monocular focus cue. Next, for astigmatism and HOAs, whose focal length varies with meridians, we computationally manipulate vector sampling rays that integrate for a 3D image to make them refocused on the retina, as Fig. 1(a) shows. The manipulation of the rays is fully computational by changing positions of the pixels. The InIm-LFD's unique feature that a voxel is formed by multiple sampling rays, whose directions are determined by digital signals, enables computational vision correction.

The proposed method is verified by taking astigmatism as an example. We adopt a previously proposed image formation model of InIm-LFDs [6] (see Fig. 2(a)), based on which a sampling rays' retinal footprint and a retinal integral image are simulated (see Fig. 2(b)). Next, the emmetropic Arizona eye model is replaced with an astigmatic eye model (+2.0D), causing the sampling rays to diverge on the y-direction, then producing an astigmatic retina image (see Fig. 2(b)). The proposed method then optimizes the pixel positions for refocused sampling rays through the genetic algorithm. As a result, the rightmost subfigure in Fig. 2(b) shows perfectly refocused rays. Nevertheless, the integral image is slightly blurred compared with the normal eye because each elemental image is inevitably astigmatic. Fortunately, the narrow beam produced by the lenslet's tiny aperture makes each retinal elemental image much less blurred than ordinary imaging, making the corrected integral image nearly as sharp as the normal eye. Figure 2 also compares a scene observed in the above three cases.

We believe the proposed vision correction method could adapt InIm-LFDs to various vision defects with no increase in system volume, complexity, and costs.

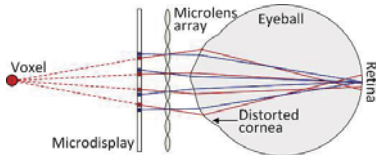

Fig 1. Manipulation of sampling rays' directions for vision correction (red & blue: original & corrected rays).

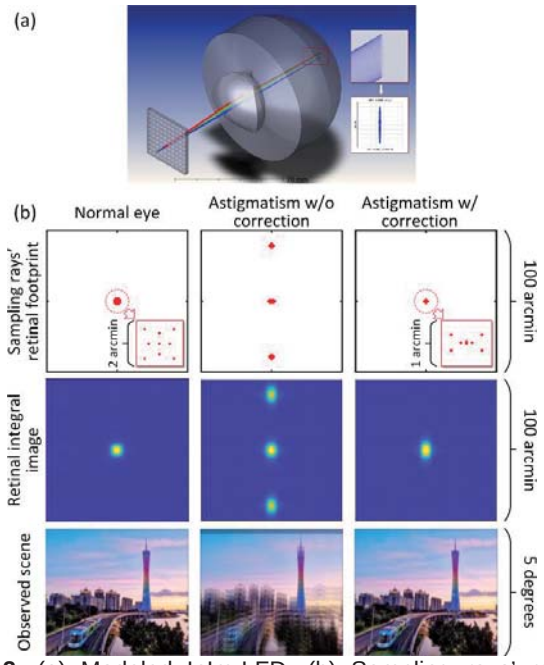

Fig 2. (a) Modeled InIm-LFD. (b) Sampling rays' retinal footprint, integral image, and an observed scene.

References

[1] N. Padmanaban, et al. *PNAS, 114(9), 2183(2017).*
[2] J.Y. Wu & J. Kim *Opt. Express, 28(5): 6225 (2020).*
[3] Y. Itoh, et al. *IEEE TVCG, 27(3), 1916 (2019).*
[4] F.-C. Huang, et al., *ACM T. Graph. 33(4), 1 (2014).*
[5] Z. Qin et al., *J. SID, 27(4), 238 (2019).*
[6] Y. Zhong & H. Gross, *JOSA A, 35(8), 1385 (2018).*

Viewing Angle Improvement of the Floating Display System Based on Dihedral Corner Reflector Array

Cheng-Hsun Tsai, Chih-Hao Chuang**, Shi-Hwa Huang***, Chien-Yu Chen****

* Graduate Institute of Photonics and Optoelectronics, and Department of Electrical Engineering, National Taiwan University, Taipei 10617, Taiwan

** Department of Photonics, Feng Chia University, 100 Wenhwa Rd., Seatwen, Taichung 40724, Taiwan

***Graduate Institute of Color and Illumination Technology, National Taiwan University of Science and Technology, Taipei 10607, Taiwan

DCRA (Dihedral corner reflector array) is a component that can project images onto parallel opposing planes [1]. Its characteristics make it suitable for applications in floating image displays. However, while generating floating images, it also introduces various degradation phenomena. Several methods have been proposed to improve these issues, such as a radial arrangement to enhance the viewing angle [2] and a louver structure to suppress ghosting [3]. Vibration to suppress image degradation [4]; each of these methods addresses specific problems. In this study, we propose a novel eight-pointed star-shaped DCRA to augment the viewing angle.

DCRA relies on the second reflection of light on two mutually perpendicular surfaces to form an image at the location of the image. This enables people to see images floating in the air. DCRA does not introduce aberrations or distortions and possesses a simple repetitive array structure with excellent projection quality, making it suitable for floating display applications.

We designed a new eight-pointed star DCRA as shown in Figure 1, with eight right angles. Firstly, the increase in right angles expands the visible range of the image, allowing the component to capture light and perform second reflections from multiple azimuths. Secondly, while the light efficiency at the front-facing right angle is lower than that of the diamond-shaped DCRA, the light efficiency remains relatively stable as the angle changes. Lastly, as the viewing angle of the diamond-shaped DCRA increases, the light efficiency drops drastically, whereas the second-reflected image of the eight-pointed star-shaped DCRA remains present, and the light efficiency remains stable.

We analyzed the conditions and principles of the second reflection in DCRA and designed the eight-pointed star-shaped DCRA to augment the viewing angle. Through the optical software *Tracepro*, we compared the light efficiency of the eight-pointed star-shaped DCRA and diamond-shaped DCRA under different viewing angles, as shown in Figure 2. We observed that the diamond-shaped DCRA's light efficiency is highest at a viewing angle of 0 degrees and decreases with increasing angles. At 45 degrees, there is no light efficiency. In contrast, although the eight-pointed star-shaped DCRA's light efficiency is only 50% at a viewing angle of 0 degrees, it does not show significant degradation as the viewing angle increases. The light efficiency returns to 50% at a viewing angle of 45 degrees. Therefore, the eight-pointed star-shaped DCRA is a novel DCRA that can augment the viewing angle.

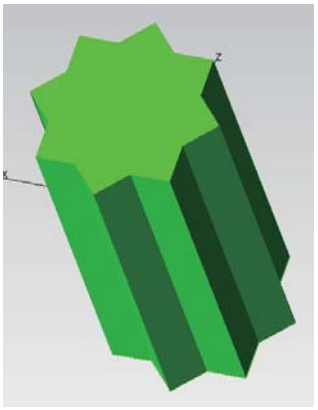

Fig. 1. Eight-pointed star DCRA structure

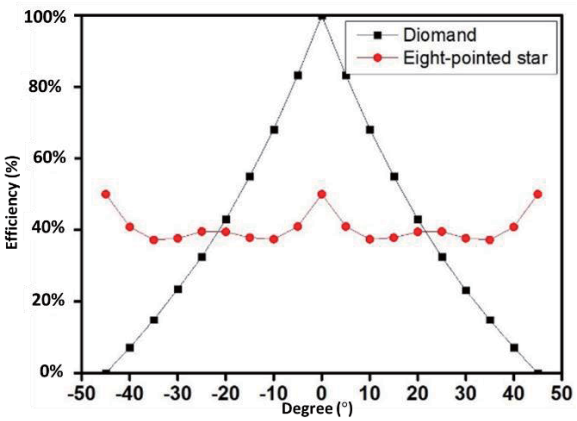

Fig. 2. Comparison of Light Efficiency Graph

References

[1] T. Yamane, S. Maekawa, Y. Utsumi, I. Okada and A. Yamaguchi, "Fabrication and evaluation of Dihedral Corner Reflector Array for floating image manufactured by synchrotron radiation," 2015 International Conference on Electronics Packaging and iMAPS All Asia Conference (ICEP-IAAC), Kyoto, Japan, 2015, pp. 436-439, doi: 10.1109/ICEP-IAAC.2015.7111052.

[2] Yuta Yushimizu, et al. " Radially Arranged Dihedral Corner Reflector Array for Wide Viewing Angle of Seamless Floating Image." Optics express 26.7 (2018): 8883-8889.

[3] Y. Osada and Y. Bao, "Design of Ghost-free Aerial Display by Using Polarizing Plate and Dihedral Corner Reflector Array," *2021 5th International Conference on Imaging, Signal Processing and Communications (ICISPC)*, Kumamoto, Japan, 2021, pp. 67-70, doi: 10.1109/ICISPC53419.2021.00020.

[4] YUCHI YAHAGI, et al. " Suppression of floating image degradation using a mechanical vibration of a dihedral corner reflector array" Optics Express 33145.

A multi-focal-plane head-up display using polarization multiplexing

Yi Liu*, Jiaqi Dong*, Bo-Ru Yang*, and Zong Qin*
***School of Electronics and Information Technology, Sun Yat-Sen University, Guangzhou, China**

Vehicle head-up displays (HUDs) project various in-vehicle information into a driver's eyes through a combiner or windshield, which can keep the driver's eyes on the road, thus significantly improving driving safety. Recently, the combination of HUD and augmented reality (AR) enables the HUD to carry richer driving information. An AR-HUD typically requires two or more focal planes, respectively presenting augmented information for interacting and basic driving information such as speed [1]. Besides that, AR-HUDs still face many technical difficulties in the optical system, including multiple focal planes, larger FOV, larger eyebox, etc., so the optical system design is demanding.

To develop an AR-HUD using a single PGU and a single freeform mirror, Qin et al. [2] proposes to divide a single PGU into two logically separated parts and optically relay one of them to a new position to create two focal planes. In this manner, the expanded volume of AR-HUDs is addressed while the resolution of the PGU is halved for either image. Therefore, in this study, we propose a practical AR-HUD with a large FOV and dual focal planes, either of which utilizes the PGU's full resolution, using a single freeform mirror. A compact volume is achieved by folding the light path with polarization multiplexing which guarantees fully utilizing the PGU's resolution.

Based on the system architecture of dual-focal-plane HUDs using two PGUs, the AR-HUD proposed in this paper folds the light path by polarizing elements and a mirror, as shown in Fig. 1(a). The specification of the proposed dual-focal-plane AR-HUD is shown in Table 1. After optical design and optimization, sufficient image quality was obtained in the entire eyebox and the FOV. All MTF values are beyond approximately 0.3 at the cutoff frequency of 6.7 cycle/mm determined by the PGU resolution, suggesting enough image clarity.

Table 1. Specification of the proposed AR-HUD

	Far virtual image	**Near virtual image**
Throw distance	10 m	2.5 m
Horizontal FOV	-6.5°– 6.5° (13°)	-5°– 5° (10°)
Vertical FOV	-5.5°– -1.5° (4°)	-7.5°– -6.5° (1°)
Eyebox	130 mm by 60 mm	
Windshield	Windshield for HUD	
Eye-relief (driver to windshield)	800 mm	
Pupil diameter	5 mm	

Apart from imaging clarity, the distortion and the vertical binocular disparity are crucial to a binocular vision system like HUDs. In an ideal system, the vertical binocular disparity should be zero. In a real HUD, the vertical binocular disparity should be within 2.5 mrad to avoid visual discomfort. Moreover, slight distortions can be solved by digital calibration. Besides that, the simulated vertical binocular disparity provided by Zemax OpticStudio is always less than 2.5 mrad, so drivers moving within the eyebox will not suffer discomfort due to vertical binocular disparity.

After the simulation results met Table 1, we built the designed HUD. The actual FOV areas are marked in Fig. 1(b) and (c) with yellow squares. By estimating the size of the image on the film, the actual FOV is 11.0° by 1.4° and 13.9° by 4.4° for near and far virtual images, respectively. The size of the real eyebox is slightly larger than 130 mm by 60 mm. The maximum value of the vertical binocular disparity calculated by the height difference of the images taken by a camera are 1.66 mrad and 3.24 mrad at the center of the eyebox spaced 65 mm apart in the horizontal direction for near and far virtual images, respectively. All results show that the system specifications meet the design requirements. The error of inaccurate manual assembly can be addressed by fixing these optical elements inside a housing that is mechanically designed in future work.

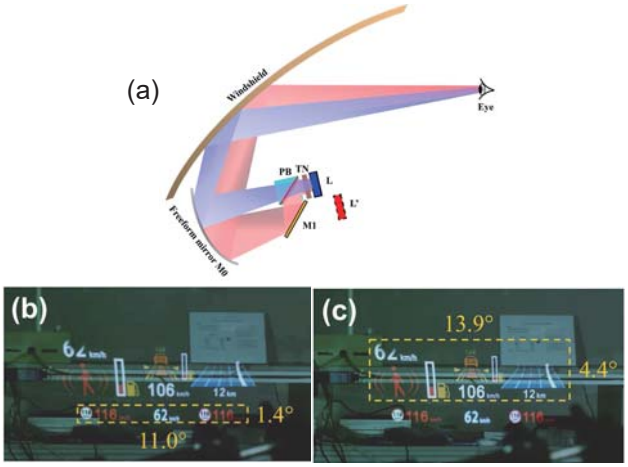

Fig. 1. (a) Proposed dual-focal-plane AR-HUD architecture using polarizing elements and a mirror to fold the light path. The FOV of (b) near and (c) far focal planes, respectively.

References

[1] Shi, Bingchuan, et al. "34.3: A dual depth head up display system for vehicle." SID Symposium Digest of Technical Papers. Vol. 49. 2018.

[2] Qin, Zong, et al. "Dual-focal-plane augmented reality head-up display using a single picture generation unit and a single freeform mirror." Applied Optics 58.20 (2019): 5366-5374.

Advancements in high quality InGaN/GaN multiple quantum wells Micro-LEDs on free-standing GaN substrate: from material to display

Yibo Liu*, Feng Feng*, Zhaojun Liu**, Hoi Sing Kwok*

***State Key Lab of Advanced Displays and Optoelectronics Technologies, HKUST, Hong Kong SAR, China**

****Dept. of Electrical and Electronic Engineering, SUSTech, Shenzhen, China.**

The pursuit of enhancing display technologies has led to a paradigm shift in the field of optoelectronics. Micro-LEDs (Light Emitting Diodes) have emerged as a promising solution, offering unparalleled brightness, energy efficiency, and picture quality. Among the various substrates explored for micro-LED fabrication, free-standing GaN (Gallium Nitride) substrates have emerged as a compelling platform. This work delves into our remarkable progress made in the domain of micro-LEDs, specifically focusing on the material engineering, device physics, and display applications.

In material epitaxy, our GaN-on-GaN structure grows on a free-standing n-GaN substrate, and the ascending structures are shown in Fig. 1(a). At the beginning, the ITO current spreading layer is deposited onto p-GaN, and the following self-aligned fabrication process can refer to our previous publication [1]. The GaN-on-sapphire structure shows significant broadening symmetric rocking curve compared to GaN-on-GaN structure. The FWHM of 002 scan is about 0.08 degree (288 arcsec) and less than 0.013 degree (46.8 arcsec) for GaN-on-sapphire and GaN-on-GaN respectively, indicating the lower threading dislocation densities (TDDs) in GaN-on-GaN, consistent to the Cathodoluminescence (CL) and TEM comparison in Fig. 1(c) and (d).

In the device characterization level, we demonstrate the peak wavelength shift and light output power for purple, blue and green GaN-on-GaN 10 μm device, and current-voltage relation and internal quantum efficiency (IQE) comparison for GaN-on-sapphire and GaN-on-GaN 10 μm device. The peak wavelength/FWHM of EL spectrum is 389.9/8.9 nm, 455.6/16.8 nm and 504.3/23.5 nm for purple, blue and green respectively, and the peak wavelength shift is 0.27, 1.21 and 4.79 nm when the current density up to 500 A/cm^2. Light output power is consistent with the external quantum efficiency (EQE), where the GaN-on-GaN blue is the highest and GaN-on-GaN purple is the lowest, which can be ascribed to the optical loss such as absorption and scattering for shorter wavelength. The IQE of GaN-on-sapphire and GaN-on-GaN blue 10 μm device is calculated by using room-temperature reference method (RTRM) [2] and fitted with ABC model Eq. (1) shown as below, and the result reveals that GaN-on-sapphire device exhibits higher defects (A parameter) and lower current injection efficiency (η_{inj}).

$$\eta_{EQE} = \eta_{LEE} \times \eta_{IQE} = \eta_{LEE} \times \frac{\eta_{inj} B n^2}{An + Bn^2 + Cn^3} \quad (1)$$

At the display level, the GaN-on-GaN micro-display boasting an impressive 3000 PPI (pixels per inch) stands out with its remarkable display uniformity and heightened brightness. The accompanying SEM figures vividly depict the indium bumps' morphology following the flip-chip bonding process. With this cutting-edge technology, the brightness achieved for a pattern display reaches an impressive 90,000 cd/m^2, coupled with an expansive field of view spanning 143 degrees, making it an exceptional choice for AR (Augmented Reality) displays.

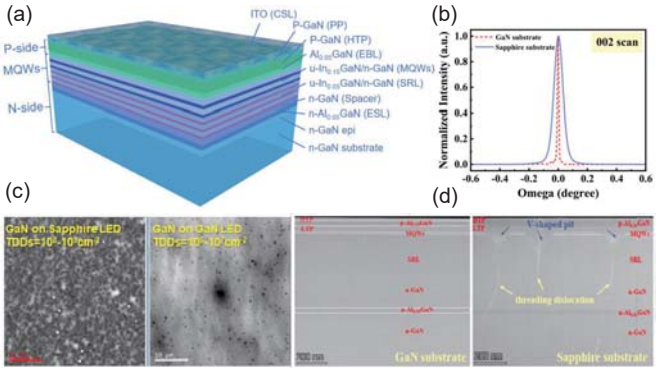

Fig. 1. (a) cross-section of epi-ready structure; (b) 002 scan of rocking curve; (c) Cathodoluminescence; (d) TEM.

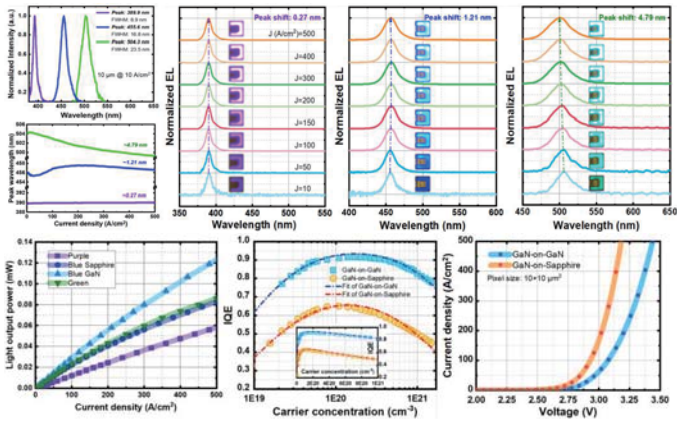

Fig. 2. Device characterization of tri-color GaN-on-GaN devices.

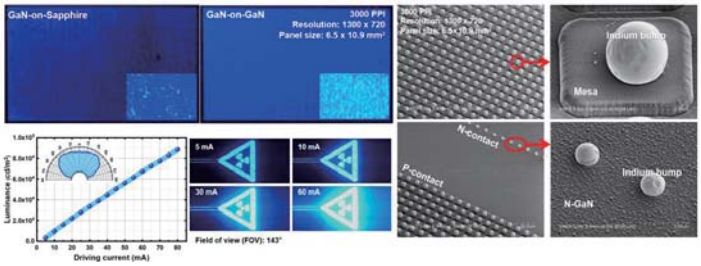

Fig. 1. Display uniformity, luminance and field of view characterization and SEM observation of display array.

References

[1] Y. Liu, et al. *Journal of Physics D: Applied Physics* 55, 315107 (2022).

[2] J.-I. Shim et al. *Nanophotonics* 7.10: 1601-1615 (2018).

High-Yield Transfer of Flip-Chip Structure Micro-LED by Flexible Film

Jiayi Li, Zhaojun Liu*

Department of Electric and Electronic Engineering, Southern University of Science and Technology, Shenzhen, China

***Corresponding Email: liuzj@sustech.edu.cn**

Micro-LED display technology has the potential to become the next generation of display technology due to its advantages such as high brightness and self-illumination. [1] Currently, micro-LED display technology still faces several important issues, including full color display and integration. In order to realize the display function, the micro-LED needs to be integrated into the drive circuit, which can be achieved through monolithic integration and mass transfer.

A common method of mass transfer is to use an elastic stamp to pick up the micro-LED array, which is anchored on the substrate by the photoresist. In this method, the micro-LED array is transferred to the target substrate for wire bonding through a single transfer. But wiring results in limited resolution. Comparing with planer structure micro-LED, flip-chip structures can have a higher pixel density. In this work, the flip-chip structured micro-LED is fabricated. Laser is used to peel off the sapphire substrate, allowing an array of individual micro-LED devices to be transferred onto the flexible film, followed by a secondary transfer to expose the electrodes.

Micro-LED array is fabricated on commercial epitaxial wafer. The structure of mesa is etched by inductively coupled plasma, using SiO_2 as a hard mask. Then, the magnet sputtering is used to deposit indium-tin oxide, act as current spreading laye. After that, electrodes composed of Ti/Al/Ti/Au are deposited by e-beam evaporation. Then the GaN is deeply etched onto the sapphire surface to make the micro-LED devices individual of each other. The structure of single micro-LED is schematically illustrated in figure 1.

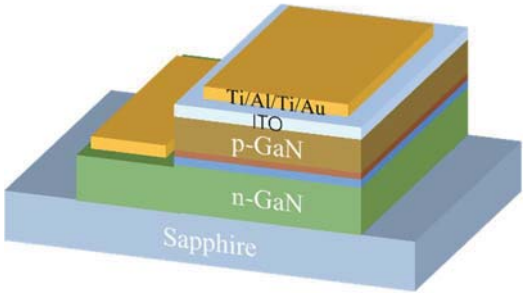

Fig. 1. Schematic diagram of the structure of a single micro-LED.

After completing the fabrication of the individual micro-LED device array, a blue film is pasted on the side of the electrode, followed by a laser introduced into the interface between the sapphire and gallium nitride. The laser used is a solid-state laser with wavelength of 266nm, pulse width of 5us and power of 0.5W. Since GaN has a band gap of 3.3eV, while sapphire has a band gap energy of 9.9eV. Thus, sapphire is transparent to the laser beam with photon energy of 4.7eV [2,3]. The laser passes through the sapphire and the irradiation causes the gallium nitride at the interface to break down into Ga droplets and N_2, so that the sapphire can be easily peeled off, leaving the micro-LED array on the blue film, as shown in figure 2(a). Next, the micro-LED is attached to a second film with higher viscosity. Due to the difference in viscosity, the first film can be easily removed, leaving the micro-LED array on the second film, prepared for the subsequent bonding.

By adjusting the viscosity of the two layers during the transfer process, the transfer yield of micro-LED can reach more than 99%. The results show that a flip-chip structured micro-LED array can be successfully transferred to a flexible surface by using laser lift-off technology and flexible film transfer. This indicates that the individual micro-LEDs of flip-chip structure have the potential to be applied to flexible or curved displays.

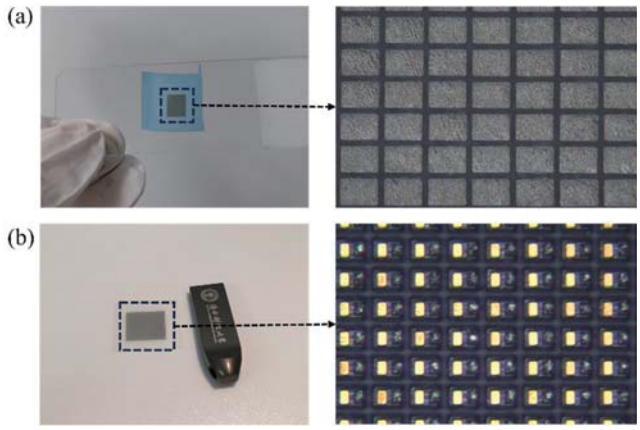

Fig. 2. (a) The micro-LED array transferred onto the blue film after LLO. (b) The micro-LED array is transferred from blue film to UV film, while exposing the electrode.

References

[1] CHEN Z, YAN S K, DANESH C. MicroLED technologies and applications: characteristics, fabrication, progress, and challenges. J Phys D Appl Phys, 2021, 54(12).

[2] Li, S. H. , Lin, C. P. , Fang, Y. H. , Kuo, W. H. , & Su, G. . (2019). Performance analysis of gan-based micro light-emitting diodes by laser lift-off process. Solid State Electronics Letters, 1(2).

[3] Gong, & Gong, Z. (2022). Laser-Based Micro/Nano-Processing Techniques for Microscale LEDs and Full-Color Displays. Advanced Materials Technologies, 2200949–. https://doi.org/10.1002/admt.202200949

Enhancing the Front LEE of Micro-LEDs via Sidewall Transparent Oxide

Tianwen Xia[1,2], Yongzhen Liu[1,2], Zhonghang Huang[1,2], Dalei Wu[1,2], Tao Liang[1,2], Enguo Chen[1,2], Jie Sun[1,2]*, Qun Yan[1,2], and Tailiang Guo[1,2]*

1.College of Physics and Information Engneering, Fuzhou University, Fuzhou 350108, China

2.Fujian Science & Technology Innovation Laboratory for Optoelectronic Information of China, Fuzhou 350108, China

Corresponding author: ceg@fzu.edu.cn

Micro-LED, with its micron-sized inorganic structure, holds great promise as a display device. However, a major challenge associated with the miniaturized size of micro-LED is the significant amount of sidewall emission, which results in crosstalk issues for display devices. To address this problem, this paper proposes an innovative micro-LED structure that incorporates a sidewall light guide structure. This structure involves the sequential addition of SiO_2 and TiO_2 layers to the micro-LED's sidewall, creating a total reflection layer. Consequently, a substantial portion of the light emitted from the sidewall can be effectively directed towards the front of the structure. Through simulations, it has been demonstrated that the implementation of the proposed sidewall light guide structure can enhance the efficiency of front emission for RGB micro-LEDs, particularly within a sidewall inclination degree ranging from 0° to 50°. Additionally, the ratio of front emission to total emission can be improved significantly, reaching 68%.

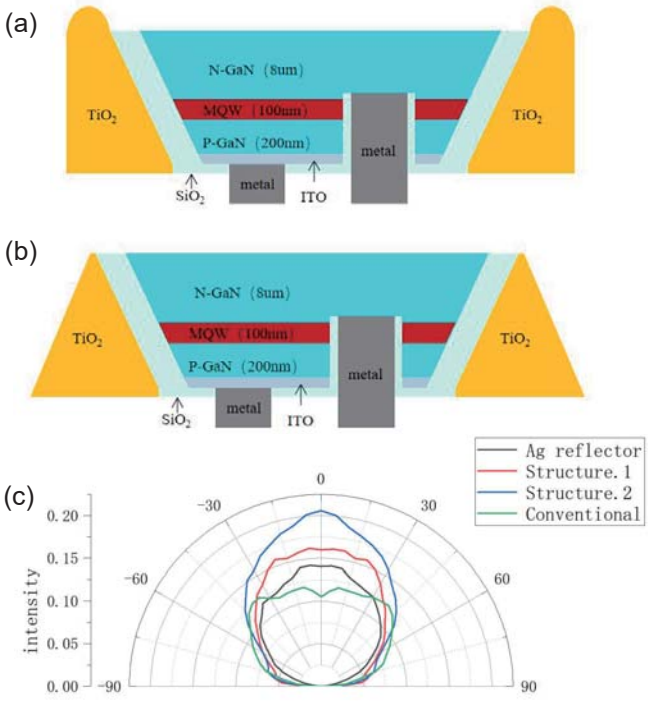

Fig. 1. Schematic diagram of (a) structure.1 and (b) structure.2 of the micro-LED with sidewall transparent media; (c) Far-field intensity distribution of the micro-LEDs with the traditional structure, sidewall Ag reflector and designed structure

Funding. National Key Research and Development Plan of China (Grant No. 2022YFB3603503); National Natural Science Foundation of China (62175032); Fujian Provincial Natural Science Foundation Project (2021J01579).

References

[1] F. Gou et al., Optics Express., 27(12), 746 (2019)

[2] X. Hu et al., Optics & Laser Technology, 154, 108335 (2022)

[3] X. Lai et al., Journal of Materials Science: Materials in Electronics., 31(23), 21361 (2020)

The full-color micro-LED display with quantum dots inkjet printing

Yonghong Lin, Wenjun Huang, Mengyuan Zhanghu, Zhaojun Liu

Department of Electrical and Electronic Engineering, Southern University of Science and Technology, Shenzhen, China

Micro light-emitting diode (Micro-LED) has become as the most promising display technology because of their unique performances, such as small size, high PPI, low power consumption, fast response time, high brightness, high contrast ratio and so on [1]. To achieve commercial application, many challenges need to be solved. The full color technology is one of the most important challenges in display area. The straightforward method is to combine red, green and blue micro-LED to achieve full color display. As the resolution increases, the transfer process has many problems, like low transfer speed, low repeatability, high costs and so on. The alternative way is to use blue or UV micro-LED to excite fluorescence materials. The unique fluorescence materials can achieve effectively red and green light under blue or UV micro-LED. This method can simplify the transfer process as only single-color micro-LED needs to be transferred [2].

Among the fluorescence materials, the colloidal quantum dots (QDs) have considered as an outstanding material for next generation display. The excellent characteristics of QDs are their tunable wavelength, narrow full width at half maximum, high quantum yield and low cost [3]. A combination of blue or UV micro-LED and red/green QDs can become a prospective display technology in the future. The QDs color conversion film needs to be patterned for the micro size of LED. The inkjet printing technology shows promising prospect for QDs deposition on micro-LED. The benefits of provided by inkjet printing are their mask free, simple process, high precision and low consumption of materials [4]. Using quantum dots inkjet printing, the full color micro-LED can be achieved in an effective and simple way.

In this work, we propose an effective way to make an ultra-thick black matrix and print an ultra-thick QDs color conversion film. The ultra-thick black matrix was fabricated using semiconductor processing technology, and this high thickness of the black matrix can remove the crosstalk in the color conversion film and form a QDs film with sufficient thickness for color conversion. Then different thicknesses of QDs films were printed using an EHD printer, and their blue light leakage was measured. Finally, we printed a red/green color conversion layer, then it was integrated on blue micro-LEDs. The film can achieve effective color conversion, and the blue leakage is reduced greatly without a color filter. The brightness of green and red films can reach 257.64 nit and 140.51 nits at the current density of 2 A/cm^2, and their color gamut is 71.19% NTSC. The results show that this method can achieve excellent full-color micro-LED displays.

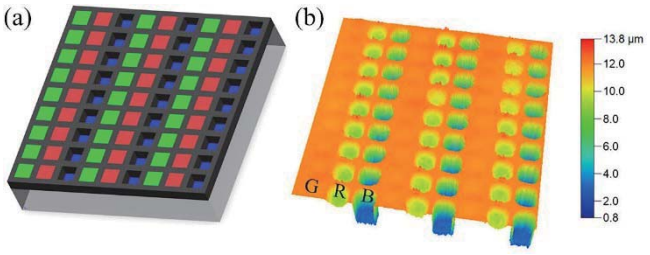

Fig. 1. (a) The schematic of QDs color conversion layer, (b) the 3D morphology image of black matrix and printed QDs ink.

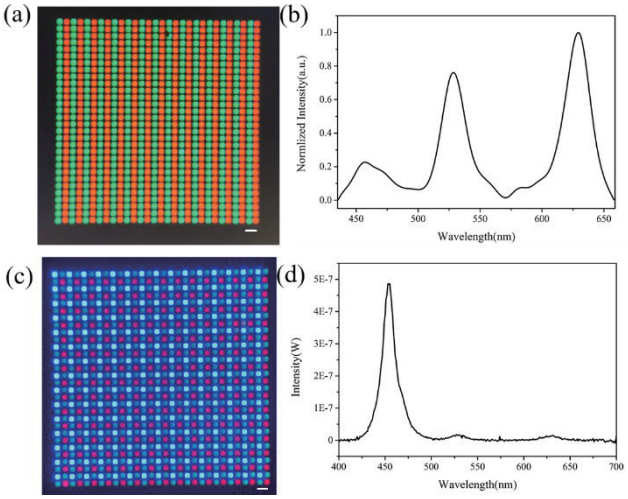

Fig. 2. The illuminous images of the RG (a) and RGGB (c) array and their spectra (b) (d). The scale bar is 30 μm.

References

[1] Wu, T.; Sher, C.-W.; Lin, Y.; Lee, C.-F.; Liang, S.; Lu, Y.; Huang Chen, S.-W.; Guo, W.; Kuo, H.-C.; Chen, Z., *Applied Sciences* 2018, 8 (9).

[2] Liu, Z.; Lin, C. H.; Hyun, B. R.; Sher, C. W.; Lv, Z.; Luo, B.; Jiang, F.; Wu, T.; Ho, C. H.; Kuo, H. C.; He, J. H., *Light: Science & Applications* 2020, 9, 83.

[3] Chen, O.; Wei, H.; Maurice, A.; Bawendi, M.; Reiss, P., *MRS Bulletin* 2013, 38 (9), 696-702.

[4] Jiang, C.; Zhong, Z.; Liu, B.; He, Z.; Zou, J.; Wang, L.; Wang, J.; Peng, J.; Cao, Y., *ACS Appl Mater Interfaces* 2016, 8 (39), 26162-26168.

Design and Application of Micro-LED Pico-Projection Based on Image Fiber

Huajian Jin [1,2], Enguo Chen [1,2,], Yun Ye [1,2], Sheng Xu [1,2], Tailiang Guo [1,2]*

[1] School of Advanced Manufacturing, Fuzhou University, Jinjiang, Fujian Province, China, 362200;

[2] National & Local United Engineering Laboratory of Flat Panel Display Technology, Fuzhou University, Fuzhou, Fujian Province, China, 350108;

*Corresponding author: ceg@fzu.edu.cn

Micro light-emitting diode (Micro LED) has the advantages of high brightness, low power consumption and long life. It has great potential and wide application prospects. Image fiber is a flexible, high resolution and small image transmitting device. The light source and image source of traditional projection system are generated by different devices with large volume and high power consumption. Using micro-LED as the light source and image source of the projection system can greatly reduce the size and power consumption of the system. However, the electrical module and optical module of the micro-LED pico-projection system cannot be separated. We designed a micro-LED pico-projection optical engine based on image fiber, and used image fiber to effectively separate the electrical module and optical module in the optical engine. This optical engine is composed of a projection lens group, an image fiber and a micro-LED. The projection lens group is composed of 5 spherical lenses, with the total length is less than 7mm, the focal length is 2.8mm and the field of view is ±20°. The modulation transfer function (MTF) is higher than 0.8@32lp/mm, and the distortion is less than 3%. The image fiber adopts a multi-core fiber with a diameter of 2mm and a resolution of 32lp/mm. Then, the overall simulation model of the optical engine was built for verification. Finally, we applied the optical engine to a near-eye display device and also built a prototype to verify its feasibility.

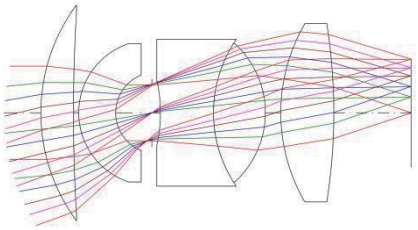

(a)

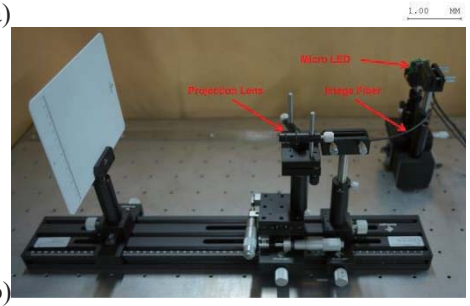

(b)

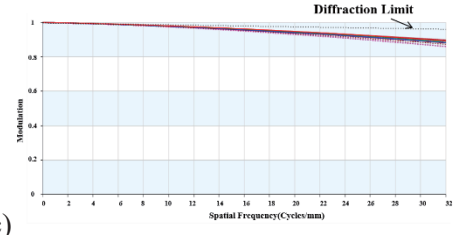

(c)

(d)

Fig. 1. Design result of the projection lens. (a) The projection lens group; (b) Fiber projection optical engine; (c) MTF curve ;(d) Fiber projection image

References

[1] Jiang H. et al. Applied Optics 60.23 (2021): 6971-6977.

[2] Chen. Z . et al. Chinese Optics Letters 17.9 (2019): 090901.

[3] T. Y et al. Optics express 26.18 (2018): 22985-22999.

Monolithically Integrated Micro-LED and AlGaN/GaN High Electron Mobility Transistor for Display

Liu Yaying[1], Liu Zhaojun[1]

[1]Dept. of Electronic and Electrical Engineering, Shenzhen, Guangdong, China

InGaN/GaN LEDs have been widely applied in solid-state-lighting for decades due to their excellent performances, such as high brightness, high efficiency, and long lifespan [1, 2]. In recent years, researches into Micro-LEDs for intelligent lighting, visible light communication, and display have been attracting increasing attention [3]. AlGaN/GaN HEMTs and InGaN/GaN LEDs are based on the same material system. It allows HEMT and LED to be monolithically integrated on the same epitaxial wafer, forming a voltage-controlled HEMT-LED structure [4-6]. Modulation of LED brightness by HEMT would benefit from excellent properties like high on-state current, low off-state current, and high reliability of HEMT.

In this work, a voltage-controlled and dimmable micro-LED is proposed by integrating Micro-LED with HEMT using the selective area regrowth (SAR) method. A 2-inch AlGaN/GaN HEMT grown on the (001) sapphire substrate is selectively etched for the SAR of Micro-LED. As shown in Fig. 1, the Micro-LED and HEMT are connected laterally by the 2-dimensional electron gas (2DEG) and the n-GaN layer. Fabrication of the Micro-LED-HEMT combines the standard Micro-LED and HEMT fabrication processes. The HEMT could provide a maximum current density of 1128 A/cm^2 for the Micro-LED. The brightness of the Micro-LED can be modulated by the drain bias and the gate bias. In addition, as shown in Fig. 4, the brightness can also be modulated by pulse width modulation (PWM) on gate bias from 20% to 100%.

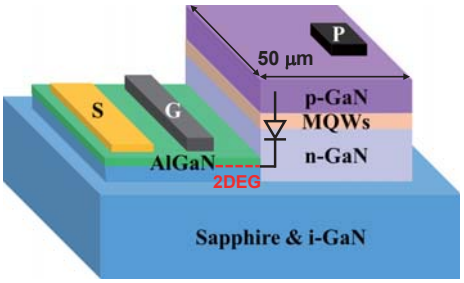

Fig. 1. Schematic diagram of voltage-controlled micro-LED

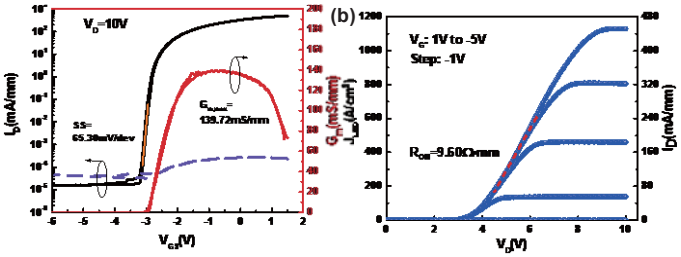

Fig. 2. (a)Transfer and (b) output characteristics of the voltage-controlled micro-LED

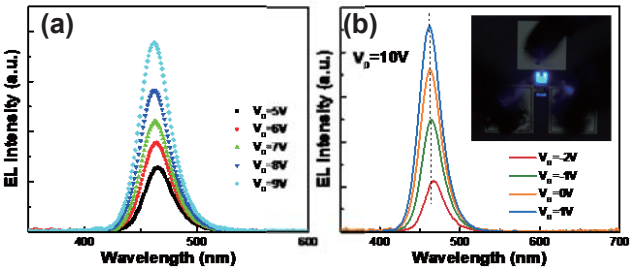

Fig. 3 EL spectra of the micro-LED under modulation of both (a) drain bias and (b) gate bias

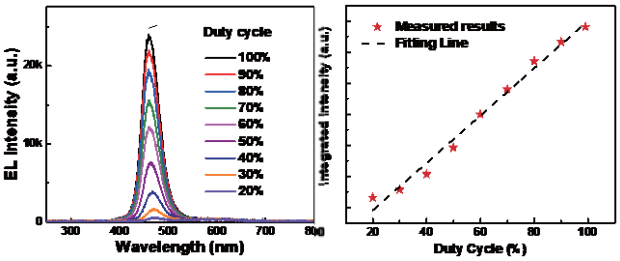

Fig. 4 (a) EL spectra of the micro-LED under gate pulse width modulation and (b) intensity with a function of duty cycle

References

[1] S. J. R. o. M. P. Nakamura, "Nobel Lecture: Background story of the invention of efficient blue InGaN light emitting diodes," vol. 87, no. 4, p. 1139, 2015.

[2] I. J. R. o. M. P. Akasaki, "Nobel Lecture: Fascinated journeys into blue light," vol. 87, no. 4, p. 1119, 2015.

[3] J. Lin and H. Jiang, "Development of microLED," Applied Physics Letters, vol. 116, no. 10, p. 100502, 2020.

[4] Y. Cai, C. Zhu, W. Zhong, P. Feng, S. Jiang, and T. J. A. M. T. Wang, "Monolithically Integrated μLEDs/HEMTs Microdisplay on a Single Chip by a Direct Epitaxial Approach," 2021.

[5] Z. Li, J. Waldron, T. Detchprohm, C. Wetzel, R. Karlicek Jr, and T. Chow, "Monolithic integration of light-emitting diodes and power metal-oxide-semiconductor channel high-electron-mobility transistors for light-emitting power integrated circuits in GaN on sapphire substrate," Applied Physics Letters, vol. 102, no. 19, p. 192107, 2013.

[6] Z. Liu, J. Ma, T. Huang, C. Liu, and K. May Lau, "Selective epitaxial growth of monolithically integrated GaN-based light emitting diodes with AlGaN/GaN driving transistors," Applied Physics Letters, vol. 104, no. 9, p. 091103, 2014.

Abstract from Poster Presentations

High Performance Ultra-Nanosheet Indium Zinc Oxide Transistor for BEOL Compatible Applications

Bo-Wei Huang, Zhen-Hao Li, Tsung-Che Chiang, Po-Tsun Liu*

***Dept. of Electronics and Computer Engineering, National Yang Ming Chiao Tung University, Hsinchu, Taiwan**

Abstract

In this work, the outstanding amorphous oxide semiconductor (AOS) material of gallium free indium zinc oxide (IZO) were applicated for low thermal budget thin film transistor (TFT) with back-end-of-line (BEOL) compatible monolithic three-dimensional integrated circuits (3D-ICs). We had successfully fabricated 2 nm amorphous indium zinc oxide thin film transistor to exhibit a high electron mobility of 30.2 $cm^2/V{\cdot}s$. While the channel thickness (t_{ch}) scaled from 4nm to 2nm, the threshold voltage (V_{th}) shifts from -0.7 V to 0.22 V, making the transistor changes from depletion mode to enhancement mode.

I. INTRODUCTION

In recent years, Monolithic Three-Dimensional integrated circuit (3D-IC) components have been widely realized by thin-film transistors (TFTs) structures. Among them, 3D-IC can reduce the occupied area to increase the density of logic circuits and effectively improved the defects of 2D stacked-structure. 3D-ICs has many advantages, such as higher transmission speed, easy formation of heterogeneous structures, reduced power, large storage capacity, and lower costs [1]. Due to low thermal budgets for 3D-ICs circuit integration are a critical engineering target for manufacturing back-end-of-line (BEOL) circuits [2]. Currently, the monolithic 3D-IC TFTs applied for BEOL technology has the limitation of the connection between the top-layer devices below the high temperature process of 400°C. Amorphous oxide semiconductor (AOS) TFTs possess significant advantages such as high electron mobility and low temperature fabrication. Therefore, one of the most used AOS materials, amorphous indium gallium zinc oxide (a-IGZO), exhibits low leakage current, goof uniformity and low thermal budget process. However, the mobility of IGZO is about 10 $cm^2/V{\cdot}s$ which is not sufficient to comparing with frond-end-of-line (FEOL) device.

II. EXPERIMENTAL DETAILS

We fabricated the Monolithic 3D-IC applicable structure of a-IZO TFTs processes on Si wafers grown with a 550 nm thermal oxide buffer layer. Schematic cross-sections of the a-IZO TFTs are shown in **Fig. 1**. First, we deposited the Mo layer on the SiO_2 by DC-sputtering as the gate electrode. Followed by bottom-gate (BG) insulator fabrication by atomic layer deposition (ALD) for HfO_2 of high dielectric constant (high-κ) material. Next, a Nano-meter-thickness of a-IZO layer was deposited by RF sputtering with IZO target and dilute HF wet etching. Source and drain (S/D) electrodes were patterned by lift-off process. Finally, the a-IZO TFTs is completed after the gate contact via was formed by dry-etching.

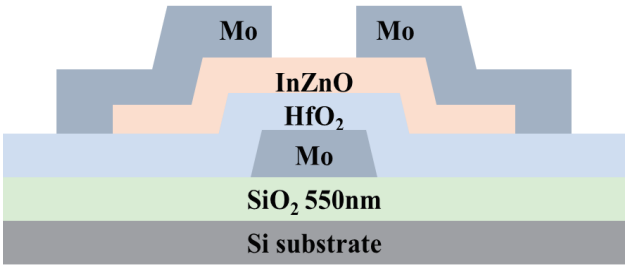

Fig. 1 The cross-section schematic of a-IZO TFTs with bottom gate inverted-staggered structure.

III. RESULT AND DISCUSSION

Figure. 2 shows the each nanosheet channel transfer curve (I_D-V_G) from 4 nm to 2 nm a-IZO TFTs. According to **fig. 2**, a-IZO TFT with 2nm channel thickness shows slightly lower mobility compared to 4nm. The electron mobility for t_{ch} of 4 nm, 3 nm, and 2 nm were 42.9, 41.4, and 30.2 cm^2 /V-s, respectively. Furthermore, by scaling the t_{ch} from 4nm to 2nm, the threshold voltage (V_{th}) shifts from -0.7 V to 0.22 V, making the transistor changes from depletion mode to enhancement mode. Also, the sub-threshold swing (SS) can approach the ideal value of 60 mV/dec. To sum up, a-IZO TFT with 2nm exhibits good performance to be applied for BEOL monolithic 3D-IC applications.

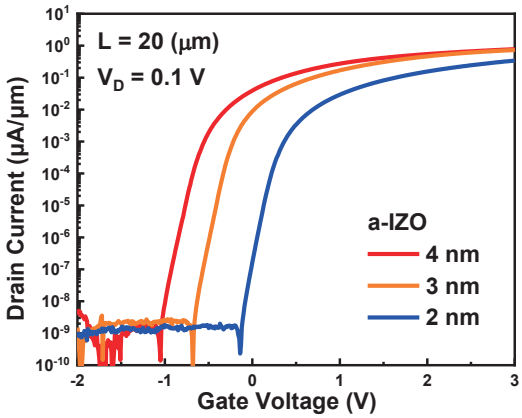

Fig. 2 The transfer curve (I_D-V_G) of TFTs with IZO.

References

[1] Y. Son, B. Frost, Y. Zhao, and R. L. Peterson, "Monolithic integration of high-voltage thin-film electronics on low-voltage integrated circuits using a solution process," Nature Electronics, vol. 2, no. 11, pp. 540-548, 2019.

[2] Kim, Hyun Jong, et al. "Reliability of amorphous InGaZnO TFTs with ITO local conducting buried layer for BEOL power transistors." Microelectronics Reliability 76 2017.

Enhanced Stability of Elevated-Metal Metal-Oxide a-IGZO TFTs through Controlled Defect Generation and Elimination

Jianming Zhu*, Lei Lu*

*** School of Electronic and Computer Engineering, Peking University, Shenzhen, China**

The stability of Oxide TFT is important and is usually associated with internal or interfacial defects in the active layer.[1] In our work, we found that the stability of the elevates-metal metal-oxide (EMMO) a-IGZO TFT is significantly influenced by the trap state at the back-channel interface.

Shown in Fig.2 is the evolution of an EMMO TFT under positive bias stress(PBS), the threshold voltage(V_{th}) shifts slightly. But under a positive bias temperature stress(PBTS), the Vth shifts towards the negative gate-voltage direction and a hump was observed. We suppress the defects by high temperature oxygen annealing after annealing of IGZO capped with sealed cover which can increase the defects of the channel, and we found it will be more stable, as indicated in Fig.3. Also, a similar phenomenon was observed after annealing after increasing defects by other ways in Fig.4. Therefore, we propose that the ionized oxygen vacancies(V_o^{2+}) trapped at the back-channel interface cause the negative shift and oxygen can be more easily diffused into the channel in the annealing process by increasing the defects in the channel first to reduce more oxygen vacancies.

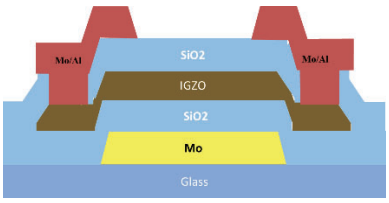

Fig. 1. Schematic cross-section of an EMMO TFT.

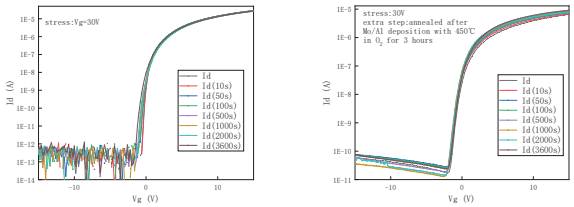

Fig. 2 Time evolutions of transfer characteristics of EMMO TFT with or without extra O_2 annealing under PBS

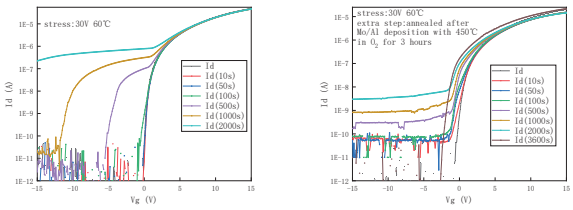

Fig. 3. Time evolutions of transfer characteristics of EMMO TFT with or without extra O_2 annealing under PBTS

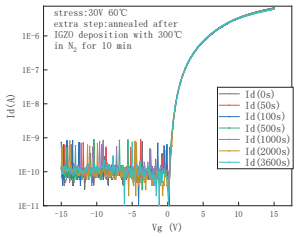

Fig. 4. Time evolutions of transfer characteristics of EMMO TFT with extra N_2 annealing under PBTS

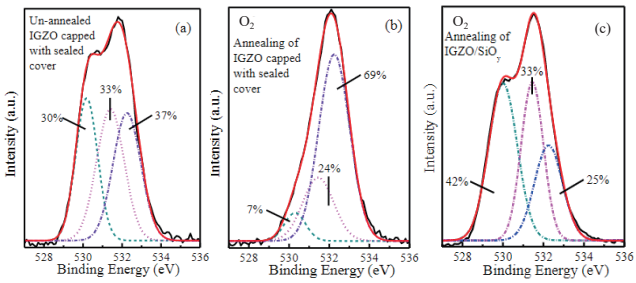

Fig. 5. The XPS spectra of O1s in the IGZO samples capped with sealed cover or SiO_x, which was unannealed or annealed in O_2 [2]

References

[1] Y. Zhang et al., *IEEE Trans. Electron Devices*, vol. 68, no. 3, pp. 1081–1087 (2021).

[2] L. Lu et al., *IEDM Tech. Dig.*,2017, pp. 3221–3224 (2017).

Improvement for Electrical Performance of Self-Aligned Top-Gate Amorphous InGaZnO Thin-Film Transistors with Pre-Annealed SiO_X Buffer

Yuhan Zhang*, Jiye Li*, Zhikang Ma*, Tengyan Huang*, Lei Lu*, Shengdong Zhang*

***School of Electronic and Computer Engineering, Peking University, Shenzhen, Guangdong, China**

Amorphous InGaZnO thin-film transistors (a-IGZO TFTs) have been successfully industrialized in flat-panel displays due to their relatively high mobility, ultra-low off current, low fabrication temperature, and good large-area uniformity [1]. Among various device architectures of a-IGZO TFTs, the self-aligned top-gate (SATG) structure is more preferred for advanced applications by virtue of its much smaller parasitic capacitance and better scalability. However, some recent reports have demonstrated that the buffer layer, which is commonly used in industrial production, has a crucial impact on the performance of the SATG transistors, including both mobility and stability, because of its direct contact with the active layer [2], [3]. Therefore, in this work, the impact of SiO_X buffer layer on the performance of SATG a-IGZO TFTs is studied and attempted to improve.

Shown in Fig. 1(a) and (b) are the schematic cross-sections of the fabricated SATG a-IGZO TFTs. The SATG TFTs without and with SiO_X buffer are labeled as device A and B. The SATG transistors with their buffer layer pre-annealing under different conditions are labeled as device C, D and E, respectively. As illustrated in Fig. 1(c), the performance of the transistor with 200-nm SiO_X buffer layer (red line) exhibits obvious degradation compared to the SATG a-IGZO TFT without buffer layer (black line), including the field-effect mobility (μ_{FE}) decreasing significantly from 17.4 $cm^2/V{\cdot}s$ to 6.4 $cm^2/V{\cdot}s$ and the subthreshold swing (*SS*) worsening correspondingly from 229.6 mV/dec to 356.1 mV/dec. These phenomena could be attributed to the unintentional diffusion of the excessive hydrogen from the PECVD SiO_X buffer layer to a-IGZO active layer, which could be aggravated by the subsequent annealing treatment during the fabrication process of SATG a-IGZO TFTs. Fortunately, pre-annealing treatment to SiO_X buffer can effectively improve the electrical properties of the SATG TFTs, especially the increase of μ_{FE} to 14.3 $cm^2/V{\cdot}s$. It suggests that pre-annealing treatment can remove excess hydrogen in SiO_X buffer in advance.

As shown in Fig. 2, the SATG a-IGZO TFT without SiO_X buffer exhibits excellent stability with only a ΔV_{TH} of +0.17 V and -0.03 V under positive bias stress (PBS) and negative bias stress (NBS), respectively. However, the PBS stability of the transistor with SiO_X buffer (device B) are significantly deteriorated, showing a ΔV_{TH} of -7.85 V. The H- related species diffusing from buffer layer could give rise to this severe PBS instability and abnormal negative V_{TH} shift. Through pre-annealing treatment in O_2 at 300 ℃ for 3 hours, the ΔV_{TH} under PBS is recovered to -2.05 V.

In conclusion, pre-annealing treatment to the SiO_X buffer can improve the electrical performance of SATG TFTs to some extent. Further improvement of the mobility and stability can be highly expected by more carefully optimizing the pre-annealing conditions.

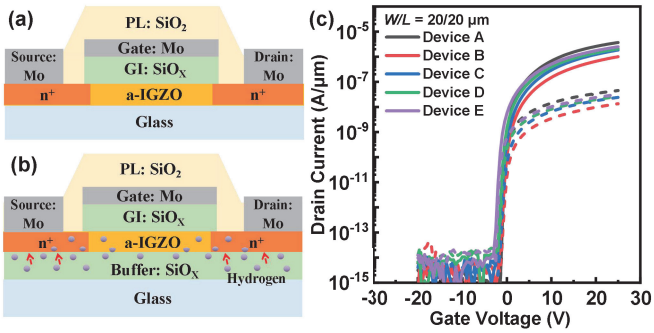

Fig. 1. Schematic cross-sections of SATG a-IGZO TFTs (a) standard and (b) with SiO_X buffer layer. (c) Transfer curves of these transistors.

Table 1. Parameter Comparison of The SATG a-IGZO TFTs with Various Process Conditions.

Device	A	B	C	D	E
Anneal conditions	--	--	350 ℃ O_2 1.5 h	300 ℃ O_2 1.5 h	300℃ O_2 3 h
μ ($cm^2/V{\cdot}s$)	17.4	6.4	10.8	10.5	14.3
SS (mV/dec)	229.6	356.1	362.7	362.7	342.0
V_{TH} (V)	-0.29	0.26	-0.05	-0.67	-1.49
ΔV_{TH} at NBS	-0.03	-0.34	-0.27	-0.25	-0.11
ΔV_{TH} at PBS	+0.17	-7.85	-5.49	-2.36	-2.05

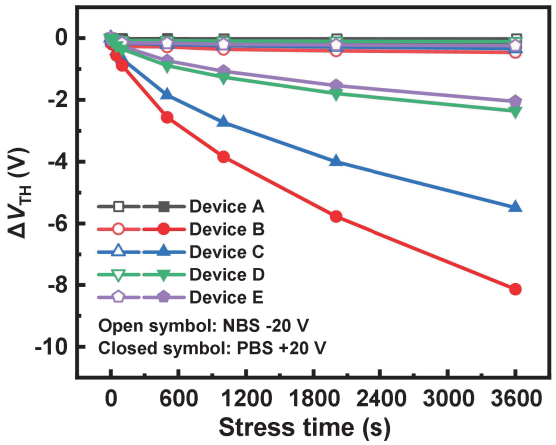

Fig. 2. Evolution of ΔV_{TH} with stress time under NBS and PBS for the fabricated SATG TFTs.

References

[1] K. Ide, et al, *physica status solidi,* vol. 216, (2019).

[2] Y.-D. Ho, et al, *SID Symp. Dig. Tech. Pap.,* vol. 48, no. 1, pp. 1246-1249 (2017).

[3] K.-L. Han, et al, *Appl. Phys. Lett.,* vol. 111, (2017).

High-Mobility Dual-Gate a-IGZO/a-IZO/a-IGZO Thin-Film Transistors

Zhikang Ma*, Huan Yang*, Lei Lu* and Shengdong Zhang*
***School of Electrical and Computer Engineering, Peking University, Shenzhen, China**

Amorphous oxide semiconductor (AOS) thin-film t ransistors (TFTs) have large mobility and good uniform ity [1], which is suitable for next-generation displays. Specificly, high-end displays including micro-LED requi re TFT with higher mobility. High-In AOSs are usually used to acquire high mobility, but resulting in negativ e threshold voltage (V_{th}) and poor stability [2]. It has been reported that multilayer-channel AOS TFT exhibit s high mobility, and also relatively reasonable V_{th} and good stability [3]. On the other hand, the dual gate (D G) TFTs can turn off more easily compared to the sin gle gate (SG) one, also be beneficial for achieving hig h mobility. Thus the multilayer channel, combined with highly conductive a-IZO (In:Zn = 5:1) and a-IGZO, AOS TFTs with DG structureare fabricated to acquire high mobility in this work.

Fig. 1 shows the schematic cross-section of the fa bricated DG TFT with self-aligned top gate. As shown, the multi-layer channel is with -nm a-IGZO/ -nm a-I ZO/ -nm a-IGZO. As shown in Fig. 2, single layer a-I ZO TFT has high drain current , but cannot turn off even at gate voltage (V_G) of -30V. However, multilayer channel TFT with the same thickness of a-IZO shows clear turn-off region with V_{th} of -8.83V, but lower on -state current.

Multilayer channel devices with different a-IZO thi ckness are also studied. As shown in Fig 3 (a) and (b), with the decreased thickness of a-IZO, the positive -shifted V_{th} and the decreased linear mobility (μ_{lin}) are observed. In addition, for these TFTs, μ_{lin} shows degra dation at high V_G region, and the values of transition V_G are nearly the same at about 18V. This can be exp lained as below, similar to earlier work [4]. As shown in Fig 4 (a), the conduction band minimum (E_c) of a -IZO is lower than a-IGZO. At low voltage, the induc ed electrons are restricted in a-IZO. With V_G increases, the E_c at GI/IGZO surface becomes lower and even l ower than that at the interface of a-IGZO and a-IZO, which means a new carrier transport path is formed (s hown in Fig 4 (b)). However, the μ_{lin} of the path in a -IGZO is lower than that in a-IZO, which causes degr adation in high V_G region.

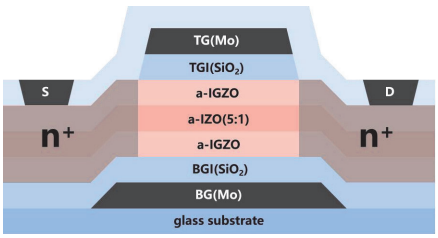

Fig. 1. Schematic cross section of the multilayer c hannel DG TFTs.

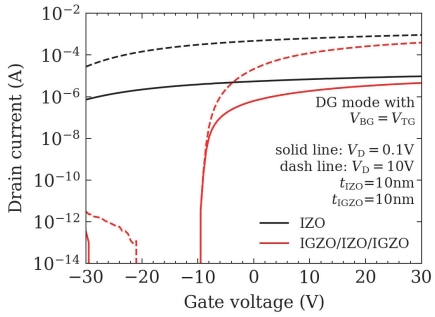

Fig. 2. Transfer curves of 10 nm single layer IZO (5:1) and multilayer IGZO/IZO/IGZO TFTs. Measure d with DG mode.

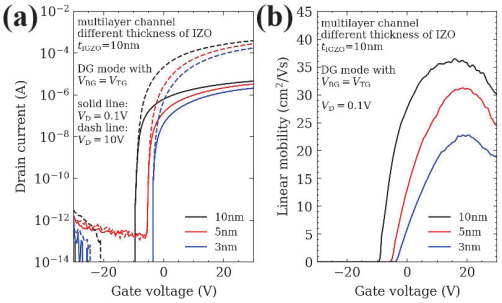

Fig. 3. (a) Transfer curves and (b) extracted linear mobility of TFTs with different thickness of a-IZO i n multilayer channel. Measured with DG mode.

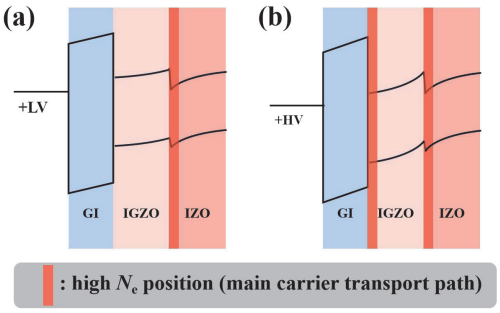

Fig. 4. Band diagrams of a-IGZO and a-IZO chan nel (part of multilayer channels) with gate bias at (a) low voltage (LV) or (b) high voltage (HV).

References

[1] K. Nomura et al, *Nature,* 432(7016), 488 (2004)

[2] T. Kamiya et al, *NPG Asia Materials*, 2, 15 (2010)

[3] X. Yu et al, *Acs Appl. Mater. Interfaces*, 5(16), 7983 (2013)

[4] M. Furuta et al, *Jpn. J. Appl. Phys*. 58, 090604 (2019)

Conductive Indium-Tin-Zinc Oxide Formed by Oxygen Plasma Treatment

Xinying Xie, Kaiqi Chen, Zhichao Zhou, Wei Jiang, Yuqi Wang, Zhihe Xia and Man Wong
Department of Electronic and Computer Engineering,
The Hong Kong University of Science and Technology, Kowloon, Hong Kong

Various doping methods have been studied to increase the conductivity of semiconducting indium-tin-zinc oxide (ITZO) to form the source/drain (S/D) regions of a TFT. These include argon plasma treatment at 200 °C **[1-3]**, reactive aluminum annealing at 200 °C in an oxygen (O_2) atmosphere **[4]**, and interlayer silicon nitride SiN_x deposited using ICP-CVD with high hydrogen content silane (SiH_4) plasma at 150 ℃ **[5]**. All these doping processes require high temperature as well as exposure of the ITZO by removing the covering gate dielectric. Presently reported is an ITZO doping technique based on O_2 plasma treatment. Doping can be achieved with the metal-oxide semiconductor covered with silicon oxide SiO_x and at room temperature. A low resistivity of ~1.5 mΩ· **cm** can be obtained in 10 mins.

The dependence of the resistivity of ITZO exposed to O_2 plasma on the thickness of the SiO_x above ITZO has been investigated and the resistivity increases as the thickness of the SiO_x increases when exposed to O_2 plasma as shown in Fig. 1a. The increasing ICP power of O_2 plasma decreases the resistivity of ITZO exposed to O_2 plasma as shown in Fig. 1b, while the bias power of O_2 plasma does not affect the resistivity of ITZO exposed to O_2 plasma as shown in Fig. 1c. The increasing time of O_2 plasma treatment decreases the resistivity of ITZO exposed to O_2 plasma as shown in Fig. 1d.

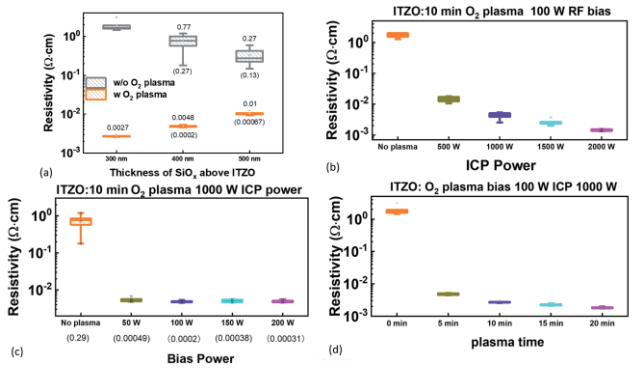

Fig. 1. The dependence of the resistivity of ITZO with or without exposure to O_2 plasma on (a) the thickness of the SiO_x above ITZO (b) RF ICP power of O_2 plasma treatment, (c) RF bias power of O_2 plasma treatment and (d) O_2 plasma treatment time.

Top-gate (TG), self-aligned (SA) ITZO TFTs have been fabricated using the O_2 plasma S/D doping technique. Shown in Fig. 2 is the drain current I_d *vs.* gate voltage V_g transfer characteristics of the TG SA ITZO TFT with different channel length L.

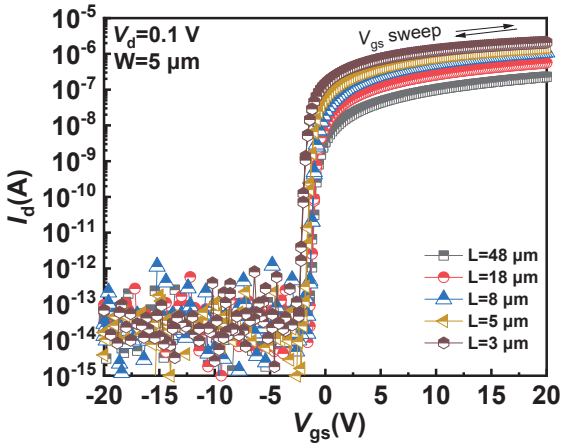

Fig. 2. I_d *vs.* V_g transfer characteristics of TG SA ITZO TFTs with different channel length

References

[1] S.-I. Cho, J. B. Ko, S. H. Lee, J. Kim, and S.-H. K. Park, "Remarkably stable high mobility self-aligned oxide TFT by investigating the effect of oxygen plasma time during PEALD of SiO2 gate insulator," *Journal of Alloys Compounds,* vol. 893, p. 162308, 2022.

[2] W. Jeong, J. Winkler, H. Schmidt, K.-H. Lee, S.-H. K. J. J. o. A. Park, and Compounds, "Suppressing channel-shortening effect of self-aligned coplanar Al-doped In-Sn-Zn-O TFTs using Mo-Al alloy source/drain electrode as Cu diffusion barrier," vol. 859, p. 158227, 2021.

[3J. Kim, D. H. Kim, S.-I. Cho, S. H. Lee, W. Jeong, and S.-H. K. Park, "Channel-shortening effect suppression of a high-mobility self-aligned oxide TFT using trench structure," *IEEE Electron Device Letters,* vol. 42, no. 12, pp. 1798-1801, 2021.

[4] N. Morosawa *et al.*, "High-mobility self-aligned top-gate oxide TFT for high-resolution AM-OLED," vol. 21, no. 11, pp. 467-473, 2013.

[5] R. Upadhyay, S. Steudel, M.-P. Hung, A. K. Mandal, F. Catthoor, and M. Nag, "Self-aligned amorphous indium-tin-zinc-oxide thin film transistors on polyimide foil," *ECS Journal of Solid State Science Technology,* vol. 7, no. 4, p. P185, 2018.

The effects of the temperature of fluorination treatment on the reliability of an indium-gallium-zinc oxide thin-film transistor

Wei Jiang *, Yuqi Wang*, Zhihe Xia*, and Man Wong*,**

***Department of Electronic and Computer Engineering, State Key Laboratory on Advanced Displays and Optoelectronics and Technologies, The Hong Kong University of Science and Technology, Hong Kong, China**

****The Hong Kong University of Science and Technology Shenzhen Research Institute, Shenzhen, China.**

Amorphous indium-gallium-zinc oxide (a-IGZO) thin-film transistors (TFT) are being deployed in active-matrix organic light-emitting diode (OLED) displays due to their compatible electrical properties, including an adequately high field-effect mobility μ_{FE} and large on/off current ratio. Furthermore, the long-term electrical stability of an IGZO TFT is critical in practical applications since the degradation of TFT characteristics will affect the pixel brightness. Several factors are responsible for the instability of IGZO TFTs, such as residual hydrogen (H) in the gate insulator or passivation layer, and un-passivated defects in the a-IGZO channel [1]. Fluorination is regarded as an effective technique of suppressing the diffusion of mobile H and passivate the defects or weakly bound oxygen in the channel [2]. Fluorine (F) can be introduced into an a-IGZO channel by means of plasma treatment, a process that is more compatible with processing of a large-area substrate while inducing less damage than implantation [3].

This study explore the effects of the temperature of fluorination by F plasma treatment on IGZO TFTs. Fig. 1a shows the I-V characteristics of IGZO TFTs fluorinated at 100, 200, 300℃, and without fluorination, respectively, while Fig. 1b shows the box plots of V_{on}. One can notice that a fluorinated TFT has a more positive V_{on} than the non-fluorinated one, and the V_{on} of a TFT fluorinated at a higher temperature is more positive than that fluorinated at a lower temperature. It is shown in Fig. 2 that TFTs fluorinated at a higher temperature have a stronger resilience against positive gate-bias temperature stress (PBTS) than those fluorinated at a lower temperature. Furthermore, TFTs subjected to higher-temperature fluorination exhibit higher stability than those treated at a lower temperature when subjected to no-oxidizing heat-treatment as shown in Fig. 3.

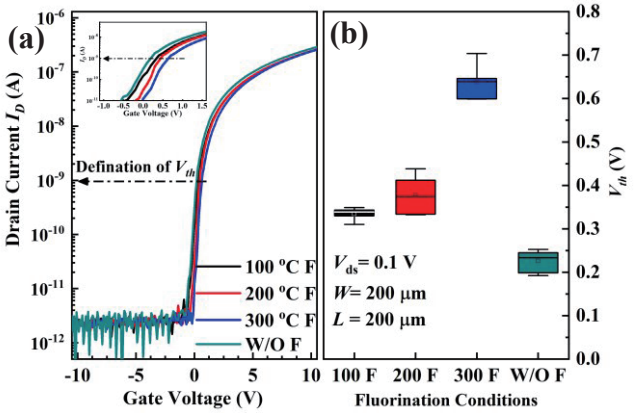

Fig. 1. (a) The I-V curves of IGZO and IGZO:F TFTs fluorinated at various temperatures. (b) Box plots of V_{on} of TFTs subjected to 4 different fluorination conditions.

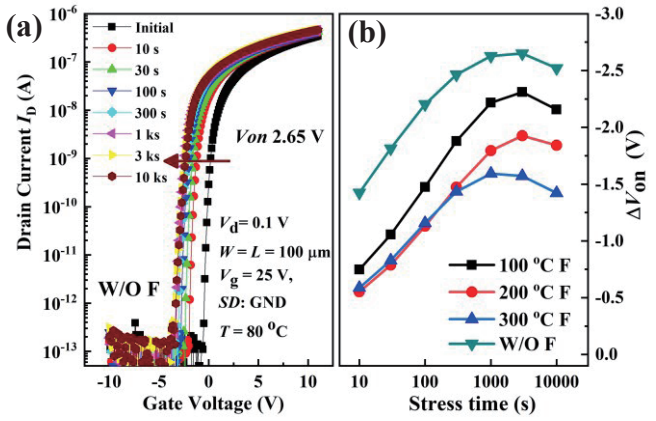

Fig. 2. (a) Time evolution of the I-V curves of non-fluorinated IGZO TFTs (*W*/*L* = 100µm/100µm) to the PBTS (V_g = 25 V at 80 °C). (b) The dependence of ΔV_{on} on the PBTS duration for IGZO TFTs fluorinated at 4 different fluorination conditions

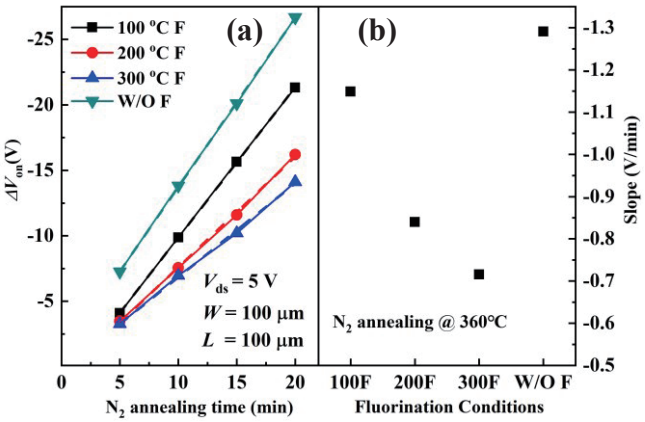

Fig. 3. (a) Change of average ΔV_{on} with increasing N_2 heat-treatment time, (b) slope of ΔV_{on} *vs.* heat-treatment time under various fluorination conditions.

References

[1] Toda T, Wang D, Jiang J, Hung MP, Furuta M. *IEEE Trans. Electron Devices*, 61(11), 3762 (2014).

[2] Lu L, Xia Z, Li J, Feng Z, Wang S, Kwok HS, Wong M. *IEEE Electron Device Lett.*, 39(2), 196 (2017).

[3] Ye, Zhi, and Man Wong. *IEEE Electron Device Lett.,* 33(8), 1147 (2012).

Temperature-Controlled Dip-Coating Carbon Nanotube Thin-Film Transistors

Lin Xu*, Wei Huang*, Rongsheng Chen ****

*School of Microelectronics, South China University of Technology, Guangzhou, China.

**State Key Laboratory of Advanced Displays and Optoelectronics Technologies, Department of Electronic and Computer Engineering, The Hong Kong University of Science and Technology, Hong Kong, China

Abstract

The large-scale fabrication of high mobility carbon nanotube thin-film transistors remains a challenge. Here, we present high-performance carbon nanotube thin-film transistors prepared using a temperature-controlled dip-coating technology, exhibiting a mobility of 27.8 $cm^2 \cdot V^{-1} \cdot s^{-1}$ and an on-state current of 8.06×10^{-5} A.

1. Introduction

Carbon nanotube thin-film transistors (CNT-TFTs) are characterized by high mobility and excellent mechanical flexibility. The carbon nanotube (CNT) film prepared via the dip-coating method exhibits excellent uniformity and is characterized by a simple preparation process, enabling large-area coverage[1]. However, the dip-coating method necessitates a preparation time exceeding 12 hours, and this method cannot yield CNT-TFTs with ideal properties[2].

Herein, CNT-TFTs were fabricated on glass substrates using the dip-coating method. The CNT-TFTs prepared via temperature-controlled dip-coating (TCDC) exhibited a field effect mobility (μ_{FE}) of 27.8 $cm^2 \cdot V^{-1} \cdot s^{-1}$, an on-state current ($I_{on}$) of 8.06×10^{-5} A, and an on/off ratio ($I_{on/off}$) of 9×10^5.

2. Experiment

Raw CNTs and PCz (poly[9-(1-octylnonyl)-9H-carbazole-2,7diyl]) were ultra-sonically mixed in toluene, and 80% of the supernatant was collected after ultracentrifugation for the CNT-TFTs preparation (Fig. 1**a**).

The CNT-TFTs were constructed using a bottom-gate structure, the device structure of CNT-TFTs is depicted in Fig. 1**b**. The CNTs film was prepared using TCDC, wherein the entire device was immersed in a CNTs solution at 20/40/80°C for 2 hours, resulting in the CNTs film serving as the active layer. Photolithography and reactive ion etching were used to pattern the CNTs film, followed by the deposition of Ti/Au to form the source-drain electrodes. The transfer characteristics and output characteristics of CNT-TFTs, prepared using TCDC at 80°C, are presented in Fig. 1**c** and Fig. 1**d**, respectively.

3. Results and Discussion

The qualitative characterization of the purified CNTs solution was performed using a spectrophotometer, The transition characteristic positions of semiconducting (S22) or metallic (M11) CNTs were indicated in Fig. 2**a**. The purified CNTs solution exhibits a significantly lower M11 metallic peak compared to the unpurified CNTs, indicating that polymer-assisted ultracentrifugation can yield a high-purity SWCNT solution. Fig. 2**b** displays the SEM image of the CNTs film prepared from purified SWCNTs.

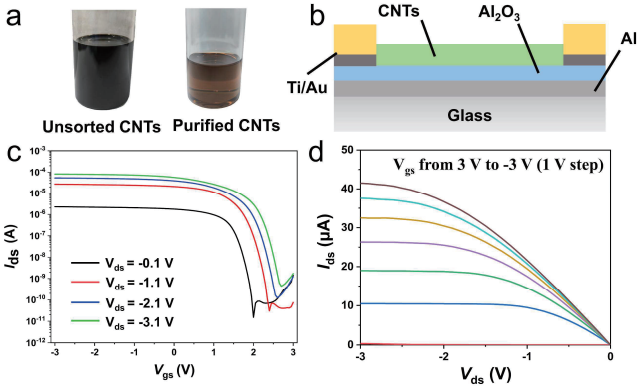

Fig. 1. a Unsorted and purified SWCNTs. **b** Schematic illustration of CNT-TFTs structure, W/L = 300/100 μm. **c** Transfer characteristics and **d** Output characteristics of CNTs-TFT prepared via TCDC at 80°C.

As shown in Fig. 2**c** and **d**, CNT-TFTs prepared at 80°C exhibit a 5-fold increase in I_{on} compared to those prepared at 20°C, reaching 8.06×10^{-5} A at V_{ds} = -3.1 V (Fig. 1**c**). The $I_{on/off} = 9 \times 10^5$ at V_{ds} = -1.1 V. The μ_{FE} increases by 5.8 times, reaching 27.8 $cm^2 \cdot V^{-1} \cdot s^{-1}$. The subthreshold swing (SS) decreases from 142 mV/dec to 122 mV/dec.

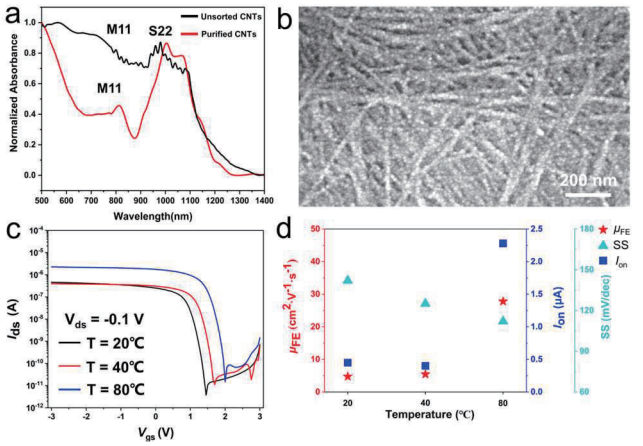

Fig. 2. a Absorption spectra of CNTs. **b** SEM image of the CNTs film. **c** Transfer characteristics and **d** characteristic parameters of CNT-TFTs at different dip-coating temperatures, V_{ds} = -0.1 V.

References

[1] L. Xiang et al., *Sci. Adv.*, 8(33), eabp8075 (2022).

[2] H. Zhang et al., *Adv. Mater.*, 30(50), e1805408 (2018).

Enhanced Performance of Self-Powered PTAA/$MAPbCl_3$ Single Crystal Film Heterojunction Ultraviolet Photodetector Based on Homologous bromides passivation

*Shilin Liu, Yijing Ding, Qing Li**

* Joint International Research Laboratory of Information Display and Visualization, School of Electronic Science and Engineering, Southeast University, Nanjing, Jiangsu, China

In the field of optical communication and sensing applications, photodetectors (PDs) are crucial core components. Perovskite materials have outstanding competitiveness in the PD field due to their longer carrier lifetime, longer diffusion length, and larger optical absorption coefficient. However, the inherently high trap density at grain boundaries in perovskite polycrystalline films is inevitable, which limits the unimpeded transport of carriers and increases the probability of carrier recombination. This has become the bottleneck for the performance improvement of perovskite PDs. In order to solve this problem, further research is needed to improve the performance and stability of perovskite materials in the PD field to promote their widespread use in optical communication and sensing applications.

Perovskite single crystal films (SCFs) are more desirable as light absorbers for photodetectors (PDs) compared to polycrystalline films (PCFs) due to their remarkable crystallinity, high mobility, and low trap density. However, the lead halide perovskites are unintentionally self-doped, resulting in undesired performance (low mobility, high carrier densities and defect density, and etc.).[1, 2]There are much less efforts devoted to enhancing the quality of perovskite single crystals in terms of controlling self-doped, despite it is well known in the community that the crystals quality is important to achieve the best properties and device performance. $MAPbCl_3$, a wide band gap semiconductor (the band gap energy: ~2.9 eV), is regarded as an attractive candidate for ultraviolet (UV) photodetection.[3] However, due to self-doping-induced defects, the photoresponsivity for the reported $MAPbCl_3$ single-crystal photodetectors is still below 50 mA W^{-1}. Furthermore, most of the PDs are operating under an external bias as the driving force, which limits their independence in real-time practical applications. To meet the demand of high efficiency, low power consumption and small electronic device size, self-powered UV PDs which can operate without any power supply are urgently needed.[4]

Here, the self-powered PTAA/$MAPbCl_3$ single crystal film heterojunction ultraviolet photodetector based homologous bromides passivation has been successfully fabricated. Homologous halide passivation effectively suppresses defects in the single crystal film, while the built-in electric field of the heterojunction ensures efficient charge separation. This device shows fast response and high responsivity for ultraviolet light, meanwhile it exhibits excellent stability in ambient conditions. Our strategy for fabricating high-performance solution-processed UV photodetectors is highly attractive for further light communication and detection techniques.

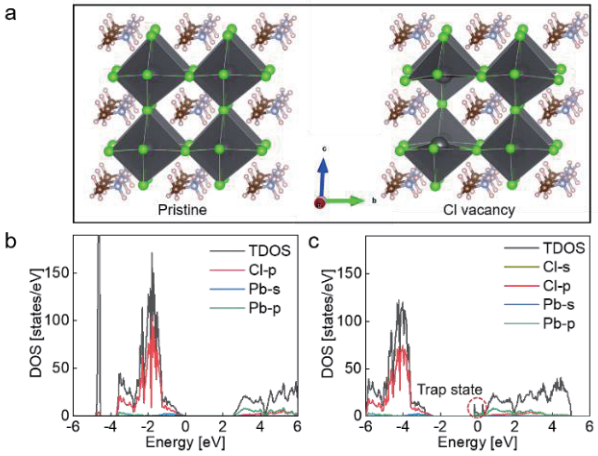

Fig. 1. (a) Optimized crystal structures for pristine $MAPbCl_3$ and $MAPbCl_3$ with Cl vacancy. DOS of pristine $MAPbCl_3$ (b) and $MaPbCl_3$ with Cl vacancy(c).

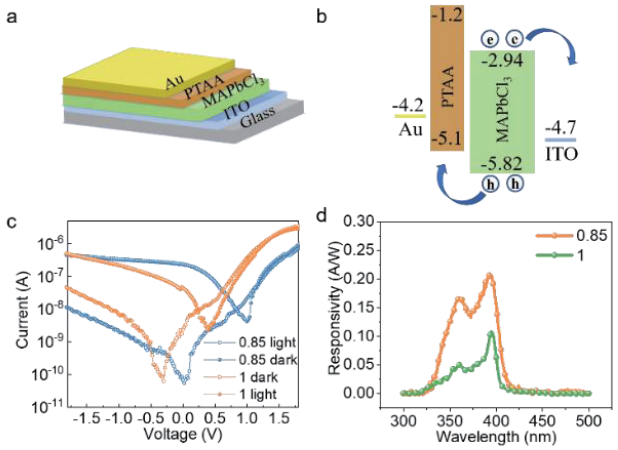

Fig. 2. (a) device schematic diagram and (b) the energy level diagram. (c) I–V curves and (d) Responsivity of the device. (The 0.85 and 1 refers to the ratio between $PbCl_2$ and MACl.)

References

[1] J. Euvrard, Nat. Rev. Mater, 6 (6), 531-549 (2021).

[2] J. Huang, Nat. Rev. Mater, 2 (7), 17042 (2017).

[3] Y. Chen, Chem. Commun., 56 (47), 6404-6407 (2020).

[4] F.Chen, Adv. Mater. Interfaces, 9 (9) (2022).

Wearable Piezoelectric Sensor Based on PVDF/ZnO Composite Membrane and ITZO TFT

Mei Yang, Rongsheng Chen*, ***

*School of Microelectronics, South China University of Technology, Guangzhou, China.

**State Key Laboratory of Advanced Displays and Optoelectronics Technologies, Department of Electronic and Computer Engineering, The Hong Kong University of Science and Technology, Hong Kong, China

Wearable flexible electronic devices are increasingly becoming an important part of the future rolling touch screen, health care equipment, electronic skin and other fields. However, large-area array pressure sensors with small size, high sensitivity, and ability to detect high-frequency dynamic forces are still key challenges in their practical applications [1]. It is worth noting that piezoelectric sensors are widely used because of their self-powered capability, fast dynamic load response, and relatively simple circuits [2]. Thin film transistors (TFTs) have been successfully used as active components in display panels and sensor devices due to their advantages of amplification effect, small size, low cost, and large-area fabrication of arrays [3][4]. Among them, ITZO TFT has high field effect mobility, low energy consumption, and can be used as an amplifier for signal amplification of flexible sensing systems. The relevant electrical parameter data are shown in Table 1.

Here, we prepared a PVDF/ZnO composite fibrous membrane as a sensor and then connected the ITZO TFT as an output signal amplifier. The device diagram is shown in Figure 1.

To study the piezoelectric properties of this sensor, we provide different pressures (0.01N, 0.05N, 0.1N, 0.5N, 1N, 1.5N) to the sensor to test its sensitivity, as shown in Figure 1. It can be seen that when the pressure is 0.01 N, the average output voltage of the sensor is 50 mV. When the pressure is 1.5 N, the average output voltage is about 3V. As shown in Figure 3, the sensor was placed on the wrist of a 28-year-old volunteer for real-time monitoring of light and heavy pressure. It is found that it can not only capture small signals, but also produce a response of up to 3V to heavy pressure.

In summary, as a low-cost and simple-to-manufacture piezoelectric sensor, the composite membrane has the advantages of porous, flexible and breathable. This sensor can also realize the detection of human physiological signals, such as throat sound, finger bending, pulse measurement and so on. With the combination of the ITZO TFT, this pressure sensor exhibits fast response speed (37.5 ms), high amplification (10 times), and lower energy consumption, meeting the requirements of wearable devices.

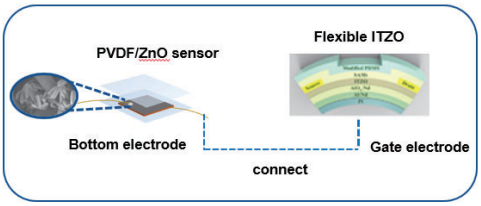

Fig. 1. The pressure sensor diagram.

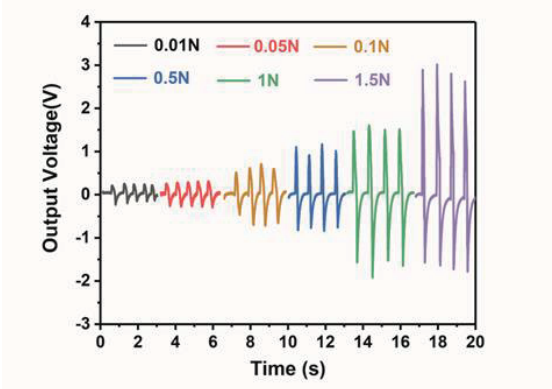

Fig. 2. The response signal of the sensor under different pressures.

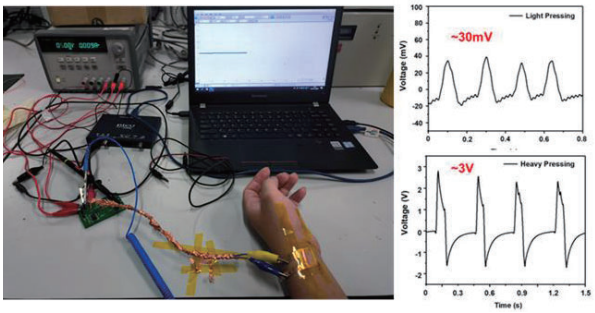

Fig. 3. Real-time signal output of integrated sensor.

Table 1. Electrical parameters of the ITZO

ITZO parameters		Sensor parameters	
μ_{FE}	20.52 $cm^2V^{-1}S^{-1}$	Φ	278 nm
SS	0.074 V/dec	ZnO *L/D*	8.5
I_{on}/I_{off}	3.42×10^{10}	*S*	1.98 V/KPa
V_{th}	1.88 V	*RT*	37.5 ms
W/L	300μm/300μm	*PR*	0.01~1.5 N

References

[1] M. L. Hammock, *Adv. Mater.,* 25(1), 5997–6038 (2013).

[2] M. D. Maeder, *J. Electroceramics*, 13(3), 385–392 (2004).

[3] Z. Zhang et al., *IEEE Electron Device Letters*, 40(1), 111–114 (2019).

[4] A. Spanu, *Organic Electron.*, 36(1), 57–60 (2016).

High Photo Response of High-Indium InZnO Thin-Film Transistors

Tengyan Huang*, Hao Liu*, Fanyou Tang*, Junjin Cheng*, Lei Lu* and Shengdong Zhang*
***School of Electronic and Computer Engineering, Peking University, Shenzhen, Guangdong, China**

The amorphous oxide semiconductor (AOS) thin-film transistors (TFTs) are promising for next-generation flat panel display (FPD) technology thanks to merits like reasonable electrical properties, high optical transparency, low processing temperature and low manufacturing costs [1]. Researchers have also discovered that AOS TFTs, especially amorphous InZnO (a-IZO) TFTs, exhibit wavelength selectivity, low dark current, and high photo responsivity, making them considered a promising photodetectors [2]. Enhancing photo responsivity is a desired objective to minimize the required light dosage for detection [3]. The active layer's composition will directly influence the photo response characteristics. Therefore, this work studies the impact of indium content in the a-InZnO layer on the photo responsivity of a-IZO TFTs.

Fig. 1(a) illustrates the employed inverted staggered bottom-gate (BG) TFT structure. The IZO active layer was sputtered using In:Zn targets with ratios of 1:1 and 3:1 under an argon-to-oxygen ratio of 20:30. Fig. 1(b) and 1(c) compare the photo response of a-IZO TFTs with In:Zn ratios of 1:1 and 3:1 under dark and under illumination at different wavelengths (λ). Under dark, the off-state currents of the a-IZO TFTs with different indium content are both relatively low (0.1 pA). The incident light power density (P) was 250 μW/cm^2. Both TFTs show noticeable photocurrent for the illumination with λ of 325–425 nm. It indicates that the absorption in the a-IZO layer under light exposure with less photon energy than 2.9 eV is largely responsible for subgap states [4]. The responsivity of the a-IZO TFTs was extracted at a gate bias of -20 V and a drain bias of 10 V, as shown in Fig. 1(d). Notably, the a-IZO TFT with an In:Zn ratio of 3:1 demonstrates higher photo responsivity than the TFT with In:Zn ratio of 1:1, surpassing 10^4 A/W under 325 nm illumination. It may be attributed to the lower binding affinity of indium atoms with oxygen in the IZO thin film. As the indium content increases, a higher concentration of oxygen vacancies is produced, resulting in increased photocurrent and responsivity of the TFTs.

The Fig. 2(a) and 2(b) show the X-ray photoelectron spectroscopy (XPS) O 1s spectra of a-IZO thin films with In:Zn ratios of 1:1 and 3:1 to verify the above hypothesis. The O 1s spectra can be deconvoluted into three Gaussian. The peak at 531.2 eV is attributed to oxygen vacancies (V_O). The XPS analysis reveals that a-IZO In:Zn ratio of 3:1 exhibits a higher concentration of oxygen vacancies (V_O). Under illumination, as shown in Fig. 2(c), ionization of V_O occurs, generating ionized oxygen vacancies that screen the gate voltage and lower the source barrier, resulting in a large photocurrent. Hence, the higher concentration of V_O in a-IZO with an In:Zn ratio of 3:1 is attributed to its enhanced photo responsivity.

In conclusion, the TFT with an In:Zn ratio of 3:1 demonstrated higher photo responsivity compared to the one with a 1:1 ratio. This enhancement is attributed to the higher concentration of oxygen vacancies in the a-IZO TFTs with an In:Zn ratio of 3:1.

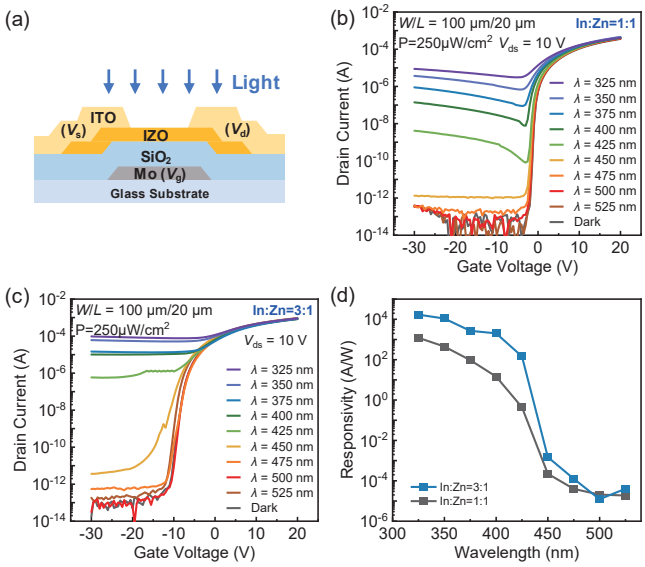

Fig. 1. (a) Schematic diagram of the BG a-IZO TFTs. (b)(c) Transfer curves and (d) photo responsivity of a-IZO TFT with In:Zn ratio of 1:1 and 3:1 under different wavelengths illumination.

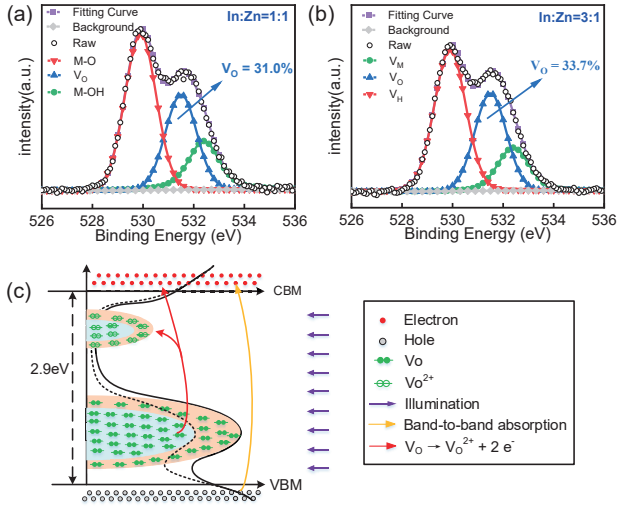

Fig. 2. (a)(b) XPS spectra of O 1s signal for a-IZO TFTs with In:Zn ratio of 1:1 and 3:1. (c) The diagram of the density of states for IZO film under illumination.

References

[1] A. Nathan, et al, *Disp. Technol.* 10 (11), 917(2014).

[2] S. Jeon, et al, *Adv. Mater.* 26 (41), 7102 (2014).

[3] H.-S. Choi, et al, *Appl. Phys. Lett.* 106 (1) (2015).

[4] A. Janotti, et al, *Appl. Phys. Lett.* 87 (12) (2005).

Bio-Inspired Ultrasensitive Optical-Electrical Strain Sensor for Human Motion Detection

Tianqi Wang[1], Gui-Shi Liu[1]*

[1]Guangdong Provincial Key Laboratory of Optical Fiber Sensing and Communications, Key Laboratory of Visible Light Communications of Guangzhou, Key Laboratory of Optoelectronic Information and Sensing Technologies of Guangdong Higher Education Institutes, Jinan University, Guangzhou 510632, China

E-mail: guishiliu@163.com

The increasing breakthroughs of nanotechnology and microelectronics technology have promoted the rapid development of electronic skin (e-skin) in the areas of virtual reality, intelligent robotics, and man-machine interaction. E-skin with a single electrical signal output is difficult to meet the needs of visual dynamic human-machine. Thus, it is necessary to develop an e-skin with optical signal output.[1]

In this work, high-performance dual-function e-skin is prepared in a simple and environmentally friendly way. Optical sensing is inspired by the guanine nanocrystal arrays of chameleons.[2] By controlling the structure of the nanoparticles in the flexible matrix, the photonic band gap (PBG) is shifted so that the e-skin can display different structural colors. A colloidal crystal assembly method is combined with the dry etching method to produce a non-closely colloidal crystal array (CCA) of PS nanoparticles. Microscale patterns of the CCA were easily fabricated through this fast and simple assembly method (Fig.1). The CCA can be transferred into a modified PDM to form a stretchable optical strain sensor. The sensor can monitor compressive and tensile strain in the range of -15%-70% with $\Delta\lambda_{max}\approx219$ nm, as shown in Fig.2.

The electrical sensors of most dual-function e-skins are comprised of nanofillers and ionic gels, suffering from low sensitivities due to the inherent limitations associated with small conductive network variations under stretching. Inspired by the cracks in spider legs, a conductive network was prepared by brittle MXene and high ductility AgNW.[3] The prepared e-skin possesses a high gauge factor (GF) of 1339.6 and ultrafast response time about 63 ms (Fig.2).

The dual-function e-skin was fabricated by integrating the CCA film with the MXene/AgNW composite membrane. The e-skin can monitor human motion by attaching to different parts of the body. The subtle physiological motor signals including pulse, facial expression and breath can be accurately and quickly monitored by the electrical sensing component, and large joint movements can be visualized by optical sensing layer. When the e-skin is installed in the throat, it can detect slight vocal cord vibration during pronunciation. A machine learning algorithm was exploited to realize the recognition of words with different pronunciations, and the accuracy rate was higher than 96%. The optical-electrical dual-mode strain sensor provides a broader optical platform for advanced visual interactive devices and smart wearable electronics.

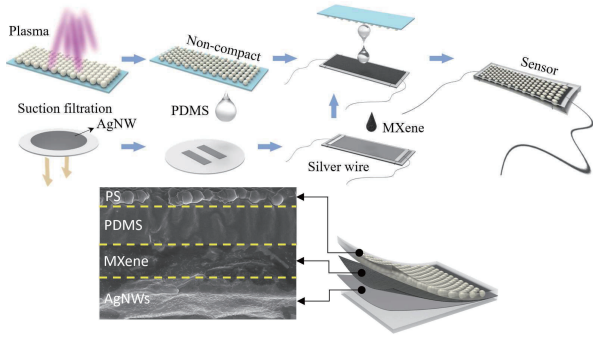

Fig. 1. Schematic of the fabrication process and structure of the e-skin

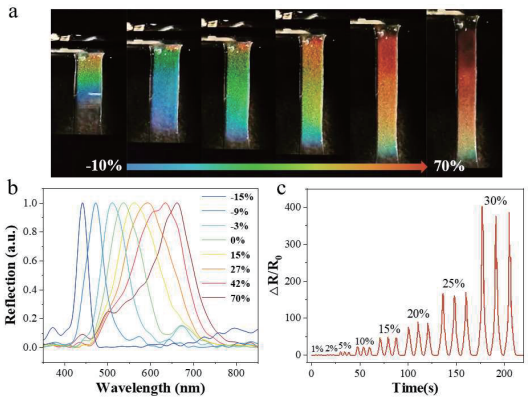

Fig. 2. (a) Photographs of the e-skin under different strains, (b) Reflectance spectra and (c) Resistance response under various strains

References

1. Sun, Y.; Wang, Y.; Liu, Y.; Wu, S.; Zhang, S.; Niu, W., Biomimetic Chromotropic Photonic-Ionic Skin with Robust Resilience, Adhesion, and Stability. *Advanced Functional Materials* **2022,** *32* (33).

2. Wang, Y.; Yu, Y.; Guo, J.; Zhang, Z.; Zhang, X.; Zhao, Y., Bio-Inspired Stretchable, Adhesive, and Conductive Structural Color Film for Visually Flexible Electronics. *Advanced Functional Materials* **2020,** *30* (32).

3. Kang, D.; Pikhitsa, P. V.; Choi, Y. W.; Lee, C.; Shin, S. S.; Piao, L.; Park, B.; Suh, K. Y.; Kim, T. I.; Choi, M., Ultrasensitive mechanical crack-based sensor inspired by the spider sensory system. *Nature* **2014,** *516* (7530), 222-6.

An “Intelligent” Gas Sensor Array based on IGZO Thin Film Transistors

Zong Liu*, Yushen Hu**, and Man Wong*

Dept. of Electronic and Computer Engineering, The Hong Kong University of Science and Technology, Hong Kong, CHINA

A gas-sensor array (GSA) is constructed based on the monolithic integration of micro hot-plates (MHPs) with indium gallium zinc oxide (IGZO) thin film transistors (TFTs) [1]. TFT-based active-matrix circuits can control the temperature of each unit and readout temperature/gas sensing signals. A die of artificial neural network (ANN) based on dual-gate (DG) TFTs has been constructed for gas analysis. Presently described is a heterogeneously packaged system employing an ANN with a hierarchical architecture consisting of cascaded networks for processing the output signals of the GSA. Gas species identification is first inferred before a species-dependent offset bias is superimposed on a subset of the GSA output signals for improved accuracy of gas concentration inference. It’s promising to realize a fully integrated “intelligent”, real-time gas sensing system.

The silicon-migration technology (SiMiT) is key to improving the integration compatibility between the MHPs and the TFTs because it can form a suspended diaphragm that is also spontaneously sealed. Shown in Fig. 1 are schematic cross-sections of the GSA and the ANN. For the latter, parallel, dual-gate (DG) indium-gallium zinc oxide (IGZO) TFTs as computation elements are fabricated. The indium–tin oxide (ITO) is used for forming the top gate because of its oxygen-permeability during the annealing process [2].

Four MHPs in the GSA are coated with the same tin (IV) oxide gas-sensitive material. Meanwhile, they are set at four different temperatures to improve their sensing specificity to ethanol, methanol, and ammonia ranging from 20 to 100 ppm. Inspired by the three stages of olfactory sensing, a three-stage hierarchical multi-layer ANN is constructed for the sequential flow of species identification using a "4 × 7 × 1" ANN followed by concentration estimation using a "2 × 4 × 1" ANN as shown in Fig. 2. The identification result in the microcontroller program is the connector between the two networks for the selection of the weights matrix of the second ANN and the superimposition of species-dependent offset bias for accuracy improving.

Shown in Fig. 3 (a) is the epochal evolution of the cost during species identification training. The correct rate for gas species identification of the training set is "44/45" as shown in Fig. 3 (b). Depicted in Fig. 3 (c) is the epochal evolution of the cost during concentration estimation training of three kinds of gases. As shown in Fig. 3 (d), the output of training sets of three gases on their respective trained ANNs shows small errors. Forty-five new data are extracted and analyzed as shown in Fig. 4. Not only a high accurate rate of identification is achieved, the concentration extraction result of untrained 80 ppm indicates the ability to estimate gas concentration continuously in a range when only a few concentration levels need to be trained.

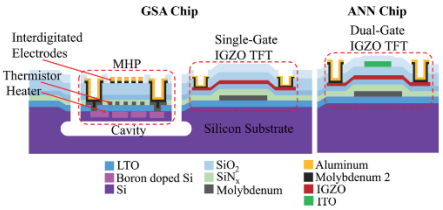

Fig. 1. Cross-sections of the GSA and the ANN

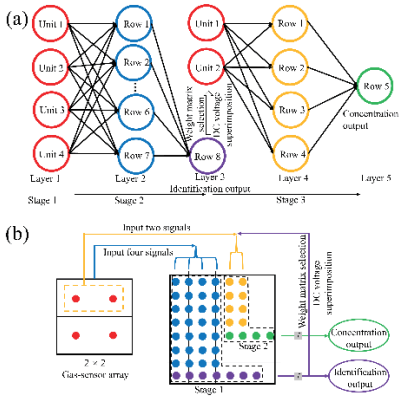

Fig. 2. The hierarchical architecture of the ANN

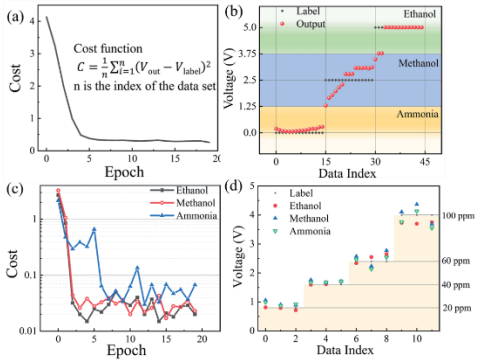

Fig. 3. ANN training and results

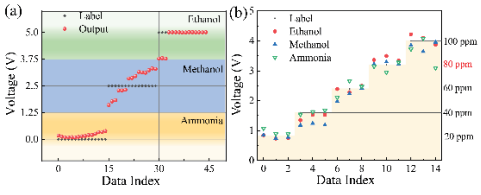

Fig. 4. New gas sensing data analysis

References

[1] Z. Liu et al., *MEMS 2023,* pp. 259-262.

[2] Y. Hu et al., *IEEE Transactions on Electron Devices*, vol. 69, no. 10, pp. 5574-5579, Oct. 2022.

A High-Reliability, Capacitorless, 1-to-4 Sharing Architecture Gate Driver with a-Si: H TFTs for TFT-LCD Application

Bor-Jiun Huang *, Guang-Ting Zheng **, Po-Tsun Liu ***

*** Department of Photonics & Institute of Electro-Optical Engineering, National Yang-Ming Chiao-Tung University, Hsinchu**

This paper proposed a novel GOA circuit with **capacitor-less**, **noise-free sharing**, **carry-stage**, and **high reliability** for a narrow bezel display application. The capacitor-less and sharing method used in circuit design could reduce the large layout area to achieve a narrow bezel. Using the carry-stage and lower voltage level to promote the issue of using a capacitor-less technique that will suffer from the output is sensitive to the noise and the severe leakage current of pre-charge nodes at high temperatures. The simulation result shows that the proposed circuit could normally operate from −40°C to 85°C. The proposed circuit has passed the reliability test for 800 hours at 85°C, which means the proposed circuit could still normally operate after a long-time operation at a high temperature. Finally, the proposed circuit demonstrated on a 4.7-inch HD panel successfully passed the test of wide temperature. Therefore, the proposed GOA circuit is suitable for integration into the narrow bezel high-reliability TFT-LCD panels.

The proposed input signal includes a high voltage signal V_{DD} (15 V), two low voltage signals V_{SS} (-12 V) and V_{SS2} (-18 V), two start pulses ST1 and ST2, two stop pulses STP1 and STP2, eight clock signals CLK1 ~ CLK8 with voltage from 15 V to −12 V, two noise-free clocks ECK and EXCK with voltage from 15 V to −18 V, and reset signal RST. The pulse width of CLK1 ~ CLK8 is 87.5 μs, and the cycle time is 200 μs. Divide CLK into 16 phases that define each phase with 1H = 12.5 us. Each CLK will overlap 5H.

Fig. 1 shows the connection between different blocks of the proposed circuit. Fig. 2 shows the circuit schematic of 1-to-4 noise-free sharing modules of the proposed circuit in every four stages. 1-to-4 noise-free sharing modules mean every four stages share one noise-free block, which provides the same noise-free function (Q[1] and Q[1X]) as the related four stages. Moreover, the two identical dual diode-connected noise-free blocks could provide the full-time noise-free function for output stages. The gate driver circuit operates by the input start signal (Vstart1 and Vstart2).

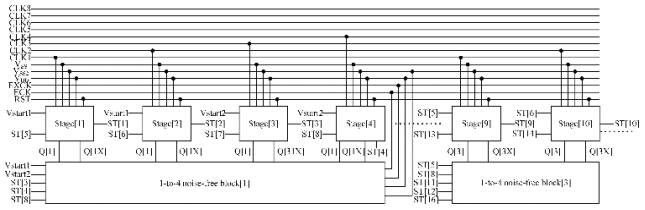

Fig. 1. The circuit schematic of 1-to-4 noise-free sharing modules of the proposed circuit

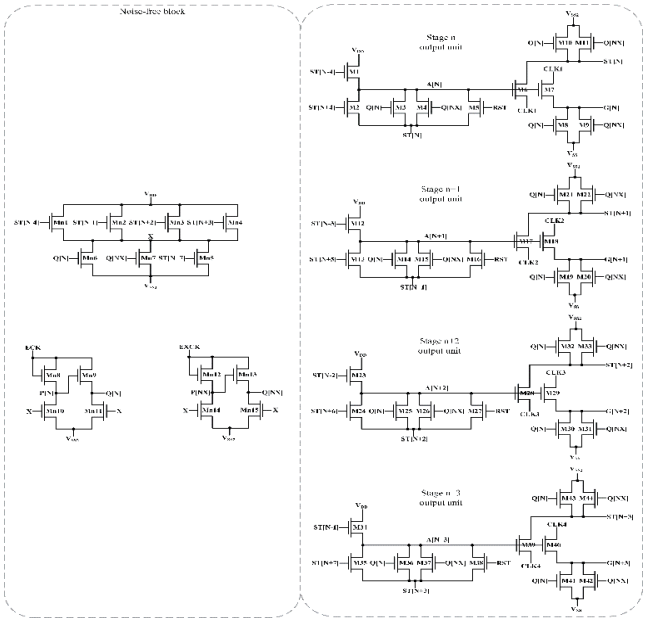

Fig. 2. The circuit schematic of 1-to-4 noise-free sharing modules of the proposed circuit

Table 1. Forward scan simulation results at 25°C

Forward scan	Rising time	Falling time	RMS
G[1]	**3.35 μs**	**3.2 μs**	**0.01 V**
G[200]	**3.34 μs**	**3.19 μs**	**0.01 V**
G[400]	**3.34 μs**	**3.19 μs**	**0.01 V**
G[640]	**3.34 μs**	**3.2 μs**	**0.01 V**

Table 2. Forward scan simulation results at 85°C

Forward scan	Rising time	Falling time	RMS
G[1]	**2.84 μs**	**2.79 μs**	**0.01 V**
G[200]	**2.85 μs**	**2.76 μs**	**0.01 V**
G[400]	**2.85 μs**	**2.76 μs**	**0.01 V**
G[640]	**2.86 μs**	**2.76 μs**	**0.01 V**

Table 3. Forward scan simulation results at -40°C

Forward scan	Rising time	Falling time	RMS
G[1]	**14.6 μs**	**11.6 μs**	**0.02 V**
G[200]	**14.4 μs**	**11.7μs**	**0.02 V**
G[400]	**14.4 μs**	**11.7 μs**	**0.02 V**
G[640]	**14.4 μs**	**11.7 μs**	**0.02 V**

References

[1] G. T. Zheng, P. T. Liu, "Design of dual-outputs-single-stage a-Si: H TFT gate driver for high resolution TFT-LCD application," JSID,vol.24, no.5, pp.330-337, 2016.

[2] Z. Wang, H. Huang, C. Dai, and D. Xia, "P-12: Novel 1-to-N Architecture of Bidirectional Gate Driver for Ultra-Narrow-Border Display," in SID Digest of Technical Papers, 2018, vol. 49, no. 1: Wiley Online Library, pp. 1223-1226.

Power and Color Shift Analysis of Driving MicroLED Display with Gamma 2.2 Correction in Low Grayscale

Wei-Lin Wu*, Jun-Wei Wu**, Ya-Hsiang Tai***

***Department of Photonics and Institute of Electro-Optical Engineering, College of Electrical and Computer Engineering, National Yang Ming Chiao Tung University, Hsinchu, Taiwan, 30010, R.O.C.**

As a potential next-generation mainstream display technology, Micro light-emitting diodes (μLEDs) displays have many advantages. However, the driving current density of μLED can cause wavelength shift and changes in external quantum efficiency (EQE). To address these challenges and ensure a proper fitting of the low grayscale gamma 2.2 curve, the Hybrid Pulse Width and Amplitude Modulation (HPP) driving method is utilized.

Increasing the PPI in HPP driving mode, the EQE value will be smaller due to the restriction to use at low brightness and PAM part to analyze whether the power consumption at low grayscale is affected more. The simulation uses actual specifications, employing Python deep learning to analyze data and extract various grayscale values.HPP power consumption is compared to PWM in Fig. 1, indicating PWM's better power performance at low grayscale. However, the difference between PWM and HPP is not significant. Fig. 1 also illustrates that as PPI increases, power difference between PWM and HPP at low grayscale reduces. Fig. 2 displays four different grayscale distribution images, which are considered representative based on hundreds of images. can confirm whether it exhibits the same trend as Fig. 1. As the proportion of low grayscale increases, the trend of decreasing power difference between PWM and HPP with higher PPI is still observed.

The driving current density can cause wavelength shift, resulting in color shift use CIE Luv, which reflects the actual magnitude of color shift, and combine it with the Python Colour library for coordinate calculations. Based on the overlay analysis, Fig. 3 reveals that the color shift ranges for RGB are very small. The maximum color shift range for the μ' coordinates of green μLED is ±0.0033. These deviations are negligible to the human eye. ($\Delta \mu' \nu' < 0.02$)

Deep learning simulation analyzed power and color shift in μLEDs using HPP driving at low grayscale with gamma 2.2. Results show a slight decrease in EQE with increasing PPI, but overall impact is not significant. Power and color shift at low grayscale are negligible. Thus, μLED driving current density issue has no significant impact. For product design, focus on circuit design if power and color shift are not critical, and choose between PWM and HPP driving methods.

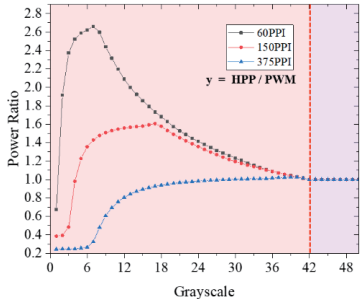

Fig. 1. Power ratio between HPP and PWM

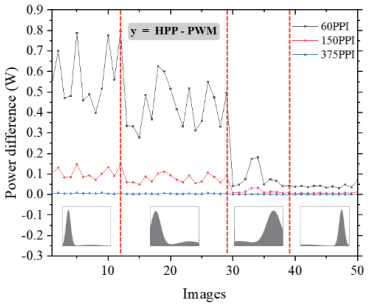

Fig. 2. Power difference vs input image

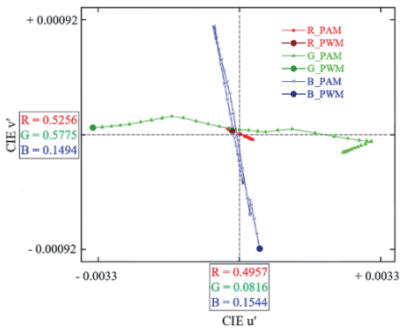

Fig. 3. RGB color shift range of Lu′v′ coordinates

References

[1] Huang, Y., Hsiang, E. L., Deng, M. Y., & Wu, S. T. (2020). Light: Science & Applications, 9(1), 105.

[2] Hong, Yong-Hoo, et al. Journal of Information Display 23.4 (2022): 243-249.

[3] Hong, Yong-Hoo, et al. SID Symposium Digest of Technical Papers. Vol. 52. No. 1. 2021.

[4] Oh, Jongsu, et al. IEEE Electron Device Letters 42.10 (2021): 1496-1499.

Progress Review of Driving Method and Color Evaluation for Color Electrophoretic Display

Xinzao Wu, Guangyou Liu, Yue Zhang, Jie Liu, Zhuohang Li, Ting Wang, Jintao Shi, Feng Xiong, Zong Qin, Bo-ru Yang*

State Key Laboratory of Optoelectronic Materials and Technologies, Guangdong Province Key Laboratory of Display Material and Technology, School of Electronics and Information Technology, Sun Yat-Sen University, Guangzhou 510275, People's Republic of China.

***Emial:Paulyang68@me.com**

Electrophoretic display (EPD) has the advantages of ultra-low power consumption, flexibility, lightness, low cost and good readability in sunlight, which has great application prospects[1]. Color EPD can provide abundant information and good reading experience. In this paper, we will summarize the current mainstream color electrophoretic display technologies in detail, and review the progress of color E-paper in driving and color evaluation in recent years.

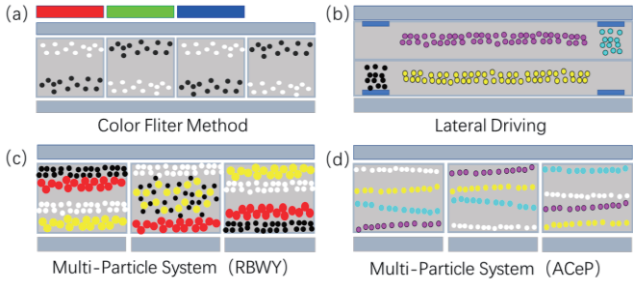

Fig. 1. Color EPD Technology

Electrophoretic display technology uses applied electric field to control the movement of electrophoretic particles in the microcavity, forming a specific spatial arrangement, thus presenting various colors and patterns. Color filter electronic paper overlays a color filter array (CFA) on top of traditional black and white electrophoretic displays. By mixing the ambient light reflected by electrophoretic particles with color filters, color effects are achieved. The color filter method has a simple and mature fabrication process suitable for mass production. However, introducing CF absorbs 70% of ambient light, affecting brightness and saturation. To improve the display performance of the color filter method, various schemes have been proposed, such as RGBW filters, optimal decomposition algorithms, and reflected color filters.

Lateral driving technology adds a control electrode at the bottom of traditional vertical driving electrophoretic displays, allowing particles to move within the plane. By controlling the particle accumulation or spreading, it enables black, white, color, and even transparent state. Canon, Sipix, and Philips have proposed their respective lateral driving colorization schemes. The lateral driving structure avoids the brightness loss issue of the color filter method. However, challenges remain regarding the trade-off between the bottom electrode and aperture ratio, and complex electrode arrangements, requiring further research[2].

Multi-particle system color electrophoretic displays contain multiple color primary particles within microcavity. This approach achieves better brightness and saturation, making it the most promising technology for color electrophoretic displays. However, increasing the number of particle types adds complexity to the system. Precise control of particle charge and threshold voltage, as well as waveform design, are crucial research areas. The current mainstream multi-particle system color electrophoretic display technologies include IMCP, ACeP, RBW and RBWY.

The driving waveform in electrophoretic displays directly affects the accuracy of grayscale and the vividness of color displays. The driving waveform for color filter-based E-paper is similar to that of black and white electrophoretic displays, including four stages: erase, DC balance, activate, and drive stages. Compared to black and white E-papers, three-color E-papers[3] add a low-level voltage and an additional red drive stage in the drive stage. Researchers have also optimized three-color electrophoretic driving, including response time, saturation enhancement, and ghosting elimination. Four-color electrophoretic particles require five-level or seven-level push-pull waveforms that need to repeat the drive stage waveform multiple times to achieve the desired display effect.

Color evaluation is an important criterion for color displays. However, there is currently no unified standard for color evaluation in electrophoretic displays[4]. As E-paper relies on ambient light for display, brightness is a significant factor in color evaluation. Therefore, three-dimensional color gamut volume can better represent its true color capability. However, the volume of color gamut space cannot directly reflect all color information, and it is difficult to compare. The recently proposed gamut rings[5] standard provides a two-dimensional mapping of color gamut volume, capturing the three elements of color on a two-dimensional plane. Therefore, comprehensive evaluation using chromaticity volume and color gamut rings is a promising choice for assessing the color capabilities of electrophoretic displays.

References

[1] Yang B-R. “E-Paper Displays”. John Wiley & Sons Ltd, Chichester, ISBN: 978-1-119-74558-7, 2022.

[2] BLANKENBACH K, HENZEN A, CHIEN L-C, et al. Improvements in in-plane electrophoretic displays [Z]. Advances in Display Technologies; and E-papers and Flexible Displays. 2011.10.1117/12.876578

[3] KAO W-C and TSAI J-C. Driving method of three-particle electrophoretic displays [J]. 2018, 65(3): 1023-8.

[4] HERTEL D, BOUCHARD A, KRUSE R, et al. Gamut rings of reflective ePaper displays with combined frontlight and ambient illumination [J]. Journal of the Society for Information Display, 2022, 30(5): 351-62

[5] MASAOKA K, JIANG F, FAIRCHILD M D, et al. 78-3: 2D Representation of Display Color Gamut [J]. SID Symposium Digest of Technical Papers, 2018, 49(1): 1048-51

Passive Matrix Driving Method of Alternating Current Electroluminescence with Multiple Grey Levels

Qitian Fan, Jintao Shi, Simu Zhu, Yifan Gu, Zong Qin, Bo-ru Yang*

State Key Laboratory of Optoelectronic Materials and Technologies, Guangdong Province Key Laboratory of Display Material and Technology, School of Electronics and Information Technology, Sun Yat-Sen University, Guangzhou, China (paulyang68@me.com)

Flexible electronics have attracted wide attention during the recent years. Currently there have been various devices with flexible displays appearing in the market. Alternating current electroluminescence (ACEL) is an intrinsically flexible luminescent device formed with electroluminescent (EL) phosphors sandwiched in between two flexible electrodes, and it is able to function stably under stretching and twisting. [1-6] ACELs are driven by high-voltage, high-frequency AC, but currently there isn't any method to manipulate AC with a display matrix, limiting its future to full color display. In this work, we propose a passive matrix based on full bridge inverter to drive ACELs in multiple grey levels.

The basic structure of our passive matrix is shown in Fig. 1, which is a full bridge inverter, consisting of 4 n-channel MOSFETs. The capacitor C1 is equivalent to an ACEL device. When Q1, Q4 are turned on and Q2, Q3 turned off, the left end of the capacitor is connected to the power source while the other is connected to the ground, resulting in a left-to-right voltage across the device. Oppositely, when Q2, Q3 are turned on and Q1, Q4 are turned off, it results in a right-to-left voltage. By repeating the previous actions, the voltage waveform across the device will be a square wave and the frequency and duty cycle of the square wave is fully configurable.

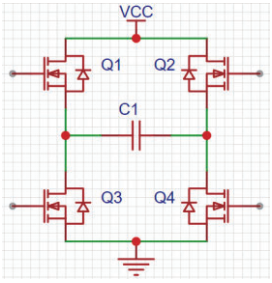

Fig. 1 Basic structure of our passive matrix

The schematic diagram of the proposed passive matrix (PM) is shown in Fig. 2. In this matrix, we output different grey levels by changing duty cycle, which in our case is the duration of voltage applied on each pixel in the matrix. The matrix is scanned by row, and when it is scanning the first row, MOSFET Q1, Q7 and Q8 turns on while the others turn off to supply voltage to pixel C1 and C2, forming the positive half of a square wave. For the negative half of a square wave, MOSFET Q3, Q4 and Q5 turns on while the others turn off. However, since the positive voltage on the same row is provided with a single MOSFET, we can't individually set the duration of positive voltage on each pixel of the same row. To solve this problem, we utilize Q3 and Q4. For example, when C1 reached its predesigned positive voltage duration, Q3 turns on and Q4 turns off, making both ends of C1 connected to the power source. With no voltage across ACEL, the device will cease to glow.

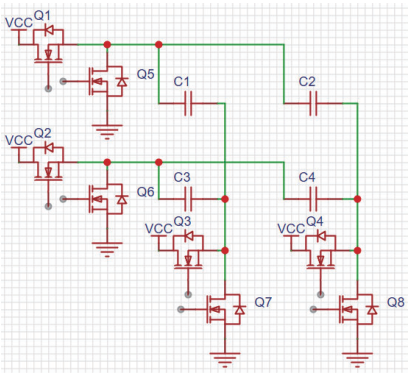

Fig. 2. Schematic diagram of proposed PM

With the previous method, we have successfully accomplished 8 grey levels with linear L*. The curve of L* in relation with duty cycle is shown in Fig. 3(a). After calibration, we can see L* changing linearly with grey level in Fig. 3(b). Also, we demonstrate a 2x2 passive matrix with 4 greyscales in Fig. 3(c).

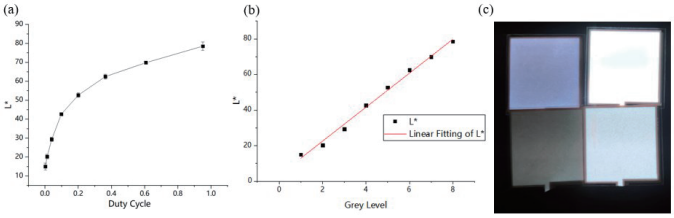

Fig. 3 (a) Curve of L* in relation with duty cycle (b) Linear grey levels (c) Demonstration of separate grey levels of GL0, GL2, GL4, GL7

References

[1] Yang B-R. "E-Paper Displays". John Wiley & Sons Ltd, Chichester, ISBN: 978-1-119-74558-7, 2022.

[2] ACS Applied Materials & Interfaces, 2017, 9(6): 5486-5494.

[3] ACS Applied Electronic Materials, 2021, 3(12): 5188-5210.

[4] Nature 591, 240–245 (2021).

[5] Journal of Materials Chemistry C, 2019, 7(3): 484-489.

[6] Nature materials, 2020, 19(2): 182-188.

A VCO-Based ADC Circuit Using N-Type Oxide TFTs

*Zhaoyu Deng *, Derun Chen*, Rongsheng Chen *, ***

***School of Microelectronics, South China University of Technology, Guangzhou, China**

****State Key Laboratory of Advanced Displays and Optoelectronics Technologies, Department of Electronic and Computer Engineering, The Hong Kong University of Science and Technology, Hong Kong, China**

In recent years, there has been a growing interest in the development of Voltage-Controlled Oscillator (VCO)-based Analog-to-Digital Converters (ADCs) utilizing Thin-Film Transistors (TFT) technology[1]. This paper provides an improved VCO-based ADC structure based on unipolar metal-oxide TFTs[1]. The ADC is powered by dual power supplies, 10V and 20V respectively. Its area is 1.617 square millimeters. Experimental results show that the proposed ADC achieves a 20S/s sampling rate with ENOB of 6.5 bits.

Fig. 1 shows the schematic of the proposed VCO. It consists of a RO, a level shifter and a sampling circuit, while the RO consists of an odd number of inverters and a non-inverting delay cell.

The VCO operates according to the following ideal working process: Assuming Va is at a high level, the capacitor C2 starts charging and Vb rises. When Vb reaches a high level, it triggers the inverters chain, causing Va to switch to a low level. At this point, the capacitor starts discharging and Vb begins to decrease. When Vb drops to a low level, it triggers the inverters chain again, causing Va to switch back to a high level. This cycle repeats, generating oscillations. The waveform of the corresponding nodes is shown in Fig. 2. The output signal of the VCO is the same as the Va node, but with less delay. By designing the charging time of the capacitor to be much shorter than the discharging time, the oscillation period approximates the discharge time (i.e., the delay of the delay unit). In this case, the output should be a series of narrow pulses as shown in Fig. 2. Due to the "regeneration" effect of the inverters chain, Vb's amplitude will be slightly smaller than Va's amplitude.

The circuit occupies an area of 1.617 mm^2 and is fully integrated on the chip, requiring no external discrete components. This design utilizes a 7-stage ring oscillator (RO). The power supply is set as VDD = 10V, VSS = 2VDD. The clock signal CLK is set to a high level to enable the sampling circuit. As shown in Fig. 3, the input signal is scanned from 2V to 7V, and the output consists of a series of pulses that can be directly processed by the subsequent counter circuit. The maximum linear error (ferror) of the circuit is 2% of the output frequency range.

Based on the spectrum plot in Fig. 4, the signal-to-noise and distortion ratio (SNDR) of the ADC is 41.1 dB. T he SNDR is the ratio of the signal amplitude to the combine d amplitude of noise and distortion. The formula to calculat e ENOB is as follows:

ENOB = (SNDR - 1.76) / 6.02.

Here, 1.76 dB accounts for the loss due to quantization noise, and 6.02 is a constant that converts the units to bits. Substituting the value of SNDR into the formula: ENOB = (41.1 - 1.76) / 6.02= 39.34 / 6.02≈ 6.53 bits

Therefore, based on the given SNDR, the calculated ENOB for the ADC is approximately 6.53 bits.

The proposed design has the potential for a smaller footprint and higher SNDR, making it suitable for flexible substrates, low-cost, and medium-speed sensor readout interfaces.

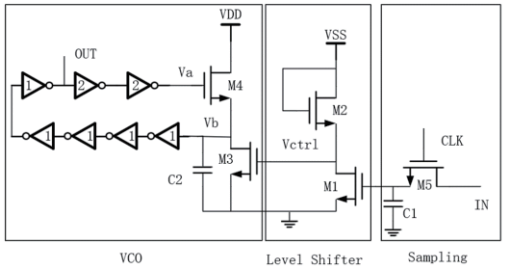

Fig. 1. The proposed VCO-based ADC

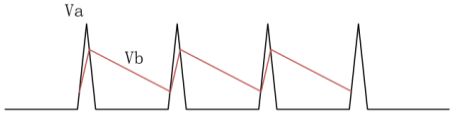

Fig. 2. The diagram of the VCO waveforms

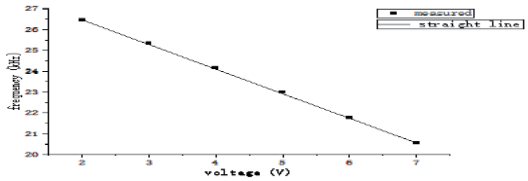

Fig. 3. Characteristic of the VCO

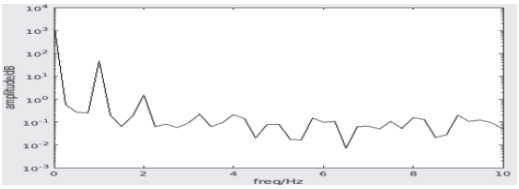

Fig. 4. The spectrum of the reconstructed signal from the ADC digital output

References

[1] Zulqarnain M, Stanzione S, Rathinavel G, et al. A flexible ECG patch compatible with NFC RF communication[J]. npj Flexible Electronics, 2020, 4(1): 13.

[2] Li B, Wei S, Zhao M, et al. A Delay-Cell-Controlled VCO Design for Unipolar Single-Gate Enhancement-Mode TFT Technologies[J]. Micromachines, 2022, 14(1): 32.

Design of High-Precision Horizontal Synchronization Circuit in Micro-LED Display Driver

Wenhao Zhang, Xinyi Liu*, Zhaojun Liu*,*

**Department of electronic and electrical engineering, Southern University of Science and Technology, Shenzhen, Guangdong, 518055, China.*

Email: 12132161@mail.sustech.edu.cn; 12051011@mail.sustech.edu.cn; liuzj@sustech.edu.cn

Abstract

With the human stepping into the information society and the rapid increase of information, various display facilities and display devices are getting unprecedented development. In the display industry, Micro-LED has become the focus of development because it has the advantages of both traditional LED and small size, and can achieve extremely high PPI. However, it is precisely because of its small size, in order to drive Micro-LED display, it is particularly important to design a separate driver circuit that meets its characteristics. In this paper, a kind of high-precision horizontal synchronization(HSYNC) circuit in Micro-LED display driver is studied. By comparing different structures, the performance of HSYNC circuits under different frequencies and process corners is analyzed. This paper introduces and analyzes the circuit structure and design flow of this HSYNC circuit. Simulation is carried out by Cadence software, and its actual performance is verified by taping out.

Author Keywords

Micro-LED; Active address; Display drive circuit

1. Background

Traditional horizontal synchronization(HSYNC) circuits typically use shift registers composed of data flip-flops. The simulation results are shown in Fig.1.

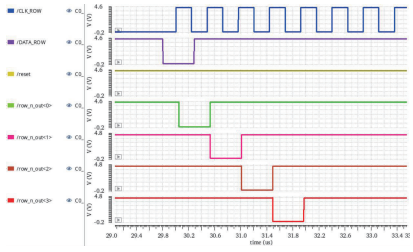

Fig.1 Traditional HSYNC circuit simulation results

As shown in Fig.2, this HSYNC signal obtained by this structure may cause errors in our pixel driver circuit.

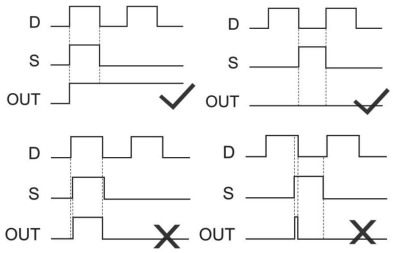

Fig.2 Errors caused by delay in pixel driver circuit

2. High-precision horizontal synchronization circuit design

The RCLK signal is delayed by 0.1 to 0.4 clock cycles. At the same time, an AND gate is added to the line scan circuit to perform an AND gate operation on the signal generated by the shift register and RCLK, reducing the high-level width of S by half. And add an OR gate, perform an OR gate operation on S and RSTX to reset S to 1, thereby resetting the entire screen. After resetting the RSTX signal, setting S to 0 will not affect subsequent logic.

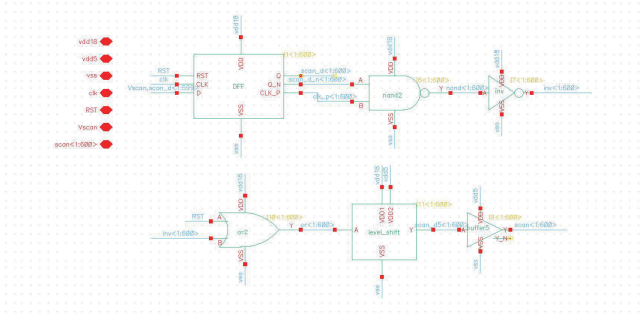

Fig.3 High-precision HSYNC circuit structure

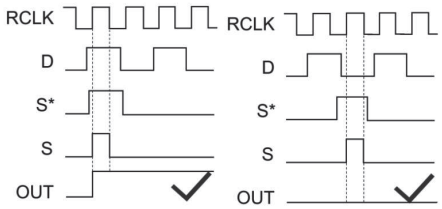

Fig.4 New HSYNC signal in pixel driver circuit

3. Simulation and test

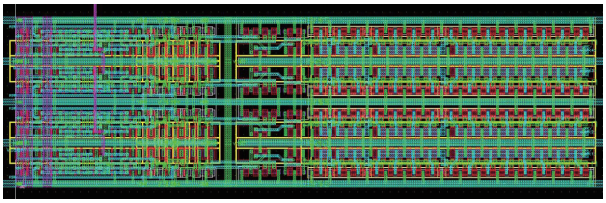

Fig.5 Layout of high-precision HSYNC circuit

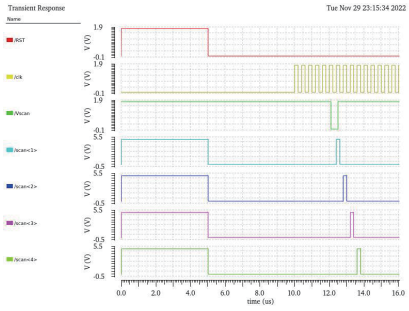

Fig.6 High-precision HSYNC circuit simulation results

A Review on Micro-LED Display Integrating Metasurface Structures in Controlling Emission Angles

Zhaoyong Liu[1,2,3], Kailin Ren[1,2,3], and Jianhua Zhang[1,2,3,]*
1 School of Microelectronics, Shanghai University, Shanghai 200444, China
2 Key Laboratory of Advanced Display and System Applications (Ministry of Education), Shanghai University, Shanghai 200444, China
3 Shanghai Key Laboratory of Chips and Systems for Intelligent Connected Vehicle, Shanghai University, Shanghai 200444, China

Abstract
Micro-LED display technology has been considered as a promising candidate for near-eye display applications owing to its superior performances such as high brightness, high resolution, and high contrast. However, optical crosstalk between pixels can lead to unclear display images and cause dizziness. Therefore, reducing crosstalk has become a hot research topic. Recently, by exploiting the capability of metasurface in wavefront modulation, researchers have achieved many excellent results by integrating metasurface structures with Micro-LEDs, including improving the light extraction efficiency, controlling the emission angle to achieve directional emission, and obtaining polarized Micro-LEDs. Among them, achieving directional emission of Micro-LEDs can solve the problem of optical crosstalk between pixels. In this paper, recent progresses on Micro-LEDs integrated with metasurface structures are reviewed in controlling angular deflection of emission.

Keywords
Micro-LED, metasurface, collimation, angular deflection

1. Introduction
Micro-LEDs have attracted much attention owing to their advantages of high luminous intensity, high resolution, high contrast, fast response speed, long life and low power consumption. Due to these excellent performance traits, Micro-LEDs are regarded as the mainstream of the next-generation display technology, for a wide range of applications, from wearable devices such as wristbands and watches to commercial billboards, public displays, and virtual reality (VR) or augmented reality (AR) devices [1],[2]. However, challenges have also arisen with th e development of Micro-LED display technology, such as optical crosstalk between pixels [3]. This is because a typical Micro-LED exhibits Lambertian-shaped emission [4]. This wide-angle emission causes light interactions between adjacent pixels to cause dizziness. Therefore, reducing the crosstalk between Micro-LED pixels has become a mainstream research direction.

The metasurface is an artificial nanostructure that is designed to control the amplitude, polarization, and phase of incident waves at the subwavelength scale [5],[6] . Metasurface structures can realize the above functions with the premise that the incident light must be coherent [7]. However, light emitted of Micro-LEDs in any direction has very low spatial coherence, so it is a key issue to realize control of the Micro-LED wavefront with metasurface. Therefore, the researchers introduced reflective mirrors at the bottom and top of the Micro-LED to form the Fabry-Perot (F-P) cavity structure [7], so that the emitted light is concentrated in a narrow angular range after resonance selection through the cavity, which can enhance the spatial coherence of the emitted light. In this case, the integration with the metasurface structure can realize the deflection of the beam angle, and the light can be emitted to the preset position to reduce optical crosstalk. This paper reviews the research progress of Micro-LEDs integrated with metasurface structures in controlling emission angles.

2. Control of the deflection of light angle
The metasurface structures can accurately control the phase of the wavefront to realize the control of the emitted light angle of Micro-LED. The nanocolumn array is integrated on the top surface of Micro-LED, which is composed of nanocolumn with different diameters in one cycle to achieve 0−2π phase coverage. The changes of the nanocolumn and phase can be changed by changing the height of the nanocolumn and the equivalent refractive index, which can be achieved by changing the diameter of the nanocolumn. The phase coverage of 2π is realized by selecting suitable nanocolumns with different diameters and adjusting different periods to achieve different emission angles.

In 2018, Liu et al. demonstrated for the first time the control of metasurface structure on light emitted by LED with a wavelength of 460 nm through simulation [7]. This paper compared the far-field graphs of LED with a directly added TiO_2 nanocolumn arrays and resonant cavity LED (RCLED) with TiO_2 nanocolumn arrays added on its surface. RCLED can achieve a 20° angular deflection by controlling the phase with the metasurface structure, while LED cannot. The result indicates that the resonant cavity structure can collimate the Lambertian-shaped emission of LED, approximating a plane wave, and enhance the spatial coherence of the emitted light from LED. Two years later, the team added the metasurface RCLED design to the GaP LED [8], proposing that as long as the reflectivity of the metasurface is low, resonators and metasurface can be designed separately and independently, showing the flexibility and universality of the metasurface design. In the GaP metasurface RCLED, the resonator consists of bottom Au mirrors and top DBR mirrors, with top nanocolumns selected with high index Si materials. However, Si material

has high absorption in the visible band, which will reduce the light output efficiency, so TiO_2 material with high refractive index can be chosen to replace it. In the paper, the 30° deflection of the emitted light beam with a wavelength of 620 nm is obtained [see Fig. 1(d)]. Fig. 1 shows the full process of angular control through the integration of the metasurface structure and RCLED.

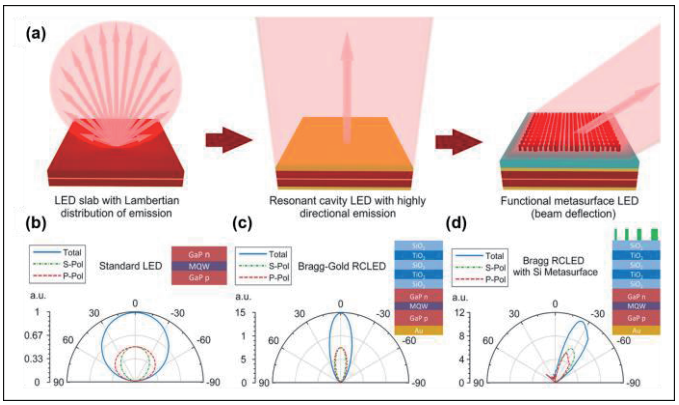

Fig. 1. (a) Schematic diagram of metasurface control of LED emitted light. The far-field diagram of (b) GaP LED, (c) Hybrid bragg-gold RCLED and (d) Hybrid RCLED with the integrated metasurface [8].

In recent years, the demand for near-eye display devices has been increasing, and Micro-LED that can be emitted in unidirectional direction is undoubtedly one of the most ideal light sources, as unidirectional emissions can reduce optical crosstalk and provide a better visual experience. Huang et al. proposed a metasurface RC Micro-LED with unidirectional emission [9]. Different diameters of nanocolumn can produce different phase changes, which can satisfy the phase coverage of 0−2π within a period. The nanocolumn with different diameters are selected to form different periods to achieve unidirectional emission of light at different angles. The structure diagram and control phase schematic diagram are shown in Fig. 2(a) and 2(b) respectively. Controllable one-way emission Micro-LED can prevent light leakage. In 3D display, unidirectional emission of light to the left eye and the right eye can reduce pixel crosstalk and improve 3D display effect, shown in Fig. 2(c). In addition, Micro-LED composed of a pixel with a variety of emission directions can produce a wider viewing angle and more 3D viewing points [see Fig. 2(d)], so as to have a better 3D display experience, providing more impetus for the future development of near-eye 3D Micro-LED displays. The team later made a 3D display using Micro-LEDs emitted in a unidirectional and compared it with a traditional 3D display [10], the schematic diagram of both is shown in Fig. 2(e) and 2(f). Through comparison, the results found that unidirectional Micro-LED pixels can effectively reduce optical crosstalk and improve the display effect.

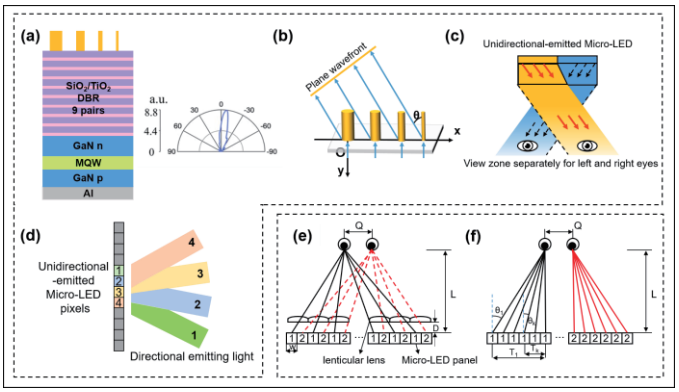

Fig. 2. (a) Device structure and far-field diagram of Micro-LED with the beam deflecting metasurface. (b) Working schematic of the beam deflection supercell. (c) Unidirectional emission Micro-LED for naked-eye 3D display. (d) Multi-view naked-eye 3D display with unidirectional emission Micro-LED pixels [9]. Autostereoscopic 3D Micro-LED display system based on (e) lenticular lens, and (f) unidirectional emission Micro-LEDs [10].

The control of the angle of emitted light by metasurface structures has also been developed in QD LEDs, which brings a new scheme for optimizing QD LEDs. Park et al. showed the control of metasurface structures on the angles of light emitted by the colloidal quantum dot (CQD) RCLEDs [11]. The CQD RCLED structure is shown in Fig. 3(a) with five pairs of DBR mirrors on both the bottom and top to form a resonator, with the top integrating TiO_2 nanocolumns to allow angular deflection. In Fig. 3(b), the relationship between the diameter and phase (red lines) of TiO_2 nanocolumns with heights of 700 nm and 300 nm is shown, respectively. The results present that the phase coverage of 0–2π cannot be achieved by the short nanocolumns, but using patterned TiO_2 nanocolumns with a high aspect ratio is difficult. Therefore, the team selected TiO_2 nanocolumns with low aspect ratios to control the angle of light by adjusting the period and phase within the period, thus reducing the difficulty of the manufacturing process. The black line represents the relationship between diameter and transmittance, and it can be observed that the high TiO_2 nanorods experience a sharp drop at a diameter of 250nm. The final simulated and experimentally measured deflection angles in this paper are both 20°, with only a 4 nm deviation in peak wavelength. Therefore, the experimental results highly match the simulation. Huang et al. conducted a simulation study on the exit angle control of QD LEDs [12]. Comparing the emission light direction diagrams of the Gaussian beam and electric dipole light sources in the RCLEDs formed by the bottom flattened Ag mirror and top DBR mirror, they found that the RC of the flattened Ag mirror and DBR mirror failed to collimate the QD LED emission of light, resulting in unrealized angle control. The team proposed that the circular patterned bottom Ag mirror and the top DBR mirror formed an RC to realize the emitted light collimation, and the different deflection angles were controlled by selecting nanocolumns of different diameters to form different cycles, shown in Fig. 3(c). This method provides a scheme for the manipulation of a single QD, and presents the structural design differences

between QD LEDs and Micro-LEDs in angular deflection.

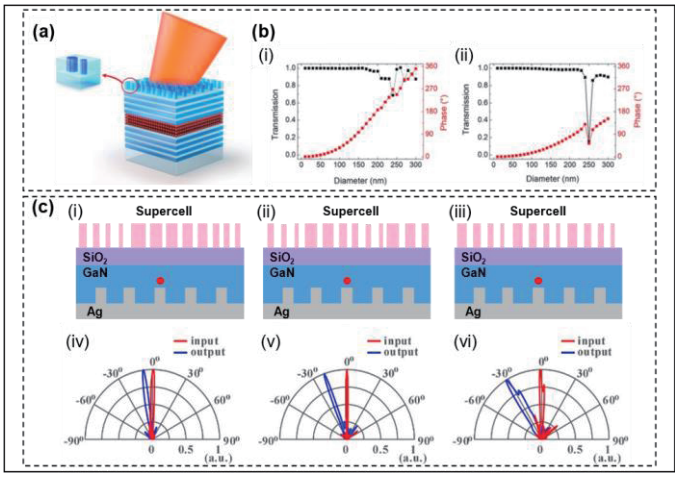

Fig. 3. (a) Schematic of CQD RCLEDs with TiO_2 metasurface. (b) Calculated look-up tables of a TiO2 nanocolumn with thicknesses of (i) 700 nm and (ii) 300 nm [11]. (c) (i–iii) Schematic structures of GaN-based QD LEDs with an Ag grating and a phase-gradient metasurface. Polar plots for the input beam and output beam of the metasurface. (iv–vi) are the cases for 10°, 20°, and 30° angle deflection, respectively [12].

In this chapter, the research on metasurface structures controlling the direction of light emitted by Micro−LEDs is summarized. Recent research findings are mostly simulation results, as the manufacturing process of multi−layer DBR mirrors and metasurface is relatively complex, and the design and fabrication of metasurface structures still face many challenges and high costs. Therefore, there might still be a long way before their application in displays.

3. Conclusions

In this paper, the applications of metasurface structures integrated with Micro-LEDs in obtaining directional emission is reviewed. In the field of display technologies such as AR and VR, optical crosstalk between pixels is a significant problem affecting the viewing experience. By using RC collimation to reduce the emission width and further applying metasurface structures to achieve directional emission, the phenomenon of optical crosstalk is significantly weakened. In addition, the integration of metasurface and Micro-LEDs has produced many positive results in improving the light extraction efficiency and polarization of Micro-LEDs. The integration of metasurface and Micro-LEDs will create more possibilities for the rapid development of Micro-LED displays.

References

[1] H.E. Lee et al., “Micro Light-Emitting Diodes for Display and Flexible Biomedical Applications,” Adv. Funct. Mater. 2019, 29, 1808075.

[2] Z. Wang, X.Y. Shan, X.G. Cui, and P.F. T, “Characteristics and techniques of GaN-based micro-LEDs for application in next-generation display,” J. Semicond. 2020, 41, 041606.

[3] A.R. Anwar et al., “Recent Progress in Micro-LED-Based Display Technologies,” Laser Photonics Rev. 2022, 16, 2100427.

[4] P.J. Parbrook, B. Corbet, J. Han, T.Y. Seong, and H. Amano, “Micro-Light Emitting Diode: From Chips to Applications,” Laser Photonics Rev. 2021, 15, 2000133.

[5] S. Chang, X. Guo, and X. Ni, “Optical metasurfaces: progress and applications,” Annu. Rev. Mater. Res. 2018, 48, 279-302.

[6] J.Y. Yang, S. Gurung, S. Bej, P.N. Ni, and H.W.H. Lee, “Active optical metasurfaces: comprehensive review on physics, mechanisms, and prospective applications,” Rep. Prog. Phys. 2022, 85, 036101.

[7] Z. Liu et al., “Using metasurfaces to control random light emission,” IEEE. CLEO-PR.

[8] E. Khaidarov et al., “Control of LED emission with functional dielectric metasurfaces,” Laser Photonics Rev. 2020, 14, 1900235.

[9] J.P. Huang, Z.L. Hu, X. Gao, Y. Xu, and L.C. Wang, “Unidirectional-emitting GaN-based micro-LED for 3D display,” Opt. Lett. 2021, 46, 3476-3479.

[10] Y. Xu, J.W. Cui, Z.L. Hu, X. Gao, and L.C. Wang, “Pixel crosstalk in naked-eye micro-LED 3D display,” Appl. Opt. 2021, 60, 5977-5983.

[11] Y. Park, H. Kim, J. Lee, W. Ko, K. Bae, K. Cho. Direction control of colloidal quantum dot emission using dielectric metasurfaces. Nanophotonics 2020, 9, 1023–1030.

[12] H. Huang, S. Zheng W. Sun. Beam manipulation for quantum dot light-emitting diode with an Ag grating and a phase-gradient metasurface. Opt. Express 2022, 30, 28345–28357.

Recent Progress of Quantum Dot Photoresist-Based Full-Color Micro-LED

Zichun Li[1], Yibo Liu[1], Feng Feng[1], Zhaojun Liu[2]

[1]Hong Kong University of Science and Technology, Hong Kong, China

[2]Southern University of Science and Technology, Shenzhen, China

Micro-LED is an array device consisting of micron-sized LED light-emitting elements and is the most promising next-generation display technology after LCD and OLED. The red-green-blue (RGB) micro-LEDs assembled into a matrix by a mass transfer process can achieve a full-color display. However, this method is still challenging with low yield and high cost. Photolithography techniques can be used for producing high-resolution Micro-LED displays and also to overcome the challenges faced in mass transfer process. Quantum dots can be combined with photoresist (PR) to form QDPR after surface modification. It is compatible with conventional lithography, which enables control of thickness and size. Therefore, QDPR provides a method for patterning multicolor QD arrays and now is regarded as an important route to achieve high-resolution full-colorized Micro-LED displays. This article reviews the principles and process flow of QDPR, describes current research progress in the field, and concludes with a discussion of the problems, which demonstrates its great potential for the fabrication of full-color Micro-LED displays.

QDPR technology is the deposition of QDs with the assistance of a photolithography process, which involves adding quantum dots to the photoresist to form a stable quantum dot photoresist blend as a basis for patterning. The basic process flow is shown in Figure 1. In addition to basic lithography process, some means or structures are often used to assist in improving device performance such as device stability or resolution. Weng et al. (2021) patterned the InP/ZnS QDPR film with laser assistance [1], and the process is shown in Figure 2. The etching depth of the film will increase with the increase of laser energy. Research shows that the thicker the InP/ZnS QDPR film thickness and the higher the quantum dot concentration will improve the luminous efficiency. They also added a distributed bragg reflector structure (DBR), which significantly reduces the transmittance of blue light at the bottom, as well as isolating air and water to avoid oxidation and thus improve quantum dot stability.

In order to expand the application range of QDPR, the quantum dots themselves can also be improved and replaced. Instead of using the common red-green primary color quantum dots, Lin et al. (2019) they prepared a four-color QDPR composed of red (R), yellow-green (YG), blue-green (BG) and blue (B) sub-pixels by a total of 118 rounds of lithography [2]. Blue light absorption has been improved both in terms of material and device structure. The prepared QDPR containing 30 wt.% of QDs with film thickness of 7.4 μm shows the OD value above 2.0 and the EQE above 30%. This QDPR film can provide an ultra-wide color gamut, which is higher than other existing color gamut extension methods. In addition, QDPR is a mixture of QDs, photoresist, and TiO2 [3], and TiO2 can act as a mirror to reflect incident blue light, which results in a significant reduction of external blue light.

Overall, the advantages of using QDPR to achieve full-color Micro-LEDs are mainly due to the simplicity of the process and the possibility of modifying the nature of the quantum dots to make them compatible with the photoresist. However, since most of the quantum dots have a strong absorption for the UV band, the QDs and photoresist in the QDPR will compete for the UV light. If the QD concentration is too low, it may lead to low conversion efficiency, and if the QD concentration is too high, the QDPR may not be able to form a pattern due to the insufficient absorption of energy, and these are the obstacles that must be solved in the process of realizing the high quality of the full-colorization Micro-LED by using the QDPR.

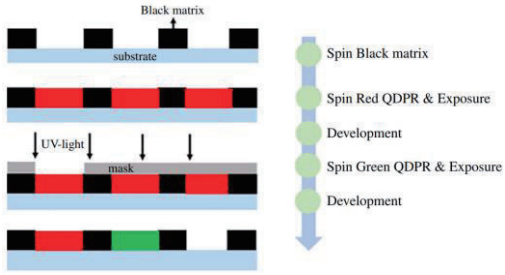

Fig. 1. Process flow of basic quantum dot photoresist method

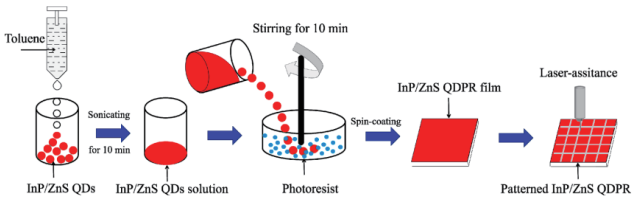

Fig. 2. Process flow of laser-assisted quantum dot photoresist method

References

[1] Weng, Y., Chen, S., Zhang, Y., Sun, L., & Wu, C.. (2021). Fabrication and color conversion of patterned inp/zns quantum dots photoresist film via a laser-assisted route. Optics & Laser Technology, 140(2), 107026.

[2] Lin, S., Tan, G., Yu, J., Chen, E., Weng, Y., Zhou, X., Xu, S., Ye, Y., Yan, Q., Guo, T.. Multi-primary-color quantum-dot down-converting films for display applications. Opt Express. 2019 Sep 30;27(20):28480-

28493.

[3] Chen, C., Chen, H., Liao, J., Yu, C., Wu, M., 2019. Fabrication and characterization of active–matrix 960*540 blue GaN-based micro-LED display. IEEE J. Quantum Electron. 55 (2), 1–6, 3300106.

Unraveling the Enhancements in Radiant Flux Density by Scaling-down AlGaN Ultraviolet-C MicroLEDs

Feng Feng*, Zhaojun Liu**, Hoi-sing Kwok***

***Hong Kong University of Science and Technology, Hong Kong S.A.R.**

****Southern University of Science and Technology, Shenzhen, China**

***** Hong Kong University of Science and Technology, Hong Kong S.A.R.**

In recent years, the industry has been abuzz with excitement over the potential of deep-ultraviolet (UVC) microLEDs with AlGaN multi-quantum wells (MQWs). These miniature wonders hold vast promise for a wide array of applications, including color conversion displays , optical wireless communication (OWC), and optogenetic neuroscience . While much attention has been devoted to understanding the high energy radiation of UVC microLEDs, little has been explored about the quest for elevating the optical power density in these ultra-fine devices.

The crafted UVC microLEDs come into being utilizing customized AlGaN epitaxial wafers. Employing the metal organic chemical vapor deposition (MOCVD) technique, the resultant epilayers on an AlN template encompass an AlGaN interlayer, a vibrant active region comprised of multiple quantum wells (MQWs) alongside an electron block layer (EBL), all followed by a p-GaN contact layer. A series of different-sized square devices (in 10×10, 20×20, 50×50, 80×80, and 100×100 μm^2) were fabricated and characterized for optical investigation. The cross-section view in Figure 1 of an investigated standalone UVC microLED was captured by scanning electron microscope (SEM).

For the purpose of optically characterizing UVC microLEDs, the Ocean Optics USB 2000+ UV-Visible spectrometer serves as the tool of choice, facilitating the acquisition of the spectral response of light intensity. In this research endeavor, the absolute optical power and EQE (External Quantum Efficiency) are deduced by integrating the light emitted from the backside of the thinned and polished wafer, expertly accomplished through the utilization of a CC-3-UV-S cosine corrector. Given that the reflectance of the integrating sphere coating tends to be relatively low for UVC light, one must remain vigilant about the potential introduction of high noise into the optical measurements. This is where the cosine corrector emerges as a savior, offering a direct approach that leads to more precise optical power evaluation for microLEDs in diminutive dimensions. To establish the backside emission measurement system, UV-Visible fiber connections are put into play, subsequently subjected to radiometric calibration via a standard light source (Ocean Optics DH-3P-BAL-CAL).

In Figure 2, we witness the visual representation of the size-dependent radiant flux of UVC microLEDs. At diminutive scales, these microLEDs demonstrate a mesmerizing brilliance, boasting intensified radiance under identical injection current density. This captivating phenomenon finds its elucidation in the augmented uniformity of current spreading, precisely aligned with the unparalleled evenness in light emission originating from the active region. Moreover, the relatively more generous surface-to-volume ratio assumes a pivotal role in fortifying the efficacy of light extraction and heat dissipation, consequently contributing to the exceptional thermal management of these miniature marvels.

In conclusion, the industry's fervent anticipation for AlGaN multi-quantum well UVC microLEDs is well-founded. As the research community delves deeper into scaling down these micro wonders, the quest for elevating optical power density assumes paramount importance. The path ahead is illuminated by the promising findings of this work, beckoning a new era of brilliance in color conversion displays, optical wireless communication, and optogenetic neuroscience. The saga of UVC microLEDs with AlGaN MQWs continues to unfold, leaving an indelible mark on the landscape of modern optoelectronics.

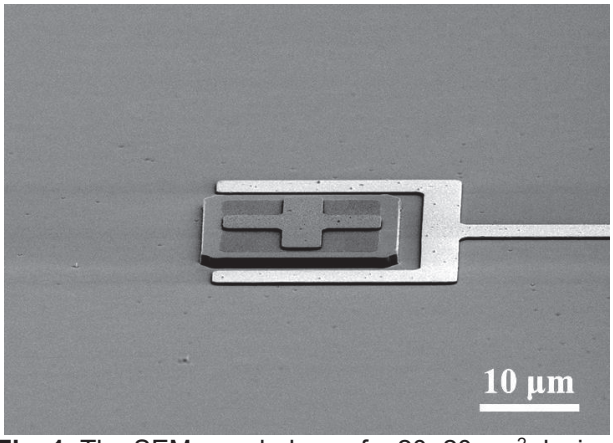

Fig. 1. The SEM morphology of a 20×20 μm^2 device.

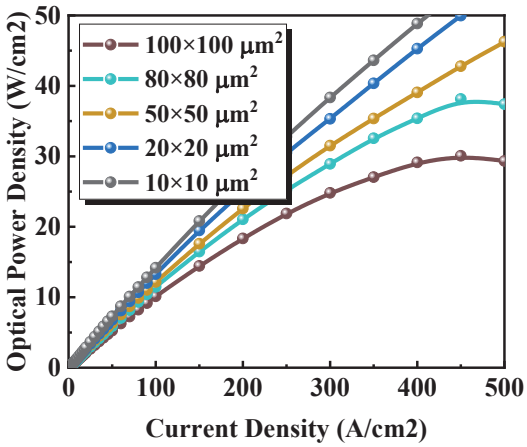

Fig. 2. The size-dependent radiant flux of UVC microLEDs.

Change in Field of Micro-LED Brought by GaN Substrate

Chunxiao Li

Department of Electronics and Information Engineering, Hebei University of Science and Technology,

Tianjin, China

Gallium Nitride is a kind of III-V compound semiconductor materials wildly used in the field of electronics, optoelectronics and power devices. GaN bandgap width is much higher than other general substrate materials such as gallium arsenide and silicon, result of the excellent performance in high-temperature and high-power environments which is essential for component.

Material	Si	GaAs	GaN	Sic
Bandgap(eV)	1.1	1.4	3.4	3.2
Critical field (10^6 V/cm)	0.3	0.4	3.5	3
Electron mobility (cm^2/V-Sec)	1450	8500	2000	900
Saturation velocity (10^6 cm/Sec)	10	12	25	22
Lattice constant (Å)	3.84	5.6	3.19	3.08
Thermal conductivity (W/cm K)	3.5	0.56	1.3	5
Coefficient of thermal expansion (CTE)	2.6	6.86	5.6	4.2

Tab. 1. A series of material properties including GaN

As a new display technology, micro-LED uses GaN as a substrate preparation material in recent years. Some of the benefits it brings include high brightness, high efficiency, fast response time, color performance, high reliability, and long life.

Fig. 1. The first GaN-on-Silicon monolithic FHD micro-led bonded display

Challenges come with opportunities at the same time like higher cost due to difficult growth, more precise operation and lattice mismatch.

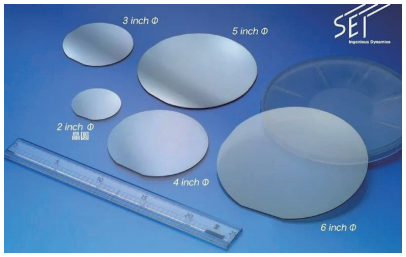

Fig. 2. Wafers that are difficult to grow in large sizes

References

[1] Anwar, A. R., Sajjad, M. T., Johar, M. A., Hernández-Gutiérrez, C. A., Usman, M., Łepkowski, S. P., Recent Progress in Micro-LED-Based Display Technologies. Laser & Photonics Reviews 2022, 16, 2100427.

[2] Zhou Wang *et al* 2020 *J. Semicond.* 41 041606
DOI 10.1088/1674-4926/41/4/041606

[3] Fulong Jiang, Feifan Xu, Zhaojun Liu, et al. Research Progress of GaN-based Micro-LED Display Technology[J]. Journal of Synthetic Crystals, 2020, 49(11).

Micro-LED structure using metasurface for collimation

Zhengui Fan[1,2], Kangkang Chen[1,2], Enguo Chen[1,2,], Yun Ye[1,2] , Sheng Xu[1,2], Tailiang Guo[1,2]*

1. College of Physics and Information Engineering, Fuzhou University, Fuzhou 350108, China
2. Fujian Science & Technology Innovation Laboratory for Optoelectronic Information of China, Fuzhou 350108, China

*Corresponding author: ceg@fzu.edu.cn

Micro-displays are playing an increasingly important role in modern technology. However, their importance demands continuous advancement in micro-display technology. Currently, higher pixel density, brightness, and color saturation are required, which LCD and OLED displays can no longer meet. Micro-LED technology has emerged as a promising solution, offering high performance with longer lifespan and lower energy consumption, making it a hot research topic in the display industry.

Micro-LED technology's application in micro-displays can improve the limitations of traditional LCD and OLED micro-displays. Its high pixel density, brightness, and color saturation make Micro-LED widely applicable in various fields, such as virtual reality, augmented reality, drone navigation, medical, and military applications.

However, Micro-LEDs also face common problems with micro-displays, such as large divergence angle and significant crosstalk. These issues lead to unclear images and a decrease in image quality. Additionally, the large divergence angle limits the amount of light that can be coupled into the optical coupler, resulting in low efficiency. Therefore, there is a need to use large-volume and complex optical collimators to collimate the light source, making the system bulky and not suitable for micro-displays.

This paper presents a novel Micro-LED structure that combines the current research hotspot of metasurfaces. The metasurface is used to control the Micro-LED's outgoing light field, achieving collimation of the Micro-LED's outgoing light. The metasurface structure is simple, easy to integrate, and has good light field control, which addresses the problems of using Micro-LEDs in micro-displays. Our proposed novel Micro-LED structure achieves excellent collimation performance, reducing the full width at half maximum (FWHM) angle to ± 7.22 ° compared to traditional Micro-LED structures. Furthermore, the central light intensity is increased by 4.14 times. The proposed structure has the advantages of easy integration, simple structure, good collimation performance, and high energy concentration, making it highly promising for micro-display applications.

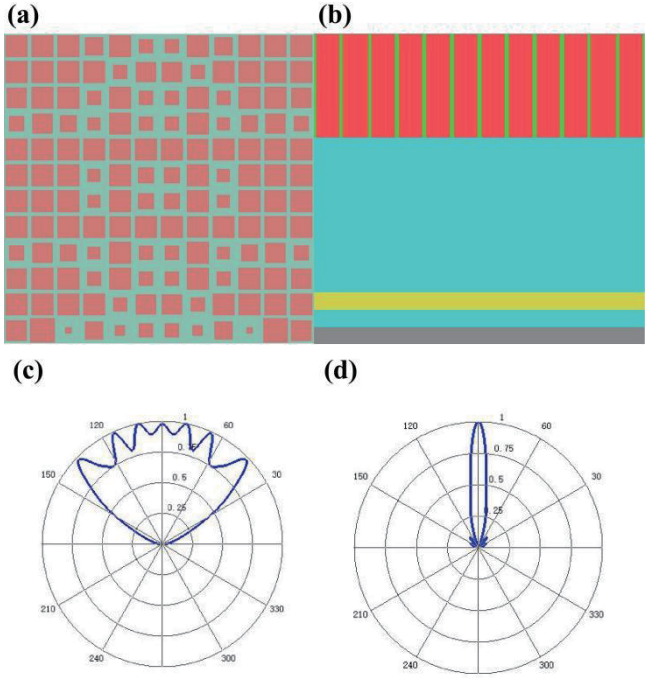

Fig. 1. (a) Top view of the proposed novel Micro-LED structure in this paper; (b) Front view of the proposed novel Micro-LED structure in this paper; (c) Normalized intensity-angular distribution diagram of the outgoing light of the traditional Micro-LED structure; (d) Normalized intensity-angular distribution diagram of the outgoing light of the proposed novel Micro-LED structure.

References

[1] Ramón P, Feng Y Y, Egor K, et al. Nano. lett., 2018, 18(3).

[2] Jinpeng H, Zelin H, Xiang G, et al. Opti. lett., 2021, 46(14).

Enhancing Device Performance of Micro-LEDs through the Ideality Factor

Mengyuan Zhanghu*, Byung-Ryool Hyun*, Yibo Liu**, and Zhaojun Liu*

*** Department of Electrical and Electronic Engineering, Southern University of Science and Technology, 518055 Shenzhen, China.**

**** Department of Electrical and Computer Engineering, Hong Kong University of Science and Technology, Hong Kong SAR, People's Republic of China.**

Micro-light-emitting diodes (Micro-LEDs) have emerged as a highly promising next-generation display technology, boasting superior optical properties such as high efficiency, low power consumption, stability, and brightness.[1] Despite their immense potential, certain fundamental electrical properties, particularly the current-voltage (I-V) characteristic and ideality factor (n_d , have remained poorly understood, particularly in GaN-based Micro-LEDs. In some cases, GaN-based Micro-LEDs produced via ICP etching have exhibited high ideality factors ranging from 3 to 10, along with disappointingly low external quantum efficiency (EQE) of less than 5%. These unfavorable characteristics were attributed to non-radiative recombination centers and carrier leakage channels that induced numerous deep traps in the active layers, leading to what is commonly known as sidewall damage. [1 - 4] However, significant advancements have been made through chemical treatments and the implementation of passivation layers, resulting in remarkable improvements in both EQE and ideality factor. In recent developments, blue or green Micro-LEDs have achieved EQE values exceeding 25% and ideality factors below 1.5. [5, 6]

The ideality factor of Micro-LEDs is expected to correlate strongly with their internal quantum efficiency (IQE) or EQE. Generally, a lower ideality factor indicates a higher IQE, as it signifies fewer non-radiative recombinations within the Micro-LEDs. Consequently, a larger fraction of injected carriers can recombine radiatively, leading to enhanced light emission [5]. Fig. 1 illustrates the size-dependent EQE and ideality factor of green Micro-LEDs, showcasing their excellent device performance across a wide size range. [6] These green Micro-LEDs exhibit impressively low ideality factors of approximately 1.35 compared to other reports.

There are several reasons behind the correlation between a lower ideality factor and a higher EQE (or IQE). Firstly, a reduced ideality factor implies improved carrier transport efficiency across the junction. Lower resistance to carrier transport allows more carriers to reach the active region of the Micro-LEDs, facilitating higher rates of radiative recombination. Secondly, a lower ideality factor points towards a lower density of defects within the Micro-LED structure. Defects can trap carriers and impede radiative recombination, thus Micro-LEDs with fewer defects tend to have higher EQE values and lower ideality factors.

While other factors such as material quality, LED structure design affecting light extraction efficiency, and manufacturing processes can also impact the EQE of Micro-LEDs, the ideality factor remains a reliable indicator of their overall efficiency. As a result, it can be effectively used to predict the EQE or IQE of an LED with a high degree of accuracy. By understanding and optimizing the ideality factor, researchers and engineers can further enhance the performance of Micro-LEDs and unlock their full potential for future display technologies.

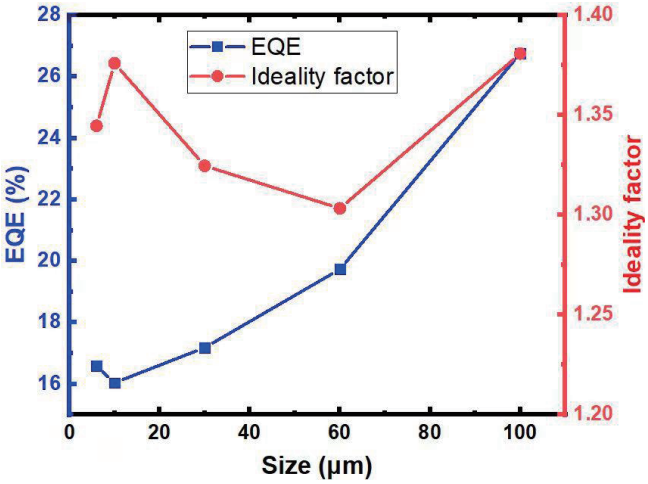

Fig. 1. The size-dependence of EQE and ideality factor of green Micro-LEDs.

References

[1] Z. Liu, C.-H. Lin, B.-R. Hyun, C.-W. Sher, Z. Lv, B. Luo, F. Jiang, T. Wu, C.-H. Ho, H.-C. Kuo, J.-H. He, *Light: Sci. Appl*. 9, 83 (2020).

[2] Lee, S.; Oh, D.; Goto, H.; Ha, J.; Lee, H.; Hanada, T.; Cho, M.; Yao, T.; Hong, S.; Lee, H.. *Appl. Phys. Lett*. 89, 132117 (2006).

[3] Sze, S.M.; Ng, K.K. Physics of semiconductor devices; John wiley & sons (2006).

[4] Yan, D.; Lu, H.; Chen, D.; Zhang, R.; Zheng, Y. *Appl. Phys. Lett.*, 96, 083504 (2010).

[5] M. Zhanghu, B.-R. Hyun, F. Jiang, and Z. Liu, *Opt. Express* 30(6), 10119 (2022)

[6] Y. Liu, F. Feng, K. Zhang, F. Jiang, K.-W. Chan, H.-S. Kwok, and Z. Liu, *J. Phys. D: Appl. Phys*. 55(31), 315107 (2022).

Optimization of a normally-off in-situ Integration HEMT-LED enabled by P-GaN Selective Epitaxy Growth

Jingyang Zhang[1], Wei Huang[2], Zhaojun Liu[1],
[1]Department of electronic and electrical engineering, Southern University of Science and Technology, Shenzhen, Guangdong, 518055, China.
[2]A State Key Laboratory of ASIC and System, Shanghai Institute of Intelligent Electronics & Systems, School of Microelectronics, Fudan University, Shanghai 200433, China.
Email: 12132159@mail.sustech.edu.cn; eehuangw@fudan.edu.cn; liuzj@sustech,edu,cn

Abstract

Building upon previous research on the fabrication of ultraviolet HEMT-LEDs using selective epitaxial growth, this study conducts simulations to investigate the optimal size for p-GaN selection. Selective epitaxy growth (SEG) enables the utilization of p-GaN as a junction termination, reducing electric field crowding at the HEMT gate, while also forming an active region through contact with the 2-dimensional electron gas (2DEG). The simulation results serve as a valuable reference for designing p-GaN grown via SEG and pave the way for integrating this approach, aligning with the goal of method selection for practical realization.

Introduction:

AlGaN/GaN HEMTs exhibit exceptional performance in high-power, high-frequency, and high-temperature applications, making them a promising choice as driving transistors for electroluminescence (EL) devices. Although there have been attempts to integrate HEMTs and LEDs monolithically, these approaches often encounter challenges related to complex processes, such as parasitic resistance and high costs, which are difficult to address fundamentally. However, a recent report highlights a potential solution to simplify the process by directly converting AlGaN/GaN HEMTs into photoluminescent devices through selective growth of p-GaN. It should be noted that the presence of a two-dimensional electron gas in GaN HEMTs renders them as normally-on devices, which can pose practical challenges in circuit design.

Figure 1 represents a schematic diagram of the designed device in this study. The p-GaN under the gate and the p-GaN in the active region can be obtained through selective epitaxial growth followed by etching. This structure is expected to realize a normally-off HEMT-LED device with a relatively simple process. In this paper, simulations were conducted to determine the thickness of the barrier layer, aiming to obtain a HEMT-LED device that meets practical application requirements.

It can be seen that the size of p-GaN selective growth can be controlled by designing a photolithographic plate, and the depth of p-GaN growth can be controlled by ICP etching time. Therefore, The appropriate thickness of selective epitaxial growth for p-GaN has a significant impact on both the active emission region and the device's switching behavior.

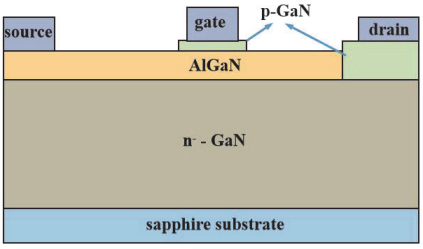

Fig.1 schematic diagram of the device

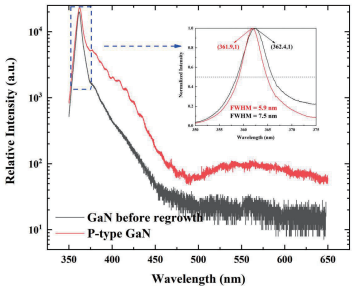

Fig.2 Photoluminescence spectra of p-GaN and GaN before growth

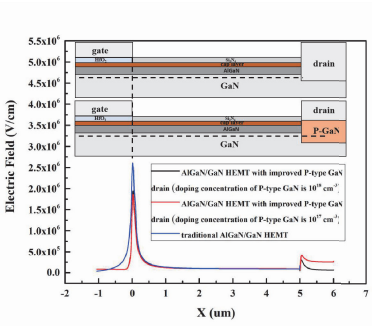

Fig.3 Electric field distribution at channel position when V_{DS}=10 V V_{GS}= - 6 V

(The following full text will analyze he in detail based on the influence of the width and depth of p-GaN grown in the selected region on the HEMT electric field distribution and the comprehensive influence of the electron hole recombination in the active region.)

The Effect of ITO Thickness on Metal Grating Linear Polarized Micro LED

Jingnan Zeng, Zhaojun Liu*
Department of Electrical and Electronic Engineering, Southern University of Science and Technology, Shenzhen, China

Micro LEDs are considered as the next generation of display technology. Polarized light sources can significantly improve the efficiency of applications of micro LEDs by reducing glare[1]. Many studies on polarized light micro LEDs have been published[2,3]. We propose a linearly polarized micro LED to obtain linear polarized light from unpolarized light source by integrating a subwavelength metal grating on top of the micro LED and researched the effect of ITO thickness on polarization by FDTD simulation.

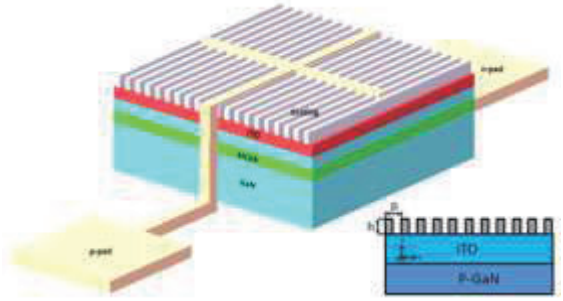

Fig. 1. The schematic structure of the linear polarized micro-LED and simulation model.

The model of metal grating micro LEDs was set up by using FDTD method of Lumerical. The schematic structure of the linear polarized micro-LED and simulation model is shown in Fig. 1. The metal grating can allow TM polarized light along the x-axis direction (perpendicular to grating direction) to pass through the polarizer, and the TE polarized light along the z-axis direction (parallel to grating direction) is absorbed to achieve linear polarized light micro LEDs. Al was selected as the material for metal gratings. The transmittance of TM and TE as a function of Al grating thickness and period is shown in Fig. 2. The duty cycle is set to 0.5.

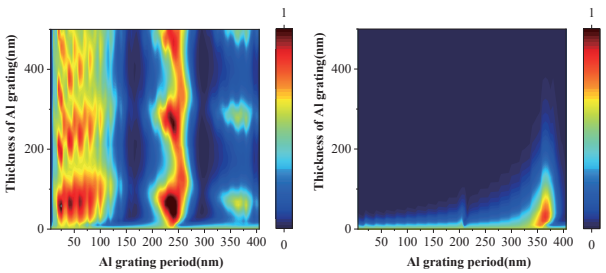

Fig. 2. The transmittance of TM and TE

P is the grating period and h is the grating thickness. At a specific p, the transmittance of TM fluctuates up and down with increase of h and gradually decreases. When p is about 260nm and less than 110nm, the TM transmittance is greater than 0.5. The transmittance of TE tends to zero before 200nm and rapidly increases after 200nm. In order to ensure a high TM transmittance and a low TE transmittance, meanwhile for process considerations, a metal grating with p=100nm and h=100nm was selected for simulation the effect of ITO thickness on linear polarized light.

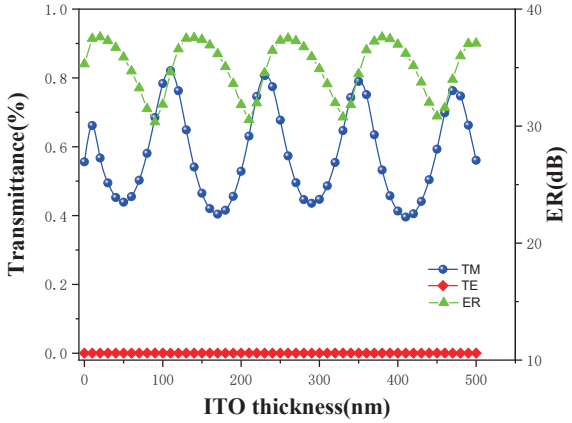

Fig. 3. TM, TE transmittance and ER

The extinction ratio (ER) can be calculated by $ER = 10\lg\frac{T_{TM}}{T_{TE}}$, where T_{TM} and T_{TE} are the transmittance values of TM and TE lights. Fig. 3 shows the changes in TM, TE transmittance, and ER with the thickness of the ITO grating. When the thickness of ITO is 0, the metal grating is directly integrated on p-GaN, and the transmittance of TM is 0.55. The transmittance of TM varies periodically with increase of thickness of ITO. When the thickness of ITO is 110nm, 230nm, 350nm, and 470nm, the transmittance of TM reaches 0.8, which is higher than that without ITO. At the same time, under the thickness of ITO within 500nm, the transmittance of TE is extremely low, resulting in an extinction ratio greater than 30dB. It can be seen that ITO gratings can not only be used for current spreading layer but also increase the polarization effect of polarized light micro LEDs at certain thicknesses.

References

[1] Haojun Zhang, Appl. Phys. Lett. 117, 181105 (2020).

[2] Guogang Zhang, Optics Letters,47, 215485-04(2022).

[3] Xiang Gao, Optics Letters,21, 112666-04(2021).

Light-field Three-dimensional Displays Based on a Mini-LED Displays

Yanzhen Yin[1], Zhaojun Liu[1#]

[1]Department of Electrical and Electronic Engineering, Southern University of Science and Technology, Shenzhen, China

[#]Corresponding Email: liuzj@sustech.edu.cn

Three-dimensional (3D) displays provide 3D images through the use of various technologies, which process complex high-dimensional data and objects and provide viewers with a sense of depth. It is an emerging display technology that is increasingly being applied in various fields such as automobiles, movies, large screen televisions, and mobile devices. 3D display is one of the new developments in the display industry, providing a very immersive 3D viewing experience. Therefore, 3D displays can bring new realism and immersive experiences to entertainment activities, such as 3D movies and 3D games. In our work, a light- field 3D display with Mini-LED is successfully demonstrated for flat panel display (FPD). By covering the display surface with a parallax barrier, a 3D display effect is formed. Finally, a 9-view, 43-degree FOV Mini-LED 3D display devices are packaged and demonstrated [1, 2].

Fig.1shows the slanted-barrier setup for Mini-LED where the RGB sub-pixels are perfectly aligned at the slant angle of arctan(1/3) ≈ 18.43 degrees, and the white-framed RGB sub-pixels form a single-view whose width is 1/3 pixel pitch (px), and height is 3 px. Thus, the area of one pixel is 1 px^2. An N-view display requires N pixels to represent N views; thus, the 3D resolution drops by N-fold.

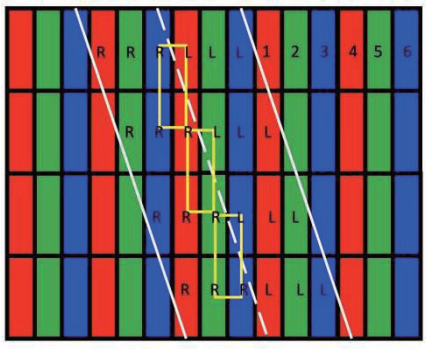

Fig.1 The matrix sub-pixel pattern of Mini-LED is implemented with a slanted barrier of angle arctan(1/3), and the size of single-view pixel is 1/3 px × 3 px, which gives the maximum 3D resolution.

Fig. 2 show that the left, central, and right perspectives to demonstrate the horizontal motion parallax relative position changes. When the views of the observers moving from left to right, it is clear that the images presents huge parallax which confirms the successful 3D reconstruction. Parameters used in the implementation are summarized in Table 1. These results clearly demonstrate some parameters and performance of this 3D display.

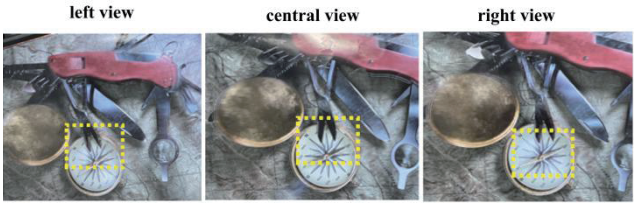

Fig.2 Left view, central view and right view of the image presented by the prototype.

Table 1. The specification and parameters for the Mini-LED light-field display.

System parameters	Barrier duty cycle	
	1/4	1/3
Viewing distance	500 mm	500 mm
Single-view Pixel pitch	31.99 um	31.99 um
Pixel pitch	95.97 um	95.97 um
effective gap	383.88 um	383.88 um
physical gap	575.82 um	575.82 um
Viewing zone pitch	41.7 mm	41.7 mm
view angle	43°	43°
barrier pitch	287.6 um	287.6 um
barrier open	71.9 um	95.9 um
Slant angle	18.43°	18.43°
Screen size	12.9 inch	
2D resolution	2732*2048	
3D resolution	910*682	
View number	9	

References

[1] J. Geng, Adv. Opt. Photonics 5(4), 456–535. (2013).

[2] A. Gershun, J. Math. Phys. 18(1-4), 51–151. (1939).

Enhancing the Light Extraction Efficiency of AlGaN-based DUV Micro-LED by Optimizing the Chip Sidewall Inclined Angle

Juan Wang, Zhaojun Liu*

***Dept. of Electronic and Electrical Engineering, Southern University of Science and Technology, Shenzhen, China.**

***Corresponding Email: liuzj@sustech.edu.cn**

AlGaN-based DUV LEDs have promising applications in sterilization, biomonitoring, UV phototherapy, and anti-counterfeit detection. However, compared with visible LEDs, the external quantum efficiency(EQE) of DUV LEDs is extremely low, and the EQE of most DUV LEDs is still lower than 10%, which is mainly caused by the very low light extraction efficiency （LEE）, which is less than 10%[1, 2]. Therefore, it is important to improve the LEE of DUV LEDs.

In this paper, the LEE of μLEDs with vertical and inclined sidewalls is established and analyzed by using a two-dimensional finite-difference time-domain (FDTD) method. The simulated device structure is shown in figure 1. The simulation boundary is set to be perfectly matched layer (PML). The dipole source is placed in the center of the quantum well to represent the light generating. The dipole source is polarized in the parallel (perpendicular) to the X-direction corresponding to the TE(TM) mode. The monitor is placed 300 nm below the sapphire. The LEE is defined as the ratio of the power received by the monitor to the power emitted by the dipole. The ($\mathrm{LEE}_{overall}$) can be determined by considering the ratio of TE and TM polarizations [3, 4].

$$\mathrm{LEE}_{overall} = 0.42 \cdot \mathrm{LEE}_{TE} + 0.58 \cdot \mathrm{LEE}_{TM} \qquad (1)$$

Firstly, we optimized the thickness of p-AlGaN in vertical sidewall structure. The light from the MQW propagates upward and downward, and the upward-propagating light is reflected downward by the electrodes. The two beams of light produce constructive or destructive interference depending on the thickness of the p-type layer. It can be seen in figure 2(a) that with the increase of the thickness of AlGaN, the LEE in both TE and TM modes oscillates with a period of about 58 nm, which is in accordance with the interference theory. It can be concluded that the $LEE_{overall}$ is maximum at about 90 nm, so the AlGaN thickness was determined to be 90 nm.

After that, we simulated different sidewall inclined angle structure. It can be seen from figure 2(b) that the variation of LEE with inclined angle is small in TE mode, which is due to the fact that the light propagates perpendicularly to the epitaxial layers in TE mode. The variation of LEE with inclined angle is larger in TM mode. The maximum LEE_{TM} and $\mathrm{LEE}_{overall}$ is achieved at 40°.

As can be seen in figure 3(a), in the TM mode, a large amount of horizontally propagating light reaches the sidewalls. For the vertical sidewall structure, the light reaching the sidewall is ejected from the sidewall. However, for the inclined sidewall structure, the light reaching the sidewall is reflected back to the sapphire side, increasing the light output of the sapphire side, as shown in figure 3(b).

In summary, we found that the maximum LEE can be obtained at p-AlGaN of 90 nm, with a sidewall inclined angle of about 40° through simulation.

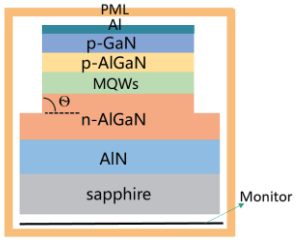

Fig. 1. simulation structure

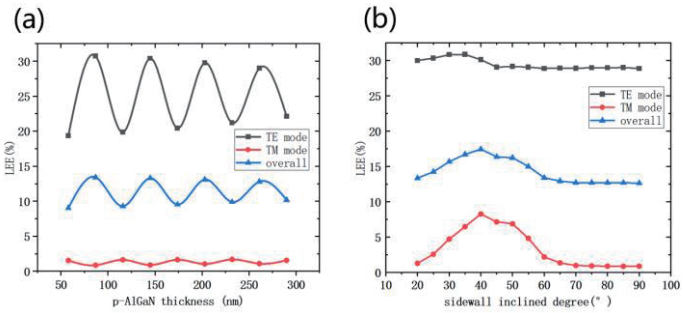

Fig. 2. LEE with (a)p-AlGaN thickness and (b)sidewall inclined angle

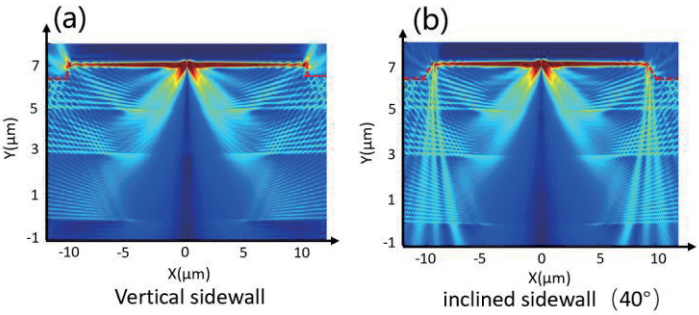

Fig. 3. TM-polarized Cross-sectional light field

References

[1] Michael Kneissl, Nature Photonics ,13(4): 233-44 (2019).

[2] Tian Meng, Optics Letter, 46(19): 4809-12 (2021).

[3] Ryu, H.-Y, Quantum Electron. 46, 1329–1335 (2014).

[4] Kolbe, T., Knauer, A., Chua, C., M. Appl. Phys. Lett. 97, 171105 (2010).

Perovskite crystals for Full-color Micro-display

Yujia Sheng*, Zhaojun Liu*
*Department of Electrical and Electronic Engineering, Southern University of Science and Technology

The obstacle of achieving full-color representation remains a challenge in the commercialization of Micro-LEDs (μ-LED) displays, especially when the pixel pitch is reduced to below 20 μm. However, the integration of quantum dots (QDs) as color converters has shown promise in overcoming this limitation. This study proposes the utilization of perovskite crystals as color converters for μ-LEDs, aiming to enable full-color display functionality.

In a previous study, the mechanical properties of a paper-based material derived from abundant plant resources were shown to be highly robust. The material exhibited excellent flexibility, allowing for both twisting and bending. Furthermore, by incorporating appropriate processes and additives, the material could be further modified to possess additional desirable properties, including flexibility and stretchability. Overall, these findings highlight the versatility and potential of this paper-based material for various practical applications. [1] In a study conducted by He et al., a paper-based photodetector was successfully fabricated using ZnO nanowires and carbon electrodes. The utilization of the Miura origami folding method resulted in exceptional deformability of the photodetector. Notably, the photodetector exhibited a stable photo-response even after undergoing 400 cycles of tension, bending, and twisting. These findings highlight the robustness and reliability of the paper-based photodetector design, showcasing its potential for various practical applications. [2] According to the above research, devices fabricated with high-efficiency blue or UV chips and flexible perovskite crystals color converters are regarded as the best way to achieve novel μ-LEDs. However, the intrinsic instability of perovskite hinders its optical properties and lifetime. To solve the optical issues, 2D/quasi-2D perovskite crystals can be used for their quantum confinement effect. CNCs, which are environmentally friendly and renewable, can be regarded as a framework for perovskite crystals. Because of their surface passivation and confinement effects, celluloses can further improve the stability of perovskite crystals as well as provide flexibility. [3-4]

The objective of this study is to investigate the production of color conversion films through the use of perovskite crystals and the vacuum filtration method. The results indicate that red perovskite crystals demonstrate relatively good stability and desirable optical properties, while green perovskite crystals exhibit favorable optical characteristics. However, the stability and protective attributes of blue perovskite crystals are insufficient, calling for further enhancements. Despite the challenges related to the optical stability and lifetime of perovskite crystals, this research highlights their significant potential in commercial applications of μ-LEDs. These findings offer promising prospects for the future utilization of perovskite crystals in various applications.

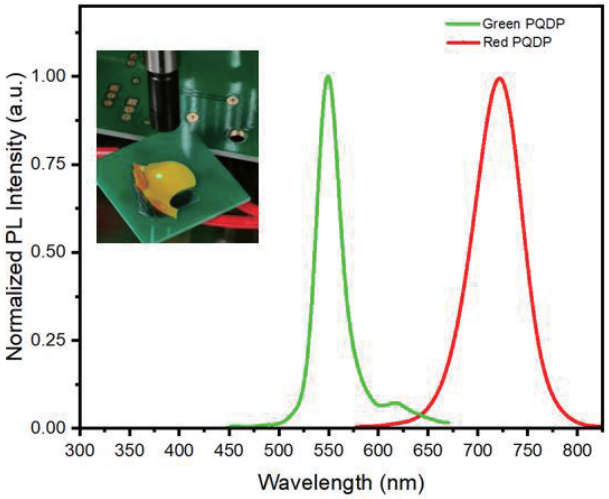

Figure 1. PL spectra (inset: Crystals excited by blue μ-LED)

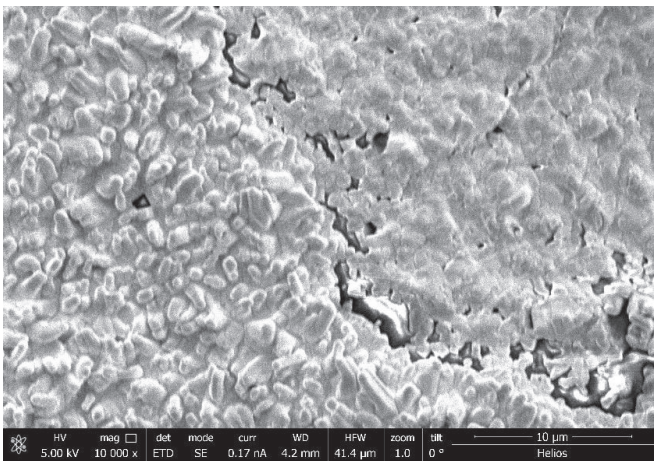

Figure 3. Scanning electron microscope morphology for the surface of the green perovskite crystal.

References

[1] H. Liu, "Fabrication and properties of transparent polymethylmethacrylate/cellulose nanocrystals composites," *Bioresource Technology*, Vol. 101, pp. 5685-5692 (2010).

[2] C. Lin, "Highly Deformable Origami Paper Photodetector Arrays," *ACS Nano,* Vol. 11, pp. 10230-10235 (2017).

[3] T. Li, "Highly UV Resistant Inch-Scale Hybrid Perovskite Quantum Dot Papers," *Advanced Science.* Vol. 7, 1902439 (2020).

[4] C. Kang, "Highly Efficient and Stable White Light-Emitting Diodes Using Perovskite Quantum Dot Paper," *Advanced Science.* Vol. 6, 1902230 (2019).

Size-Independent Current Density-Voltage Characteristic of Micro-LEDs

Hang Yang1, Wen Jun Huang1, Yong hong Lin1, Meng yuan Zhang Hu1, Zhao-jun Liu1*

1Department of Electrical and Electronic Engineering, Southern University of Science and Technology, Shenzhen, Guangdong, China

Abstract

Various individual Micro-LEDs were designed and fabricated with size from 10 μm to 100 μm. The effects of Size-independent current density-voltage characteristic of Micro-LEDs were investigated. It is found size effect didn't have obvious impact on the J-V characteristics (current density-voltage), because of the optimized current route of the current spreading layer. Meanwhile, the device leakage current was less than 10^{-11} A, while the contact resistance between p-GaN and contact metal is 5.9E-3 Ω·cm^2. The forward voltage is 2.36V with the current density of 10 A/cm^2, and external quantum efficiency is 13.6%.

Keywords

Micro-LEDs Fabrication; size effect; external quantum efficiency (EQE).

1. Introduction

As a third-generation semiconductor material, GaN material has high luminous efficiency because it is a direct band gap material. GaN-based Micro-LEDs have many advantages, such as high resolution, high brightness, high contrast, long life time and fast response speed [1]. Therefore, it has received more and more attention and is expected to become the next-generation mainstream display technology. In this work, we have fabricated Micro-LED devices using micro-nano processing technology, and obtained Size-independent current density-voltage characteristic of Micro-LEDs.

Generally, external quantum efficiency (EQE) is used to describe of LED devices' luminous efficiency. Light extraction efficiency (LEE) and internal quantum efficiency (IQE) are multiplied to get EQE. IQE can also be explained by classic ABC model. A coefficient represents non-radiative recombination (for example, Shockley-Read-Hall Recombination), the B coefficient represents the radiation recombination, the C coefficient represents the Auger recombination, and n is carrier concentration of quantum well. Currently, it is reported that the peak EQE of InGaN/GaN Micro-LEDs is usually less than 15% [2, 3]. There are several reasons for limiting the GaN-based Micro-LEDs' EQE: SRH recombination coefficient, ratio between the perimeter and the mesa area, and quantum confinement Stark effect (QCSE).

$$EQE = IQE \times LEE \tag{1}$$

$$IQE = \frac{Bn^2}{An + Bn^2 + Cn^3} \tag{2}$$

According to reports, the Auger recombination coefficient is hardly affected by the device size and remains constant as the figure is shown in Fig.1(a), but the Shockley-Read-Hall (SRH) recombination increases when the size of the LED decreases (see Fig.1(b)) [2]. Therefore, it has every reason to believe that Micro-LEDs' EQE will be significantly affected by SRH non-radiative recombination. When the size of Micro-LED is further reduced, surface defects may dominate. So, great efforts are required to inhibit the surface recombination rate.

To our knowledge that Micro-LEDs have better current spreading effect in small size, which means that carriers could reach the edge of the mesa easily, resulting in significant surface non-radiative recombination. For traditional LEDs with large mesa sizes, it will not greatly sacrifice performance of LEDs, although surface non-radiative recombination still exists. Because the ratio between perimeter and mesa area (P/A) of traditional LEDs is much smaller than that of Micro-LEDs. When the chip size decreases, the P/A ratio increases, so when the chip size decreases, EQE continues to decrease [4, 5, 6, 7].

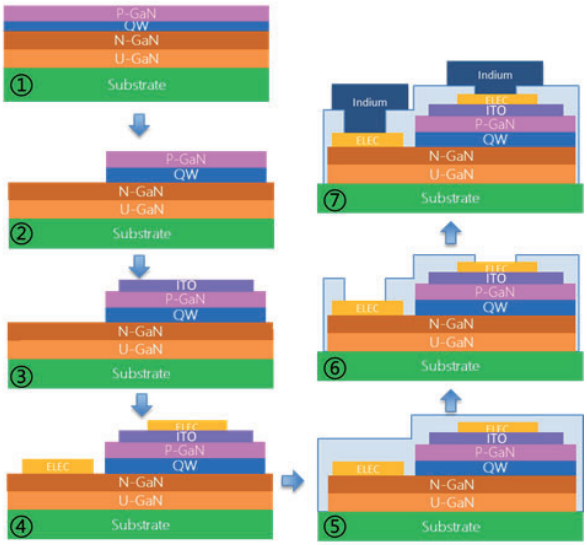

Figure 1. Fabrication process of Micro-LEDs ① Epitaxial wafer, ② mesa, ③ current spreading layer, ④ electrode, ⑤ silicon nitride passivation layer, ⑥ contact hole, ⑦ indium electrode

The evident quantum confinement Stark effect (QCSE) is another reason for the low EQE, which is based on the characteristics of the GaN material itself. At the present stage, InGaN/GaN LEDs are mainly grown in the [0001] direction. [0001] direction in GaN material will generate a strong spontaneous polarization and piezoelectric polarization effect in multiple quantum wells (MQWs). The polarized electric field causes the energy band to bend,

and the wave functions of electrons and holes do not coincide, which is called QCSE. The radiation recombination rate of InGaN/GaN MQWs could be reduced by QCSE [8].

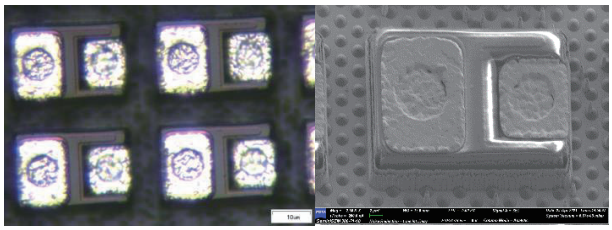

(a) (b)

Figure 2. Microscope picture (a) and SEM (scanning electron microscope) figure (b) of the device.

2. Experiments

The Micro-LEDs structure (from Xiamen Changelight Co., Ltd) were grown on a (0001) c-plane patterned sapphire substrate by metalorganic chemical vapor deposition (MOCVD), as shown in Figure 1(epitaxial wafer). The LED had a typical p-i-n structure with an u-GaN buffer layer, n-GaN layer, InGaN/GaN multiple quantum wells (MQWs), and a p-GaN layer. Photolithography and inductively coupled plasma (ICP) etching, with SiO_2 as a hard mask, were performed to define the mesa structure. Then current spreading layer (CSL) was deposited with a 100 nm Indium Tin Oxide (ITO) layer by sputter. In order to achieve ohmic contact between CSL and p-GaN, Rapid Thermal Processing (RTP) was used in an atmosphere of nitrogen and oxygen. A Ti(20nm) /Al(100nm) /Ti(20nm) /Au(50nm) stack layer was evaporated onto the CSL and n-GaN as the p-electrodes and n-electrodes by E-Beam Evaporator. 600nm silicon nitride is used as passivation layer, which is realized by Plasma Enhanced Chemical Vapor Deposition (PECVD) at 300°C. ICP technology is used to open contact holes to expose metal electrodes. Subsequently, 2 μm of indium was deposited by thermal evaporation as the metal of the lead-out electrode. Microscope picture (a) and SEM (scanning electron microscope) figure (b) of the device are shown in Figure 2.

After grinding and polishing, the samples were cut and wire-bonded. Micro-LEDs were tested with Agilent B1500A, probe station, obtaining the current-voltage characteristics of the device. External quantum efficiency of devices measured by integrating sphere.

3. Results and discussion

Devices from 10μm to 100μm are good in electricity properties, which leakage current is less than 10^{-11} A and ρ_c is 5.9E-3Ω·cm^2(p-GaN), especially, the 10A/cm^2 voltage is 2.32V. Micro-LEDs of different sizes exhibit different current-voltage curves, but the overall trend of the curves is very similar. Large-sized Micro-LEDs have larger mesas and can pass more current, so under the same voltage, large-sized Micro-LEDs have larger currents. As shown in Figure 3. Current-Voltage characteristic and Current density-Voltage characteristic of Micro-LEDs after electrode processing. It can be observed that the relationship between current density and voltage does not change greatly with the size of the Micro-LEDs in Figure 3.(b), thanks to the optimized current route of the current expansion layer.

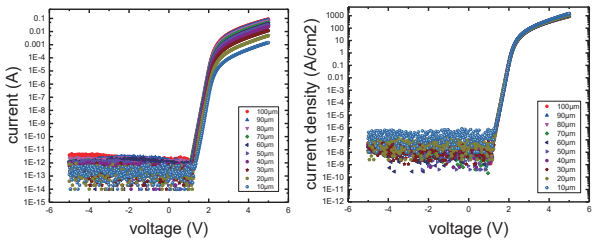

(a) (b)

Figure 3. Current-Voltage characteristic (a) and Current density-Voltage characteristic (b) of Micro-LEDs

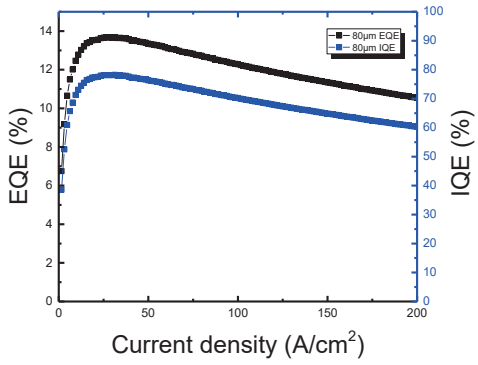

Figure 4. The EQE (External Quantum Efficiency) and IQE (Internal Quantum Efficiency) of the 80μm Micro-LED

After the sample is wired, the EQE test is performed on the 80μm Micro-LED. The EQE of the 80μm Micro-LED device was measured as a function of current density, and the EQE first increased and then decreased slowly, with a maximum value of 13.6% in Figure 4. At the same time, the device achieved a maximum IQE of 78%.

4. Conclusion

Single devices GaN-based Micro-LED with good performance and uniformity with size from 10um to 100um were proposed. The effects of Size-independent current density-voltage characteristic of Micro-LEDs were observed. The current path is optimized by the current expansion layer, leading to the improvement of electrical characteristics of the Micro-LED device better. Even if the size of the device changes, the current flowing through the unit area is basically the same. The research work showed great potential to further improve the EQE of the device,

and the follow-up work will continue to optimize the process parameters to reduce damage to the device and improve the luminous efficiency of the device.

5. Acknowledgements

The authors would like to thank Mr. Guo-cai Wu for his kind assistance with the research work. The authors also would like to thank Dr. Ke Zhang for her assistance with writing. The authors also would like to thank Core Lab in SUSTech and Sitan Technology in Shenzhen for technical support in this work.

6. References

[1] Zhang, Xu, et al. "Active matrix monolithic micro-LED full-color micro-display." Journal of the Society for Information Display 29.1 (2021): 47-56.
[2] Olivier, F. , et al. "Shockley-Read-Hall and Auger non-radiative recombination in GaN based LEDs: A size effect study." Applied Physics Letters 111.2(2017):669.
[3] Tian, P. , et al. "Size-dependent efficiency and efficiency droop of blue InGaN micro-light emitting diodes." Applied Physics Letters 101.23(2012):2217.
[4] Hwang, D. , et al. "Sustained high external quantum efficiency in ultrasmall blue III–nitride micro-LEDs." Applied Physics Express 10.3(2017):032101.
[5] Kou, J. , et al. "Impact of the surface recombination on InGaN/GaN-based blue micro-light emitting diodes." Optics Express 27.12(2019):A643.
[6] Olivier, et al. "Influence of size-reduction on the performances of GaN-based micro-LEDs for display application." Journal of Luminescence: An Interdisciplinary Journal of Research on Excited State Processes in Condensed Matter (2017).
[7] Malinverni, M. , D. Martin , and N. Grandjean . "InGaN based micro light emitting diodes featuring a buried GaN tunnel junction." Applied Physics Letters 107.5(2015):051107.
[8] Hwang, J. I. , et al. "Development of InGaN-based red LED grown on (0001) polar surface." Appl.phys.express 7.7(2014):071003.

GaN Micro-LED Array Based Underwater Wireless Optical Communication Using Flip-Chip Technology

Xinyi LIU*, Wenhao Zhang*, Zhaojun LIU**
***Department of Electrical and Electronic Engineering, Southern University of Science and Technology, Shenzhen, China**
****liuzj@sustech.edu.cn**

With the development of modern oceanography, more and more observation devices are arranged in various locations in the ocean. However, collecting high-resolution videos and images from observation devices has become an extremely challenging problem. Therefore, it is very necessary to set up a set of reliable high data rate underwater wireless communication links. Underwater acoustic communication technology is currently the most used underwater wireless communication technology. Its communication distance can reach several kilometers, but the bandwidth is low, resulting in very limited data rates. Secondly, it will be affected by multipath propagation, resulting in severe inter symbol interference (ISI). While underwater wireless radio frequency (RF) communication technology can provide a higher transmission rate than acoustic communication, the attenuation of RF signals in water is very serious, it is limited to short-distance propagation. It also requires huge antennas to generates signals, so the communication system is not easy to establish. Considering those limitations, underwater wireless optical communication (UWOC) has been paid enough attention by researchers. It can provide high-speed transmission and low latency, the communication range can reach ten to hundreds of meters. Moreover, UWOC can utilize the low attenuation window in the visible light spectrum, that is, the blue-green light band with a wavelength range of 450-560 nm. Therefore, high-speed UWOC technology has extremely broad development prospects.

Micro-LED has attracted much attention as a potential UWOC light source due to its excellent performance. Due to its small size and high current density, it can provide high modulation bandwidth. According to numerous studies [1-3], the modulation bandwidth of Micro-LED can reach hundreds of MHz or even GHz. Compared with LED and LD, Micro-LED has higher modulation bandwidth, larger beam divergence angle, and does not require additional heat dissipation system, making it more suitable for high-speed UWOC systems. The prominent attenuation issue in underwater environment is the main reason that limit the Micro-LED using in long-distance UWOC with the low light power. To overcome this impediment, a GaN Micro-LED array using flip-chip technology was fabricated to increase the output optical power.

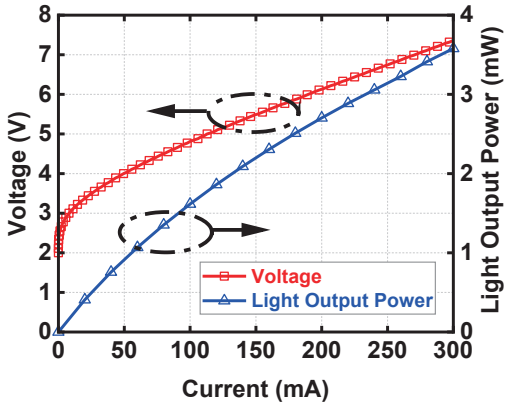

Fig. 1. Measured V-I and L-I characteristics of Micro-LED array.

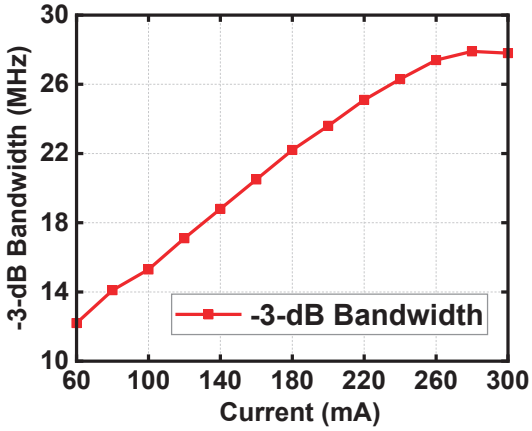

Fig. 2. The -3-dB bandwidth under different bias currents of the Micro-LED array.

References

[1] J. J. McKendry, *J. Light. Technol.*, 30(1), 61-67 (2012).

[2] M. S. Islim, *Photonics Res.*, 5(2), (2017).

[3] R. X. Ferreira, *IEEE Photon. Technol. Lett.*, 28(19), 2023-2026 (2016).

Micro LED pixel-level collimator for direct-type pico-projectors

Ziming Yao[1,2], Enguo Chen[1,2,], Yun Ye[1,2], Sheng Xu[1,2], Tailiang Guo[1,2]*

1. College of Physics and Information Engineering, Fuzhou University, Fuzhou 350108, China.
2. Fujian Science & Technology Innovation Laboratory for Optoelectronic Information of China, Fuzhou 350108, China.

*Corresponding author: ceg@fzu.edu.cn

Micro LED is a promising light source whose main advantages are high brightness and long lifetime. Applying Micro LED to projection display and other fields will be the future direction. Using a micro led as a projector light source requires that it be collimated first. Direct-type pico-projectors is characterized by the absence of complicated relay system, the overall structure is composed of light source, collimation device and projector lens, so the shaping of the light source is the key to the efficient work of the Direct-type pico-projector device[1,2].

Because of the Lambertian characteristics of LEDs, there have been very much research on the light out shaping of LEDs, such as CPC, free-form lenses and so on. However, these traditional methods will have many problems on micron-scale Micro LEDs, such as difficult to process, too high cost, and so on. Therefore, we consider whether we can use an easy-to-process device with good collimation effect, and finally we choose to use a reflector-coupled hemispherical lens for collimation[3]. The principle and simulation schematic are shown in Fig.1.

The collimation effect of a hemispherical lens with a reflector can be determined from Snell's law and the law of reflection alone. As shown in equations 1 and 2 below.

$$n_1 \sin(\theta_1) = n_2 \sin(\theta_2) \quad (1)$$

$$\theta_{in} = \theta_{out} \quad (2)$$

Obviously, a large angle of light through the reflection of the reflector will be a relatively small angle into the hemispherical lens, and the material of the hemispherical lens is PMMA, its refraction coefficient is 1.44, so the light from the hemispherical lens into the air should be more convergence, so this combination can achieve efficient collimation and the use of large-angle light.

Simulation setup of a single Micro LED pixel 20 microns long and 15 microns wide with a pixel pitch of 20 microns. Simulation results show that the outgoing half-angle is limited to 20°, and the luminous flux within ±20° accounts for 70% of the total luminous flux, which improves the luminous flux within ±20° by a factor of 4.6 and the maximum luminous intensity by a factor of 10 compared to that before the addition of the device. The device has a simple morphology, iseasy to produce, and can perform pixel-level collimation well, which can be well used for micro-projection and other directions. The light pattern and illumination results are shown in Figs. 2 and 3.

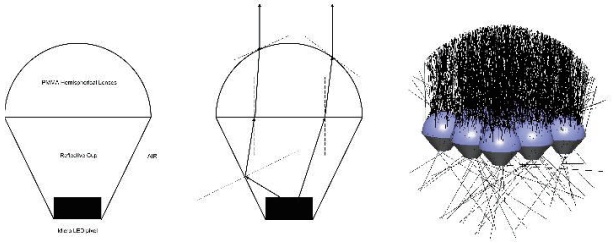

Fig. 1. Schematic of the principle and simulation array of the device

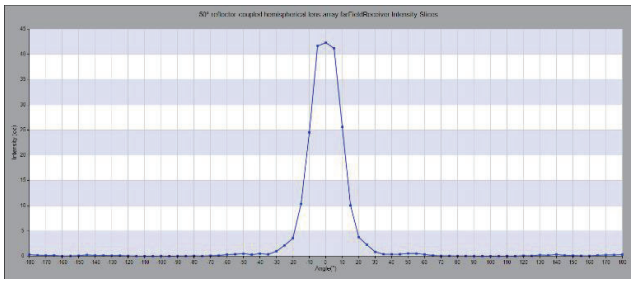

Fig. 2. Light pattern after combination of 50° reflector and hemispherical lens

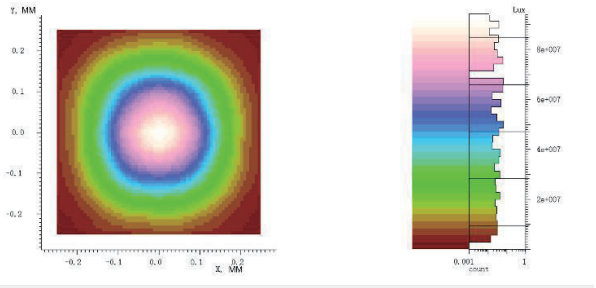

Fig.3. exit illuminance diagram

References

[1] Vázquez-Moliní D, Montes MG, Fernandez BA. Optim Eng. 2010; 49(12):123001.O.V.

[2] Zhang X, Chen A, Yang T, et al. IEEE Photonics J. 2022; 14(2): 1– 7.

[3] Chong WC, Ou F, Xu Q. SID Int Symp: Dig Technol Pap. 2018; 49: 339– 42.

Research progress on Micro-LED light extraction and beam shaping

*Tao Liang[1,2], Tianwen Xia[1,2], Yongzhen Liu[1,2], Jie Sun[1,2], Enguo Chen[1,2] *, Qun Yan[1,2], Tailiang Guo[1,2]*

1. College of Physics and Information Engneering, Fuzhou University, Fuzhou 350108, China

2. Fujian Science & Technology Innovation Laboratory for Optoelectronic Information of China, Fuzhou 350108, China

Corresponding author: ceg@fzu.edu.cn

Micro-LED technology is the prime promising emerging technology with great potential in display and lighting. Light extraction and optical rectification, as two important research directions in Micro-LED technology, can enhance the luminous efficiency of Micro-LEDs, and the optical shaping technology can make the light from Micro-LEDs evenly distributed on the display panel to enhance the display quality and visual experience, which will be helpful for the application in the fields of Virtual Reality (VR), Augmented Reality (AR), wearables, and so on.

Fangwang Gou's team from the University of Central Florida used a flip-flop Micro-LED chip with an inverted trapezoidal structure, and a light intensity distribution pattern showing a Rumbo distribution was also obtained. Xingzhen Bao's team at the University of Chinese Academy of Sciences analyzed and designed a red light Micro-LED array structure containing reflective media in the sidewalls, and filled the pixel spacing with polyimide material containing uniformly doped single-crystal silicon nanoparticles, which was calculated to reflect 16.695% of the light emitted from the sidewalls.

Recently, Enguo Chen's team at Fuzhou University has made new progress in Micro-LED beam shaping and light extraction.Among them, a small light emission dispersion angle blue light Micro-LED structure design with the light emission angle limiting film layer is utilized to inhibit the structure of the excess large-angle light emission in order to obtain a smaller dispersion angle, and the specific structure is shown in Fig. 1.And Fig. 2(a) shows the arrangement of photonic crystals and the selected periodic simulation unit, and Fig. 2

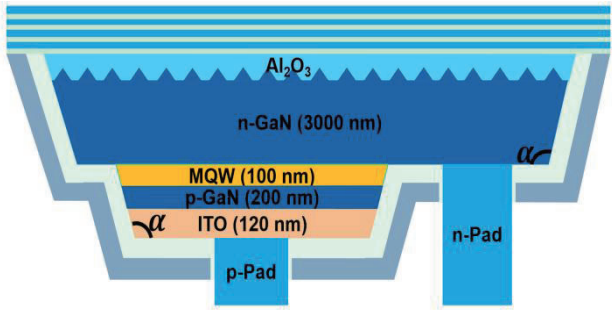

Fig. 1. Micro-LED chip structure with small light dispersion angle

(b) represents the established simulation model of photonic crystals, which shows that the photonic crystal structure consists of an n-type GaN surface etching, which is then covered with an Al_2O_3 support layer.

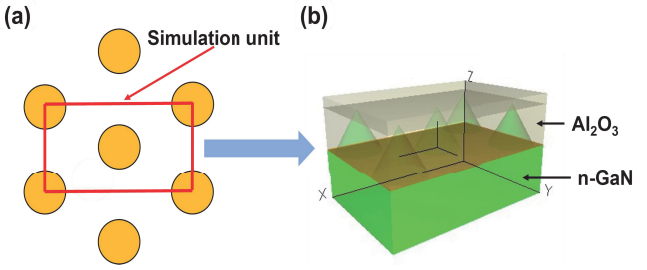

Fig. 2. (a) Photonic crystal arrangement and periodicity simulation unit, (b) Photonic crystal modeling

The principle of angle limiting film layer is similar to that of distributed Bragg reflector, which mainly utilizes the interference principle of fluctuating optics. At small incidence angles, the interference phase length is dominant; at large incidence angles, the interference phase cancellation is dominant.

Fig. 3 shows a Micro-LED sidewall light-guiding structure composed of SiO_2 and TiO_2, which transfers the light from the sidewalls of Micro-LEDs outward to the front side of the structure outward through a total reflection mechanism, has a higher light extraction efficiency and normal intensity. It has higher frontal light extraction efficiency and normal light intensity.

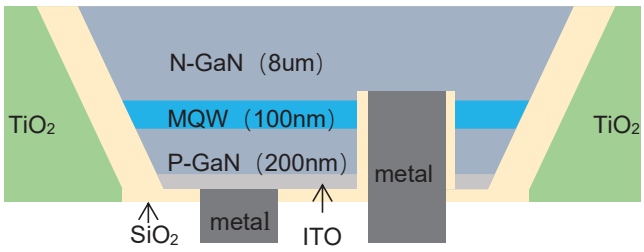

Fig. 3. Schematic of Micro-LED structure with side wall light guide structure

References

[1] Liu Y, Xia T, Liang T, ,et al.Opt. Lett. 48(7), 2023: 1650-1653.

[2] Hu X , Cai J , Liu Y ,et al.Optics and Laser Technology, 2022:154.

Double perovskite for full color E-paper display

Xingke Zheng[1], Aochen Du[1,2], Yun Ye[1,2,*], Enguo Chen[1,2], Sheng Xu[1,2], Tailiang Guo[1,2]

[1]Fujian Science & Technology Innovation Laboratory for Optoelectronic Information of China, Fuzhou 350108, China

[2]College of Physics and Information Engineering, Fuzhou University, Fuzhou 350108, China

***Corresponding author, E-mail: yeyun07@fzu.edu.cn**

Electronic paper (E-paper) refers to the reflective digital displays that mimic the appearance of conventional ink on paper.[1] Since the pioneering work of Jacobson and others, electrophoretic displays (EPD) have been a promising technology applied to E-paper because of its interesting features such as light-weight, thinness, good contrast ratio, wide viewing angles, flexibility, and low power consumption. Though the RGB tricolor was realized by placing a color filter array on the electrophoretic film, it is still a challenge to meet the requirements of the consumers viewing experience because a color filter array not only limits the brightness to less than a third of the incident light, but it also sacrifices the saturation of the colors.[2] Research on a novel structure and simple process for full-color EPD with good brightness and color sharpness are still in progress.[3] In all the solutions, the tricolor (CYM or RGB) electrophoretic particles and the corresponding electronic ink with vivid color were necessary and irreplaceable.

EPD, as an analogous paper reflective display, is more suitable for reading than standard display technologies due to its low power consumption, non-radiation, wide viewing angle and light weight.[4] Fig. 1 shows the preparation idea of organic pigment-high brightness quantum dots, where the high brightness quantum dots are coated on the surface of organic pigment, and the organic polymer with hydroxyl groups is communicated using the grafting method. Fig. 2 gives the microscopic morphology and elemental analysis, which further verifies that the elements are uniformly distributed, which facilitates the excitation of quantum dots and improves the screen display effect. Fig. 3 tested the high temperature resistance of the high brightness electrophoretic particles, further proving that the organic pigment-quantum dots can be applied to electronic paper display.

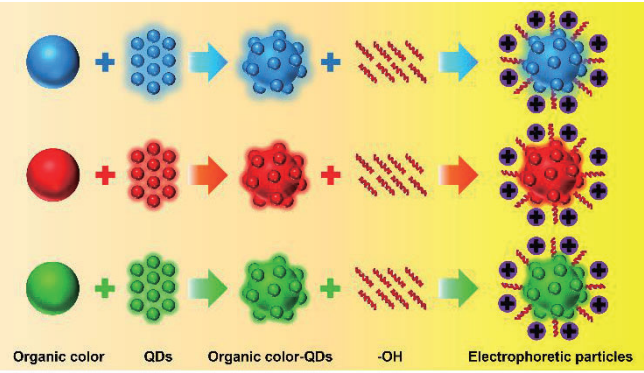

Fig. 1. Synthetic organic pigment-high brightness quantum dot composite particles

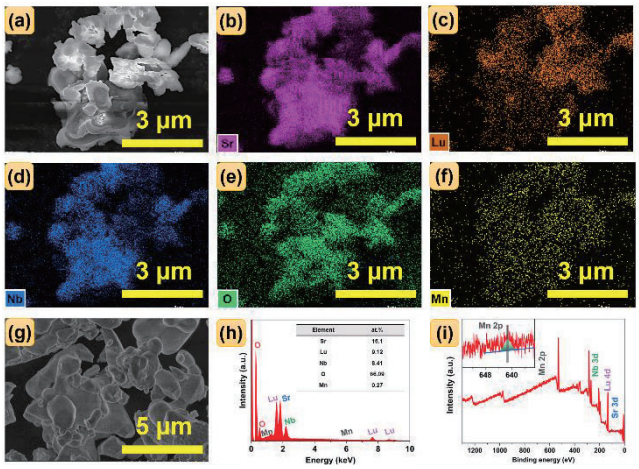

Fig. 2. SEM, Mapping, EDS and XPS

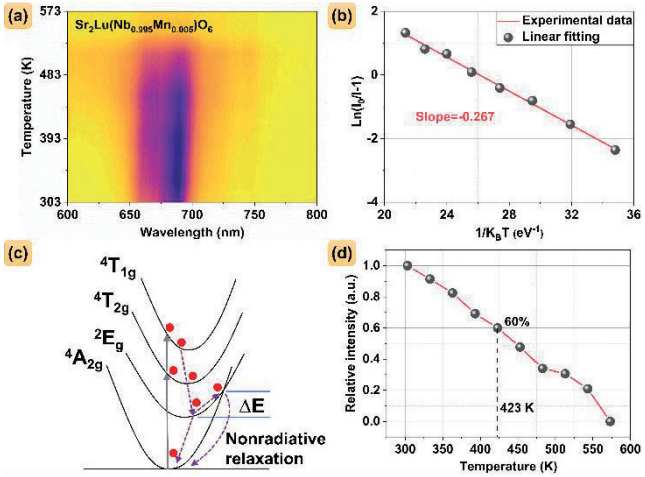

Fig. 3. Luminescence performance under high temperature

References

[1] Y. Fang, J. J. Wang, L. L. Li, et al. *J. Mater. Chem. C,* 4, 5664 (2016).

[2] Y. Hu, S. A. S. Al-Shujaa, B. Zhen, et al. *RSC Adv.,* 11, 20760 (2021).

[3] B. Serment, C. Brochon, G. Hadziioannou, et al. *RSC Adv.*, 9, 34125 (2019).

[4] G. G. Bao, W. Y. Yu, Q. Q. Fu, et al. *J. Mater. Chem. C,* 11, 3513 (2023).

Coaxial spherical cavity Micro-LED for near-eye display based on curved surface metal bonding engineering

Liwen Deng[1], Tao Liang[1], KangKang Chen,[1] Zhilin Sun,[1] Enguo Chen[1,2]*, Tailiang Guo[1,2]

1. College of Physics and Information Engineering, Fuzhou University, Fuzhou 350108, China

2. Fujian Science & Technology Innovation Laboratory for Optoelectronic Information of China, Fuzhou 350108, China

***Corresponding author: ceg@fzu.edu.cn**

Micro-LED (Micro Light Emitting Diode) is a new type of display technology and is considered to be one of the candidates for the next generation of display technology. It uses tiny leds as pixel units, each of which is a self-illuminating light source. Compared with traditional liquid crystal display (LCD) and organic light-emitting diode display (OLED), people have higher expectations for Micro-LED, believing that it will become a leading display technology in the future. It is expected to be widely used in high-end TVS, virtual reality devices, smart watches and wearables.

At present, Micro-LED has several disadvantages in its application. First, the divergence Angle of the Micro-LED is about 120 degrees, causing the light to scatter over a wide range of angles. While this is attractive for wide-field TV applications, it is less efficient in augmented reality (AR) systems, where only light emitted in the near-normal direction can be used effectively, so its optical efficiency is relatively low. In order to improve the efficiency of the entire system, the directional transmission display concentrates the display power into the normal view to achieve higher optical efficiency.

In addition, the emission spectrum of Micro-LEDs is wider, which causes the problem of diffraction dispersion. Diffraction dispersion can cause a rainbow to appear in the image, reducing the quality of the display. This is because the light emitted by the Micro-LED has a wide spectrum, and different wavelengths of light experience different refraction and deflection during the propagation process, resulting in the effect of diffraction dispersion.

In order to solve the above problems, researchers have introduced mirrors at the bottom and top of the Micro-LED to form a Fabry-Perot (F-P) cavity structure, so that the emitted light is concentrated in a narrow Angle range after resonance selection through the cavity, which can enhance the spatial coherence of the emitted light, and the collimation of the emitted light also improves the LEE.

However, OLED and LED are only a few hundred nanometers thick, while Micro-LEDs are only a few micrometers. Therefore, the interference effect of F-P cavity is more obvious in OLED and LED. Moreover, due to differences in device structure, the emission position of the Micro-LED is within a multi-quantum well (MQW), resulting in different light source heights, which makes the microcavity effect more complex. The actual prepared planar cavity Micro-LED often can not meet the needs of near-eye display.

In this paper, a Micro-LED with coaxial spherical cavity structure is proposed. Based on the actual situation of the light-emitting chip applied to the near-eye device, combined with the optimization strategy of coaxial spherical cavity and light extraction efficiency in the micro-cavity theory, the luminous collimation effect and light extraction efficiency of the micro-cavity can exceed the existing parallel plane cavity scheme. In the very small size of the Micro-LED, even if the material efficiency is greatly reduced, it can improve the light performance by reducing the geometric deflection loss, converging the emitted light and resonating. After simulation calculation, the common GAN-based Micro-LED is used as the basis of the simulation model, the chip size is 6μm*6μm*4μm. After adding the upper and lower two layers of curved metal mirrors and using dipoles as the light source for simulation, the optical far-field distribution of the three RGB colors is 4.98°, 5.1°, 3.87°, and the light transmission rate is, respectively. 15.4%, 18.9%, 13.7%.

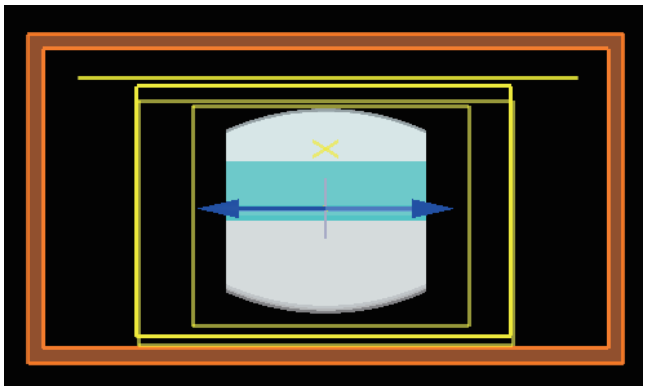

Fig. 1. Diagram of FDTD simulation model

Acknowledgement

National Natural Science Foundation of China (62175032); Fujian Provincial Natural Science Foundation Project (2021J01579); Fujian Provincial Key Science and Technology Project (2021HZ021001); Fujian Science & Technology Innovation Laboratory for Optoelectronic Information of China (2020ZZ111).

References

[1] L Chen, et al., *Research Article,* 6, 2102090 (2022).

[2] C L Lin, et al., *Applied Physics Letters,*87,021101(2005).

[3] Joo et al., Science ,370, 459–463 (2020).

A single layer all-optical diffraction neural network based on liquid crystal

Lisheng YAO*, Wanlong ZHANG*

*** Nanophotonics Research Centre, Institute of Microscale Optoelectronics, Shenzhen University, Shenzhen,518060, China**

Compared with traditional neural networks, all-optical neural networks have the advantages of high parallelism, high speed calculation and low power consumption[1]. The all-optical diffraction neural network framework is physically formed by multiple layers of diffractive surfaces. The design of the diffraction surface is done by computer, while the physical network to achieve specific functions is optical.

The feasibility of all optical diffraction neural networks in image recognition and classification has been proved[1]. And a single modulation layer has a good effect on digit classification[2]. In this paper, a single liquid crystal box is used to classify digital images, and the accuracy rate reaches more than 90 percent. The confusion matrix shows the simulation blind test results, as shown in Fig.1.

In the simulation, the Angle spectrum method was used to construct the light propagation model, and the MNIST handwriting database was used to train the phase modulation layer. Fig.2 shows the phase parameter image obtained by model training. The digital image is irradiated on the liquid crystal box after a distance propagation, and the liquid crystal box modulates the light information, and after another distance propagation, the resulting map is obtained at the detection position. Fig.3a is one of the seven in the MNIST handwriting database, the digital seven image passes through the phase modulation layer, and the light intensity is the strongest for the detection area of the digital seven in the result layer, which is shown in Fig.3b.

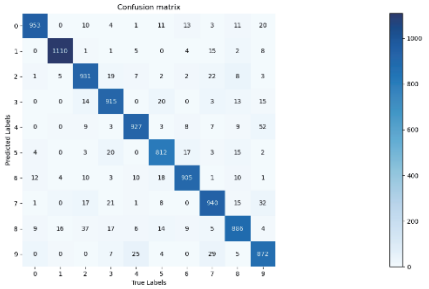

Fig. 1. Confusion matrix

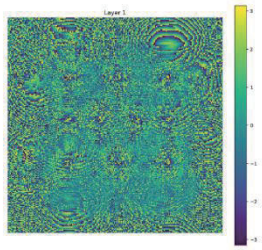

Fig. 2. Phase parameter image

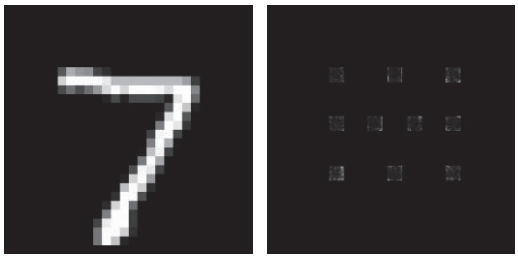

(a) (b)

Fig. 3. The result of the digital image passing through the phase modulation layer

References

[1] Lin X, Rivenson Y, Yardimci N T, et al. All-optical machine learning using diffractive deep neural networks[J]. Science, 2018, 361(6406): 1004–1008.

[2] Zheng M, Shi L, Zi J. Optimize performance of a diffractive neural network by controlling the Fresnel number[J]. Photonics Research, 2022, 10(11): 2667.

A Realization of Dynamic Continuous Adjustable Phase Based on Liquid Crystal-Integrate All-dielectric Metasurface

Liu Liu*, Wanlong Zhang*

Nanophotonics Research Centre, Institute of Microscale Optoelectronics, Shenzhen University, Shenzhen,518060, China

Composed of sub-wavelength metallic/dielectric nanostructures (meta-atoms), metasurfaces are made of nanopillars using two-dimensional materials to be arranged periodically. With the superior performance of low-loss and high refractive index, dielectric metasurfaces have developed rapidly in nonlinear optical field. The performance metasurfaces are mainly determined by the size and arrangement of nanopillars, which makes it difficult to be adjusted. In recent years, some researchers have embedded anisotropic liquid crystal molecules with metasurface to achieve the dynamic phase modulation of the incident light[1][2]. Due to the unique anisotropy of LC, which can be manipulated by electric fields, magnetic fields, and temperature. In this paper, we demonstrate the liquid crystal embedded metasurface device for continuous phase modulation at working wavelength of 1550nm. Under the modulation of voltage, the tilt angle of LC can be changed to realize particular character. By designing the dielectric nano-antenna structure, the electric dipole and magnetic dipole resonances are superimposed, which can generate phase modulation of 0-2pi near the resonance peak.

The model of continuously tunable metasurface by modulating the tilt angle of LC(Fig. 1). The FDTD simulation results of the device is shown in Fig.2. By applying the external voltage, the LC molecules are controlled with different tilt angles, resulting the change of dielectric environment and resonance of the nanopillar array, achieving 2pi phase changes at C-band, which are essentially important for optical communication system.

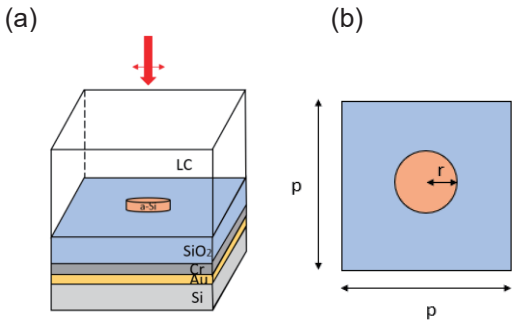

Fig. 1. Reflective liquid crystal metasurface structure (a) Side view; (b) Top view

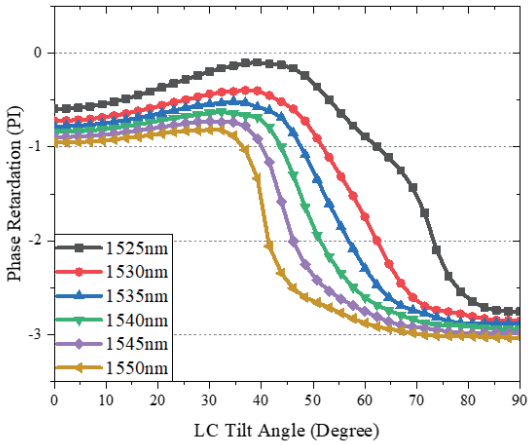

Fig. 2. The simulated phase modulation of the LC-Metasurface device

References

[1] Li, S., Xu, X., Maruthiyodan Veetil, R., Valuckas, V., Paniagua-Domínguez, R., & Kuznetsov, A.I. (2019). Science, 364, 1087 - 1090.

[2] Kim, I., Ansari, M. A., Mehmood, M. Q., Kim, W. S., Jang, J., Zubair, M., Kim, Y. K., & Rho, J. (2020). Advanced materials (Deerfield Beach, Fla.), 32(50), e2004664.

High Order Laguerre Gaussian Generation System based on liquid crystal

Haidong Shi*, Wanlong Zhang*

*** Nano-photonics Research Centre, Shenzhen Key Laboratory of Micro-scale Optical Information Technology, Institute of Micro/Nano Optoelectronics, Shenzhen University, 518060, China**

Optical vortices have been of interest for decades as with phase singularities. In the case of tight focusing, they both have unique focusing properties. At the same time, it is the hope for increasing the capacity of optical communication system and realizing the new generation of optical communication. To generate optical vortices, Pancharatnam-Berry Phase Optical Elements (PBOEs) are used by modulating the spatially varying geometrical phases associated with the polarization of light. [1] It can also be used for imaging, beam shaping and optical pattern classification. PBOEs can be realized based on self-assembled nanostructures, metasurfaces and photoaligned liquid crystals (LCs).

In order to achieve flexible manipulation of the angular order of a vortex beam, we have designed a vortex beam generation system that can generate angular orders from -99 to +99. The system consists of several liquid crystal vortex waveplates and one-half waveplates. The order of the vortex light is adjusted by applying a voltage to the liquid crystal waveplates.

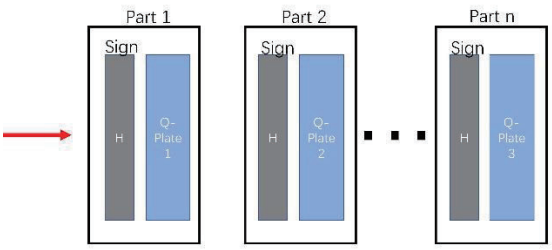

Fig. 1. Schematic diagram of an order-adjustable vortex waveplate system

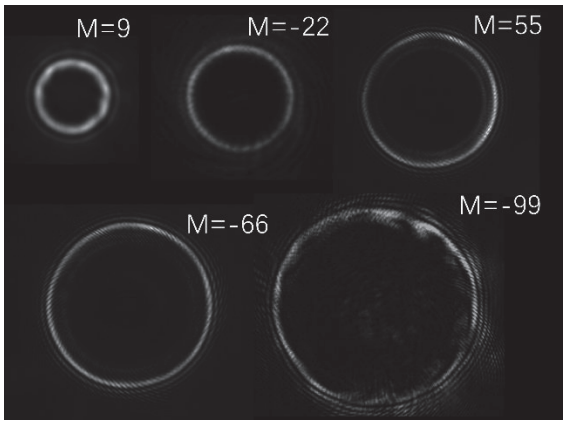

Fig. 2. Images of experimental results with different vortex light

References

[1] Lin Zhu, Chun-Ting Xu, Peng Chen,* Yi-Heng Zhang, Si-Jia Liu, Quan-Ming Chen, Shi-Jun Ge, Wei Hu, and Yan-Qing Lu*Light Sci. Appl. 11, 135

The complete LCD design process based on Empyrean Technology platform

Xiaoxin MA*, Wanlong ZHANG**

*** Nano-photonics Research Centre, Shenzhen Key Laboratory of Micro-scale Optical Information Technology, Institute of Micro/Nano Optoelectronics, Shenzhen University, 518060, China**

The significance of higher charging rate lies in improving battery charging speed and efficiency, while EDA software provides advanced electronic design automation tools to assist engineers in designing, validating, and implementing complex integrated circuits and electronic systems.

In this study, EDA software was used for schematic design, and through layout design, TFT performance was optimized, resulting in an increased pixel charging rate of 90.715%. The layout size was restricted to 1200um*3996um. GOA bilateral driving: On one side, the GOA unit drives only odd-numbered rows, while on the other side, the GOA unit drives only even-numbered rows. They do not interfere with each other, achieving the purpose of sequentially activating each row."Figure 1 below shows the simulated measurement of the charging rate for nine selected pixel points in the GOA unit output.

An entire LCD simulation circuit was constructed using EDA software. Figure 2 represents the schematic circuit of the GOA unit (gate driver circuit), while Figure 3 shows the goa_unit layout that perfectly matches the circuit. Figure 4 shows the layout of TFTs with different channel widths (channel length is 3.5um).

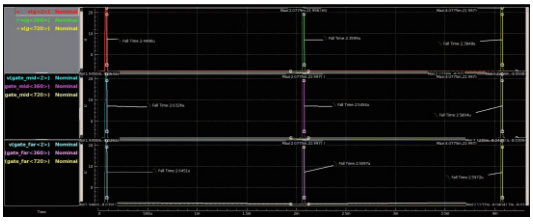

Figure 1 the simulated measurement of the charging rate

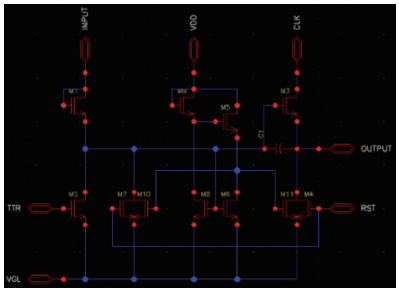

Figure 2 the schematic circuit of the GOA unit (gate driver circuit)

Figure 3 the goa_unit layout that matches the circuit.

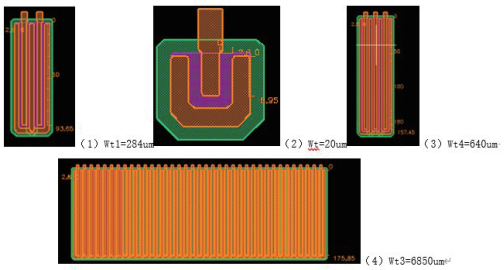

Fig.4. the layout of TFTs with different channel widths

References

[1] Dennis Goldstein.Polarized Light. The Chemical RubberCompany Press,2003

[2] Yue Kuo. THIN FILM TRANSISTORS. KLUWER ACADEMIC PUBLISHERS , 2004

High Efficiency Full-phase Continuous Modulator Based on Liquid Crystal Metasurface

Cong Liu*, Wanlong Zhang**,

Nanophotonics Research Centre, Institute of Microscale Optoelectronics, Shenzhen University,

Shenzhen,518060, China

All-dielectric metasurfaces can avoid the losses of metals and effectively improve the efficiency of metasurfaces. Liquid crystals have dielectric and optical anisotropy. When the external environment changes, such as the electric field, magnetic field, and temperature, the liquid crystal will transform between isotropy and anisotropy, thereby changing its dielectric constant and refractive index characteristics.In recent years, some researchers have embedded anisotropic liquid crystal molecules with metasurface to achieve the dynamic phase modulation of the incident light[1][2].In this paper, we combined liquid crystal modulation technology with all-dielectric metasurfaces. By changing the azimuth angle of liquid crystal molecules and designing the dielectric nanoantenna structure, the electric dipole and magnetic dipole resonances are superimposed, which can generate phase modulation of 0-2pi near the resonance peak.Through design and simulation, we achieved over 0-2π full-phase continuous modulation at five wavelengths in the optical communication C-band, and the average reflectance reached 90%.

The model of liquid crystal metasurface by modulating the azimuth angle of LC(Fig. 1). The FDTD simulation results of the device is shown in Fig.2. By liquid crystal optical orientation technology technology, the LC molecules are controlled with different azimuth angles, resulting the change of dielectric environment and resonance of the nanopillar array, achieving 2pi phase changes at C-band, which are essentially important for optical communication system.

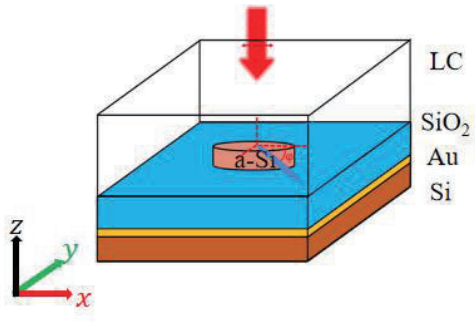

Fig. 1. Reflective liquid crystal metasurface structure

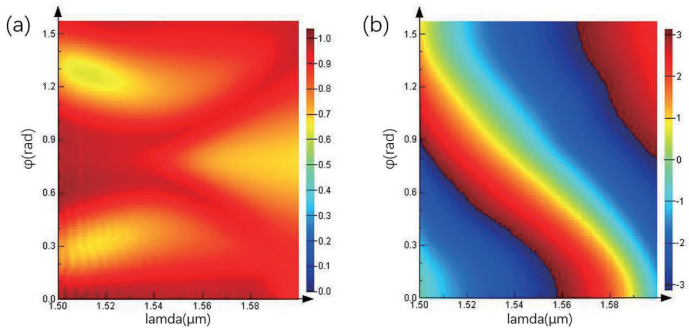

Fig. 2. The simulated of the LC Metasurface device

(a) Reflectance; (b) Phase modulation

References

[1] Lin X, Rivenson Y, Yardimci N T, et al. All-optical machine learning using diffractive deep neural networks[J]. Science, 2018, 361(6406): 1004–1008.

[2] Zheng M, Shi L, Zi J. Optimize performance of a diffractive neural network by controlling the Fresnel number[J]. Photonics Research, 2022, 10(11): 2667.

Passive Vibration Sensor Using Deformed Helix Ferroelectric Liquid Crystal Electro-optical Modulator

Xinyi Yu, Vigneshwaran Swaminathan, Valerii V. Vashchenko, Abhishek Kumar Srivastava*

***State Key Laboratory of Advanced Display and Optoelectronics,**
Hong Kong University of Science and Technology
***Tel: +852- 3469 2485, Email: eeabhishek@ust.hk**

Keywords: Passive sensing; Threshold-less liquid crystal; Vibration sensor; Ferroelectric liquid crystal

Abstract

In this work, we proposed a passive vibration sensor using threshold-less deformed helix ferroelectric liquid crystal (DHFLC) electro-optical (EO) modulator. Combining a DHFLC cell, a passive vibration transducer and an optical detector, the sensor can transform a slight vibration into light intensity signal without power supply. The sensor was tested using 2 kinds of passive vibration transducers and 2 vibration generators. We proved the feasibility of the sensor and found it can reach the sensitivity of 165 V/(m/s) and the linearity <1% full range output. The proposed sensor will be combined with optical fibers to play an important role in various vibration sensing array applications.

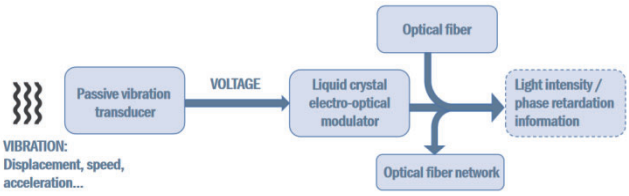

Figure 1. The mechanism of the proposed system.

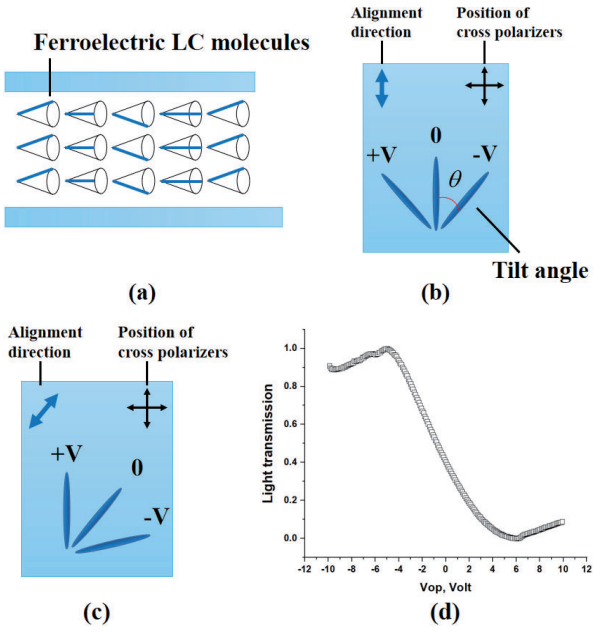

Figure 2. (a) The schematic diagram of molecules orientation of DHFLC. The relative of cross polarizers and alignment direction of (b) displays and (c) LC modulator in proposed system. (d) The TVC of DHFLC.

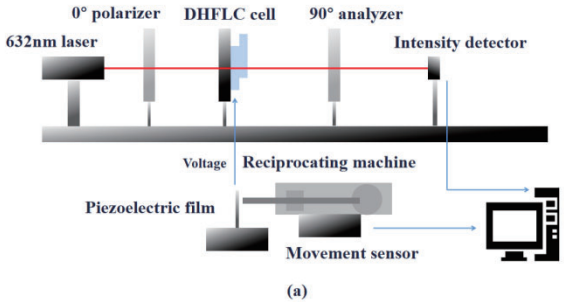

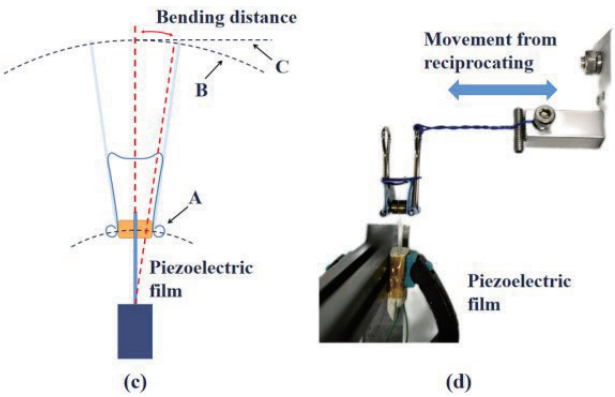

Figure 3. (a) The measurement setup using piezoelectric film and reciprocating machine. (b) The picture of piezoelectric film, whose sensing mode is the bending along the long axis. (c) The schematic diagram of the piezoelectric film movement model. (d) The picture illustrating the connection of movement structure.

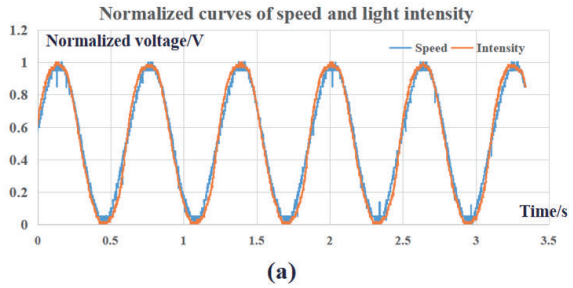

(a)

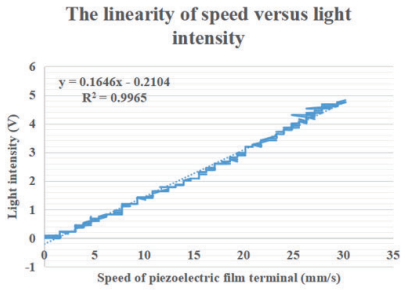

(b)

Figure 4. (a) The synchronous time versus normalized speed and light intensity. (b) The linearity of speed versus light intensity curve.

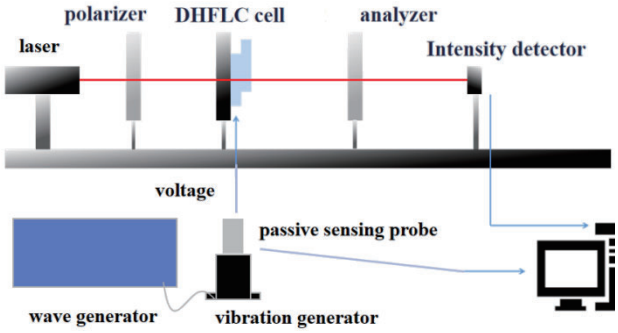

(a)

(b)

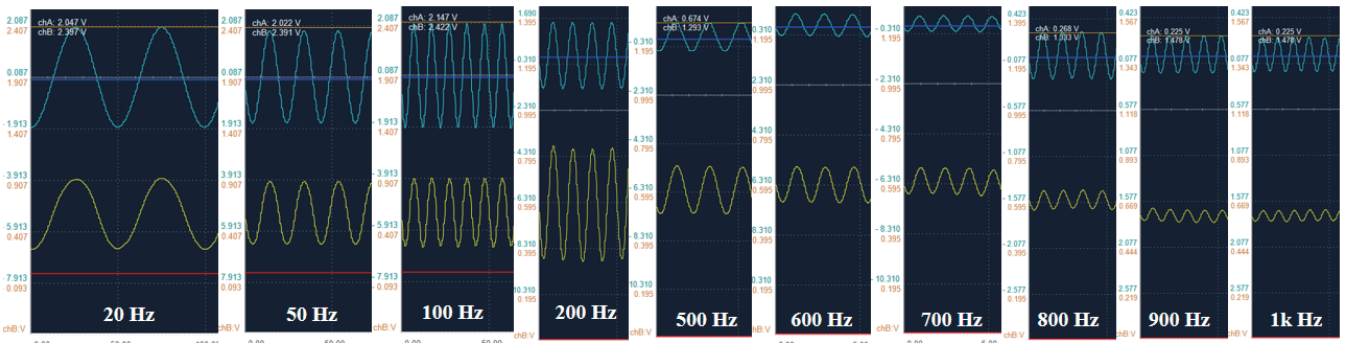

(c)

Figure 5. (a) The measurement setup using electromagnetic transducer and sine vibration generator. (b) The figure of bonding of electromagnetic transducer and sine vibration generator. (c) The optical output corresponding to the movement of the vibration generator at various frequency.

Conclusions

Combining threshold-less DHFLC EO modulator with a wide linear range, an optical system and a passive vibration transducer, the proposed passive vibration sensing sensor shows a feasibility of applications. The performance is measured using a 632 nm laser setup and 2 kinds of vibration generator. The sensor has a sensitivity of 164.6V/(m/s) and provides a good linearity of 0.35% FRO. The proposed sensor can be optimized further and is believed to be applied to diverse passive sensing networks.

Acknowledgement

We acknowledge the support of The State Key Laboratory of Advanced Displays and Optoelectronics through the Innovations and Technology Commission of Hong Kong and Hong Kong Gov. Innovations and Technology Commission of Hong Kong grant number PRP/049/19FX.

Advanced Color Conversion LCD with Photoluminescent Color Filter and In-Cell Polarizer

Yi-Yang Gao, Yue-Chu Cheng, Jian-Xin Song, Man-Chun Tseng, Jacob Yeuk-Lung Ho, Olena Vashchenko, Shu-Tuen Tang, Valerii Vashchenko, Fion Sze-Yan Yeung, Abhishek Srivastava, and Hoi-Sing Kwok*

*** State Key Laboratory of Advanced Displays and Optoelectronics Technologies,**

Department of Electronic and Computer Engineering,

The Hong Kong University of Science and Technology,

Hong Kong S.A.R, China

Color conversion is promising technology to innovate LCD for high end display. An approach to developing a thin-film polarizer with high polarization efficiency in liquid crystal cells is presented. The in-cell polarizer facilitates the realization of novel color-conversion liquid crystal displays, where advanced quantum color-converters are used as photoluminescent color filter arrays (PLCF). The PLCF replace traditional absorptive type color filter arrays, endowing the LCD with higher energy efficiency, wider viewing angle and broader color gamut. The in cell polarizer is ultrathin and is integrated between the PLCF and LC. The in-cell structure solve problem of depolarization and parallax thus ensuring the improved LCD operation. We systematically designed the device structure and fabrication process. And we experimentally demonstrated using azo-dye-based embedded polarizers for color-conversion liquid crystal displays for the first time.

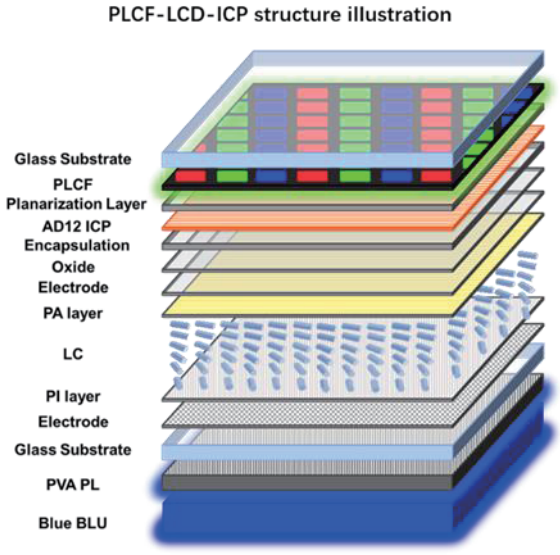

Fig. 1. Structural Illustration

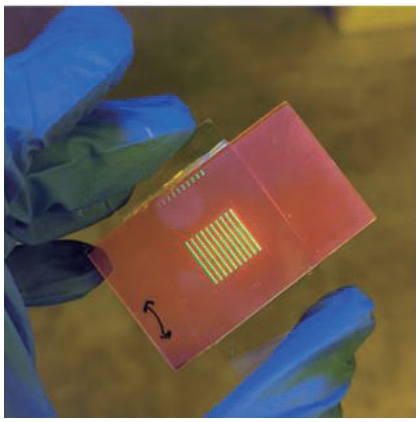

Fig. 2. Photo of a PLCF-LCD with ICP sample

References

[1] Pan, S., Ho, J. Y., Chigrinov, V. G., & Kwok, H. S. (2018). Novel photoalignment method based on low-molecular-weight azobenzene dyes and its application for high-dichroic-ratio polarizers. ACS applied materials & interfaces, 10(10), 9032-9037.

[2] Gupta, S. K., Prodanov, M. F., Zhang, W., Vashchenko, V. V., Dudka, T., Rogach, A. L., & Srivastava, A. K. (2019). Inkjet-printed aligned quantum rod enhancement films for their application in liquid crystal displays. Nanoscale, 11(43), 20837-20846.

[3] Tseng, M. C., Yaroshchuk, O., Bidna, T., Srivastava, A. K., Chigrinov, V., & Kwok, H. S. (2016). Strengthening of liquid crystal photoalignment on azo dye films: passivation by reactive mesogens. RSC advances, 6(53), 48181-48188.

Integrated Display and Communication: High-capacity MIMO Visible Light Communication Enabled by LCDs with mini-LED Backlight

Zhiqing Zhao*, Yuqing Qiu*, Guowei Zou*, Bo-Ru Yang*, Zong Qin*
***School of Electronics and Information Technology, Sun Yat-Sen University, Guangzhou, China.**

Optical wireless communication (OWC) technology has been considered as a promising RF-alternative option for future beyond-5G (6G) communication [1]. Visible light communication (VLC) is an OWC technology that leverages visible light as the communication medium, featuring high bandwidth capacity, unlicensed spectrum, high security and negligible electromagnetic interference. Moreover, transmitters in the visible are ubiquitous and inexpensive, such as lighting fixtures and displays. Compared with lighting fixtures that provide simultaneous illumination and communication, it is more attractive to use a display as a transmitter because the display and VLC are performed at the same time. In addition, the temporal resolution of the human visual system is around 60 Hz, while the modulation bandwidth of modern LEDs can easily be at kHz or even MHz. Thus, a display-based VLC system can intrinsically multiplex display and communication signals, which we call *Integrated Display and Communication* (IDAC).

LCD is an ideal choice for IDAC—the LC panel refreshes at 60 or 120 Hz while the backlight flickers at a much higher frequency, as proposed by previous studies [2,3]. However, those studies usually adopted an edge-lit backlight, which dominated the LCD market in the past due to its compactness compared with direct-lit. The edge backlight was used like a lamp bulb transmitting 1D signals. In this manner, the display-based VLC does not show superiority to lighting-based systems except by being integrated into a normally working display.

However, things are changing since the mini-LED technology emerged. With mini-LEDs, direct-lit LCDs can be as thin as edge-lit. More importantly, contrast comparable with OLEDs and higher peak brightness can be achieved through local dimming with massive segments, not to mention the power consumption saving. Thus, mini-LEDs make direct-lit LCDs popular for high-end products.

Besides the benefits to display technology, we here propose, for the first time to our knowledge, the mini-LED also opens up a promising opportunity for IDAC by introducing massive local dimming segments. Specifically, each backlight segment is independently controlled in a mini-LED LCD, so we have multiple (in fact, massive) outputs. On the other hand, a commercial camera can be used as an arrayed receiver for spatiotemporal signals, i.e., multiple inputs. In this manner, we have a fascinating multi-input and multi-output (MIMO) system. Noticeably, the channel number in our MIMO system is the dimming segment number, which is hugely higher than radio-band MIMO. However, we will hardly encounter channel crosstalk, the radio band's main obstacle, because a camera's spatial resolution is too high. In essence, the area of optics always pursues high spatial resolution by modulating spatially, while the area of communication pursues high temporal resolution by modulating temporally. When the two areas meet, the camera's spatial resolution greatly exceeds our requirement.

One more thing. Local dimming for LCDs requires each segment to be dimmed according to image content for higher contrast and lower power. Meantime, VLC also requires the source to be dimmed because meaningful signals (e.g., 0-1-0-1) must reduce the brightness. The requirements from display and communication naturally fit in IDAC.

This study proposes a concept-of-proof IDAC LCD, as shown in Fig. 1. We utilize the camera's rolling shutter effect (RSE), which takes advantage of the sequential reading characteristic of a CMOS sensor [2]. That is, in a frame time of the camera, rows in the image sensor can sequentially reflect the signal flow from the transmitter, for a capacity determined by the sensor's row number (usually very high). In the column direction, each backlight segment is interpedently controlled, for a multiplied capacity. Here, we adopt ten columns, which for sure can be expanded easily.

Moreover, we like to further exploit the high spatial resolution of the camera. Combined with local dimming and multi-pulse position modulation (MPPM), the proposed system was able to achieve a data rate of 46.2 kbps. Figure 2 shows the experiment setup of the system. A frame captured by the camera is shown in Figure 3.

More importantly, the communication capacity is estimated, as given by Table 1. With such a low device modulation bandwidth and a commercial camera, a mini-LED LCD can achieve 462 kbps by extending the dimming segment columns to 100.

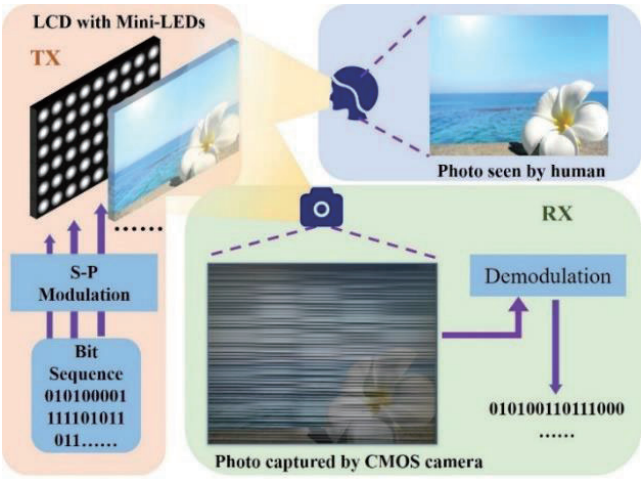

Fig. 1. System of IDAC LCD

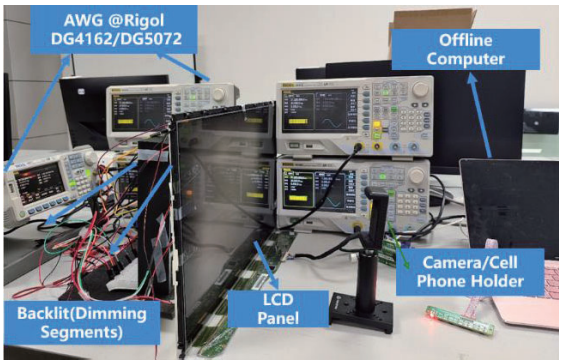

Fig. 2. Experiment Setup

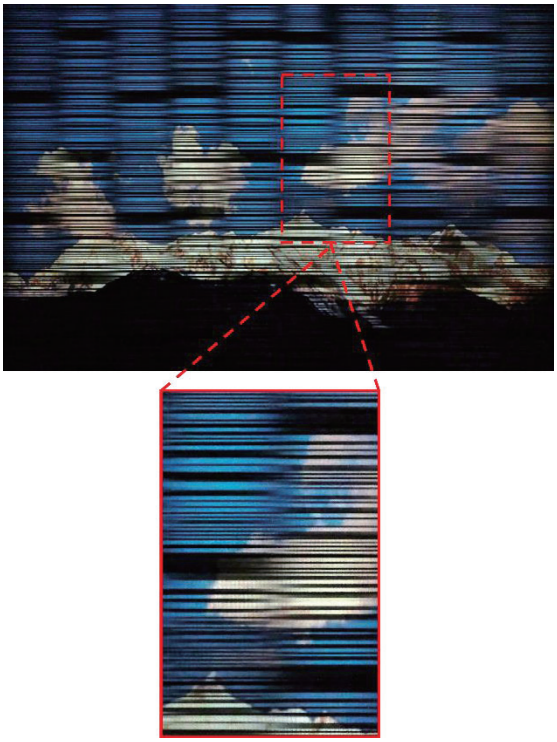

Fig. 2. Rolling Shutter Patterns

Table 1. Rate of IDAC LCD

Symbol Number per Column	11
Bit Rate per Column	55~77
Bit Rate per Frame(10 columns)	550~770
Bit Rate/kbps(60fps,10 columns)	33~46.2
Bit Rate per Frame(100 columns)	5500~7700
Bit Rate/kbps(60fps, 100 columns)	330~462

References

[1] Li, Xianbo, et al. IEEE Photonics Journal 11.1 (2019): 1-8.

[2] Chow, Chi-Wai, Chung-Yen Chen, and Shih-Hao Chen. Optics express 23.20 (2015): 26080-26085.

[3] Liang, Kevin, Chi-Wai Chow, and Yang Liu. Optics express 24.15 (2016): 17505-17510.

Progress Review in Materials and Structures toward Stretchable Light-Emitting Diodes

Lisha Peng, Zhiguang Qiu, Yifan Gu, Simu Zhu, Feng Xiong, Zong Qin, Bo-Ru Yang*

Dept. of Electronics and Information Technology, Sun Yat-Sen University, Guangzhou, China
***Email: paulyang68@me.com**

Among various display technologies[1], light-emitting diodes (LED) has developed for several decades of years. However, the demand of stretchability has posed new technical challenges for LED display. In this paper, we summerize the strategies and latest developments for achieving stretchability in LED displays, with detailed explanations from both material and structural scales.

The intrinsic stretchable LED display device consists of three functional layers: i) Encapsulation layer; ii) Emission layer and iii) Electrode layer, as shown in **Fig.1**. These layers required to be stretchable and modulus matched to prevent device delamination under strain.

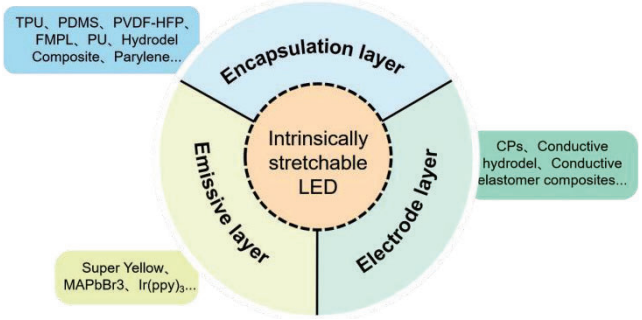

Fig.1 A schematic of different functional layers of LED and the example materials

For encapsulation layers, the material is usually required to be environmental stability. Commonly used include thermoplastic polyurethanes (TPU), polydimethylsiloxane (PDMS), polyurethanes (PU), hydrodel composite, parylene, acrylic based tape, etc. For the emission layer, luminescent materials and viscoelastic materials are usually mixed together to reduce the Young's modulus to achieve modulus matching. The commonly used light-emitting material is super yellow. In addition, there are phosphorescent light-emitting layers[2], $MAPbBr_3$, and RGB three color light-emitting films[3], which are blended with poly (9-vinylcarbazole) (PVK) and Tris (2-phenylpyridine) iridium ($Ir(ppy)_3$). For the electrode layer, the commonly used materials are mainly divided into three categories: i) Conductive polymers (CPs): polymers generate conductivity from doped charge carriers and have good mechanical processing properties. The representative material is PEDOT:PSS; ii) Conductive elastomer composites: an electrode with both conductivity and extensibility can be obtained by combining conductive filler and elastomer. The conductive filler includes metal nanowires (NWs), metal nanoparticles (NPs), carbon nanotubes (CNTs), Graphene, etc. The representative elastomer materials include PDMS, PU, styrene-butadiene-styrene block copolymer (SBS), Ecoflex, etc; iii) Conductive hydrogel: it can be mixed with PEDOT:PSS, metal NWs and other conductors, but it has the disadvantage of environmental instability, so it needs to make gel water retaining method.

On the other hand, stretchable structure strategies mainly include four types: pre-strain/wrinkled structure[4], island bridge structure, textile structure[5], and Kirigami structure[6], as shown in **Fig.2**.

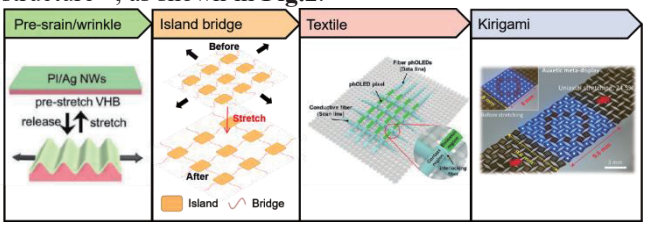

Fig.2 A schematic of different structural designs of LED[4-6]

The pre-strain/wrinkle strategy can achieve amplification of the device's luminescent area during stretching by preparing ultra-thin LED display device layers on pre-stretched substrates. The island bridge structure provides mechanical isolation for each rigid LED through stretchable interconnects (such as liquid metal (LM), silver nanowires (AgNWs), etc.). The LED array designed thereby can achieve stretchable high-resolution LED display when combined with stretchable (thin film transistor) TFT array, such as a 12 inch 100 PPI Active Matrix Micro-LED with 20% extensibility[7]. The textile structure is based on fibers, and can achieve display functions to fabric like stretchability through the weaving of conductive fibers and luminescent fibers, and can even achieve site selection display. The Kirigami structure can be obtained through laser cutting, providing positional stability for the LED during stretching by rotating the structure, which can achieve distortion free stretchable display devices.

References

[1] B-R. Yang, "E-Paper Displays". *John Wiley & Sons Ltd, Chichester*, ISBN: 978-1-119-74558-7, (2022).
[2] J. H. Oh, et al. *ACS Appl Mater Interfaces,* 15, 33784-33796 (2023).
[3] M. W. Jeong, et al. *Sci Adv,* 9, eadh1504 (2023).
[4] Y. F. Li, et al. *Adv. Mater.s,* 31 (2019).
[5] Y. H. Hwang, et al. *Adv. Funct. Mater.,* 31 (2021).
[6] B. Jang, et al. *Adv. Funct. Mater.,* 32 (2022).
[7] H. Jung, et al. *J Soc Inf Disp,* 31, 201-210 (2023).

Improving the Response Time of Electrophoretic Display by Waveform with Invisible Shaking

Tao Zhou[1], Debo Zeng[1], Guangyou Liu[1], Yue Zhang[1], Xinzao Wu[1], Zong Qin[1], Bo-ru Yang[1,]*
State Key Laboratory of Optoelectronic Materials and Technologies, Guangdong Province Key Laboratory of Display Material and Technology, School of Electronics and Information Technology, Sun Yat-Sen University, Guangzhou 510275, People's Republic of China.
***Email:Paulyang68@me.com**

The electrophoretic displays (EPDs) hold great promise for various applications due to their low power consumption, high environmental contrast and flexibility.[1] However, the response time of the EPDs remains a challenge, as it can be as long as hundreds of milliseconds. One effective approach to improve the response time is by optimizing the driving waveform. However, current waveform designs aimed at improving the response time often include additional phases before or after the display stage, such as an activation phase[2], leading to extra time cost. In this study, we have proposed a new waveform without additional phase to improve the response time of EPDs.

In this proposed waveform, the particle driving stage is divided into two phases: the direct current (DC) driving phase and the "invisible shaking" phase. Firstly, we apply a direct voltage to drive the EPDs to the desirable state (black or white). Secondly, instead of maintaining the direct voltage, we introduce a small-amplitude shaking voltage whose integral over time is opposite to the direct voltage applied earlier. Importantly, the shaking voltage here does not alter the grayscale of the EPDs, allowing us to include it in the display stage seamlessly. The driving waveform is shown in Fig. 1.

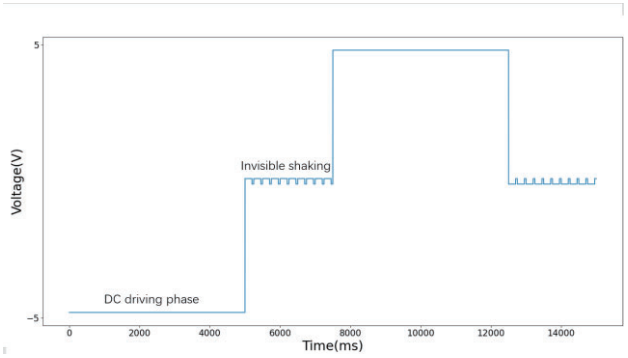

Fig. 1. Driving waveform with invisible shaking. The duty ratio of invisible shaking after the negative DC driving phase is 80% , and the duty ratio of invisible shaking after the positive DC driving phase is 20% .

To assess the effectiveness of the proposed waveform, we conducted experiments using three different waveforms on the EPD and recorded response time respectively. The first waveform is three-phase waveform[2], which has reset phase and activation phase before transferring to different display stages; The second waveform is direct shift waveform, which just sets different voltages when transferring to different display stages; The third waveform is the proposed waveform. The result is shown in Table 1. According to the experimental result, we can find that the response time of the proposed waveform is 260ms and 100ms, which is improved significantly compared to that of the direct shift waveform. Although the response time of proposed waveform is little longer than the three-phase waveform, the proposed waveform doesn't need additional phases before display stage. For the validity of the waveform, we have the following explanations.

Waveform	Initial state	Final state	Response time(ms)
Three-phase waveform	white	black	200
	black	white	80
Direct shift waveform	white	black	600
	black	white	300
Invisible shaking	white	black	260
	black	white	100

Table 1. Response time of three different waveforms

The charged particles and charged inverse micelles (CIMs) will drift to the two sides of EPDs under the influence of direct voltage and shield the external electric field, which the prolongs response time. By employing the "invisible shaking" waveform, we can drive the CIMs to the center of the EPDs before transferring between different states, while maintaining most of the charged particles in their original positions, as shown in Fig. 2, thus improves the response time.

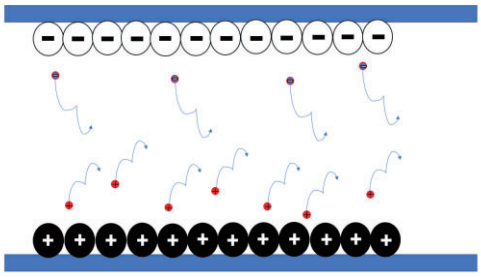

Fig. 2. Motion of CIMs under invisible shaking .

References

[1] Yang B-R. "E-Paper Displays". John Wiley & Sons Ltd, Chichester, ISBN: 978-1-119-74558-7, 2022.

[2] W.C. Kao, H. Chen, Y. Liu, S. Liou. *J. Disp. Technol.*

Hardware engine for supporting gray-tone paintbrush function on electrophoretic papers. (2014), 10, 138–145.

Key printing processes and applications of roll-to-roll in flexible display

*Jintao Shi, Qitian Fan, Yifan Gu, Zhiguang Qiu, Zong Qin, Bo-Ru Yang**

State Key Laboratory of Optoelectronic Materials and Technologies, Guangdong Province Key Laboratory of Display Material and Technology, School of Electronics and Information Technology, Sun Yat-Sen University, Guangzhou, Guangzhou 510275, People's Republic of China.

***Email:** paulyang68@me.com

The development of display devices is aligning with the trend towards flexible electronic devices. Display devices have transitioned from traditional large-area rigid screens to foldable and even stretchable, leading to the emergence of new wearable display technologies, which have experienced significant advancements in recent years [1]. Commercial display devices consist of complex multilayered thin-film structures, making them well-suited for fabrication using the Roll-to-Roll (R2R) printing process. Compared to traditional discontinuous processes on flat planes, R2R offers distinct advantages as a continuous flexible electronic printing technology, with features like high throughput, low production costs, and suitability for large-scale production.

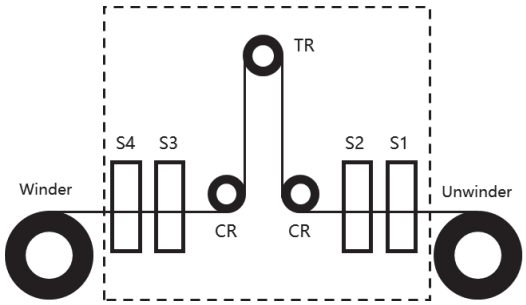

Figure 1：Schematic of an R2R operating system

R2R systems, despite their variations based on different applications and products, share common features and operating principles. A typical working schematic of an R2R system is shown in Figure 1. The uncoated or pre-coated substrate enters the R2R processing system (indicated by the dashed box in the figure) through the unwinder roller. The flexible substrate is then continuously transported at a controlled speed between multiple processing steps (S1, S2, etc.) and finally wound up into the finished roll by the winder roller. Besides the unwinder roller, winder roller, and process rollers, a complete R2R system includes several transport rollers (CR) and tension rollers (TR), which ensure flatness, planarity, and defect-free processing throughout the entire manufacturing process[2].

R2R systems can integrate various traditional flat-plane processes, including various printing and coating techniques, photolithography, lamination, and thin-film deposition methods like sputtering and chemical vapor deposition. Table 1 concludes some features of printing methods used in R2R[3, 4].

The entire R2R process relies on the continuous treatment of the web, which simultaneously serves as the device substrate. Commonly used substrate materials include inorganic thin glass, polymer films, and metal foils. There are also many examples of hybrid substrates combining two or more materials to leverage their respective advantages.

Table 1. Categories, parameters and characteristics of R2R printing process

R2R Printing category	Common feature size	Printing speed	System complexity	Cost
Gravure printing	5~10 μm	High（up to 15 m/s）	Low	Low
Flexographic printing	5~10 μm	High	Medium	Low
Rotary screen printing	50~100 um	High（>100 m/min）	Medium	High
Reverse offset printing	>0.5um	Medium（<50 mm/s）	Medium	Low
Inkjet printing	15-20um	Low	High	Low
Nanoimprint	>10nm	Low	Medium	Low

The production of flexible display devices using R2R technology is currently a research hotspot. For instance, in LCDs, R2R is used for high-throughput processes, such as designing color filter films, backlight modules, polarization films, and functional layers like microstructured films for viewing angle enhancement. In OLED displays, R2R processes involve the fabrication of transparent electrodes, moisture and oxygen barrier layers, and other functional layers such as HIL, EIL, and EML. In EPD, R2R is used for novel micro-cups and top-sealing techniques for SiPix and for directly attaching EPD films to TFT arrays to achieve display effects.

As of now, the biggest challenge for future R2R printed electronic products lies in improving device yield, performance, and reliability, as well as further reducing the overall production cost. If achieved, the commercialization potential of R2R equipment on a large scale would significantly increase in the current context.

References

[1] Yang B-R. *"E-Paper Displays". John Wiley & Sons Ltd, Chichester, ISBN: 978-1-119-74558-7,* 2022.

[2] J. Greener. *Roll-to-Roll Manufacturing: Process Elements and Recent Advances*, 1-17 (2018).

[3] A. Sneck, et al. *Flexible and Printed Electronics,* 3, 014001 (2018).

[4] R. R. Søndergaard, et al. *Journal of Polymer Science Part B: Polymer Physics,* 51, 16-34 (2013).

A Stretchable Electrophoretic Display Device for Textile Display Application

Simu Zhu, Feng Xiong, Yifan Gu, Ting Wang, Hao Lu, Zhiguang Qiu, Zong Qin, Bo-ru Yang*

State Key Laboratory of Optoelectronic Materials and Technologies, Guangdong Province Key Laboratory of Display Material and Technology, School of Electronics and Information Technology, Sun Yat-sen University, Guangzhou, 510275, China. * Email: *paulyang68@me.com*

Nowadays, the Internet of Things (IOT) is evolving rapidly.[1] Wearable display devices have become a popular choice for obtaining information and monitoring human health in various applications. However, devices that have been commercialized still can't balance flexibility, long battery endurance, outdoor visibility, low driving voltage (<36 V, human-safe voltage[2]) at the same time. There have been a lot of attempts on self-emissive display devices desiring to cover all the advantages above. But neither organic light emitting diode (OLED) displays nor alternating current electroluminescent (ACEL) displays has made it now. Under this precondition, we propose to combine both advantages of electrophoretic display (EPD) and stretchable display, the dream may come true.

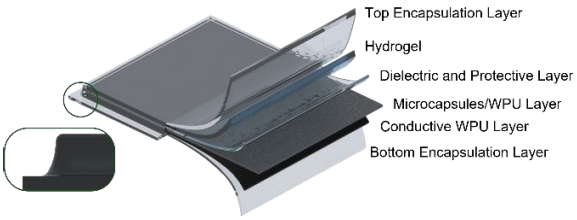

Fig. 1. Structure of the stretchable electrophoretic paper display device.

Based on the results of previous studies, our device chose inherently stretchable materials as much as possible to guarantee the flexibility of the overall device.[3] Waterborne polyurethane (WPU) and doped WPU materials with conductive properties were selected to form most of the function layers. And ionic conductive hydrogel was used as the top electrode, its colorless and transparent properties avoided to affect the display effect. The structure of the entire device is shown in Fig. 1.

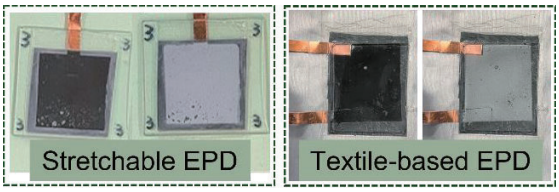

Fig. 2. The real images of two kinds of EPDs driving under the same voltage (24 V).

In order to make the device more fit to the human body while maintaining comfort, we chose textile as the substrate material of the device. Compared with traditional substrate materials such as ultra-thin glass, PI, PET, textiles possess excellent flexibility, water and air permeability, making them potentially to be the substrate material for the flexible displays.[4] By using the hot-pressing progress, we managed to combine the stretchable EPD and textile materials into textile-based EPD. The display effect and the flexibility of the device was preserved after hot-pressing. And the real images of the EPDs are shown in Fig. 2.

In addition, a dielectric protection layer was added between the top electrode and the display layer.[5] This protection could prevent the ions in the hydrogel for penetrating into the display layer and cause the ink in the microcapsule to sink. This improvement has resulted in a significant increase in the lifetime of our devices, namely 5 mins to 14 days and longer. The contrast ratio of the device during the 14-day durability test is shown in Fig. 3.

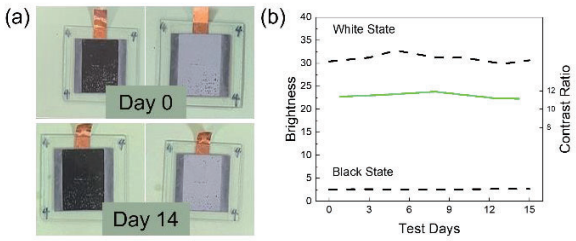

Fig. 3. 14-day durability test of the EPD device. (a)Real images and (b) Contrast ratio of the device.

References

[1] Zhang Z. Light-emitting materials for wearable electronics. Nature Reviews Materials. 2022;7(11):839-40.

[2] Bridges JE, Ford GL, Sherman IA, Vainberg M. PREFACE. In: Bridges JE, Ford GL, Sherman IA, Vainberg M, editors. Electrical Shock Safety Criteria: Pergamon; 1985. p. viii.

[3] Li X-C, Yao L, Song W, Liu F, Wang Q, Chen J, et al. Intrinsically Stretchable Electroluminescent Elastomers with Self-Confinement Effect for Highly Efficient Non-Blended Stretchable OLEDs. Angewandte Chemie International Edition. 2023;62(2):e202213749.

[4] Shi X, Zuo Y, Zhai P, Shen J, Yang Y, Gao Z, et al. Large-area display textiles integrated with functional systems. Nature. 2021;591(7849):240-5.

[5] Qiu Z, Zhu S, Lu H, Gu Y, Wu Z, Zhang G, et al. An electrophoretic e-paper device with stretchable, washable, and rewritable functions. Journal of the Society for Information Display. 2022;30(5):452-61.

Sealing Considerations for Electrophoretic Displays of Ink-on-Array ™

Debo Zeng, Yue Zhang, Jie Liu, Zong Qin, Bo-Ru Yang*

Dept. of Electronics and Information Technology, Sun Yat-Sen University, Guangzhou, China.
***Email: paulyang68@me.com**

Electrophoretic e-paper displays (EPDs) have demonstrated market potential in replacing actual papers due to their advantages such as comfortable reading experience and low-power consumption [1]. In order to reduce particles aggregation in the electronic ink, two mature kinds of partitioning device structures, micro-capsule and micro-cup based types, are developed for commercial. Their EPD products are made by laminating a well-packaged e-paper film (aka front panel) onto a TFT array backplane. By controlling the addressing and driving scheme of the TFT backplane, the EPD can show different reflectivity for black, white, and gray states. Furthermore, if adopting multiple color particles and complex driving waveforms, the EPD can perform full-color images [2]. However, compared with this mature type of out-cell EPD, in-cell EPD, here we term it Ink-on-Array™ (IoA) technology, seems to be a better approach for realizing higher performance because of its less interfaces. Besides, this in-cell EPD can be totally compatible with LCD's conventional fabrication process, which is possible to shorten the supply chain lead time and further cost down for EPD products to be even more prevailing.

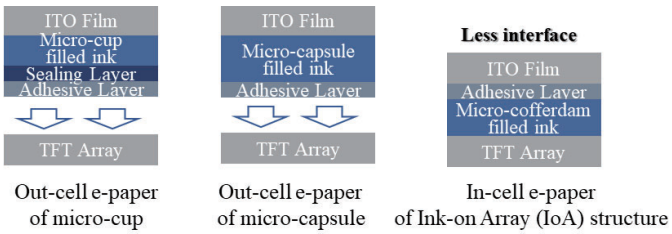

Fig. 1. EPD structure comparison of micro-cup, micro-capsule, and Ink-on-Array (IoA)

A comparison of conventional EPD structures of micro-cup, micro-capsule, and IoA structure is shown in Fig. 1. The implementation of this IoA device structure involves constructing a micro-cofferdam on a substrate, getting electronic ink filled and then sealed. But same as the micro-cup based EPD structure, the process of enclosing the electronic ink is difficult [3]. Underlying reason is analyzed as follow: the solvent can completely spread on the surface of the micro-cofferdam material, resulting in residual electronic ink on the top of the wall after filling, which seriously weakens the interfacial strength of the adhesive. Based on this, we propose some methods to avoid residual electronic ink on the top of the wall to ensure a clean top is used for sealing or adhesive. Since the solvent of our electronic ink is isopar-g, an alkane solvent, an oleophobic surface treatment of the top of the wall may avoid the residual electronic ink. However, oleophobic surface usually means low surface energy, which is unfavored for adhesive or sealing. In view of this, we selected a coating material with a contact angle about 48 degree of white electronic ink. And after test, we found that the white ink slides off on an oleophobic surface inclined at 20 degree without any residual electronic ink. After coating this material on the top of the wall and then ink filling, we found that there was almost no residual electronic ink on the top of the wall, shown in Fig. 2, which is consistent with our expected results. Next, we will perform some microstructure treatment to the oleophobic surface to further improve the adhesive or sealing performance. Similarly, to obtain a clean top of the wall, ink filled by ink jet printing may be another method, which can totally avoid residual electronic ink on the top of the wall. But some issues also need to be considered, such as nozzle blockage caused by volatile solvent and uniform ink filling of each micro-cell.

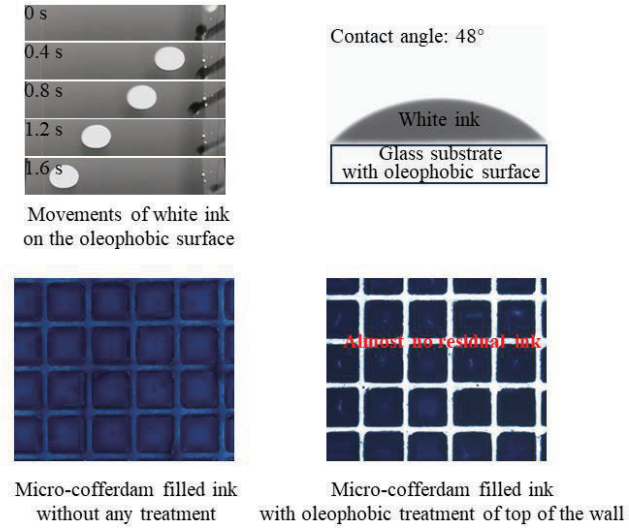

Fig. 2. Optical images of testing after oleophobic treatment

At last, we hope this IoA device structure will further prevail the market potential for EPDs after a good sealing.

References

[1] B.R. Yang, E-Paper Displays, New Jersey, Hoboken, p.2 (2022).

[2] S.J. Telfer and M.D. McCreary, *SID Symp. Dig. Tech. Pap*, 47, 574-577(2016).

[3] H.M. Zhang, Composition and Process for the Sealing of Micro-cup in Roll-to-roll Display Manufacturing, US Patent no. 7, 005, 468 (2006).

Increasing Particle Response Speed with Mixed Surfactants in Electrophoretic Display

Jinglan Yang, Feng Xiong, Zhuohang Li, Guangyou Liu, Debo Zeng, Yue Zhang, Zong Qin, Bo-Ru Yang*

Dept. of Electronics and Information Technology, Sun Yat-Sen University, Guangzhou, China

***Email: paulyang68@me.com**

With the benefits of low power consumption, high ambient contrast ratio and flexibility, electrophoretic displays (EPD) are well suited to the demands of display screens in the Internet of Things era. Therefore, EPD has great commercial potential, and it employed in a variety of areas including electronic books, supermarket shelf labels, and bus stop signs at present. Despite the many advantages of electrophoretic display, the response speed of EPD is not high enough. A commonly used method in commercial to improve the response speed is to mix two charge control agents (CCA) [1,2]. However, there are few studies focusing on the mechanism of improving the response speed of EPD by mixed CCA [3,4]. Herein, we attempt to find out the mechanism. At the same time, it is found that it is inconsistent with the widely accepted theory about zeta potential to explain the response time of electrophoretic particles, and we also put forward opinions on this discovery.

According to an experiment of $CuCrO_4$ black particles in two ionic surfactants, sodium dioctylsulfosuccinate (AOT) and Poly dimethyl diallyl ammonium chloride (PDDA) environment, it can be seen from Fig. 1b that under the same CCA mass fraction, the response time of mixed CCA is 4.3 times and 3.3 times faster than that of AOT only and PDDA only, respectively. The device shown in Fig. 1a is used for this experiment. Particles in a mixed CCA environment do not have a higher zeta potential than those in a single CCA environment, as shown in Fig. 1c. But contrary to our experimental findings, it is widely accepted that particles with higher zeta potential respond faster. In this regard, we have the following explanations.

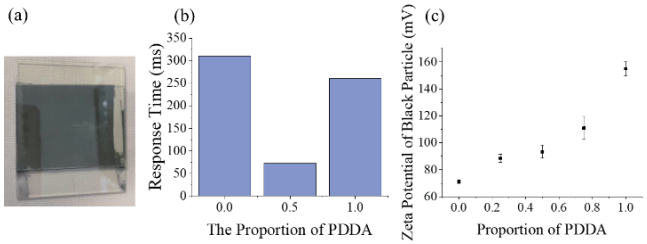

Fig. 1. (a) Electrophoretic display device. (b) Response time and (c) zeta potential of black particle with different proportion of PDDA

Firstly, zeta potential of particles is affected by electric field [5], and the electric field intensity of the particles in the driven state in the EPD device is an order of magnitude larger than that of the instrument measuring zeta potential. As a result, it is possible that the zeta potential of particles measured by the instrument is not the actual one in the environment of EPD device. Secondly, AOT is an anionic surfactant and PDDA is a cationic surfactant, both of which may be neutralized in the solvent after mixing, reducing the electric field shielding caused by charged inverse micelles (CIMs). Moreover, when the electrophoretic display device is driven by a phase in which the particles are activated by high frequency voltage of opposite polarity, we believe that various CCA have varying adhesion strength to particle double electric layer. As shown in Fig. 2, when the two CCAs are mixed, the negatively charged AOT CIMs is more likely to escape from the double electric layer due to inertia, which increases the particle charge and quickens the reaction time.

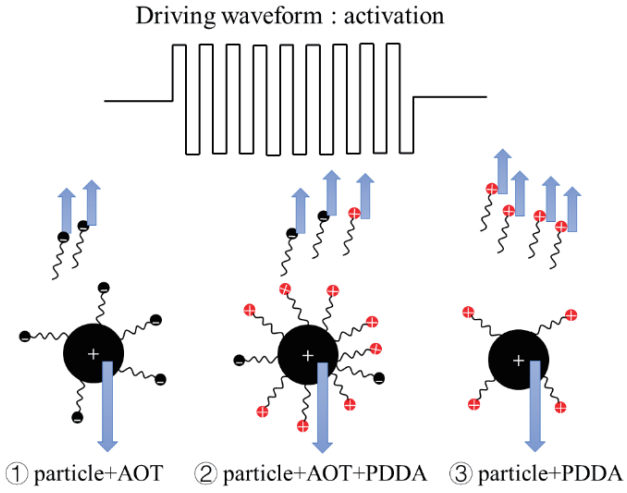

Fig. 2. Motion of CIMs of electric double layer and particles under activation driving waveform

References

[1] Jr Paolini, J Richard, D D Miller, et al., U.S. Patent No. 7,079,305 (2006).

[2] R M Webber, T H Whitesides, G M Danner, et al., U.S. Patent No. 7,339,715 (2008).

[3] B S Ponto, J C Berg, *Colloids Surf., A*, 586, 124275 (2020).

[4] B R Yang, *E-paper Displays*, John Wiley & Sons (2022).

[5] C E Espinosa, Q Guo, V Singh, et al., *Langmuir*, 26(22), 16941-16948 (2010).

Surface Modification of Black Electrophoretic Particles via Thiol−Ene Click Reactions

*Feng Xiong, Yue Zhang, Guangyou Liu, Xinzao Wu , Zong Qin, Bo-Ru Yang**

State Key Laboratory of Optoelectronic Materials and Technologies, Guangdong Province Key Laboratory of Display Material and Technology, School of Electronics and Information Technology, Sun Yat-Sen University, Guangzhou 510275, People's Republic of China.
***Email:** paulyang68@me.com

Abstract

With the rapid rise of the Internet of Things (IoT), electrophoretic display (EPD) has become widely applied in various electronic devices, such as electronic books, electronic shelf labels, bus signs, smart blackboards, and smart windows. Compared with other display technologies like organic light-emitting diode and liquid crystal display, EPD offers unique advantages including bistability, low power consumption, eye protection, and high ambient contrast ratio.[1] The principle behind EPD involves the directional movement of particles with positive or negative charge under electric field. However, how to simultaneously optimizing black particles with good dispersity and the charge is a challenge.

In order to address this challenge, two methods for particle modification can be employed: chemical modification and physical modification.[2] Chemical modification methods involve free polymerization reactions occurring on the particle surface, while physical modification methods rely on weak interactions such as Coulomb action or acid-base action. Physical modification is simple but easily fall off the charge control agent and lack electric charge during driving. On the other hand, chemical modification provides better results, but it is difficult to accurately control the thickness and charge of the grafted polymer layer. To overcome these limitations, we propose a particle modification method based on Thiol−Ene click reactions, which offers a simple and effective way to prepare particles for electrophoretic display. by utilizing the efficiency and high selectivity of click chemistry.[3]

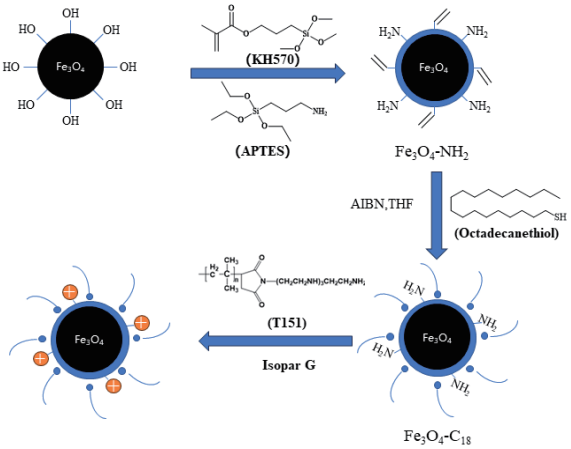

Figure 1 Preparation of Fe_3O_4 black particles.

The preparation process of black particles is shown in Figure 1. Firstly, black Fe_3O_4 particles are ball-milled with silane coupling agents (KH570 and APTES) in toluene. This ball-milling process facilitates the grafting of amino and vinyl functional groups onto the surface of Fe_3O_4 particles (Fe_3O_4-NH_2). Subsequently, in a N_2 environment, a mixture of Fe_3O_4-NH_2, octatethanethiol and initiator (AIBN) s added to the solvent (THF). Through the click chemical reaction between vinyl and sulfhydryl groups, an alkyl chain can be grafted onto the particle surface (Fe_3O_4-C_{18}). Lastly, the charged iron black particles are obtained by ball milling Fe_3O_4-C_{18} particles with T151.

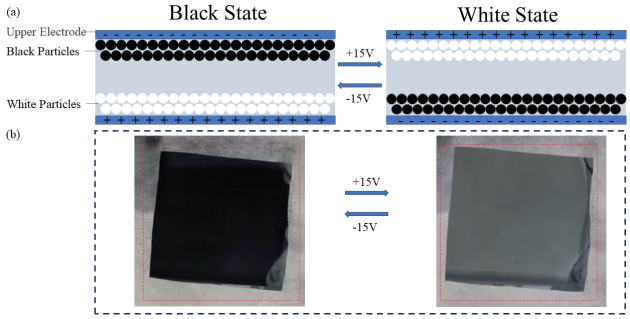

Figure 2 The illustration(a) and photographs(b) of EPD device

The EPD device was prepared to investigate the driving effect of Fe_3O_4 black particles. The cell consisted of two ITO electrodes adhered with OCA and was filled with an e-ink containing negatively charged white particles and positively charged Fe_3O_4 black particles. When the upper electrode was given -15V, the black and white particles were separated, with the black particles being driven to the upper electrode, resulting in a black state of the device. Conversely, when the upper electrode was given +15V, the white particles were driven to the upper electrode, causing the EPD to exhibit a white state. The contrast ratio of EPD device up to 11.4 with the concentration of white and black particles at 2:1.

References

[1] Yang B-R. “E-Paper Displays”. John Wiley & Sons Ltd, Chichester, ISBN: 978-1-119-74558-7, 2022.

[2] Ivanova, et al. Russian Journal of Inorganic Chemistry 65: 1985 - 2005(2020).

[3] Goldmann, et al. Macromolecules, 42(11): 3707–3714. (2009)

A Transparent Electrophoretic Display Prototype Based on In-Plane Lateral Driving

*Yunhe Liu, Qitian Fan, Guangyou Liu, Zong Qin, Bo-ru Yang**

State Key Laboratory of Optoelectronic Materials and Technologies, Guangdong Province Key Laboratory of Display Material and Technology, School of Electronics and Information Technology, Sun Yat-Sen University, Guangzhou 510275, People's Republic of China.

***Email:** paulyang68@me.com

Electrophoretic displays (EPDs), known for their low power consumption, excellent readability in strong light, and wide viewing angle, have gained increasing popularity in recent years.[1,2] Transparent electrophoretic displays (TEPDs) are an emerging field of technology, which can display both traditional reflective and transparent images, making it potential for applications in smart watches, windows, glasses, and so on.[3,4,5]

This paper presents a prototype of TEPD based on in-plane lateral driving. The prototype incorporates optimized electrode structures and driving waveform. Compared to other related studies, our device exhibits simpler structure, faster response time, and higher transmittance. Fig.1 illustrates the working principle of the TEPD. By controlling the applied driving voltage, particles would move horizontally and accumulate in collection region. Due to the particles' excellent light reflective performance, the pixels can freely switch between opaque and transparent states.

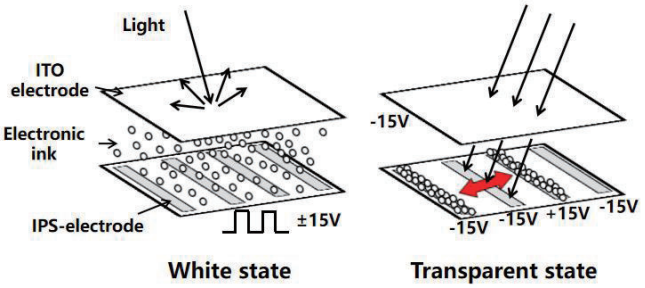

Fig. 1. Schematic representation of the working principle of TEPD

Then, we made several prototypes of TEPD, and the production process is shown in Fig. 2. The TEPD cell comprises ITO electrodes, optically clear adhesive (OCA), encapsulation layer, and in-plane switching (IPS) electrodes. Electronic-ink was introduced into the cell using capillary action through a dropper.

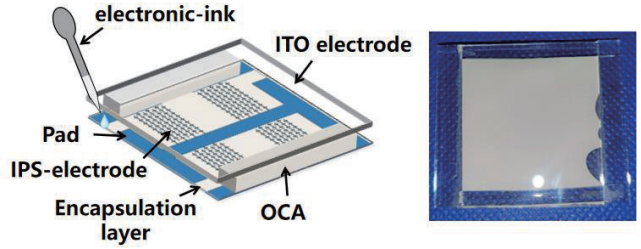

Fig. 2. The production process of TEPD cell in experiments

In the final stage, we successfully fabricated a TEPD prototype by assembling the cell with a thin-film transistor (TFT) panel. Fig. 3(a) and Fig. 3(b) respectively illustrate the operational states of pixels with two different electrode structures. The device exhibits three primary operational states: W (White state), I (Intermediate state), and T (Transparent state). The response time for transitioning from the W state to the T state is approximately 100~200ms and the highest transmittance of the device can reach about 50% in the T state.

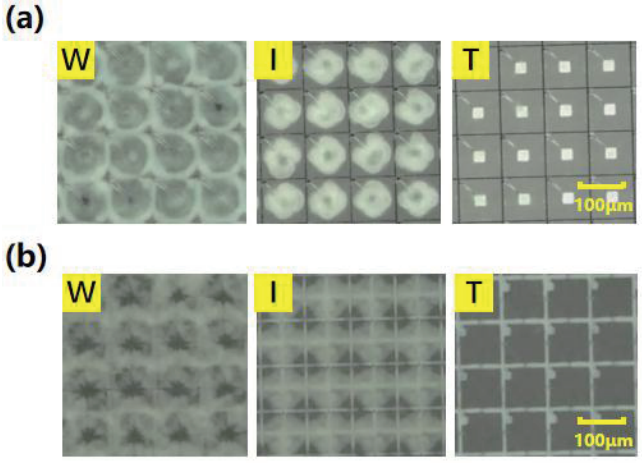

Fig. 3. Operational states of pixels in W (White state), I (Intermediate state), and T (Transparent state) with different electrode structure: (a) square-shaped, (b) cross-shaped

References

[1] B. Comiskey, et al. *Nature*., 394(6690), 253 (1998).
[2] B. R. Yang. *John Wiley & Sons Ltd, Chichester*, ISBN: 978-1-119-74558-7 (2022).
[3] Swanson S A, et al. *SID'00 Technical Digest*, vol. 31: 29 (2000).
[4] Mukherjee S, et al. *Applied Optics.*, 54(17): 5603-5609 (2015).
[5] M. D. McCreary, et al. *SID'19 Technical Digest,* vol. 50, p. 497 (2019).

Cation modified composite film to optimize the bi-stability of transparent electrophoretic display

Zhuohang Li, Guangyou Liu, Yunhe Liu, Jie Liu Zong Qin and Bo-Ru Yang*
Dept. of Electronics and Information Technology, Sun Yat-Sen University, Guangzhou, China
***Email: paulyang68@me.com**

The development of IoT applications and wearable consumer electronics has raised the requirement of longtime sustainability. However, emissive display like Organic Light-Emitting Diode (OLED) and transmissive display Liquid crystal display (LCD) couldn't reach the demand because of their high-power consumption. Thus, reflective display EPD as a technology only consume power during the image changing has enormous advantage over these emissive displays in such condition.[1] The low-power consumption feature of EPD comes from the bi-stability of the colloidal particles. There are several forces affect charged particles when they are driven by external electrical field and these forces should be equilibrium for particles to be static, but when external electrical field is removed the electrical force will be vanished so that particles will start to diffuse. Therefore, by adding thickener such as polyethylene can increase the viscosity of solvent and these forces can be re-equilibrium. However, adding thickener is tested to be inefficient for lateral-driven EPD, because for vertical electric field, particles will vertically drive to electrode with different polarity and particles will diffuse vertically when the field is removed, but for lateral electric field things are more complicated, in contrast, charged particles driven by lateral electric field will diffuse laterally which is much easier to be observed and has a direct effect on the transmittance of device, making lateral bi-stability harder to be achieved.

The operational principle was realized by laterally driven EPD. As shown in Fig. 1, an EPD with in-plane switching electrodes (IPS-EPD) can provide electric field to drive particles laterally. When the electric field is applied, negatively charged white particles will migrate to positive electrode making EPD to be transparent. IPS-EPD has numerous application potential for it can switch from transparent display to traditional reflective display [2-3], however, to apply IPS-EPD, bi-stability in lateral direction has to be achieved. Lateral driving experiment indicates that the bi-stability of colloidal particles is not only achieved by the equilibrium of force but also affected by some mechanism of surfactant. In our previous study, we proposed a mechanism how adsorption/desorption behavior of charged inverse micelles (CIMs) formed by surfactant molecules in e-ink can affect the bi-stability of EPD, in which the unabsorbed CIMs will cause a diffusion current to reversely drive colloidal particles. Herein, we fabricated an anionic modified composite film on electrode by using cation modifier Poly dimethyl diallyl ammonium chloride (PDDA) to modify polyvinyl alcohol (PVA) film. Such composite film can provide a tiny electric filed to retard the diffusion of unabsorbed CIMs, thus improve the bi-stability of EPD.

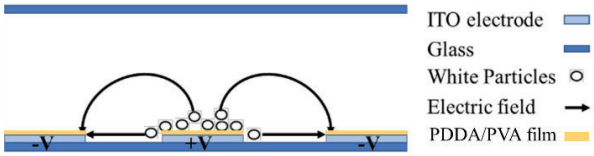

Fig. 1. Schematic diagram of IPS-EPD with PDDA/PVA composite film

The prototype of the laterally driven EPD device can perform perfectly both transparent state and opaque state; meanwhile, sustaining the bi-stability while power ing off. As shown in Figure 2, IPS-EPD with composite film could maintain transparent state for 10 minutes after power is cut-off. We further use optical test platform to test the transmittance of IPS-EPD with/without cation composite film after power is cut-off and the results are shown in Table 1. It turns out that cation modified PVA film could significantly improve the bi-stability of EPD, and it gives a new way to consider the bi-stability of EPD apart from adding viscosity of e-ink.

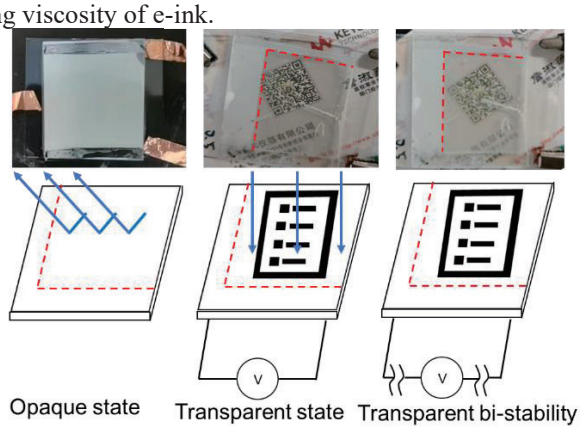

Fig. 2. IPS-EPD with cation composite film can maintain transparent display without power supply for a longtime.

Table 1. Transmittance of IPS-EPD with/without anionic composite film after power is cut-off

IPS-EPD \ Power-off	0 s	30s	50s	240s
Bare ITO	72%	38%	0%	0%
0.1%PDDA/1%PVA film	72%	59%	58%	58%
0.2%PDDA/1%PVA film	72%	55%	53%	52%

References

[1] Yang B-R. "E-Paper Displays". John Wiley & Sons Ltd, Chichester, ISBN: 978-1-119-74558-7, (2022).

[2] Michael D, Richard J, et al. SID Digest, 36(1):497-500 (2019).

[3] G. Liu, et al., Chemical Engineering Journal (2023).

High efficiency pure blue perovskite light-emitting diode based on interface engineering

Zhiqing Zhang, Huibo Yan, Fanghao Ye, and Guijun Li

Key Laboratory of Optoelectronic Devices and Systems of Ministry of Education and Guangdong Province, Shenzhen University, Shenzhen, China.

Metal halide perovskite light-emitting diodes (PeLEDs) have gained significant attention in recent years due to their exceptional photoelectric properties. The performance of PeLEDs heavily relies on the interface between different layers. In this study, we demonstrate that interface engineering using quaternary ammonium ionic liquid can effectively enhance the efficiency of blue PeLEDs. Our findings indicate that interface engineering helps in achieving a balanced injection of holes and electrons. Moreover, the presence of quaternary ammonium cation facilitates the growth and nucleation of the blue perovskite emitter, leading to improved film morphology and reduced occurrence of defects. Additionally, the use of the ionic liquid interfacial layer helps to suppress ion migration in the perovskite under forward bias operation. In conclusion, the incorporation of the quaternary ammonium ionic liquid interfacial layer significantly enhances the luminous efficiency of PeLEDs.

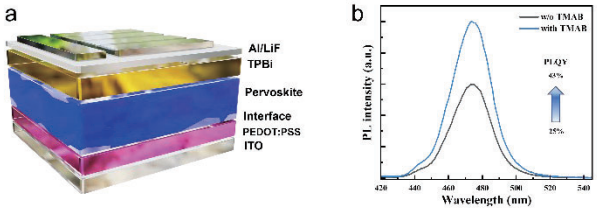

Fig. 1. (a) Structure diagram of PeLED (b) PL spectra of the perovskite film with and without TMAB.

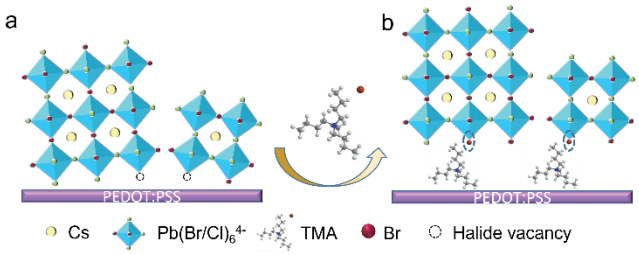

Fig.2. Schematic illustration of perovskite precursor deposited on (a) PEDOT:PSS and (b) TMAB.

References

[1] Ye, F., et al., Interface Engineering with Quaternary Ammonium-Based Ionic Liquids toward Efficient Blue Perovskite Light-Emitting Diodes. ACS Applied Materials & Interfaces, 2022. 14(44): p. 50393-50400.

Innovative Interfacial Engineering of Hole Transport Material for High-Performance Perovskite Photovoltaics

Fengning Yang*, Yen-Hung Lin**, Henry Snaith*

***Dept. of Physics, University of Oxford, Oxfordshire, UK**

**** Department of Electronic and Computer Engineering, The Hong Kong University of Science and Technology, Clear Water Bay, Kowloon, Hong Kong SAR, China**

fengning.yang@wolfson.ox.ac.uk

Recently, the perovskite solar cell and light-emitting diode have raised more attention due to their ease of fabrication, cost-effectiveness, and lower processing temperature for the fabrication of large-scale and flexible devices. However, compared with traditional semiconductor material, it still needs a great effort to push the performance close to theoretical limits and uncover the mechanism. The efficiency and stability of both types of devices are mainly determined by the non-recombination process that happened on the interface. We build a conjugated organic molecule layer between the halide metal perovskite layer and the commercial polymeric hole transporting layer. During the interfacial engineering process, we could adjust the orientation of molecules to enhance the pi-pi stacking which supplementally improves the charge mobility and align the energy level so that getting positive influence on hole extraction, transportation and perovskite crystallization.

The C8 molecule is one kind of conjugated and highly oriented organic molecule, it shows a specific edge-on angle when it is distributed into the PTAA polymer (**Fig.1**). The angle between substrate normal and molecule face (111) is around 79.2 degrees. In this case, the perovskite active layer will directly deposit on the alkyl chain, which may affect the crystallization process of perovskite.

Therefore, we test the photoluminescence behavior of the half stack of the devices (**Fig.2**). Here we induce a comparing material, polystyrene, which is a commercial isolator. As the bandgap of C8 molecules is larger than the commonly used transport layer material, we try to clear the effect of the dielectric layer and passivation layer. Fig. 2a shows that during the early delay period of TRPL, the blend C8/PTAA thin layer still has a great carrier extraction, compared to the Glass and Polystyrene film. While Fig. 2b shows that the modified layer could passivate the quenching of carriers. So that it gives clear evidence to show the C8 could passivate the perovskite layer, which shows great potential to apply to the PV cell and LED devices.

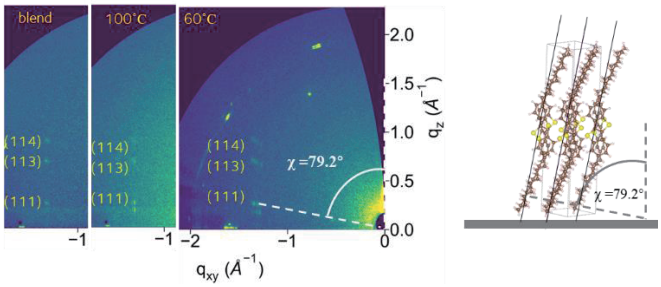

Fig. 1. The Grazing-incidence wide-angle scattering data (left) and orientation illustration figure(right) of the C8 organic molecules in PTAA thin film.

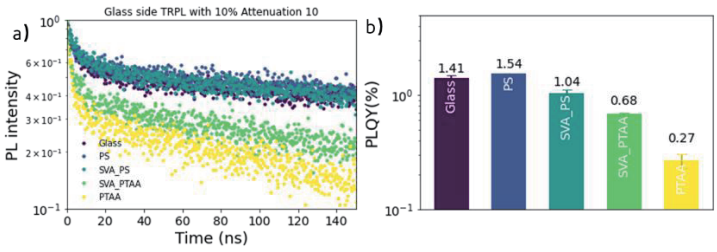

Fig. 2. a) Time-resolved photoluminescence (TRPL) spectroscopy results. b) Photoluminescence Quantum Yield (PLQY) results.

Pixelated Polarized Luminescent Color Filters Based on Down-converting Nanorods

*Jianxin SONG, Yiyang Gao, Maksym F. Prodanov, Chengbin Kang, Valerii V. Vashchenko, and Abhishek K. Srivastava**

*State Key Laboratory of Advanced Displays and Optoelectronics Technologies, Department of Electronics and Computer Engineering, The Hong Kong University of Science and Technology, Clear Water Bay, Hong Kong, China.

*Centre for Display Research, The Hong Kong University of Science and Technology, Clear Water Bay, Hong Kong, China.

Email: jsongbb@connect.ust.hk

Recently, a top emitting color filter technology that utilizes nanoparticles as photoluminescent fluorescent materials has gained widespread attention, with spherical quantum dot materials emerging as one of the most crucial advancements. Top emitter display devices enhanced by nanomaterials offer broader viewing angles, increased color gamut, and greater absorption ratios, resulting in improved display efficiency. However, one issue to consider for the display applications of fluorescent materials is the fluorescent reflection caused by the excitation effect of ambient light. As a special quantum dot material, luminescent quantum rods have gradually become an excellent alternative to quantum dot materials. Quantum rods not only have the excellent properties of quantum dots, but also have unique linear luminescence characteristics and greater Stokes shift, wider absorption cross-section, etc.[1][2][3][4][5]

In this work, we employ down-conversion nanorods as the photoluminescent material, mixing them with liquid crystal monomers to fabricate homogeneous hybrid color filter films. We then use photo-alignment technology to align the nanorods, achieving polarized luminescence. The photo-aligned color filter can convert unpolarized light into linearly polarized light, effectively mitigating the issue of fluorescent reflection and enhancing the display's luminous efficiency.

We propose photolithography and inkjet printing as two viable techniques for pixelating the color conversion layer and achieving full-color conversion. To enhance measurement accuracy, we introduce a test scheme for evaluating a single luminescent pixel. After testing, the single pixel of the polarized light-emitting color filter exhibits a polarization ratio as high as 4.27:1. Furthermore, by leveraging T-ligand quantum rods, we have achieved superior dispersion of quantum rods at higher concentrations and uniform film formation, surpassing previous reports.

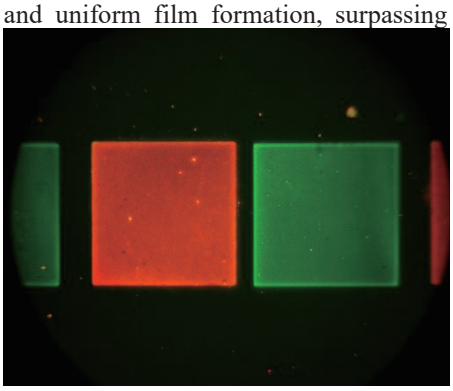

(a)

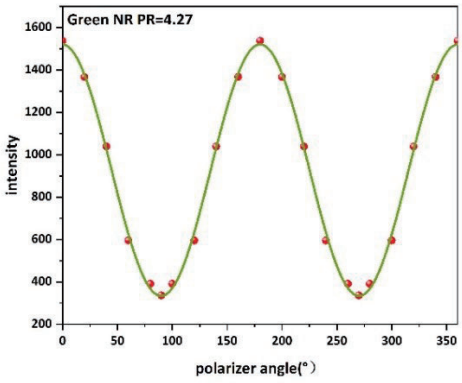

(b)

Figure 1. (a) Pixelated Polarized Luminescent Color Filters; (b) Polarization ratio result: the emission intensity as a function of the polarizer axis rotation angle

References:

[1] M. F. Prodanov et al., 'Unidirectionally aligned bright quantum rods films, using T-shape ligands, for LCD application', Nano Res., vol. 15, no. 6, pp. 5392–5401, Jun. 2022, doi: 10.1007/s12274-021-4019-2.

[2] Y. Gao et al., 'Stable bright perovskite nanoparticle thin porous films for color enhancement in modern liquid crystal displays', Nanoscale, vol. 13, no. 13, pp. 6400–6409, 2021, doi: 10.1039/D0NR07313J.

[3] 'P-86: Ink-Jet Printed Stable Full-Color Perovskite and Quantum Rod Color Filter - GAO - 2022 - SID Symposium Digest of Technical Papers - Wiley Online Library'. https://sid.onlinelibrary.wiley.com/doi/abs/10.1002/sdtp.15761 (accessed May 17, 2023).

[4] 'Inkjet-Printed, Flexible Full-Color Photoluminescence-Type Color Filters for Displays - Gao - 2022 - Advanced Engineering Materials - Wiley Online Library'. https://onlinelibrary.wiley.com/doi/full/10.1002/adem.202101553 (accessed May 17, 2023).

[5] 'Inkjet printed patterned bank structure with encapsulated perovskite colour filters for modern display - Nanoscale (RSC Publishing) DOI:10.1039/D2NR00849A'.

Transparent Quantum Dot Light-Emitting Diodes with a Current Focusing Structure

Guohong Xiang[1,2,3], Jingrui Ma[1,3], Xiangwei Qu[1,3], Kai Wang[1,3], Hoi Sing Kwok[2] and Xiao Wei Sun[1,3 *]

1 Institute of Nanoscience and Applications, and Department of Electrical and Electronic Engineering, Southern University of Science and Technology, Shenzhen 518055, China

2 State Key Laboratory of Advanced Displays and Optoelectronics Technologies, the Hong Kong University of Science and Technology, Hong Kong, China

3 Key Laboratory of Energy Conversion and Storage Technologies (Southern University of Science and Technology), Ministry of Education, Guangdong University Key Laboratory for Advanced Quantum Dot Displays and Lighting, Guangdong-Hong Kong-Macao Joint Laboratory for Photonic-Thermal-Electrical Energy Materials and Devices, and Shenzhen Key Laboratory for Advanced Quantum Dot Displays and Lighting, Southern University of Science and Technology, Shenzhen 518055, China

E-mail: sunxw@sustech.edu.cn

We report transparent quantum dot light-emitting diodes with a current focusing structure. By depositing a SiO_2 thin film to form the current focusing structure, the DC current density and luminance significantly increased to over 8700 mA/cm^2 and 360000 cd/m^2, respectively. The emission spectra and current densities as functions of SiO_2 thickness and aperture width have been investigated and discussed. This current focusing design is proved effective and can be further applied to other planar light-emitting diode devices.

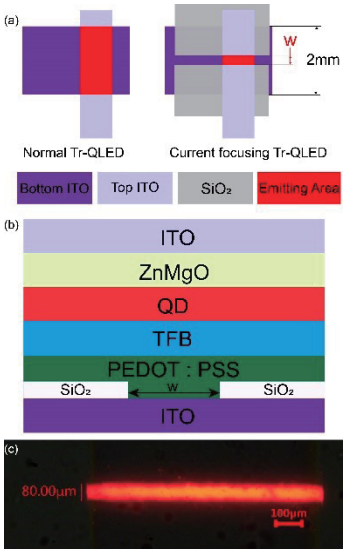

Fig. 1. (a) Top view schematic diagram of the normal Tr-QLED and the current focusing Tr-QLED. SiO_2 thin film is used to block the current and form the aperture. (b) The sectional view of the device, where the w denotes the width of the SiO_2 aperture. (c) Microscope image of the 80 μm width current focusing Tr-QLED.

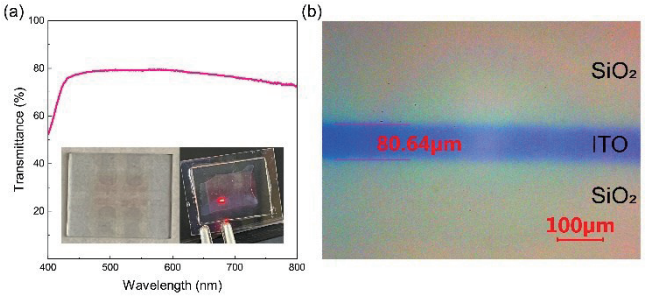

Fig. 2. (a) The transmittance of the encapsulated Tr-QLED. Insets: the fabricated Tr-QLED before encapsulation and light-emitting image with encapsulation. (b) The optical microscope image of the 80 μm width SiO_2 thin film deposited on the bottom ITO electrode.

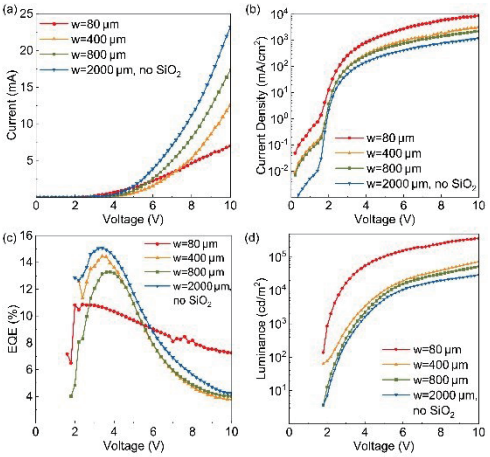

Fig. 3. Device performance of the current focusing Tr-QLED with different width of SiO_2 aperture. The thickness of SiO_2 is 10 nm. (a) I-V characteristics (b) Current density over voltage (c) EQE over voltage (d) Luminance.

Synthesis and Optical Properties of Fluorine Doped Double-cationic perovskite quantum dots / molecular sieve composites

*Xiaogang Chen[1,2], Junhu Cai[1,2], Enguo Chen[1,2] *,Yun Ye[1,2] , Sheng Xu[1,2], Tailiang Guo[1,2]*

1.College of Physics and Information Engineering, Fuzhou University, Fujian 350108, China
2.Fujian Science & Technology Innovation Laboratory for Optoelectronic Information of China, Fuzhou,350108, China

***Corresponding author : ceg@fzu.edu.cn**

Metal halide perovskite nanomaterials (ABX_3, A=MA, FA or Cs; B=Pb or Sn; X=Cl, Br or I), due to its adjustable luminous wavelength from ultraviolet to near-infrared region (400nm-750nm) and high luminous efficiency (PLQY can reach nearly 100 %) [1], light-emitting half-peak width and narrow (can be less than 15nm) [2], excellent color conversion performance and other characteristics make it widely used in the field of flat panel display. The typical structure of perovskite is a combination of A^{1+}, B^{2+} and X^{1-}. According to the tolerance factor (t), it can be determined whether the A-bit cation is suitable for the cavity in the BX_6 octahedral frame.

$$t = \frac{(R_A + R_X)}{\sqrt{2}(R_B + R_X)} \qquad (1)$$

Due to the relatively small A-bit cation, all inorganic $CsPbX_3$ perovskite nanocrystals have defects with a relatively small tolerance factor (t). And for the most common thermal injection method for perovskite synthesis, although the synthesized perovskite quantum dots have relatively high performance, the time consumed by the thermal injection method is relatively long, the high-temperature injection process is complex, and there are many uncontrollable factors and other problems are still inevitable [3].

Based on this, this paper replaces the relatively small Cs ions with larger MA cations proportionally by using the "three-step one pot method" based on ligand-assisted reprecipitation (LARP) method, which can increase the tolerance factor to nearly 1. By adding BF^{4-}, F ions are used to modify perovskite by using its water interpretation. Compared with bromide (Br), F has higher electronegativity, smaller radius, and stronger binding energy with Pb^{2+}. Therefore, when F anions occupy the surface Br space, the surface defects of perovskite can be reduced, making perovskite the performance of quantum dots has been greatly improved. In the synthesis process, molecular sieve materials are added to realize the crystallization growth of perovskite in the molecular sieve pore. Among them, the molecular sieve can not only protect perovskite well, but also limit its domain and control its particle size, so as to achieve simple and convenient preparation of perovskite with high stability, high fluorescence intensity and high color purity PQDs/SBA-15. Finally, the morphology and optical properties of the obtained material are analyzed. The results show that through the introduction of element F, the PLQY of perovskite quantum dots has been improved by up to 20%. As shown in Figure 1, through Mapping, it can be clearly seen that perovskite has filled the hole well.

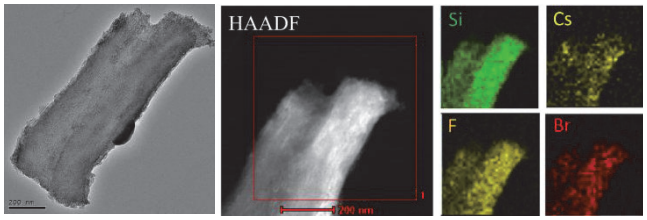

Fig 1. TEM and HAADF STEM of PQDs/SBA-15 NPs.

The obtained composite material has been placed in the air for more than two months, but there is no obvious fluorescence attenuation as shown in Figure 2. Finally, the experiment was combined with the blue LED to prepare a light-emitting device based on the quantum dot molecular sieve composite color conversion film. It provides a feasible path to achieve LED full-color display with high stability and superior luminous performance.

Fig 2. Pictures of PQDs solution and PQDs/SBA-15 NPs in natural light.

References

[1] LIU F, ZHANG Y, DING C, et al.ACS Nano. 2017; 11(10):10373-83.

[2] PROTESESCU L, YAKUNIN S, BODNARCHUK M I, et al. Nano Lett. 2015; 15(6):3692-6.

[3] LV W, LI L, XU M, et al.Adv Mater. 2019; 31(28): e1900682.

Correction Algorithm of AR-HUD Holographic Image Based on Distortion Model

Han-Syuan Chen *,Tzu-An Chou, Chih-Hao Chuang***, Chien-Yu Chen*,**
*** Graduate Institute of Color and Illumination Technology, National Taiwan University of Science and Technology, Taipei, Taiwan**
****Graduate Institute of Electro-Optical Engineering, National Taiwan University of Science and Technology, Taipei City 10607, Taiwan (R.O.C.)**
*****Department of Photonics, Feng Chia University, 100 Wenhwa Rd., Seatwen, Taichung 40724, Taiwan**

Head-Up Display (HUD) is a display technology that projects driving information onto the windshield, including navigation directions, vehicle speed, and fuel level, to assist drivers in safer driving [1]. The HUD's display enhances driving safety by providing essential driving assistance information without requiring drivers to look down. However, HUD technology also faces certain technical challenges, such as image distortion correction. When images are projected onto the windshield, they may be affected by the curvature and thickness of the glass, leading to image distortion. To address this distortion issue, various methods have been proposed, such as chessboard and warping maps [2], specialized sensors [3], and other devices or auxiliary software for automotive AR-HUD calibration.

Most of the above methods require additional hardware and software for implementation. In contrast, this study proposes a vehicle HUD system based on holographic technology. The system integrates an angled windshield and a projection device, combined with the MGSA (full name) algorithm, to construct the AR HUD system [4]. To validate the experimental results and optimization performance, we conducted tests in a self-built simulated cockpit. To tackle the image distortion problem, we extended the original algorithm by adopting a point-array-based approach for distortion correction. This algorithm first calculates the distortion model of the holographic image on the windshield based on its curvature. Subsequently, the distortion model is used to correct the holographic image, as depicted in Figur 1.

According to the research findings, the correction algorithm used in our study achieved excellent distortion correction results for the holographic images, as shown in Figure 2. We conducted a comparative analysis of the resulting images and employed several metrics, such as distortion coefficient, maximum distortion, average distortion, and root mean square error [5], as presented in Table 1. As shown in Table 1, the distortion amount is 4.81%. The maximum distortion and average distortion decreased by 44.64% and 42.86%, respectively. Finally, we found that the optimization value of root mean square error reached 0.19.

In conclusion, our research has successfully achieved distortion correction for holographic AR HUD images. By introducing the distortion model and MGSA technology, we effectively optimized the holographic images, transforming them from curved deformations into rectified forms. This study provides an effective solution to address the holographic image distortion caused by windshield curvature and thickness, offering greater technical support for the application of AR HUD technology. Such advancements are crucial for enhancing driving safety and driving experience.

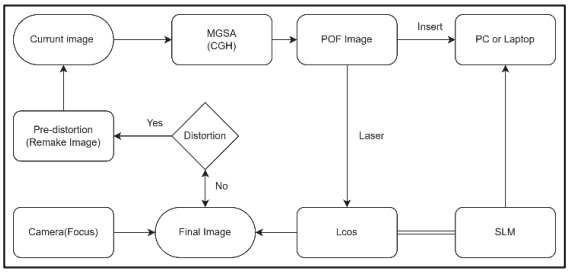

Fig. 1. The flowchart

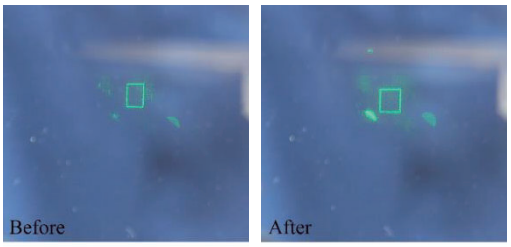

Fig. 2. 512x512 hologram aberrated vs. corrected

Table 1. Before and after distortion

Parameter	Before Distortion	After Correction
Shape	Elongated	Normal
Position	Shifted	Normal
Distortion Amount	4.81%	
Maximum Distortion	0.57	0.32
Average Distortion	0.35	0.2
RMSE	0.23	0.19

References

[1] T. Poitschke, M. Ablassmeier, G. Rigoll, S. Bardins, S. Kohlbecher, and E. Schneider. 2008. Contact-analog information representation in an automotive head-up display. In Proceedings of the 2008 symposium on Eye tracking research & applications (ETRA '08). Association for Computing Machinery, New York, NY, USA

[2] Xiang Gao, Marc Necker, and Wilhelm Stork "A low-complexity yet accurate calibration method for automotive augmented reality head-up displays", Proc. SPIE 11605, Thirteenth International Conference on Machine Vision, 116050B (4 January 2021)

[3] Deng, N., Zhou, Y., Ye, J. and Yang, X., 2018, March. A calibration method for on-vehicle AR-HUD system using mixed reality glasses. In 2018 IEEE Conference on Virtual Reality and 3D User Interfaces (VR) (pp. 541-542). IEEE.

[4] Chou, T., Pan, T., Chuang, C., Huang, B. and Chen, C. (2022), P-145: *Student Poster:* AR HUD System Realized By Holographic Display Technology. SID Symposium Digest of Technical Papers, 53: 1185-1187.

[5] Perceptual Image Distortion, First IEEE International Conference on Image Processing, vol 2, pp 982-986, November 1994

Research on Light Field 3D Display Based on Field Sequential Color Image Source

Qimeng Wang, Yunfan Cheng, Zeyu Wang*, Guowei Zou*, Boru Yang*, Zong Qin**

***School of Electronic and Information Technology,**

Sun Yat-Sen University, Guangzhou, China

The three-dimensional display technology is dedicated to reproducing the real three-dimensional space, providing viewers with an immersive visual experience. Researchers have proposed many three-dimensional display technologies, including Depth-fused 3D Display, Varifocal 3D Display, Maxwellian View 3D Display, Volumetric 3D Display, Holographic 3D Display, and Light Field Display. Among the 3D display technologies, the Integral Imaging Light Field Display (InIm LFD) technology has attracted wide attention because of its superior performance, such as monocular focus cue, compact volume, and feasible implementation. However, the InIm LFD still has some disadvantages, such as insufficient depth of field, small field of view, and low resolution. Among the drawbacks, the low resolution is the main hindrance, so improving the resolution of the InIm LFD is of great significance.

In order to improve the resolution of the Inlm LFDs, this paper investigates the image sources commonly used in VR/AR equipment. The traditional LCD needs a backlight and realizes multicolor display based on spatial color mixing, which leads to its shortcomings, e.g., low resolution and large thickness, which makes it unsuitable for VR/AR. However, the emergence of Mini LEDs eliminates the large thickness. At the same time, if adopting temporal color mixing and removing the color filter array of an LCD, the display quickly presents three images of red, green and blue in one frame. With the visual persistence of human eyes, a user can see color images, and the resolution can also be increased by three times. This technology is called Field Sequential Color (FSC) LCD.

This paper combines the FSC LCD and the InIm LFD to achieve a threefold resolution. We realize the Inlm LFDs based on an FSC image source by calculating elemental images, calculating sub-frame images, and performing an optical experiment, which verifies that the FSC LCD can benefit the InIm LFD and realizes the corresponding true-3D display. Moreover, this paper also simulates the Color Breakup (CBU) phenomenon caused by human eye movement and further realizes the 240Hz-Stencil FSC driving algorithm, which can significantly inhibit CBU. The simulation and experimental results (Fig.1 and Fig.2) show that the 240Hz-Stencil algorithm has an obvious inhibitory effect on CBU compared with the traditional RGB algorithm.

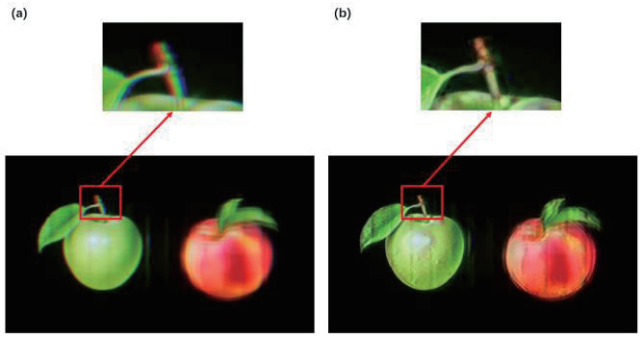

Fig. 1. 3D images with CBU on the reconstructed depth plane of the InIm-LFD, focused on the Apple: (a) RGB algorithm; (b) 240Hz-Stencil algorithm

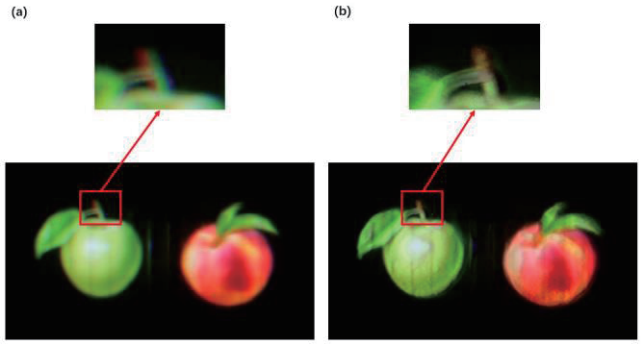

Fig. 2. 3D images with CBU on the reconstructed depth plane of the InIm-LFD, focused on the Peach: (a) RGB algorithm; (b) 240Hz-Stencil algorithm

References

[1] Wang T H , Deng H , Xing Y ,et al.High-resolution integral imaging display with precise light control unit and error compensation[J].Optics Communications: A Journal Devoted to the Rapid Publication of Short Contributions in the Field of Optics and Interaction of Light with Matter, 2022(518-):518.

[2] Yang W , Cheng Y , Zou G ,et al.Spatial resolution-tripled integral imaging light field displays with no loss of angular resolution by recombining subpixels with zero sampling error[J].SID International Symposium: Digest of Technology Papers, 2022(2):53.

[3] Guowei Zou, Zeyu Wang, Yutong Liu, Juanli Li, Xingyun Liu, Jiahui Liu, Bo-Ru Yang, and Zong Qin, "Deep learning-enabled image content-adaptive field sequential color LCDs with mini-LED backlight," Opt. Express 30, 21044-21064 (2022)

An AR Retina Projection Optical System with Switchable Multi-viewpoints Based on Dammann Grating

Haonan Jiang[1], Enguo Chen[1,2,3,], Qun Yan[1,2,3], Tailiang Guo[1,2,3]*

[1] National & Local United Engineering Laboratory of Flat Panel Display Technology, Fuzhou University, Fuzhou, Fujian, China

[2] College of Physics and Information Engineering, Fuzhou University, Fuzhou, Fujian, China

[3] Fujian Science & Technology Innovation Laboratory for Optoelectronic Information of China, Fuzhou, China

*Corresponding author: ceg@fzu.edu.cn

In recent years, Augment Realty (AR) system has received considerable interest in advanced display market. However, most of the current products have technical problems on Vergence-accommodation conflict (VAC), which causes people to feel dizzy when wearing the AR device for a long time. To lessen this problem, previous research had focused on the retina projection [1].

Generally, retina projection is based on Maxwellian view. Compared with traditional imagining, it is more like a pinhole imagining system, which has a relatively wide depth of field (DOF). A wide DOF means that people can avoid VOC because it promises the wide range of clarity of everything in the picture, which makes human eyes not focus many times anymore. However, Maxwellian display also faces relatively small eyebox and narrow field of view (FOV), which are the deadly drawbacks for the practical application. At present, people mainly solve these problems by viewpoint replicating [2] and viewpoint moving [3]. Whereas, in viewpoint replicating, the distance among multi-viewpoints is fixed all the time. As a result, different people with different pupil diameters may see the visual image display discontinuously or image overlay because of the unsuitable distance of viewpoint. To overcome such problem, we design a retina AR system with switchable multi-viewpoints to provide just one viewpoint to the pupil in one time, which is aimed to avoid the problem mentioned above.

The theory of the retina AR system is shown in Fig. 1, which is based on the 4f system and Dammann grating. The whole system mainly consists of laser beam, character picture, collimation lens, focal lens, light selector, and dammann grating. Firstly, light is shaped by the character picture and then divided into 7*7 light spots by the dammann grating. Then, light selector chooses one spot that is closest to the pupil and let it pass through, while the other spots are blocked. In this way, human eyes will always see one visual image which appears on the center of pupil all the time.

After a series of optimization, the parameter of the system is as the Table 1 shows. Finally, we built an optical platform (as Fig. 2 shows) for the verification and the test effect is shown in Fig. 3.

Table 1. The parameter of AR retina system

Focal length	50mm
Grating period	50μm
Collimation light aperture	15mm
FOV	17.1°
Eyebox	6*6mm

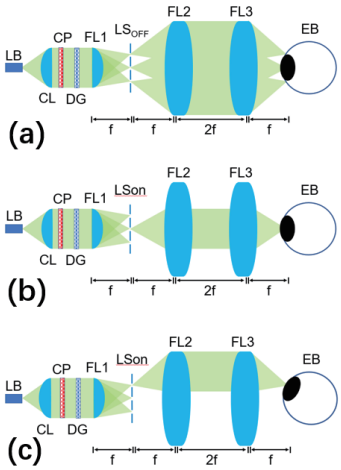

Fig. 1. Theory of the retina AR system. (a) Light selector is off. (b) Light selector selects the central viewpoints. (c) Light selector selects the edge viewpoints. LB: Laser Beam CL: Collimation Lens CP: Character Picture DG: Dammann Grating LS: Light Selector FL: Focal Lens EB: Eyeball

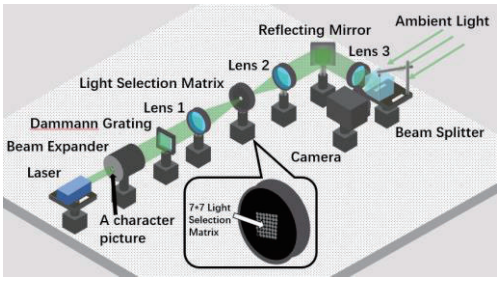

Fig. 2. The 3D model of the optical platform

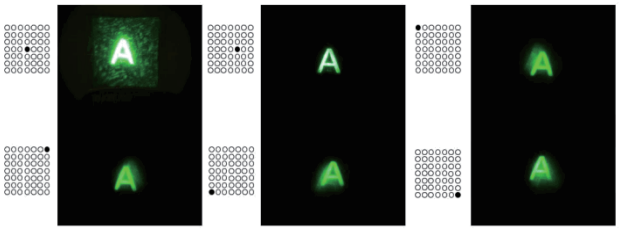

Fig. 3. Test effect of a few specific viewpoints

References

[1] S. B. Kim, et al., *Opt. Lett.,* 43(4), 767 (2018).

[2] P. K. Shrestha, et al., *Research*, 2019, 9273723(2019).

[3] J. H. Xiong, et al., *Opt. Lett.*, 46(7), 1760(2021).

Photopatterned nanoparticle films for advanced photonic and optoelectronic applications

D. Bhadra[1,2], C. Kang[1,2], V. Swaminathan[1,2], M. Kumar[1,2], J. Song[1,2], X. Yu[1,2], B. Mnaidar[1,2], and A. K. Srivastava[1,2,3]*

[1] State Key Laboratory on Advanced Displays and Optoelectronics Technologies
[2] Centre for Display Research, Hong Kong
[3] IAS Center for Quantum Technologies
The Hong Kong University of Science and Technology, Clear Water Bay, Hong Kong SAR, China
email: dbhadra@connect.ust.hk

Photopatterning has gained considerable interest in the realm of liquid crystal (LC) alignment technologies in recent decades due to its facile fabrication and micro-scale resolution capabilities. Such photopatterning technologies also allow for patterned, aligned nanoparticle thin films using LC as an intermediate layer. Quantum rods (QR), elongated 1-dimensional nanoparticles, have been of great interest due to their superior properties compared to other nanoparticles such as polarized emission, large Stokes shift, and highly tuneable emission bands. Photopatterning methods have been used to pattern and align such QRs into separate domains allowing for applications in advanced optoelectronic components such as photodetectors, and display enhancement films. Realization of such patterned aligned nanoparticle films seems to be the next crucial milestone in the advancement of photonic and optoelectronic technologies.

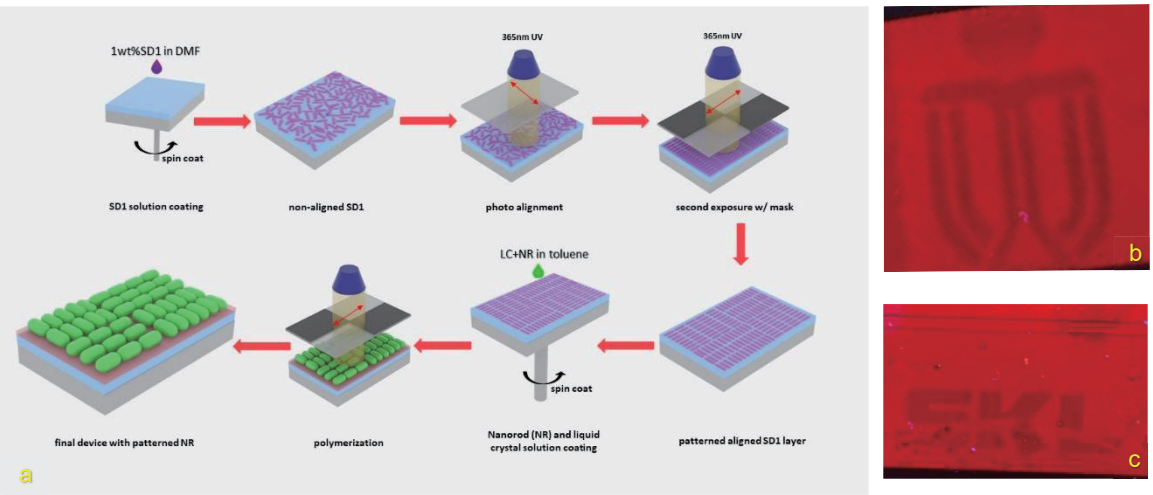

Fig. 1.a) Quantum rod photopatterning process flow, b) Patterned QR film showing HKUST logo exposed with non-polarized UV light c) Patterned QR film showing SKL logo exposed with non-polarized UV light.

Acknowledgement

This work was supported by the RGC of Hong Kong SAR for The State Key Laboratory of Advanced Displays and Optoelectronics Technologies.

References

1. Srivastava, Abhishek K., et al., *Advanced Science* 6, 1901345 (2019).
2. Abed, S.M., Mohammad, S.M., Hassan, Z. *et al. J Mater Sci: Mater Electron* **33**, 26322–26342, 10.1007/s10854-022-09315-1 (2022).
3. Dechao Chen, et al., Nano Energy, Volume 89, Part A, 106348 (2021).

Exploring the Intermediate State in CoFeB Pillar Devices Integrated with Thin Film Transistors

Shun Kong Cheung*, Wei Jiang*, Qiming Shao*

* State Key Laboratory of Advanced Displays and Optoelectronics Technologies. and Center for Display research, Hong Kong University of Science and Technology, Water bay road, Kowloon, Hong Kong

Magnetic Random Access Memory (MRAM) has emerged as a potent contender for AI applications [1]. Nonetheless, it grapples with inherent limitations characterized by fixed ON/OFF resistance states, restricting its capacity to store only a single bit of information and precluding analog behavior. Furthermore, MRAM's non-linear operational characteristics, restricted adaptability, and heightened power consumption pose challenges in its widespread application across diverse domains. Conversely, Thin Film Transistors (TFTs) have witnessed extensive utilization in pixel display and a myriad of sensor types [2]. Their commendable high mobility renders them well-suited for driving MRAM functionalities.

Fig.1 illustrates the integration of the Thin Film Transistor (TFT) and the CoFeB pillar device. To evaluate the perpendicular magnetization component of the pillars, Hall resistance measurements based on the anomalous Hall effect were conducted. In this experimental setup, the current is applied along the x-direction, and the resulting Hall voltage is recorded along the y-direction of the pillar device.

In Fig. 2, the output characteristic of the TFT is presented, with a width of 200 µm and a length of 2 µm. As the gate voltage increases, the collector current reaches a sufficient level to initiate the switching of the pillar device. In Fig. 3, the experimental result of current-induced switching, combined with the TFT under a gate voltage of 25V, are displayed. Notably, the pillar devices demonstrate successful switching behavior, and intriguingly, the emergence of the intermediate state is also observed.

In conclusion, we have successfully integrated TFT and pillar devices, showcasing both full and intermediate switching states. These additional states hold significant potential for enhancing AI applications and advancing electronic devices.

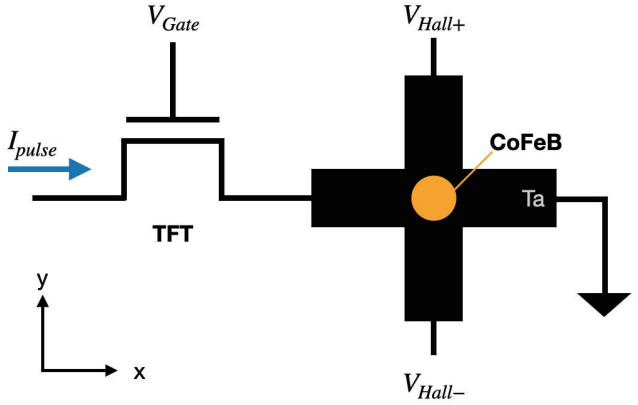

Fig. 1. Experiment set up with TFT and CoFeB pillar.

device.

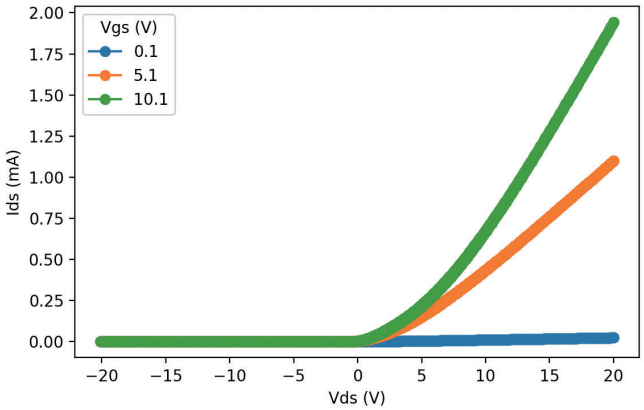

Fig. 2. Output characteristic of TFT with width is 200 µm and is length 2 µm.

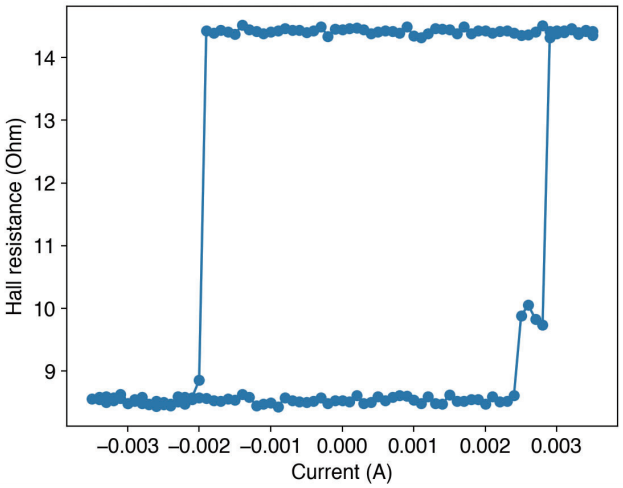

Fig. 3. Intermediate state measurement with current-induced switching.

References

[1] Q. Shao, Z. Wang, and J. J. Yang, "Efficient AI with MRAM," Nature electronics, vol. 5, no. 2, pp. 67–68, 2022, doi: 10.1038/s41928-022-00725-x.

[2] G. Zhu et al., "Significant Degradation Reduction in Metal Oxide Thin-Film Transistors via the Interaction of Ionized Oxygen Vacancy Redistribution, Self-Heating Effect, and Hot Carrier Effect," IEEE transactions on electron devices, pp. 1–8, 2023, doi: 10.1109/TED.2023.3283940.

Laser-induced Film Release, Bending and Movement under Electrostatic Field

Yi Chen, Min Tan, Haosong Zhong, Mitch Guijun Li*
Division of Integrative Systems and Design, The Hong Kong University of Science and Technology, Clear Water Bay, Kowloon, Hong Kong SAR, China
***Email: mitchli@ust.hk**

Digital micromirror devices (DMDs) are a type of commercial digital light processors and spatial light modulators (SLM).[1] Since its invention in 1987, DMDs have been developed to have an array with millions of micromirrors. Each DMD pixel is an aluminum micromirror, beneath which are a yoke and hinge layer, metal standing layer, and CMOS memory layer. These three layers form the function to switch the top micromirror between +12º and -12º (relative to flat state) under electrical signal modulation. Changing angles results in the in-situ shaping of wavefronts, to achieve the ON and OFF states. Due to the rapid development of Micro-Opto-Electromechanical System technology (MEMS), DMSs have been applied in emergent fields such as laser beam shaping[2], surface plasma resonance biosensors[3], micro stereo-lithography[4], and high-resolution biological microscopy[5].

Compared to other display techniques, DMDs feature high-speed, efficient, and controllable spatial light modulation. However, the complex traditional semiconductor manufacturing process leaves it expensive and limits its application. In this research, we propose a laser-induced method to fabricate bending silver films that are responsive to electrostatic fields. This method uses a commercial fiber laser marking machine to introduce localized heat and corresponding thermal stress on a thin silver film deposited on a glass substrate, making the sputtered silver film peel off from the glass substrate and bend. The bending silver film can move in response to the electrostatic field. Here patterns are defined by laser writing. By fixing one side and peeling off the other three sides via laser scanning, the curved silver films can do a mechanical behavior similar to the micromirrors under an external electrostatic field. Therefore, the proposed method t fabricating thin curved film has much potential in the DMDs manufacturing process.

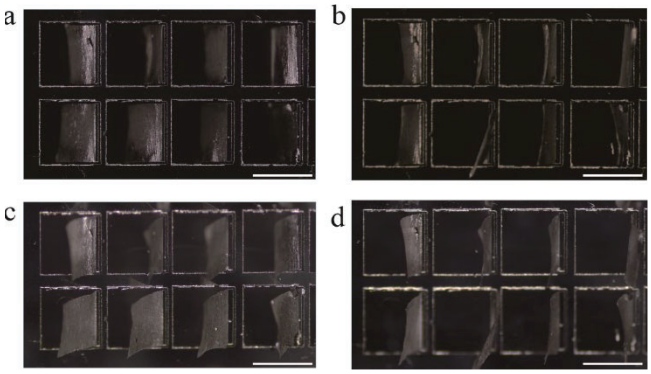

Fig. 1. (a, b) The top view of an array of curved silver films before and with an electrostatic field. (c, d) The tilted view of an array of curved silver films before and with an electrostatic field. All the scale bars are 1 mm.

References

[1] A. B. Ayoub and D. Psaltis, *Scientific Reports* **2021**, *11*.
[2] J. M. Yang, Q. Z. He, L. X. Liu, Y. Qu, R. J. Shao, B. W. Song and Y. Y. Zhao, *Light-Science & Applications* **2021**, *10*.
[3] D. Cebeci, B. R. Mankani and D. Ben-Amotz, *J Imaging* **2018**, *5*.
[4] P. Juskova, A. Ollitrault, M. Serra, J. L. Viovy and L. Malaquin, *Analytica Chimica Acta* **2018**, *1000*, 239-247.
[5] X. Dong, G. Tong, X. K. Song, X. C. Xiao and Y. T. Yu, *Microsystems & Nanoengineering* **2021**, *7*.

Electronic Properties of $(Ni_xGa_{1-x})_2O_3$ Alloys by First Principles Investigation

Hanqin Zhou*, Man Hoi Wong*, Chee-Keong Tan*,**
***Dept. of Electronic and Computing Engineering, The HKUST, Hong Kong, China**
****Advanced Materials Thrust, Function Hub, The HKUST (Guangzhou), Nansha, Guangzhou, China**

β-Ga_2O_3 has become a very strong contender for the development of the next-generation power electronics technology, attributed to its ultra-wide band gap (4.8 eV), high breakdown voltage (8 MV/cm) and low cost [1, 2]. However, one of the most fatal problems is the lack of p-type conductivity in Ga_2O_3 material, which means that p-type Ga_2O_3 is nearly impossible to be realized [1]. Traditional chemical doping can barely create acceptor defects since high ionization and formation energy is needed. A promising approach to mitigate this problem is to adjust the band structure of β-Ga_2O_3 by alloying.

NiO, as a p-type wide-bandgap transition metal oxide with a bandgap ~3.6 eV, has been proven to be a good candidate to form bipolar heterojunctions with n-type β-Ga_2O_3 [2]. A high position of valence band maximum of NiO (~4.8 eV below vacuum level) is expected to lift the valance band of β-Ga_2O_3 by alloying, thereby reducing the formation energy of some potential acceptors and achieving a p-type material.

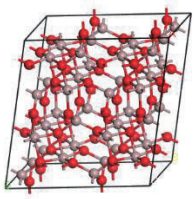

Figure 1. 80-atom β-Ga_2O_3 1×2×2 supercell.

In this work, the potential p-type ability of the β-$(Ni_xGa_{1-x})_2O_3$ alloys with Ni-content (x) up to 12.5% are investigated using density function theory (DFT) calculations. 5 models of NiGaO alloys are constructed based on an 80-atom β-Ga_2O_3 1×2×2 supercell, which contains 32 gallium atoms and 48 oxygen atoms in total, as shown in Fig. 1. The gallium atoms located at octahedral sites will be substituted by nickel atoms to achieve the desired Ni contents. Vienna Ab-initio Simulation Package (VASP) is employed, assisted with both the GGA-PBE and hybrid functional by HSE06. The Hartree-Fock exchange parameter is set at a=0.32. The cutoff energy of the plane-wave expression is set at 520 eV, and the Hellmann-Feynman force for structure optimization is set at 0.02 eV $Å^{-1}$. For all structures, the Brillouin zone is constructed using a 2×8×4 Monkhorst-Pack k-mesh, and energy convergence tolerance is set to 1×10^{-5} eV/atom.

In general, the hybrid functional by HSE is more accurate than the semilocal (GGA) approach, especially in defected conditions. In contrast, the semilocal approach has a lower calculation cost compared to the hybrid functional by HSE. The band gap errors from the semilocal approach can be corrected by applying the scissor operator to provide a closely acceptable result, which will be used to compare with the results calculated by the hybrid functional.

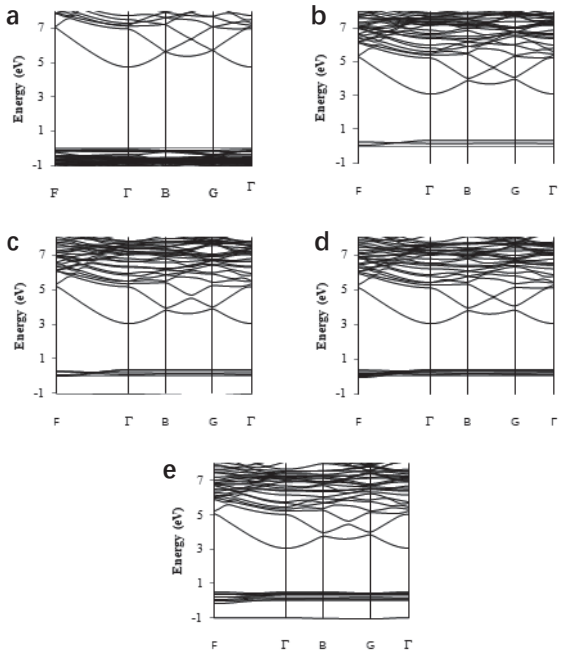

Figure 2. Band structures of β-$(Ni_xGa_{1-x})_2O_3$ alloys with (a) x = 0%, (b) x = 3.125%, (c) x = 6.25%, (d) x = 9.375%, and (e) x =12.5%.

Figure 2 illustrates the corrected GGA-PBE calculated band structure of β-$(Ni_xGa_{1-x})_2O_3$ alloys with (a) x = 0%, (b) x = 3.125%, (c) x = 6.25%, (d) x = 9.375%, and (e) x =12.5%. In all cases, the valence bands are flat and band structure analysis indicates indirect bandgaps. The conduction band minimum is always located at the Γ point, while the valance band maximum is always off the Γ point. It is interesting to point out that the difference between the direct and indirect bandgap is extremely small for all β-$(Ni_xGa_{1-x})_2O_3$ alloys (~0.03 eV). It is also important to point out that as the Ni content increases from 0% to 12.5%, the indirect energy bandgaps reduce from 4.83 eV to 2.50 eV. This trend meets our expectation, but the numerical accuracy needs to be validated. Further calculations carried by hybrid functional by HSE will be processed for verification. In summary, electronic properties of β-$(Ni_xGa_{1-x})_2O_3$ alloys with x up to 12.5% have been studied using DFT calculations.

References

[1] Kyrtsos, A., Matsubara, M., & Bellotti, E. (2018). On the feasibility of p-type Ga_2O_3. *Applied Physics Letters*, *112*(3), 032108.

[2] Kokubun, Y., Kubo, S., & Nakagomi, S. (2016). All-oxide p–n heterojunction diodes comprising p-type NiO and n-type β-Ga_2O_3. *Applied Physics Express*, *9*(9), 091101.

Optimization of information computational capacity for an alternating-driven magnetic tunnel junction

Xuezhao WU*, Qiming SHAO*

***State Key Laboratory on Advanced Displays and Optoelectronics,**

Department of Electronics and Computer Engineering, The Hong Kong University of Science and Technology,

Clear Water Bay, Kowloon, Hong Kong

The latest display technologies, from organic LED displays to electrophoretic displays, have become increasingly popular due to their high resolution and suitability for a wide range of applications, including head-up displays and advertising [1]. However, these displays still rely on traditional computer frameworks for information processing, which involves saving information into memory storage and processing it before it is transformed into display output. This information shuffling process results in high power consumption and delayed responses. To address this issue from the conventional von Neumann structure, a novel computing framework has been proposed that enables information to be processed directly in memory storage. This eliminates the requests for information transferred between processing units and memory, reducing power consumption and improving response times [2]. Magnetic random-access memory (MRAM) is a promising non-volatile memory device for this purpose, owing to its natural stability and high-speed response due to spintronics [3]. A magnetic tunnel junction, consisting of two ferromagnetic layers (fixed layer and free layer) and one barrier layer, is the fundamental unit in MRAM. When the magnetization directions of the two ferromagnets are antiparallel (parallel), it exhibits high (low) resistance due to the tunnel magnetoresistance effect. The magnetization in the fixed layer is pinned by utilizing the exchange bias effect from antiferromagnetism, while the magnetization in the free layer can be easily controlled through current or magnetic field via the spin transfer torque. In this paper, a current-controlled magnetic tunnel junction is utilized to establish a reservoir computing system using time multiplexing methods. Short-term memory and parity-check tasks are employed to assess the performance of the system. Additional alternating current was applied to adjust the dynamic properties of the magnetic tunnel junction. The Largest Lyapunov exponents and synchronization index are calculated to evaluate the system's dynamics properties. The information processing capacity spectra demonstrate that the magnetic tunnel junction-based reservoir computing system can be optimized by only tuning the alternating current.

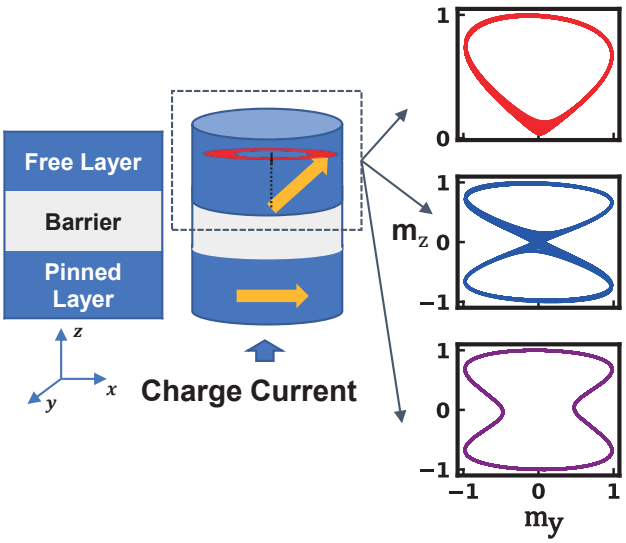

Fig. 1. Schematic of a magnetic tunnel junction. The applied charge current generates a spin transfer torque into free layer, resulting in diversified dynamics.

References

[1] Jing Yan, Xiangwen Fan, Yifan Liu, Ying Yu, Yuming Fang, and Ruo-Zhou Li, Chin. Opt. Lett. 20, 013301-(2022).

[2] Sebastian Abu, Le Gallo Manuel, Khaddam-Aljameh Riduan, and Eleftheriou Evangelos, Nat. Nanotechnol. 15, 529–544 (2020).

[3] Sumio Lkegawa, Frederick B.Mancoff, Jason Janesky, and Sanjeev Aggarwal, IEEE Trans. Electron Devices, 67, 1407-1419 (2020).

Laser-enhanced nanoimprinting of optical metasurfaces with fluorescent materials

Yee Him Timothy Chan, Zhengong Meng, Mitch Guijun Li*
Division of Integrative Systems and Design, The Hong Kong University of Science and Technology, Clear Water Bay, Kowloon, Hong Kong SAR, 999077, China
***Email:** mitchli@ust.hk

Optical metasurfaces have been widely used to precisely control signal processing, encoding, spatial filtering, and transformation [1]. It has also emerged as a potential solution to enhance the performance of fluorescent materials, which is widely used as a selective sensing detector and bioimaging indicator [2]. In this study, we further investigated using the optical metasurface as a gain medium of the fluorescence materials. This research can increase the optical performance and manipulate the fluorescence output with variable sensing environments and longer fluorescence lifetime.

The fabrication process involves the use of a polydimethylsiloxane (PDMS) mold, laser-printed graphene, and 1064 nm continuous wave laser, which is shown in Fig. 1. The PDMS mold is used to duplicate the desirable metasurface pattern onto the fluorescence crystal by laser-induced nanoimprinting, other flexible polymers can be used as the metasurface mold, such as Ecoflex. Laser-induced nanoimprint is used instead of pressure-driven nanoimprint because precise laser control can provide selective printing to control the nanoimprint area. The laser-printed graphene is produced by the same 1064 nm laser with polyimide thin film onto aluminum foil, which is placed on top of the PDMS layer to absorb the laser energy and convert it to kinetic energy to create the nanoimprint pressure to replicate the metasurface pattern onto crystal surface during crystallization. The fabricated crystal would contain a metasurface structure on top, and the pattern would modify the crystal's optical properties, as shown in Fig. 2., which can increase the optical absorption to improve its performance as a gain medium.

The combination of nanoimprint and laser would provide a simple and cost-effective fabrication method to construct a selective metasurface that can be used as an optical modulating layer for the fluorescence crystal. The flexible PDMS allows a quick molding of the metasurface to fine-tune the pattern according to different fluorescence materials to match the fluorescence wavelength. Also, different patterns of the metasurfaces can be easily replicated onto the crystal for testing and structural redesign. This technique's abilities offer exciting potential for integrating metasurface technology and fluorescent materials. By optimizing metasurfaces as modulating layers, we can substantially improve fluorescent materials' optical properties and performance, opening new possibilities in sensing, imaging, and optoelectronic devices.

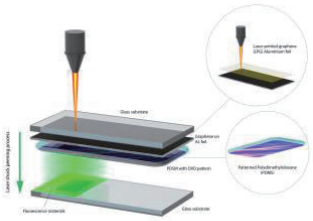

Fig. 1. Schematic of Laser-induced Nanoimprint

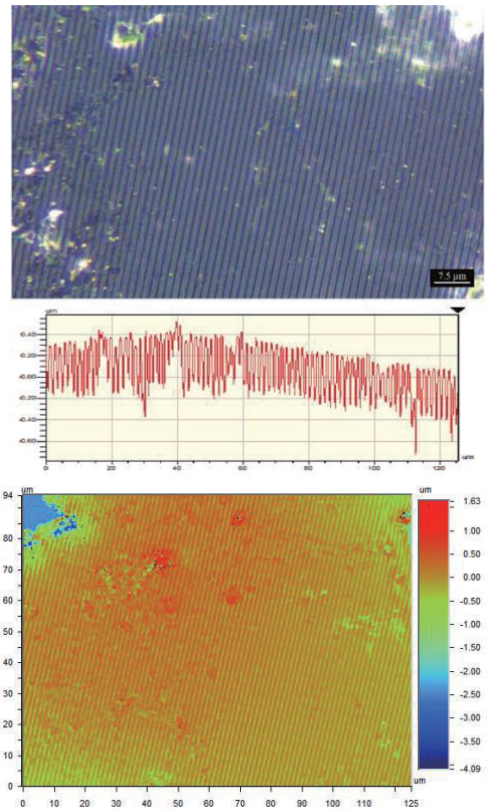

Fig. 2. Parallel line patterns from CD surface is mold onto crystal by laser-enhanced nanoimprint

References

[1] J. Hu, S. Bandyopadhyay, Y. Liu, L. Shao, *Front. Phys*, 8 (2021).

[2] Z. Chen, S. Feng and D. Wang, *Polymers*, 15, 332 (2023).

Uniformity Improvement in a Floating Aerial Display Using Off-axis Freeform-mirror

Ding-Yu Zhuo, Chih-Hao Chuang**, Chien-Yu Chen****

* Graduate Institute of Color and Illumination Technology, National Taiwan University of Science and Technology, Taipei 10607, Taiwan

** Department of Photonics, Feng Chia University, 100 Wenhwa Rd., Seatwen, Taichung 40724, Taiwan

***Graduate Institute of Color and Illumination Technology, National Taiwan University of Science and Technology, Taipei 10607, Taiwan

There are several methods for the floating display system at this stage, such as using double concave mirrors to achieve the floating display effect [1], but the overall volume is too large, and there is a problem of image deformation. The light field floating display technology [2] can present a multi-view information display, but it requires high accuracy and stability of the structure. As for the semi-transmissive film floating display technology [3], although the system structure is relatively simple, there will be restrictions on the viewing angle. Although aerial imaging by retro-reflection (AIRR) [4] or the dihedral corner reflector arrays (DCRA) [5] has a relatively good viewing angle and volume, the production of this technology is expensive. When the components' resolution is insufficient, the image will be deformed, fuzzy, and other issues.

This research adopts the freeform optical system, and its approach is shown in Figure 1. The system is an off-axis reflective optical structure. First of all, the reflective optical system can avoid the problem of chromatic aberration.

Secondly, in the off-axis optical system, the final image can have stronger illuminance, and at the same time, the system can be made more compact to achieve the purpose of miniaturization. However, off-axis reflective optics are prone to aberration problems, but they can be effectively improved by optimizing optical freeform. This study will use the optical simulation program *Zemax OpticStudio* to design and construct a floating display system.

We will refer to the head-up display's design method and use the backtracking design technique to complete the design and optimization [6]. By reversing the start and end ray tracing, the target value becomes the initial value, such as floating height, field of View, etc. The advantage of the backtracking design is that the target value can be set directly. In addition to the design can be adjusted at any time according to the demand, it can also reduce the optimization conflict caused by too many targets. According to the system's axisymmetric basis, the freeform selection in this study adopts the iconic. Surface as the base and adds x and y polynomial terms as the reflective freeform surface equation, as shown in Formula 1.

$$z(x,y)=\frac{c_x x^2+c_y y^2}{1+\sqrt{1-(1+k_x)c_x^2x^2-(1+k_y)c_y^2y^2}}+\sum_{i=1}^{N_x}\alpha_i x^i+\sum_{i=1}^{N_y}\beta_i y^i \quad (1)$$

where c is the curvature, k is the conic, α and β are polynomial terms, and N is the polynomial order.

Due to the backtracking design of this study, by defining optimization variables combined with the merit function, ray tracing can be started, and aberration correction can be optimized.

Finally, continuously adjust the weights of the merit function until the image evaluation reaches the ideal. The result is that the distortion is 1%, as shown in Figure 2. And When 8per/mm, the modulation transfer function is below 0.5, as shown in Figure 3.

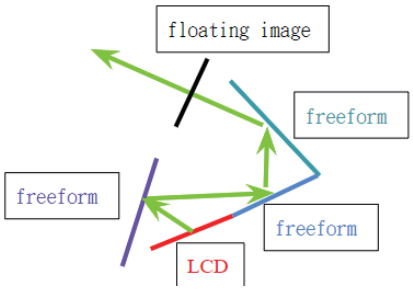

Fig. 1. optical system structure

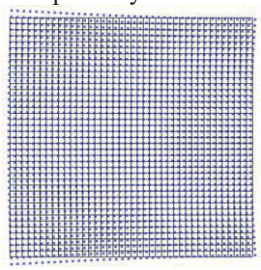

Fig. 2. distortion

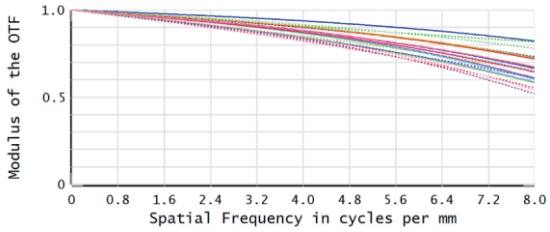

Fig. 3. modulation transfer function

References

[1] Zhao, Wu-Xiang, et al. "Aerial projection 3D display based on integral imaging." Photonics. Vol. 8. No. 9. MDPI, 2021.

[2] Sang, Xinzhu, et al. "Interactive floating full-parallax digital three-dimensional light-field display based on wavefront recomposing." Optics express 26.7 (2018): 8883-8889.

[3] Greenslade Jr, Thomas B. "Pepper's Ghost." The Physics Teacher 49.6 (2011): 338-339.

[4] Yamamoto, Hirotsugu, Yuka Tomiyama, and Shiro Suyama. "Floating aerial LED signage based on aerial imaging by retro-reflection (AIRR)." Optics express 22.22 (2014): 26919-26924.

[5] Maeda, Yuki, et al. "Volumetric display using rotating prism sheets arranged in a symmetrical configuration." Optics express 21.22 (2013): 27074-27086.

[6] Qin, Zong, et al. "Dual-focal-plane augmented reality head-up display using a single picture generation unit and a single freeform mirror." Applied Optics 58.20 (2019): 5366-5374.

Simulation of a 2D array of 1×12 wavelength selective switches with LCoS

Yu- Chia Cheng, and Hoang-Yan Lin
Graduate Institute of Photonics and Optoelectronics, National Taiwan University, No. 1, Sec. 4, Roosevelt Road, Taipei, 10617, Taiwan

In optical communication, in order to effectively use the network, optical add-drop multiplexers (OADM) are often used as photonic switches. Wavelengths can be dropped or added at specified input ports or output ports by OADM .

Liquid crystal on silicon (LCoS) spatial light modulators (SLM) can be used as an optical modulation element, which can flexibly switch the wavelength to any/multiple fiber ports by changing the pixel voltage [1].

WSS is a new type of network switch designed with dispersion and selection, which can reduce the complexity of optical fiber network and enhance the flexibility of network nodes. The system is shown in Fig. 1.

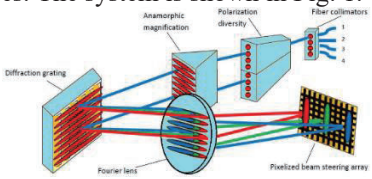

Fig. 1. 1 × K WSS system [2]

The two-dimensional optical fiber array can make the design of WSS more flexible and can also increase the number of ports and space utilization. We design a 1x13 WSS with a 2D fiber array and use an optimized iterative Fourier transform algorithm (IFTA) to switch different wavelengths to any/multiport ports.

In the case of one-to-one switching, it can be simulated with the IFTA, which is without any restrictions. However, if the input information would be transmitted to multiple receiving ports, The IFTA should be confined to uniformity conditions, as shown in Fig. 2. When the light intensity of each iteration peak result is lower or higher than a certain range, the light intensity of the peak will be increased or suppressed. If the peak value is in the target range, the value would be the next iteration. [3]

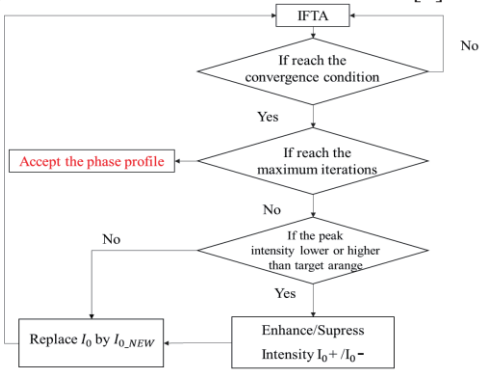

Fig. 2. Uniformity optimized IFTA process. [3]

The 1x12 WSS was designed as shown in Fig. 3(a). Different colors represent different wavelengths. The pitch of the output ports is 250 μm, and arranged in a diamond shape as a 2D fiber array, as shown in Fig. 3(b). The spot size on LCoS is scaled by a 2F system. We use a transmission grating to separate the spectrum on the dispersion axis and use LCoS to modulate the same wavelength to switch or split on the switch axis. Because the LCoS loads the phase modulation pattern generated by uniformity optimized IFTA on LCoS to split light. If it returns to the fiber array in the original way, it will cause loss off-axis, so finally use a BS to separate the optical path, and use lens3 to correct the optical path, so that the light enters the fiber arrays.

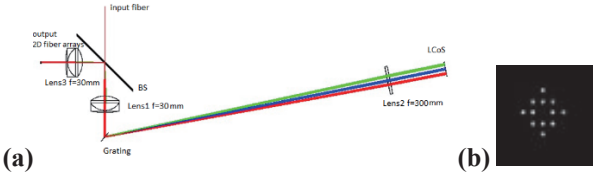

Fig. 3. (a) 1x12 WSS System design diagram (b) Schematic diagram of 2D fiber array

In this simulation, the theoretical coupling efficiency T of these output ports is about 96 % to 97 % at a wavelength of 1547 nm, about 80 % to 82 % at a wavelength of 1537 nm and about 74 % to 75 % at a wavelength of 1557 nm.

$$\mathbf{T} = \frac{|\iint \boldsymbol{F_r(x,y)W'(x,y)dxdy}|^2}{\iint \boldsymbol{F_r(x,y)F_r'(x,y)dxdy} \iint \boldsymbol{W(x,y)W'(x,y)dxdy}} \quad (1)$$

Finally, we designed a 1×12 wavelength selective switch with a 2D fiber array, and compared with the theoretical coupling efficiency of our previous design, the simulation results increased by about 30%-50%.[4]

REFERENCES

[1] Zih-Yuan Wong, et al. ,Proc. IDW ’21 LCTp1-1 (2021)

[2] Mi Wang, et al., “LCoS SLM Study and Its Application in Wavelength Selective Switch.” Photonics 2017, 4(2), 22;

[3] Hung-Pin Chen and Hoang-Yan Lin ,“Design and Optimization of 2×5 Wavelength Selective Switch with Single Mode Fiber.” Master thesis from National Taiwan University(2022)

[4] Han-Yu Lin “1x10 Wavelength Selective Switch System Modeling and Validation.” Master thesis from National Taiwan University(2022)

All Optical Diffraction Neural Network Digital Recognition Based On Photoalignment Technology

Quanzhou LONG*, Cong LIU*, Wanlong ZHANG*, Lingxiao ZHOU*, Xiaocong YUAN*
***Nanophotonics Research Center, Institute of Microscale Optoelectronics,**
Shenzhen University, Shenzhen, 518060, China

Artificial neural network is a mathematical processing method that simulates neurons in the biological nervous system. Due to the limitations of related factors such as Moore's Law, the traditional neural network model based on electronic computation still has challenges in terms of energy efficiency and operation speed [1]. Optical neural network has lower power consumption and faster computing speed, and has great research space in image classification, object detection and recognition [2]. The photoalignment technology is a kind of optical signal processing technology using the orientation of liquid crystal molecules, which can be applied to the physical processing of optical neural networks [3].

In optical neural networks, the photoalignment technology can be used to adjust the connection weight and nonlinear activation function between neurons. Specifically, the photoalignment technology can achieve a weighted summation of the input signal through the optical coherence effect. In this way, the calculation of connection weights between neurons can be completed at the optical level, thus avoiding a lot of multiplication and addition operations in traditional electronic computing, and reducing energy consumption.In addition, the orientation state of liquid crystal molecules can be used to realize the nonlinear activation function. This nonlinear transformation is the key to the realization of complex functions of optical neural networks. By adjusting the orientation of liquid crystal molecules, nonlinear characteristics can be introduced, thus giving the network more powerful expression and superior feature extraction ability.

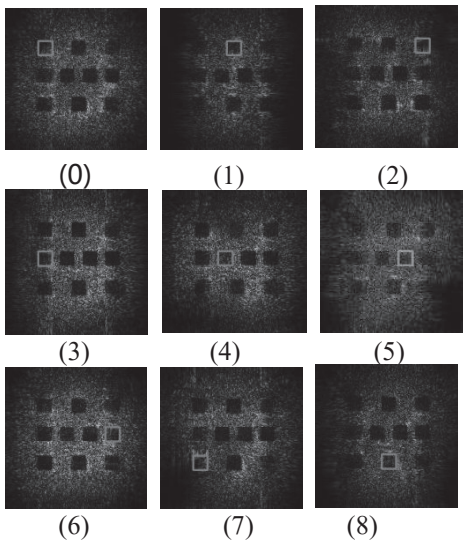

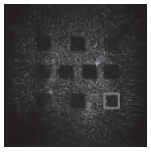
(9)

Fig. 1. Digital 0-9 all-optical neural networks recognize images

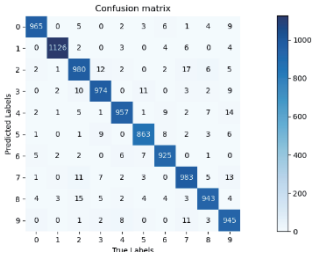

Fig. 2. Confusion matrix for simulation

In this paper, the recognition function of handwritten d igits is completed by processing optical neural network bas ed on photoalignment technology, and the function of optic al neural network in image classification is verified.The res ulting image of recognition is shown in Fig 1. The confusi on matrix of simulated digital recognition is shown in Fig 2.

References

[1] Gupta S, Agrawal A, Gopalakreshnan K, Narayanan P. Deep learning with limited numerical precision[J]. JCML'15,2015,1737-1746

[2] Lin X, Rivenson Y, Yardimci NT, Veli M, Luo Y, Jarrahi M, Ozcan A. All-optical machine learning using diffractive deep neural networks[J]. Scinence,2018,361.

[3] Pan JT, Qian JX, Ma LL, Wang ZY, Zheng R, Wang N, Li BX, LU YQ. Dual photopatterning of rotational fingerprint superstructures[J]. Opt Lett,2023,21.

A New Fast Elemental Image Array Rendering Method for Computer-generated Integral Imaging Light Field Display

Yunfan Cheng*, Bo-Ru Yang*, Zong Qin*

***School of Electronics and Information Technology, State Key Laboratory of Optoelectronic Materials and Technologies, Guangdong Province Key Laboratory of Display Material and Technology, Sun Yat-Sen University, 132 East Waihuan Rd., Guangzhou, 510006, China**

The integral imaging light field display (InIm-LFD) is currently one of the most promising true 3D display technologies due to its feasible implementation and compact volume [1]. The InIm-LFD utilizes a microlens array (MLA) to reconstruct images through elemental image arrays (EIAs) captured by a camera array or generated through computer-generated integral imaging (CGII). Although CGII aims to achieve real-time rendering, it often involves massive calculations. Previous studies adopt parallel computing [2] and sparse viewpoints [3] to improve rendering speed. However, these methods necessitate an essential tradeoff among system complexity, accuracy and speed. Therefore, we propose a new EIA generation method for fast rendering without sacrificing system complexity and accuracy.

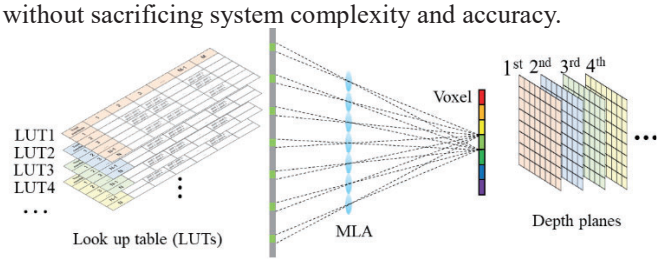

Fig. 1. The sketch map of the offline preprocessing for our real-time EIA generation method.

Our method consists of two main steps: offline preprocessing and online rendering. During the offline preprocessing stage, a finite number of voxels are on a definite depth plane with their positions explicitly defined. Therefore, we trace the chief rays from each voxel to the display panel through lenses and obtain the invariantly voxel-pixel mapping. These mappings are stored in a lookup table (LUT) shown in **Fig. 1**. Each cell in the LUT contains the coordinates of all homogeneous pixels that constitute a voxel. In the online rendering, we resample the 3D scene with a voxel matrix and rasterize it into RGB-D values. Subsequently, the EIA is generated through ultra-fast lookup operations. Our LUT-based method can achieve a rapid rendering speed by only optimizing rendering algorithms.

To verify the rendering speed with no hardware complexity increasing, we adopt an inexpensive laptop with an ordinary CPU (Intel i5-13500H) and no standalone GPU. The rendering speed (excluding I/O) is as fast as 7 ms (a MATLAB code with the core LUT function written by C), a spectacular benefit of merely executing LUT operations.

We also build a real-time InIm-LFD prototype for further demonstration. The whole pipeline is shown in **Fig. 2.** Although the prototype includes a long data pipeline (e.g., data conversion, a large amount of image I/O), the actual rendering speed can also arrive at 10 FPS. This result indicates that real-time EIA rendering could be easily achieved in an optimized all-in-one (AIO) InIm-LFD machine.

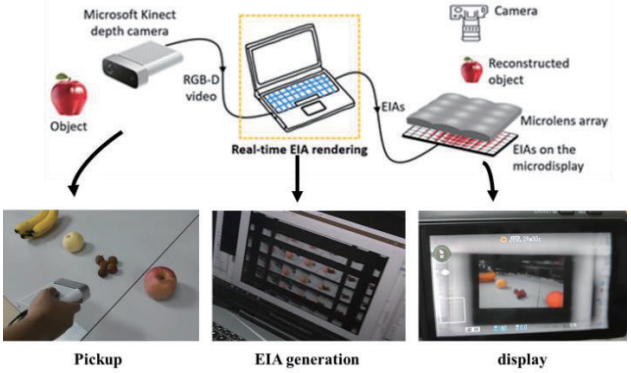

Fig. 2. Experiment to prove the EIA rendering speed.

The significant challenge of our method comes from the memory requirements. A 3D scene is formed by multiple depth planes whose number affects the demand memory. Each depth plane in our method needs several megabytes of memory for the LUT, and this demand increases proportionally with the number of depth planes. Fortunately, five to ten depth planes are generally sufficient [4], and memory demand expanding several times should still be acceptable for the RAM of modern electronic devices.

In conclusion, we propose a new EIA rendering method for CGII InIm-LFD. The EIAs are generated by ultra-fast lookup operation using LUTs stored in advance. Compared with traditional methods, the LUT-based rendering method does not need to sacrifice critical parameters: system complexity, accuracy and speed. The limitation of the proposed method is the memory requirements, which is not intractable for modern electronic devices.

References

[1] B. Javidi, A. Carnicer, J. Arai, T. Fujii, et al. Opt. Express 28(22), p. 32266 (2020).

[2] Y. Guan, X. Sang, S. Xing, Y. Li, et al. Opt. Express 27(20) p. 29309 (2019).

[3] H. Li, S. Wang, Y. Zhao, J. Wei, M. Piao, Disp. 69, p. 102025 (2021).

[4] A. Aghasi, B. Heshmat, L. Wei, M. Tian, Opt. Express 29(7), p. 9878 (2021).

Waveguide Coupler Based on Polarization Volume Gratings for Large Full-color Field of View

Zijian Lin[1,2], Enguo Chen[1,2*], Yun Ye[1,2], Sheng Xu[1,2], Qun Yan[1,2], Tailiang Guo[1,2]

[1]College of Physics and Information Engneering, Fuzhou University, Fuzhou 350108, China

[2]Fujian Science & Technology Innovation Laboratory for Optoelectronic Information of China, Fuzh ou 350108, China

Corresponding author: ceg@fzu.edu.cn

Polarization volumetric grating (PVG) have shown great potential in the field of AR optical waveguides, with their large refractive index modulation system and unique polarization characteristics, and this diffraction device has been extensively studied. However, in the PVG-based waveguide display schemes, although the multi-layer waveguide transmission optical path can expand the colorized field of view, it cannot avoid increasing the volume and weight of the waveguide system, in addition, using a single-layer full-color waveguide still cannot meet the requirements of the large field of view and has serious dispersion and ghosting can not be solved, and the waveguide with both thinness, full color and large field of view is still to be developed. In this paper, a coupler structure based on polarization volume grating is proposed for a single-layer transmission optical path to realize a colorized waveguide display system. Using the polarization characteristics of PVG, the full-color optical path is divided and controlled, combined with K-sapce analysis of the field limit, the theoretical realization is that under the refractive index of the waveguide is 1.57 and the maximum diffraction angle is 80°, the full-color horizontal field of view angle of single-layer waveguide transmission reaches 22°, and the horizontal field of view angle of 532nm wavelength and 630nm wavelength reaches 32°.

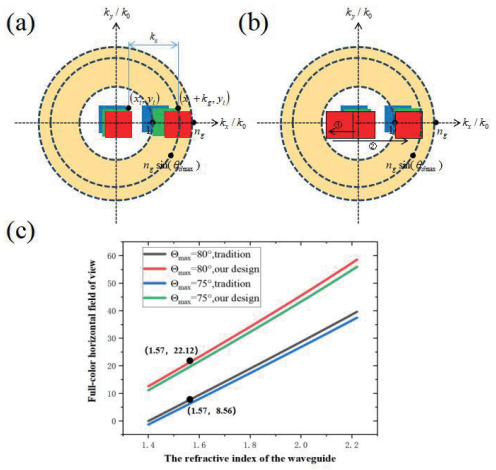

Fig. 1.(a)The k-vector diagram for a traditional single-layer color waveguide;(b)The k-vector diagram for a single-layer color waveguide in this design;(c)The limit of the field of view obtained by K-space analysis

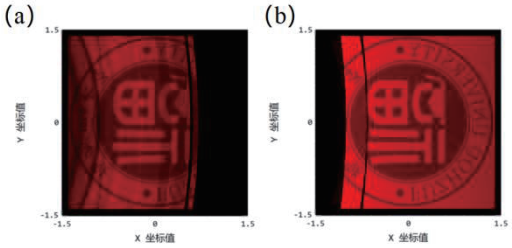

Fig. 2. Imaging simulation of PVG waveguides. (a)630nm imaging using a traditional single-layer color waveguide scheme;(b)630 nm imaging using the single-layer color waveguide scheme in this paper

References

[1] Ding Y, et al. Journal of the Society for Information Display, DOI: 10.1002 (2023).

[2] Gu Y, et al. Crystals, 12(12): 1805 (2022)

A new One-Drop-Filling (ODF) machine

HUO Yipeng, Jacob HO, SUN Zhibo, Ken Tseung, Hoi Sing KWOK
Dept.of Electric Engineering, HKUST
Clearwater Bay, HongKong

Liquid crystal devices are ubiquitous in modern day life, and faster and more accurate manufacture of these devices is required to meet increasing global demand. The optimisation of the manufacturing process generally involves attempting to reduce manufacturing time by increasing flow velocities and filling speeds.

A common method of filling the liquid crystal layer in liquid crystal devices (LCDs) used by display manufacturers is the One-Drop-Filling (ODF) method.[1].These days, we have refitted a new ODF machine, it can achieve heating FLC and glue in one reaction pot. There are photos(picture1, 2, 3, 4 and 5) about our machine.

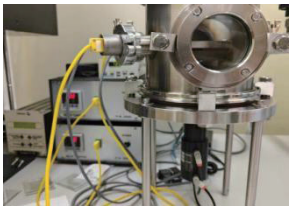

Fig.1. Hole body

Fig.2. Bump

Fig.3. Valve

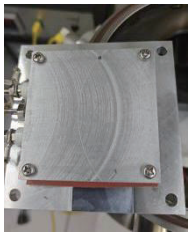

Fig.4. Hot surface top

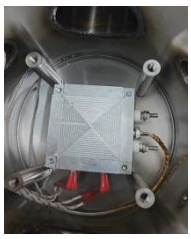

Fig.5. Hot surfaces down

We had made a lot of empty cells. During the process, we find a big problem about the work is glue. The glue will influenced the hole process a lot. So we had tested three kinds of thermal glue. The last one-we named it 86TH can be slightly successful. We use the FLC11030 as a testing materials. The result shows good.

The glues' viscosity will change when be heated to a high temperature (higher than 70°C). So finding a suitable glue is an important problem we need to solve.

References:

[1] A. Hirai, I. Abe, M. Mitsumoto, and S. Ishida., "One drop filling for liquid crystal display panel produced from larger-sized mother glass," Hitachi Review, Vol. 57, No. 3, pp. 144–148 (2008).

Large-scale planar and spherical light-emitting diodes based on arrays of perovskite quantum wires

Daquan Zhang*, Qianpeng Zhang*, Zhiyong Fan*

***Department of Electronic and Computer Engineering, The Hong Kong University of Science and Technology, Clear Water Bay, Kowloon, Hong Kong SAR, China**

High photoluminescence quantum yield (PLQY) is required to reach optimal performance in solar cells, lasers and light-emitting diodes (LEDs). Typically, PLQY can be increased by improving the material quality to reduce the non-radiative recombination rate. It is in principle equally effective to improve the optical design by nanostructuring a material to increase light out-coupling efficiency and introduce quantum confinement, both of which can increase the radiative recombination rate. However, increased surface recombination typically minimizes nanostructure gains in PLQY.

Here a porous alumina membranes (PAMs) template-assisted close-spaced-vapor-reaction (CSVR) growth of perovskite nanowire (NW) arrays with unprecedented control of NW diameter from the bulk (250 nm) to the quantum-confined regime (5.7 nm) is demonstrated, while simultaneously providing a low surface recombination velocity of 18 cm s^{-1}. This enables an obvious PLQY enhancement from 0.33 % up to 42.6 % for $MAPbI_3$ quantum wires (QWs), and up to ~ 92 % for $MAPbBr_3$ QWs, exclusively using nanophotonic design. After carrying out a hydrophobic treatment on the PAM surface to dramatically increase the water contact angle from 14.3 ° to 117.3 °, the as-obtained hydrophobic $MAPbBr_3$ QW arrays show an excellent water-repellent property, with a PL lifetime (T_{PL50}) of 5,644 hrs.

They have been fabricated into LEDs on rigid and flexible planar substrates with a single device size up to 4-inch wafer scale. Intriguingly, thanks to the conformity of the vapor phase growth approach, unique three-dimensional (3-D) spherical LEDs with outstanding uniformity have been demonstrated. The result suggests the approach developed here can be generalized to fabricating other unconventional 3-D LEDs in the future. The simple extension of this technique to a wide variety of semiconductors and the ultra-high density of vertical QWs may also provide interesting opportunities in quantum transport, electronics and memory devices in the future.

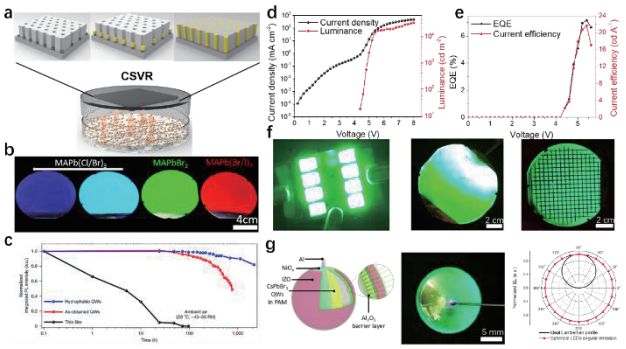

Figure 1. Perovskite QWs growth and their applications in large-scale planar and 3D spherical LEDs.

References

[1] D. Zhang, Q. Zhang, B. Ren, Y. Zhu, M. Abdellah, Y. Fu, B. Cao, C. Wang, L. Gu, Y. Ding, K. Tsui, S. Fan, S. Poddar, L. Shu, Y. Zhang, D. Kuang, J. Liao, Y. Lu, K. Zheng, Z. He, Z. Fan, *Nat. Photon.*, 16, 284 (2022).

[2] D. Zhang, L. Gu, Q. Zhang, Y. Lin, D. Lien, M. Kam, S. Poddar, E. Garnett, A. Javey, Z. Fan, *Nano Lett.*, 19 (5), 2850 (2019).

Micro-heater Integrated Nanotube Array Gas Sensor for Parts-Per-Trillion Level Gas Detection and Single Sensor-based Gas Discrimination

Wenying TANG*, Zhesi CHEN*, Zhiyong FAN*

***Dept. of Electronic and Computing Engineering, The Hong Kong University of Science and Technology, Kowloon, Hong Kong SAR, China**

Detection of various life-threatening gaseous molecules is of paramount importance in many fields like environmental monitoring, food quality evaluation, industrial safety, explosive detection and healthcare, *etc*. Conventionally, costly, bulky, and power-hungry devices, such as optical gas sensors and electrochemical gas sensors, are used for this purpose. In fact, metal oxide (MOX) semiconductor gas sensors possess several alluring attributes such as low-cost, small formfactor, reasonable lifetime, excellent compatibility with other electronic components [1]. Thus, they are ideal candidates for a highly integrated sensor systems, in principle. However, poor selectivity and sensitivity of the mainstream MOX sensors have been the main roadblocks hindering their wide applications. Meanwhile, the high operating temperature (300 ~ 400℃) also limits the deployment of MOX-based gas sensor in portable electronics due to high power consumption.

Researchers have been working to improve MOX-based gas sensors by adding a porous overlayer or functionalizing the surface with noble metals or oxides [2]. Gas sensor arrays have also been developed to discriminate multiple gases, but they require complicated construction and data processing. To implement gas discrimination with a single sensor, some have proposed adding a molecular sieve [3] or using temperature modulation to extract kinetic information [4]. However, these methods have their own limitations and the transient characteristics of multivariable response have been rarely explored in the past.

Herein, we demonstrate a dual-mode micro-heater integrated nanotube array gas sensor (MINA sensor), which can detect multiple gases down to ppt level under CH mode and discriminate the gases when working under PH mode. A MINA sensor was built on nano-porous anodic aluminum oxide (AAO) templates with top-bottom electrodes structure to enable much enhanced surface area for the molecular access. The ultrathin and conformal SnO_2 thin film and Pd nanoparticles (NPs) were deposited by atomic layer deposition (ALD) as the sensing material layer. When operating under CH mode, the MINA sensor could detect hydrogen, acetone, toluene and formaldehyde with measured LODs as low as 100 ppt, 100 ppt, 100 ppt, 4 ppb, with the corresponding theoretical LODs as 6.96 ppt, 11.88 ppt, 16.52 ppt, 70.06 ppt, respectively. Under PH mode, the MINA sensor showed intriguing transient responses toward different gases because of the variations of gas diffusion and activation energy of surface reactions. Gases of hydrogen, acetone, toluene and formaldehyde have been distinguished by extracting conductance and slope features from each pulse. Moreover, the pulse heating mode saved 66.7% energy compared with traditional continuous heating mode. The ppt level gas detection and pulse-heating enabled gas discrimination of a single MINA sensor can open a new pathway toward high-performance, low-power and miniature smart gas sensors for sensor networks and mobile/wearable electronic applications [5].

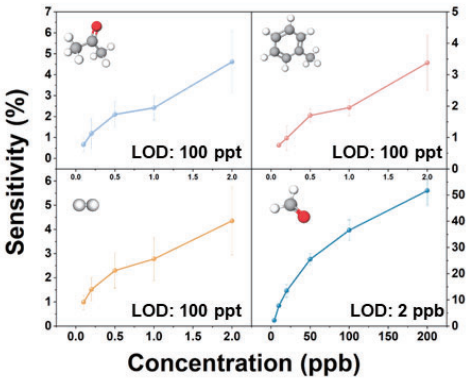

Fig. 1. Trace VOCs detection

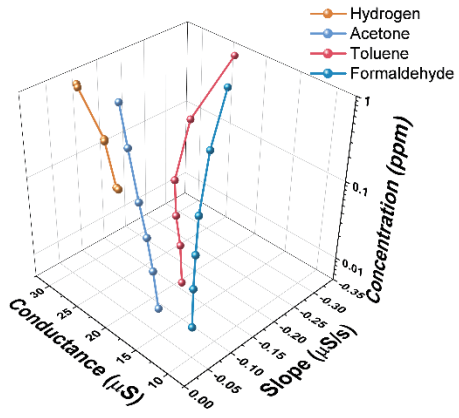

Fig. 2. Single device-based gas discrimination

References

[1] Dey, A., *Mater. Sci. Eng.,* 229, 206-217 (2018).

[2] Song, Z. L., *ACS Nano, 15,* 7659-7667 (2021)

[3] Van den Broek, J., *Nat. Commun*, 3, 280-289 (2020)

[4] Liu, H. Y., *Sens. Actuators, B*, 293, 342-349 (2019)

[5] TANG, W. Y., *ACS Nano,* 7, 10968-10978 (2022)

A perovskite nanowire array based bionic eye integrated with color imaging and signal preprocessing functions

Zhenghao Long*, Zhiyong Fan*

***Dept. of Electric and Computer Engineering, The Hong Kong university of Science and Technology, Clear Water Bay, Kowloon, Hong Kong SAR, China.**

Evolution developed extraordinary vision systems t hat support the everyday behavior of animals, including human. A human eye has many powerful features, tha t are originated from its elegant and efficient design. T he hemispherical geometry of the retina ensures the lo w aberration imaging ability even with few simple opti cs. The cone cells with color distinguish ability provid e us the precious color vision. The dense vertical align ment of the neuron array supports our high-resolution vision. And the retinal signal preprocessing gives us en ergy efficient visual signal processing. The optics of o ur eyes provides us adaptable visions. The crystalline l ens with switchable thickness makes us able to see obj ects from different distance, and the iris with adjustabl e pupil enhance the dynamic range of our eye. All ab ove outstanding functions are highly desired to be repli cated in artificial vision systems, which can support m ore powerful machine vision and robotics applications.

Cameras are essentially biomimetic device mimicki ng human eyes. However, conventional complementary metal-oxide-semiconductor (CMOS) image sensors are l imited by its design. The planar geometry cause misma tch between image sensor and the Petzval field curvatu re, result in the requirement of complex multiple lense s, which significantly increase the size and weight of t he system. The color vision is based on a color filter array, which increase the complexity and reduce pixel density. The signal is processed by redundant, separates units, which lead to low energy efficiency. Moreover, traditional cameras are based on mechanical switching optics, that are relatively slower in operation and caus e increasing of energy consumption.

Herein, we developed a bionic eye device that int egrated the advanced features of human eye. We fabric ated a hemispherical artificial retina based on a dense vertical aligned perovskite nanowire array. The device exhibit color imaging ability by utilizing the wavelengt h dependent optical penetration in nanowires. And the device has in-device signal preprocessing function base d on its synaptic photo response (Fig. 1). Moreover, w e integrated an electronic lens and an electronic iris to enhance its adaptivity (Fig. 2). This work demonstrate s a novel biomimetic approach to break the fundament al limitation of conventional imaging systems.

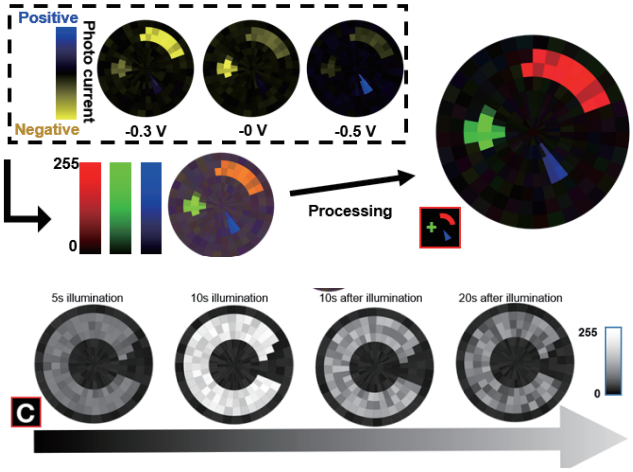

Fig. 1. Color imaging and in-device contrast enhancement

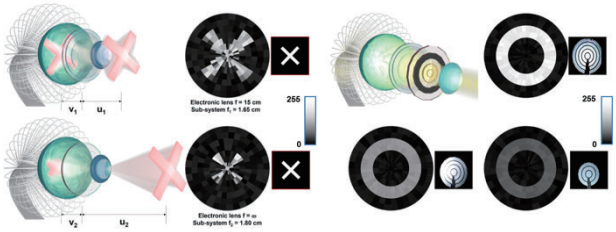

Fig. 2. Improved adaptivity with electronics optics

References

[1] Ding, Y. *et al. Sci. Adv.* **8**, 31 (2022).

[2] Gu, L. *et al. Nature* **581**, 278–282 (2020).

[3] Long, Z. *et al. Nat. Commun.* **14**, 1972 (2023).

Highly Efficient Blue Light-Emitting Diodes Based on Perovskite Film with Vertically Graded Bandgap and Organic Grain Boundary Passivation Shells

Lei Shu [*] **,** ***Zhiyong Fan*** [*]

[*]**Department of Electronic and Computer Engineering, The Hong Kong University of Science and Technology, Clear Water Bay, Kowloon, Hong Kong SAR, China**

The metal halide perovskite materials have emerged as a powerful candidate for the next generation of light-emitting diodes (LEDs) and high-definition displays. Over the past 9 years, the development of green and red emissive PeLEDs have rapidly increased, and the advancement of external quantum efficiency (EQE) have exceeded 20%. However, the achievement of pure and deep blue PeLEDs still lags far behind that of green and red PeLEDs. On the other hand, most reported blue PeLEDs articles are sky-blue emission, due to the cascade energy transfer process in quasi-2D perovskite materials. Therefore, it is still challenging to achieve pure blue and deep blue emissions.

Herein, for the first time, we demonstrated a wavelength tunable pure and deep blue PeLEDs with high EQE of 17.5% and 10.8% for emission wavelengths of 472 nm and 461 nm, respectively. The high performance of the blue PeLED EQE is achieved using quasi-2D perovskite film with vertically graded bandgap and grain boundary organic shells structure. And the unique structure is formed by controlling the doping of Cl to form the graded distribution of organic ligand $PDABr_2$ in the perovskite film, and the graded distribution of organic ligand can lead to the formation of the vertically graded bandgaps and organic shells. It opens up a novel avenue to fabricate high-performance pure and deep blue PeLEDs for future lighting and display applications.

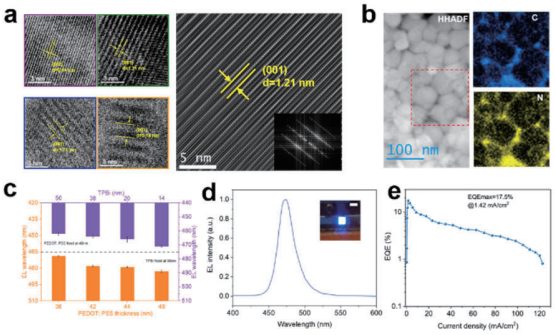

Fig.1. a, the low dose cryo-HRTEM images of different n value phases of the perovskite film; b, the organic grain boundary passivation shells; c, the tunbale EL wavelength; d, EL spectrum under forward bias; e, EQE-J curve of the champion device, the peak EQE is 17.5% (1.42mA cm^{-2}).

Designing Efficient and Aesthetically Pleasing Semitransparent Perovskite Solar Cells for Building-Integrated Photovoltaics: A Biomimetic Approach

Yiyi Zhu, Lei Shu, Qianpeng Zhang Yudong Zhu, Swapnadeep Poddar, Chen Wang, Zhubing He, and Zhiyong Fan

Department of Electronic and Computing Engineering, The Hong Kong University of Science and Technology, Kowloon, Hong Kong SAR, China

The emergence of semitransparent perovskite solar cells (ST-PSCs) has made them an attractive option for building-integrated photovoltaics, especially for power generation windows that must convert sunlight into electricity while transmitting daylight to illuminate indoor spaces. In addition to power conversion efficiency (PCE), attributes such as average visible transmittance (AVT), color, and longevity are critical for ST-PSCs. Tuning the perovskite thickness or surface coverage can adjust AVT, with an AVT of 20%–30% typically sufficient for power-generating windows. However, the conventional structure of ST-PSCs, consisting of continuous ultrathin perovskites, often results in an undesired reddish-brown hue.

To address this challenge, we present a highly efficient, robust, and neutral-colored ST-PSC inspired by the moth's eye surface architecture. The moth eye-inspired structure (MEIS) uses hexagonally arranged microcavity structures to trap photons in the wavelength range where the human eye is less sensitive, resulting in a record-high figure-of-merit for ST-PSCs.

To create the structure, we used the Langmuir-Blodgett technique to assemble polystyrene spheres on planar-ITO as a mask for patterning, which we then covered with sputtering deposition of ITO. We subsequently removed the spheres to obtain a biomimetic structure. Next, we deposited SnO2 using atomic layer deposition to achieve uniform and full coverage of the as-fabricated structure. We then applied spin-coating deposition to add the perovskites, followed by a layer of spiro-OMeTAD. Finally, we added a buffer layer of MoO3 and 100 nm IZO sputtering to serve as a transparent electrode.

We characterized the optical and electrical properties of our moth eye-inspired perovskite solar cells using various techniques, including scanning electron microscopy, X-ray diffraction, UV-Vis spectroscopy, and current-voltage measurements. Our results showed that the MEIS modification provided a AVT of 33%, which is important for maintaining aesthetics in BIPV applications. Our perovskite solar cells exhibited a high power conversion efficiency of over 10%, comparable to that of conventional opaque perovskite solar cells. We compared the performance of our moth eye-inspired perovskite solar cells to that of other semitransparent solar cells reported in the literature and demonstrated that our devices outperform them in terms of efficiency, AVT, and color neutrality.

We also tested the long-term stability of our perovskite solar cells and found that they exhibited excellent performance over a period of 224 days, indicating that they can withstand harsh environmental conditions. This study demonstrates the potential of using biomimetic approaches to design novel perovskite solar cells with improved optical and electrical properties and highlights the importance of developing solar cells that are both efficient and aesthetically pleasing for building-integrated photovoltaic applications. Our moth eye-inspired perovskite solar cells have the potential to revolutionize the field of building-integrated photovoltaics and accelerate the adoption of renewable energy sources in urban environments.

Record External Quantum Efficiency of Blue Quantum Rod Light Emitting Diodes achieved with Positive Aging Effect

Kumar Mallem*, Zebing Liao*, Maksym F. Prodanov*, Abhishek K. Srivastava*

***State Key Laboratory on Advanced Displays and Optoelectronics Technologies, Department of Electronics and Computer Engineering, The Hong Kong University of Science and Technology**

Over the last twenty years, extensive research on QLEDs has focused on synthesizing QDs, optimizing device structure, and improving electron-hole transportation, resulting in QLEDs reaching commercial standards for efficiency and stability in the display and lighting industry. Recently, demonstrations of QLEDs in red, green, and blue colors have achieved an external quantum efficiency (EQE) above 20% which is the theoretical limit of the conventional QLEDs structure, and a lifetime T50 of red and green QLEDs reached over 100,000 hours at an initial luminance of 100 cd/m^2. To further improving the EQE of the QLEDs is a big challenge due to the limitation of the outcoupling efficiency of the spherical QDs.

Semiconductor quantum rods (QRs) have distinct advantages over spherical quantum dots (QDs) such as linearly polarized emission and higher outcoupling efficiency, resulting in double the external quantum efficiency in QR-based light emitting diodes (LEDs). However, traditional synthesis approaches for CdSe/CdS core-shell QRs are limited to producing red QRs due to fast kinetics and a large bathochromic shift during the synthesis of w-CdSe seeds, making it challenging to synthesize blue QRs. The study aimed to address the challenge of achieving high-performing blue QRLEDs by synthesizing CdSe/$Zn_xCd_{1-x}S$/ZnS QRs with a high PLQY of 87% at an emission wavelength of 480 nm. Additionally, the study investigated the origin of the positive aging process observed in the blue QRLEDs.

The positive aging effect led to the achievement of blue QR-LEDs with a record-high EQE of 9.8% at an emission wavelength of 480 nm. The aging process improved the interfacial morphology of the QRs/ZnMgO/Al interface, which suppressed FRET in the device, resulting in an improvement in the PLQY and TRPL of the QRs film. The aging process also suppressed exciton quenching at the QRs/ZnMgO interface and improved the electron current of the device. As a result, the EQE and luminance of the devices increased by 2.2 and 3 folds after 5 days compared to the fresh device.

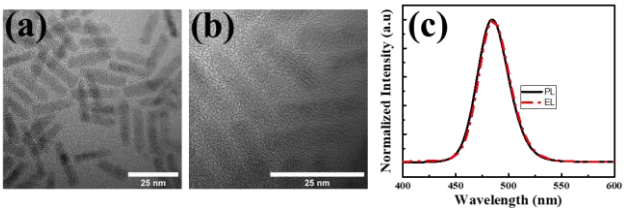

Figure 1 (a) and **(b)** The TEM image of CdSe/$Zn_xCd_{1-x}S$/ZnS QRs, the length of QRs around 20 nm. **b)** The PL and EL spectrum of QRs.

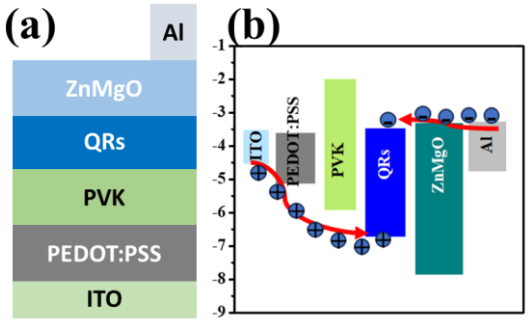

Figure 2 a) The QRLED device structure and **b)** energy level diagram.

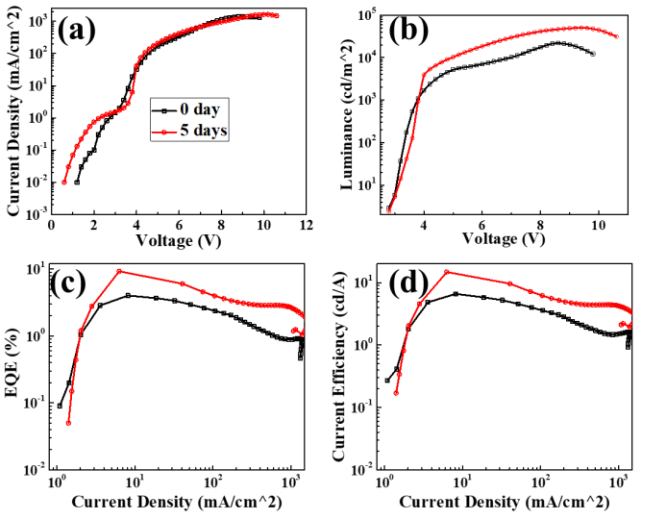

Figure 3 a) current density verse voltage. c) luminance verse Voltage. c) The EQE verse current density, and d) The current efficiency current density.

References

[1] Mallem, Kumar, et al. "Solution-Processed Red, Green, and Blue Quantum Rod Light-Emitting Diodes." *ACS Applied Materials & Interfaces* 14.16 (2022): 18723-18735.

[2] Prodanov, Maksym F., et al. "Thermally stable quantum rods, covering full visible range for display and lighting application." Small 17.3 (2021): 2004487.

[3] Kang, Chengbin, et al. "Quantum-Rod On-Chip LEDs for Display Backlights with Efficacy of 149 lm W− 1: A Step toward 200 lm W− 1." Advanced Materials 33.49 (2021): 2104685.

[4] Mallem, Kumar, et al. "65-5: Improved Brightness and Efficiency of Green Quantum-Rod-Based Light-Emitting Diodes." SID Symposium Digest of Technical Papers. Vol. 52. No. 1. 2021.

Invisibly Patterning Silver Nanowire Electrode through the Plateau-Rayleigh Instability

Hongteng Wang[1], Gui-Shi Liu[1]*

[1]Guangdong Provincial Key Laboratory of Optical Fiber Sensing and Communications, Key Laboratory of Visible Light Communications of Guangzhou, Key Laboratory of Optoelectronic Information and Sensing Technologies of Guangdong Higher Education Institutes, Jinan University, Guangzhou 510632, China

E-mail: guishiliu@163.com

Most of the electrodes in current optoelectronic devices are primarily made of indium tin oxide (ITO), but they have significant drawbacks such as brittleness and indium scarcity. Currently, silver nanowire (AgNW)-based transparent electrodes (TE) have been proposed as an attractive alternative to ITO due to their excellent flexibility, high figure of merit (FoM), and compatibility with large-scale manufacturing.[1,2] The patterning of AgNW TEs is crucial in constructing various optoelectronic devices. Therefore, there is a need for a simple, cost-effective, high-resolution, designable, and scalable process to form AgNW electrodes.

In this study, we employed a simple and cost-effective approach to fabricate patterned invisible electrodes. We modified AgNWs with a mixed solution containing a DPIN component (Figure 1). This method helps facilitate surface atom diffusion of metal nanowires at low temperatures.[3] This induced the Plateau-Rayleigh instability (PRI) to induce NW fragmentation at low temperatures. The effect of the mixed solution on reducing the melting point of AgNWs is illustrated in Figure 1. Since the DPIN is light dissociative, the DPIN-decorated AgNW film can be patterned using a photolithography-like method. Specifically, by placing a mask on the substrate and irradiating ultraviolet light above the mask, the DPIN composite in the irradiated area decomposed, thereby losing the effect of reducing the melting point of the AgNWs. The AgNWs in the unirradiated area has poor thermal stability due to the DPIN modification. Subsequently, the heating temperature was adjusted to be higher than the melting point of the unirradiated region but lower than the melting point of the irradiated region. After heating, the AgNWs in the unirradiated region melted and lost their conductivity, while the AgNWs in the irradiated region remained unaffected, thus forming the desired optically invisible patterned electrodes.

In our proposed method, the patterned ANW TEs are achieved by heating at temperatures ranging from 75 to 120° C. This significantly reduces the fabrication cost while achieving excellent disappearing effects, as shown in Figure 2. The method allows for the fabrication of multi-layer TEs on flexible substrates, making it suitable for fabrication of flexible touch panel. We have already achieved preliminary fabrication of touch electrodes that can accurately, quickly, and sensitively recognize touch signals. The fabricated touch panel holds the potential for efficient touch interaction in various electronic devices and applications.

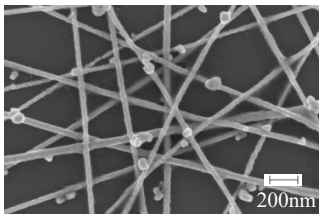

Fig. 1. Scanning electron microscope image of the AgNW network modified with DPIN

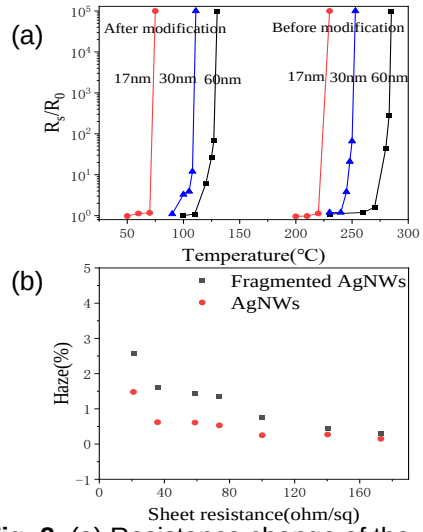

Fig. 2. (a) Resistance change of the AgNW networks with different diameters after thermal annealing for 3 minutes. (b) Haze at 550 nm wavelength of the AgNW networks and the fragmented AgNW networks.

References

1. Layani, Michael, Alexander Kamyshny, and Shlomo Magdassi. "Transparent conductors composed of nanomaterials." Nanoscale 6.11 (2014): 5581-5591.
2. Ye, Shengrong, et al. "Metal nanowire networks: the next generation of transparent conductors." Advanced materials 26.39 (2014): 6670-6687.
3. Liu, Gui-Shi, et al. "Self-assembled monolayer modulated Plateau-Rayleigh instability and enhanced chemical stability of silver nanowire for invisibly patterned, stable transparent electrodes." Nano Research 15.5 (2022): 4552-4562.

SKL
先進顯示與光電子技術
國家重點實驗室
State Key Laboratory of
Advanced Displays and Optoelectronics Technologies

香港科技大學
THE HONG KONG UNIVERSITY OF
SCIENCE AND TECHNOLOGY

中山大學
SUN YAT-SEN UNIVERSITY

南方科技大學
SOUTHERN UNIVERSITY OF SCIENCE AND TECHNOLOGY

北京大學
PEKING UNIVERSITY

華南理工大學
South China University of Technology

深圳大學
SHENZHEN UNIVERSITY

中國科學院大學
University of Chinese Academy of Sciences

福州大學
FUZHOU UNIVERSITY

國立陽明交通大學
NATIONAL YANG MING CHIAO TUNG UNIVERSITY

國立臺灣大學
National Taiwan University

國立臺灣科技大學
NATIONAL TAIWAN UNIVERSITY OF SCIENCE AND TECHNOLOGY